



ISSN 2518-718X (Print)
ISSN 2663-4872 (Online)

BULLETIN

OF THE KARAGANDA UNIVERSITY

CHEMISTRY

Series

№ 1(105)/2022

ISSN 2663-4872 (Online)
ISSN-L 2518-718X (Print)
Индексі 74617
Индекс 74617

ҚАРАҒАНДЫ
УНИВЕРСИТЕТІНІҢ
ХАБАРШЫСЫ

ВЕСТНИК
КАРАГАНДИНСКОГО
УНИВЕРСИТЕТА

BULLETIN
OF THE KARAGANDA
UNIVERSITY

ХИМИЯ сериясы

Серия **ХИМИЯ**

CHEMISTRY Series

№ 1(105)/2022

Қаңтар–ақпан–наурыз
30 наурыз 2022 ж.

Январь–февраль–март
30 марта 2022 г.

January–February–March
March, 30th, 2022

1996 жылдан бастап шығады
Издается с 1996 года
Founded in 1996

Жылына 4 рет шығады
Выходит 4 раза в год
Published 4 times a year

Қарағанды, 2022
Караганда, 2022
Karaganda, 2022

Main Editor

Doctor of Chemical sciences
M.Zh. Burkeyev

Responsible secretary

Candidate of chem. sciences
I.A. Pustolaikina

Editorial board

- Z.M. Muldakhmetov**, Academician of NAS RK, Doctor of chem. sciences, Institute of Organic Synthesis and Coal Chemistry of the Republic of Kazakhstan, Karaganda (Kazakhstan);
- S.M. Adekenov**, Academician of NAS RK, Doctor of chem. sciences, International Research and Production Holding “Phytochemistry”, Karaganda (Kazakhstan);
- S.E. Kudaibergenov**, Doctor of chem. sciences, Institute of Polymer Materials and Technologies, Almaty (Kazakhstan);
- V. Khutoryanskiy**, Professor, University of Reading, Reading (United Kingdom);
- Fengyun Ma**, Professor, Xinjiang University, Urumqi (PRC);
- Xintai Su**, Professor, South China University of Technology, Guangzhou (PRC);
- R.R. Rakhimov**, Doctor of chem. sciences, Norfolk State University, Norfolk (USA);
- M.B. Batkibekova**, Academician of the Engineering Academy of the Kyrgyz Republic, Doctor of chem. sciences, Kyrgyz State Technical University named after I. Razzakov, Bishkek (Kyrgyzstan);
- S.A. Beznosyuk**, Doctor of phys.-math. sciences, Altai State University, Barnaul (Russia);
- B.F. Minaev**, Doctor of chem. sciences, Bohdan Khmelnytsky National University of Cherkasy, Cherkasy (Ukraine);
- I.V. Kulakov**, Doctor of chem. sciences, University of Tyumen (Russia);
- R.P. Bhole**, PhD, Associate Professor, Dr. D.Y. Patil Institute of Pharmaceutical Sciences and Research, Sant Tukaram Nagar, Pimpri, Pune (India);
- A.M. Makasheva**, Doctor of techn. sciences, Zh. Abishev Chemical-Metallurgical Institute, Karaganda (Kazakhstan);
- M.I. Baikenov**, Doctor of chem. sciences, Karagandy University of the name of acad. E.A. Buketov (Kazakhstan);
- L.K. Salkeeva**, Doctor of chem. sciences, Karagandy University of the name of acad. E.A. Buketov (Kazakhstan);
- Ye.M. Tazhbaev**, Doctor of chem. sciences, Karagandy University of the name of acad. E.A. Buketov (Kazakhstan);
- O.G. Yaroshenko**, Doctor of Pedagogical Sciences, Academician of the National Academy of Pedagogical Sciences of Ukraine, Institute of Higher Education of the National Academy of Educational Sciences of Ukraine, Kyiv (Ukraine);
- V.N. Fomin**, Cand. of chemical science, Head of the laboratory of engineering profile “Physical and chemical research methods”, Karagandy University of the name of acad. E.A. Buketov (Kazakhstan)

Postal address: 28, University Str., Karaganda, 100024, Kazakhstan

Tel./fax: (7212) 34-19-40.

E-mail: chemistry.vestnik@ksu.kz; meyram.burkeyev@ksu.kz; irina.pustolaikina@ksu.kz

Web-site: <http://chemistry-vestnik.ksu.kz>

Editors Zh.T. Nurmukhanova, S.S. Balkeyeva, Z.E. Ramazanova

Computer layout V.V. Butyaikin

Bulletin of the Karaganda University. Chemistry series.

ISSN 2663-4872 (Online). ISSN-L 2518-718X (Print).

Proprietary: NLC “Karagandy University of the name of academician E.A. Buketov”.

Registered by the Ministry of Information and Social Development of the Republic of Kazakhstan. Rediscount certificate No. KZ27VPY00027382 dated 30.09.2020.

Signed in print 29.03.2022. Format 60×84 1/8. Offset paper. Volume 16,5 p.sh. Circulation 200 copies. Price upon request. Order № 44.

Printed in the Publishing house of NLC “Karagandy University of the name of acad. E.A. Buketov”.

28, University Str., Karaganda, 100024, Kazakhstan. Tel.: (7212) 35-63-16. E-mail: izd_kargu@mail.ru

CONTENTS

PREFACE

Karagandy University of the name of academician E.A. Buketov is pleased to announce that "Bulletin of the Karaganda university. Chemistry series" scientific journal has been accepted for indexing in the Scopus abstract database 4

ORGANIC CHEMISTRY

Bhole R.P., Swamy M.R., Wavhale R., Bonde C.G., Chikhale R. Design of potential vitamin-drug conjugate for enhanced anticancer activity 6

Burkeyev M.Zh., Zhunisova M.S., Plocek J., Kazhmuratova A.T., Zhumagalieva T.S. Properties of cross-linked copolymers of polypropylene glycol maleate with acrylic acid obtained at various concentrations of the RAFT agent 15

Kassanova A.Zh., Yestayeva M.T., Turtubayeva M.O. Arenediazonium sulfonates: synthesis, comparison of structural and physicochemical properties 25

Mendigalieva S.S., Birimzhanova D.A., Irgibaeva I.S., Barashkov N.N., Sakhno Y.E. Aggregation-induced emission of 5-(benzylidene) pyrimidine-2,4,6-triones 39

PHYSICAL AND ANALYTICAL CHEMISTRY

Annavarapu T., Kamepalli S., Kondala S.K., Kotra V., Challa S.R., Rudrapal M., Bendale A.R. Anti-inflammatory and antioxidant activities of 4-allylpyrocatechol and its derivatives with molecular docking and ADMET investigations 50

Asgaonkar K.D., Patil S.M., Chitre T.S., Wani S.D., Singh M.T. QSAR tool for optimization of nitrobenzamide pharmacophore for antitubercular activity 60

Galiyeva A.R., Tazhbayev Ye.M., Zhumagalieva T.S., Sadyrbekov D.T., Kaikenov D.A., Kariyeva B.N., Shokenova S.S. Polylactide-co-glycolide nanoparticles immobilized with isoniazid: optimization using the experimental Taguchi method 69

Jalmakhanbetova R.I., Suleimen Ye.M., Abe N., Oyama M., Metwaly A.M., Eissa I.H., Ishmuratova M.Yu., Ibatayev Zh.A. Isolation and in silico SARS-CoV-2 main protease inhibition potential of chrysoeriol from *Chondrilla brevirostris* Fisch. & Mey C.A. 78

Sarsenbekova A.Zh., Bolatbay A.N., Morgun V.V., Havlicek D., Davrenbekov S.Zh., Nasikhataly E. Study of thermal stability and determination of effective activation energy values during degradation of unsaturated polyester copolymers in the air atmosphere 86

INORGANIC CHEMISTRY

Aliyev F.R., Orujlu E.N., Babanly D.M. Synthesis and study of a new mixed-layered compound GeBi_3Te_4 belonging to the $n\text{Bi}_2-m\text{GeBi}_2\text{Te}_4$ homologous series 92

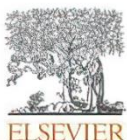
CHEMICAL TECHNOLOGY

Sagyndikov M.S., Salimgarayev I.I., Ogay E.K., Seright R.S., Kudaibergenov S.E. Assessing polyacrylamide solution chemical stability during a polymer flood in the Kalamkas field, Western Kazakhstan 99

Yuminova A.A., Giniyatullina E.A., Kariyeva L.M., Chekanova L.G. Physical-chemical properties of FM-1 reagent as a potential collector for ion flotation of lanthanoids 113

Shlyapov R.M., Amerkhanova Sh.K., Uali A.S., Omarbekov T.B., Belgibayeva D.S. Thermodynamics of chalcocite dissolving in solutions of flotation reagents 122

PREFACE



Elsevier BV
Radarweg 29
1043 NX Amsterdam
Netherlands
t +31 20 485 3911
f +31 20 485 2912
elsevier.com

III Amsterdam 31158902 | vat no. NL 005013010801

Ref. No. TRMC-CA/KZ-Jan10

“10” января 2022

**Председателю Правления – Ректору
Карагандинского государственного университета
имени академика Е.А. Букетова,
Дулатбекову Н. О.**

Уважаемый господин Нурлан Орыбасарович,

Позвольте искренне поздравить Вас и Ваших коллег с включением журнала **Bulletin of the Karaganda University Chemistry Series** (ISSN: 2518-718X, E-ISSN: 2663-4872, Издатель: Е.А.Букетов Karaganda State University Publish House) в реферативную базу данных **Scopus!**

Мы искренне верим в наше плодотворное сотрудничество и в выбранный Вами вектор, который непременно приведет Карагандинский государственный университет имени академика Е.А. Букетова к числу ведущих научных и образовательных центров Евразийского региона.

С уважением,

Дамир Рахметов
**Региональный представитель
компании Elsevier по Центральной
Азии и Азербайджану**



ELSEVIER
Scopus

Karagandy University of the name of academician E.A. Buketov is pleased to announce that the “Bulletin of the Karaganda University. Chemistry Series” scientific journal has been accepted for indexing in the Scopus bibliographic database.

Scopus is the world’s largest abstract and citation database of peer-reviewed scientific literature, developed and owned by Elsevier Publishing Corporation. The inclusion of the “Bulletin of the Karaganda University. Chemistry Series” in the Scopus database demonstrates the commitment of the journal’s editorial policy to ethical rules and principles supported by the community of leading scientific periodicals publishers; legal requirements for copyright; principles of scientific integrity; rejection of plagiarism and slander.

Е.А. Бөкетов атындағы Қарағанды университеті «Қарағанды университетінің хабаршысы. «Химия» сериясы» ғылыми журналы Scopus реферативті мәліметтер базасына индекстеу үшін қабылданғанын хабарлайды.

Scopus — бұл Elsevier баспа корпорациясы қолдайтын және рецензияланған ғылыми әдебиеттердің дәйексөзін бақылауға мүмкіндік беретін ең үлкен библиографиялық және рефераттық деректер базасы. «Қарағанды университетінің хабаршысы. Химия сериясының» Scopus базасына енуі — журналдың редакциялық саясатының жетекші ғылыми мерзімді басылымдарды шығарушылардың қауымдастығы қолдайтын этикалық ережелер мен принциптерге; авторлық құқыққа қойылатын заң талаптарына; ғылыми ақиқатқа, ғылыми адалдық, плагиат пен жала жабудан бас тарту принциптеріне адалдығын көрсетеді.

Карагандинский университет имени академика Е.А. Букетова сообщает, что научный журнал «Вестник Карагандинского университета. Серия Химия» был принят для индексирования в реферативную базу данных Scopus.

Scopus — крупнейшая библиографическая и реферативная база данных, поддерживаемая издательской корпорацией «Elsevier» и позволяющая отслеживать цитируемость рецензируемой научной литературы.

Включение «Вестника Карагандинского университета. Серия Химия» в Scopus демонстрирует приверженность редакционной политики журнала этическим правилам и принципам, поддерживаемым сообществом ведущих издателей научной периодики, законодательным требованиям в отношении авторского права, принципам научной истины, научной честности, неприятия плагиата и клеветы.

ORGANIC CHEMISTRY

Article

UDC 544.42+519.242.7

<https://doi.org/10.31489/2022Ch1/6-14>

R.P. Bhole^{1*}, M.R. Swamy¹, R. Wavhale¹, C.G. Bonde², R. Chikhale³

¹*Dr. D.Y. Patil Institute of Pharmaceutical Sciences and Research, Pimpri, Pune, India;*

²*NMIMS School of Pharmacy, Shirpur, Dist: Dhule, India;*

³*UCL School of Pharmacy, London, United Kingdom*

(*Corresponding author's e-mail: ritesh.bhole@dypvp.edu.in)

Design of potential vitamin-drug conjugate for enhanced anticancer activity

5-Fluorouracil, a primary molecule widely used in the treatment of various cancer stages, is rapidly metabolized to an inactive form, namely 5,6-dihydro-5-FU and various mutational changes in chemotherapy. We utilized a carbodiimide catalyst to form a conjugate with folic acid. As folic acid receptors are over-expressed in cancerous tissues, it increases the bioavailability of 5-FU. This work represents design and synthesis of the new vitamin-drug conjugate, possibly enhancing anticancer activity. 5-Fluorouracil has potent action on breast, colorectal, stomach, and skin cancer tissues. Folic acid aided in targeting FR α receptors of cancer cells selectively. 5-FUFA was subjected to spectral characterization to confirm successful conjugation. The molecular dynamics simulation was studied in the Schrodinger suite and validated by molecular trajectory in CPPTRAJ software. This conjugate was further studied for molecular modeling studies and the docking score of the conjugate represented a higher binding score than 5-FU, i.e., -8.0 Kcal/mol. The drug-receptor interaction was further validated using molecular dynamics simulation in the Schrodinger suite and molecular trajectory CPPTRAJ software for 100 ns. The molecular dynamics simulation results showed stability with slight conformational change at 25 ns from 2–4 Å.

Keywords: 5-Fluorouracil, folic acid, synthetic conjugate, molecular docking, molecular dynamics, drug design, chemotherapeutic agent, human thymidylate synthase.

Introduction

5-Fluorouracil (5-FU) has been 3rd most commonly prescribed antimetabolite cytotoxic drug in treatment of various malignant forms of tumors, namely breast, head, and neck, as well as pancreas, stomach, and skin since 1957. It is an aromatic water soluble heterocyclic compound structurally common to pyrimidine nitrogenous base pairing found in DNA and RNA. 5-FU is a prodrug, which is bio activated by nucleotides, namely 5-fluoro-2'-deoxyuridine 5'-monophosphate (5-FdUMP), 5-fluoro-2'-deoxyuridine 5'-triphosphate (5-FdUTP) and 5-fluorouridine triphosphate (5-FUTP) [1–5]. 5-FU administered IV for tumors located within body tissues has several issues. It is rapidly metabolized into inactive form i.e., 5,6-dihydro-5-FU (80–90 %). It has low bioavailability and non-specificity to cancer cells. Large doses, namely 400–600 mg/m² are needed for optimum therapeutic effect. Another primary reason of resistance to 5-FU was observed due to overproduction of Bcl-2, Bcl-XL, Mcl-1 proteins, augmentation of drug inactivation and mutation of target leading to anomalous conformation [6]. In a study by Yu & co-workers [7] it is stated that Rosmaric acid increases sensitivity to gastric carcinoma SGC7901 cells by downregulating miR-6785-5p and miR-642a-3p leading to increase in expression of FOXO4 in 5-FU treatment regime. In another study by Zheng & co-workers [8] Oridion was proposed to enhance cytotoxicity of 5-FU in renal carcinoma cells by inducing necroptosis.

The study carried out in France showed that among 76,200 patients who received fluoropyrimidine as chemotherapy 1,200 suffered from life threatening toxicity and 150 (0.197 %) died each year might be due to the lack of dihydropyrimidine dehydrogenase (DPD) activity [9].

DPD is a vital enzyme in catabolism of pyrimidine bases uracil and thymidine. It is highly expressed in liver and blood. It is found in monocytes followed by lymphocytes, granulocytes and platelets. In contrast, no effect on erythrocytes is detected. Wörmann & et al. [10] state that activity of DPD prior administration of 5-FU, capecitabine and tegafur is blocked by folinic acid, increasing intracellular concentration leading to increase in active metabolite rate. Thus, pharmacologically blocking of DPD increases intracellular concentration, increasing active metabolite rate.

Folic acid is a water-soluble vitamin consisting of pteridine, *p*-aminobenzoic acid and glutamic acid. It is a fully oxidized folate. Folates play an essential role in DNA synthesis and methylation, responsible for maintaining DNA integrity, metabolizing amino acid, gene expression, and remethylation of homocysteine to methionine [11–12].

Folates obtained from food intake have presence of extra glutamate residues that are hydrolyzed to single glutamate within gut before absorption by active transport across intestinal mucosa. Whereas passive diffusion is observed in doses of pharmacological administration. Monoglutamate is converted to tetrahydrofolate, further converted to methyl or formyl forms. Folates are in 5-methyl-THF forms in blood. Some folates are also circulating in blood unaltered, i.e., unmetabolized folic acid [13].

Folates are transported by Reduced Folate Carrier (RFC), Proton-Coupled Folate Transporter (PCFT), and Folate receptors α , β , respectively [14–16]. FR α and FR β are glycosylphosphatidylinositol (GPI)-anchored cell surface glycoproteins and FR γ is a secretory protein [17]. The uptake of folates by FR α and FR β is receptor-mediated endocytosis [18]. FR α is mostly expressed in epithelial cells of uterus, placenta, choroid plexus, retina, and kidney. It is also expressed in cancers of epithelial origin, namely adenocarcinoma of breast, ovary, cervix, uterus, kidney, lung, bladder, and pancreas [19–22].

Folate transporters, PCFT are active in acidic pH, while RFC has low binding to non-reduced FA. Hence, we estimate that the hypothesized folate receptor α (FR α) may take up the 5-FUFA scaffold, as it is upregulated in many primary and metastatic cancer, namely epithelial and over 90% of non-mucinous OCs also platinum-resistant ovarian cancer. Thus, targeting cancer cells selectively, associated side effects (non-specificity, resistance, toxicity, high doses, etc.) are overcome. The bioavailability of 5-FU within cancer cells is improvised with either cleavage by amidase enzyme or showing action as a whole, e.g., CT900. At concentration as low as 100–250 nM, i.e. in nanomolar range, it is possible to overcome drug resistance issues by not affecting levels of HTS and having allosteric action [23–29].

The present study aims to design a new vitamin-drug conjugate by utilizing folic acid and 5-fluorouracil as a primary compound to form 5-fluorouracil folic acid (5-FUFA). The conjugate is expected to have the targeted drug activity with minimal side effects [30–33].

Experimental

Chemicals: 5-Fluorouracil was a kindly gifted sample from Intas Pharmaceuticals, Ahmedabad. Folic acid (FA) was purchased from Sigma Aldrich Chemicals Pvt. Ltd. Dimethylformamide (DMF), 4-dimethylaminopyridine (DMAP), isopropanol, and N-hydroxysuccinamide (NHS) were purchased from SD Fine Chem Ltd. 1-(3-Dimethylaminopropyl)-3-ethylcarbodiimide HCl (EDC. HCl) was purchased from AVRA Laboratories Pvt. Ltd. Ethyl acetate and methanol were purchased from HiMedia Laboratories Pvt. Ltd.

Instruments used: Melting-boiling point apparatus (Veego) was used to determine the melting point. FTIR analysis was carried out to obtain the FTIR spectra on FTIR spectrophotometer Shimadzu FTIR 8400S. Mass spectra were recorded on a mass spectrometer, Shimadzu LCMS-8040. MD simulation was executed on Nvidia V100-SXM2-16GB Graphic Processing Unit using the PMEMD.CUDA module installed on the Computational Shared Facility (CSF3), UCL School of Pharmacy, UK.

Methodology:

Synthesis of 5-Fluorouracil Folic acid (5-FUFA)

1. Folic acid activation

3 g of FA were activated by EDC and NHS in 15 mL of DCM (molar ratio of FA:EDC:NHS =1:1:1) at room temperature under nitrogen gas for 24 h.

2. Conjugation

The 2° amine group of 5-FU (1 g) was conjugated to the carboxylic group of FA through the amide bond. 5-FU dissolved in 5 mL of DMF was added to the activated FA in DMF then EDC & DMAP were added at room temperature under nitrogen gas for 24 h.

Marverti et al. [34] performed peptide conjugates of folic acid that would selectively enter cancer cells by thymidylate synthase dimer. Presented research work utilized their synthetic scheme by incorporating various synthetic procedures with variations in catalyst to form an amide linkage between folic acid and 5-fluorouracil, respectively. Initially, 3 g of FA were activated in the presence of an equimolar concentration of EDC.HCl, NHS, (4 mL) DMF, inert atmosphere for 24 h followed by adding 1 g of 5-FU dissolved in 1 mL of DMF and equimolar concentration of DMAP in the same reaction mixture continued to stir for another 24 h (Fig. 1). EDC is a water-soluble carbodiimide that creates a zero-length linker between carboxyl and amine groups. EDC coupled with NHS reacts with the carboxyl group of FA to form a semi-stable NHS-ester intermediate. The secondary amine of 5-FU reacts with the ester intermediate to form an amide bond. Resultant was treated with 10 mL of ethyl acetate and 10 mL of methanol. Unreacted FA & 5-FU were separated. FA is insoluble in methanol, precipitates out, and 5-FU is soluble in ethyl acetate. Thus, the product formed is present in insoluble methanol form. It was checked for purity and homogeneity by TLC. It was concentrated and dried to evaporate. This was further utilized for spectral analysis to confirm amide linkage formation.

The melting point of 5-FUFA was found to be 155°C. Rf was 0.5.

Physical and spectral data for 5-FUFA: IR (KBr, cm^{-1}): Amide I bond at 1687.77 (C=O stretching), amide II bond at 1591.33 (N-H bending), O-H of carboxylic acid at 3244.66, (N-C stretching) at 1379.15 & (N-H wag) at 802.41, 3163.23 (C-H stretching). Ms: m/z (%) = 554.15 (M+1).

Protein structure preparation: The protein crystal structure of human Thymidylate Synthase (TS) enzyme (PDB ID- 1HVY) was retrieved from Protein Data Bank with the resolution of 1.90 Å. The enzyme structures were checked for missing atoms, bonds and contacts. The hydrogen atoms were added to the enzyme structure. The water molecules and bound ligands were deleted manually. The parameters during protein preparation were set with ionization and tautomerization using the Epik module for a pH range of 7 to 9.

Molecular docking studies: The compounds were subjected to docking with extra precision (XP) molecular docking using the Glide module of the Schrodinger suite. Before performing the docking studies, a grid generation protocol was performed to determine the binding site. The already bound ligand was used as a reference site for the grid generation with the Glide grid module. The generated grid was further used for the docking experiment. For the docking method, the van der Waals radii and scaling factor were set to 0.80 and 0.15, respectively, to soften the potential of nonpolar parts on drug molecules. No restraints were applied to the ligands during the entire docking protocol. Post-docking minimization was allowed to provide minimized docked structures with a maximum of five best poses per ligand to include in the docking output file. The drug molecules were allowed to be flexible during the docking process. The RMSD, docking score, Glide score, and binding energy were recorded for each molecule.

Molecular Dynamics Simulations: To explore the docked complex's structural, energetic status, and steric refinement, an all-atom MD simulation of 100 ns was performed using the AMBER18 software package. The docked complexes were immersed in a truncated octahedron of TIP3P water, giving 24,515 water molecules to the system. A sufficient number of Na^+ and Cl^- counter ions were added to neutralize the system and achieve an ionic strength of 0.1M to mimic the physiological pH. The ff14SB force field was used for protein topology generation. The entire experiment of MD simulation was executed on Nvidia V100-SXM2-16GB Graphic Processing Unit using the PMEMD.CUDA module installed on the Computational Shared Facility (CSF3), University of Manchester, UK. Simulations were run at 300 K using the Langevin thermostat with a collision frequency of 2 ps⁻¹; at 1 atm using a Monte Carlo barostat with volume exchange attempts every 100 fs. A 2-fs integration step was employed. Covalent bonds involving hydrogen constrained using SHAKE algorithm. A cut-off of 8 Å was used for short-range non-bonded interactions, while long-range electrostatics were treated using the particle mesh Ewald method. Equilibration comprised rounds of NVT and NPT equilibration for 10 ns in total. Production MD run was performed for 100 ns. Root-mean-square deviation (RMSD), root-mean-square fluctuation (RMSF), and other interactions were analyzed using CPPTRAJ over full trajectory, taking configuration every 4 ps.

Results and Discussion

5-FUFA conjugate was synthesized. The melting point and TLC were performed to ascertain its purity and homogeneity. Spectral analytical data confirmed formation of conjugate.

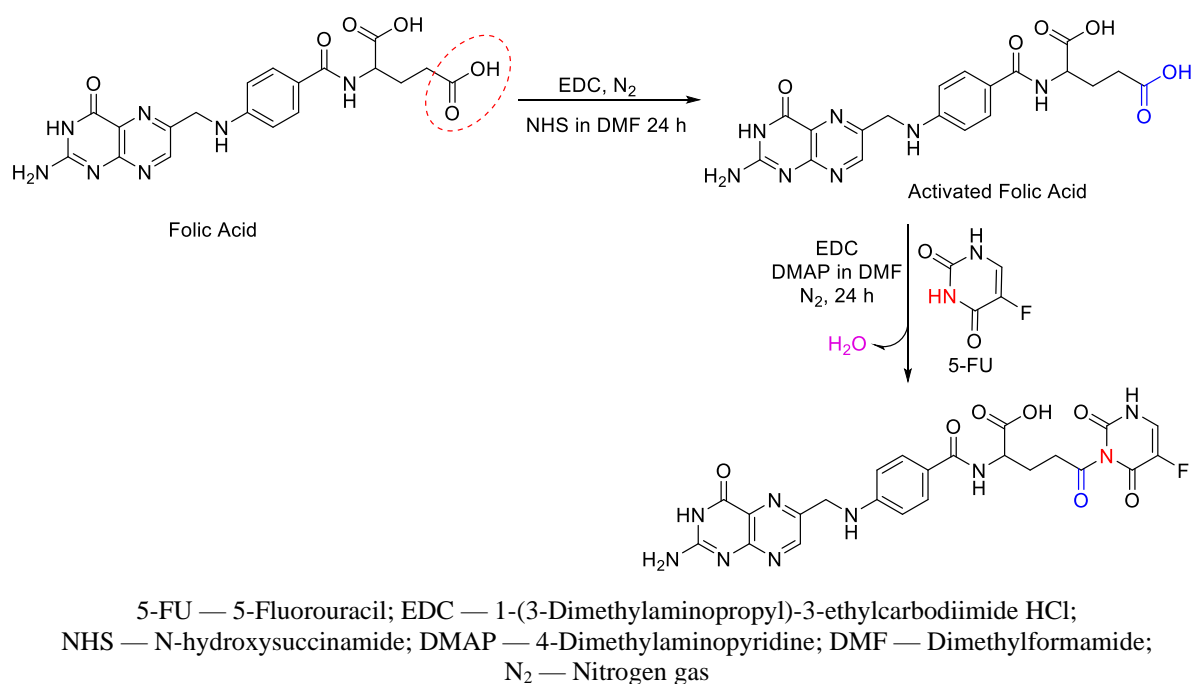


Figure 1. Proposed scheme for synthesis of 5-Fluorouracil folic acid (5-FUFA)

FT-IR

There are observed peaks at 1687.77 (C=O stretching) for an amide I bond and 1591.33 (N-H bending) for an amide II bond, which are characteristic of an amide C=O bond. These peaks in the IR spectra of 5-fluorouracil folic acid demonstrate the formation of 5-fluorouracil folic acid conjugate via the formation of an amide linkage.

Mass Spectroscopy

Mass spectra of 5-FUFA conjugate were recorded for its structural confirmation. The mass spectra of 5-FUFA conjugate showed the molecular ion peak at 554.15 m/z, confirming the conjugation of 5-FUFA by forming an amide linkage and forming the final product, i.e., 5-FUFA conjugate.

Molecular simulation:

The molecular docking study was conducted to understand the binding of 5-fluorouracil-folic acid conjugate (5-FUFA) on the human thymidylate synthase (PDB: 1HVY). The crystal structure of human thymidylate synthase is complexed with dUMP and Raltitrexed. During the processing of the target receptor, water molecules and other crystallographic solvents were removed. The protein was minimized in the Glide protein preparation protocol. The Grid generation was performed with Raltitrexed as a reference ligand and the 5-FUFA was docked with the extra precision (XP) method. The docking studies showed that 5-FUFA conjugate interacted at Asn226, Cys195, Asn112, Asp49 and Lys47 of the human thymidylate synthase proteins through hydrogen bonding and arene interaction with the π stacking with the Asp218 and the phenyl ring from the conjugate respectively with a binding score of -8.0 Kcal/mol (Figures 2, 3), which was higher than 5-FU, i.e., -3.475 . So, it was proved that forming 5-FUFA conjugate showed greater binding to the target protein.

Molecular docking studies were performed in the Schrodinger suite utilizing the Glide module with the extra precision method. 5-FUFA was bound on human thymidylate synthase, which was complexed with dUMP & Raltitrexed as a reference ligand. Followed by Molecular Dynamic simulation was carried on AMBER18 software for 100 ns, and later to validate further the resultant docking score analysis of full trajectory was done using CPPTRAJ, resulting in possible variations by a ligand and a receptor (Figure 4).

protein preparation protocol. The Grid generation was performed with Raltitrexed as a reference ligand, and the 5-FUFA was docked with the extra precision (XP) method. The docking studies showed that 5-FUFA conjugate interacted at Asn226, Cyc195, Asn112, Asp49, and Lys47 of the human thymidylate synthase proteins through hydrogen bonding and an arene interaction with the π stacking with the Asp218 and the phenyl ring from the conjugate respectively with a binding score of -8.0 Kcal/mol, which was higher than 5-FU, i.e., -3.475. So, it was proved that forming 5-FUFA conjugate showed greater binding to the target protein.

The MD simulation suggests that the receptor residues form several new interactions during simulation with the formation of hydrogen bonds with Asn226, Cyc195, Asn112, Asp49, and Lys47. It forms the arene interaction with the π stacking with the Asp218 and the phenyl ring from the conjugate (Figure 3). The analysis of the MD trajectory was performed with the help of CPPTRAJ, and plots were prepared with XMGRACE software. The RMSD of the protein suggests a smooth transition and convergence between 1–2.5 Å. The RMSF for most of the residues was below 2.0 Å throughout the simulation. It was also found that the ligand underwent a conformational change, which was reflected in its RMSD (Figure 4c) around 25 ns. The ligand RMSD fluctuated from 2 to 4 Å and then remained stable for the remaining simulation time. All these findings suggest good docking and further good stability for most of the MD simulation time.

Conclusions

We conclude scaffold formed by simple carbodiimide catalyst (EDC.HCl) and 5-FUFA conjugate between 5-FU and folic acid was successfully synthesized. The characterization of the synthesized compounds was in line with the structure proposed. The drug design studies reveal that 5-FUFA forms hydrogen bonds with the residues in the active site of the receptor, i.e., Agr50 and Tyr258 form hydrogen bonds whereas the Gly222 and Asn226 form π - π stacking interactions with the best dock pose to present -8.0 Kcal/mol, which represents the highest dock score. By assessing the stability of the drug-receptor complex, the docked pose was subjected to molecular dynamics simulation in the Schrodinger suite and validated by molecular trajectory CRPPTRAJ software for 100 ns. It was found to be stable, with a slight conformational change at 25 ns from 2 to 4 Å.

Thus, the conjugate may be a potential molecule to increase the bio efficiency of 5-FU and decrease associated side effects by selectively targeting cancer cells, such as the uptake of folic acid by cancer cells during folate receptor endocytosis. However, this hypothesis may be further tested by performing detailed anti-cancer evaluation in the future.

Acknowledgments

The authors are grateful to Principal Dr. D.Y. Patil Institute of Pharmaceutical Sciences, Pimpri, Pune, for providing necessary facilities for research.

References

- 1 Longley, D.B., Harkin, D.P., & Johnston, P.G. (2003). 5-fluorouracil: mechanisms of action and clinical strategies, *Nat. Rev. Canc.* 3, 330. <https://doi.org/10.1038/nrc1074>.
- 2 Grem, J.L. (1997). Mechanisms of action and modulation of fluorouracil. *Semin. Radiat. Oncol.* 7, 249–259. [https://dx.doi.org/10.1016/S1053-4296\(97\)80023-9](https://dx.doi.org/10.1016/S1053-4296(97)80023-9).
- 3 Diasio, R. B., & Harris, B.E. (1989). Clinical pharmacology of 5-fluorouracil. *Clinical pharmacokinetics*, 16(4), 215–237. <https://doi.org/10.2165/00003088-19816040-00002>.
- 4 Thomas, D.M., & Zalberg, J.R. (1998). 5-Fluorouracil: A pharmacological paradigm in the use of cytotoxics. *Clinical and experimental pharmacology and physiology*, 25(11), 887–895. <https://doi.org/10.1111/j.1440-1681.1998tb02339.x>.
- 5 Mader, R.M., Müller, M., & Steger, G.G. (1998). Resistance to 5-fluorouracil. *General Pharmacology: The Vascular System*, 31(5), 661–666. [http://dx.doi.org/10.1016/S0306-3623\(98\)00191-8](http://dx.doi.org/10.1016/S0306-3623(98)00191-8).
- 6 Barin-Le Guellec, C., Lafay-Chebassier, C., Ingrand, I., Tournamille, J. F., Boudet, A., Lanoue, M. C., ... & Etienne-Grimaldi, M.C. (2020). Toxicities associated with chemotherapy regimens containing a fluoropyrimidine: a real-life evaluation in France. *European Journal of Cancer*, 124, 37–46. <https://doi.org/10.1016/j.ejca.2019.09.028>.
- 7 Yu, C., Chen, D.Q., Liu, H.X., Li, W.B., Lu, J.W., & Feng, J.F. (2019). Rosmarinic acid reduces the resistance of gastric carcinoma cells to 5-fluorouracil by downregulating FOXO4-targeting miR-6785-5p. *Biomedicine & Pharmacotherapy*, 109, 2327–2334. <https://doi.org/10.1016/j.biopha.2018.10.061>.
- 8 Zheng, W., Zhou, C.Y., Zhu, X.Q., Wang, X. J., Li, Z.Y., Chen, X.C., Che, X.Y., & Xie, X. (2018). Oridonin enhances the cytotoxicity of 5-FU in renal carcinoma cells by inducing necroptotic death. *Biomedicine & Pharmacotherapy*, 106, 175–182. <https://doi.org/10.1016/j.biopha.2018.06.111>.

- 9 Amstutz U., Henricks L.M., Offer S.M., Barbarino J., Schellens J.H., Swen J.J., et al. (2018). Clinical Pharmacogenetics Implementation Consortium (CPIC) Guideline for Dihydropyrimidine Dehydrogenase Genotype and Fluoropyrimidine Dosing: 2017 Update. *Clin Pharmacol Ther.* 103(2), 210–216. <https://doi.org/10.1002/cpt.911>.
- 10 Wörmann, B., Bokemeyer, C., Burmeister, T., Köhne, C. H., Schwab, M., Arnold, D., ... & Hofheinz, R.D. (2020). Dihydropyrimidine dehydrogenase testing prior to treatment with 5-fluorouracil, capecitabine, and tegafur: a consensus paper. *Oncology research and treatment*, 43(11), 628–636. <https://doi.org/10.1159/1159/00510258>.
- 11 Shane, B. (2008). Folate and vitamin B12 metabolism: overview and interaction with riboflavin, vitamin B6, and polymorphisms. *Food and nutrition bulletin*, 29(2_suppl1), S5-16. <https://doi.org/10.1177/15648265080292s103>.
- 12 Blount, B.C., Mack, M.M., Wehr, C.M., MacGregor, J.T., Hiatt, R.A., Wang, G., Wickramasinghe, S.N., & Ames, B.N. (1997). Folate deficiency causes uracil misincorporation into human DNA and chromosome breakage: implications for cancer and neuronal damage. *Proceedings of the National Academy of Sciences*, 94(7), 3290–3295. <https://doi.org/10.1073/pnas.94.7.3290>.
- 13 Ducker, G.S., & Rabinowitz, J.D. (2017). One-carbon metabolism in health and disease. *Cell metabolism*, 25(1), 27–42. <https://doi.org/10.1016/j.cmet.2016.08.009>.
- 14 Desmoulin, S.K., Hou, Z., Gangjee, A., & Matherly, L.H. (2012). The human proton-coupled folate transporter: Biology and therapeutic applications to cancer. *Cancer biology & therapy*, 13(14), 1355–1373. <https://doi.org/10.4161/cbt.22020>.
- 15 Elnakat, H., & Ratnam, M. (2004). Distribution, functionality and gene regulation of folate receptor isoforms: implications in targeted therapy. *Advanced drug delivery reviews*, 56(8), 1067–1084. <https://doi.org/10.1016/j.addr.2004.01.001>.
- 16 Bhole, R.P., Chikhale, R.V., Wavhale, R.D., Asmary, F.A., Almutairi, T.M., Alhajri, H.M., & Bonde, C.G. (2021). Design, synthesis and evaluation of novel enzalutamide analogues as potential anticancer agents. *Heliyon*, 7(3), e06227. <https://doi.org/10.1016/j.heliyon.2021.e06227>
- 17 Lu, Y., & Low, P.S. (2002). Folate-mediated delivery of macromolecular anticancer therapeutic agents. *Advanced drug delivery reviews*, 54(5), 675–693. [https://doi.org/10.1016/s0169-409x\(02\)00042-x](https://doi.org/10.1016/s0169-409x(02)00042-x).
- 18 Parker, N., Turk, M.J., Westrick, E., Lewis, J.D., Low, P.S., & Leamon, C.P. (2005). Folate receptor expression in carcinomas and normal tissues determined by a quantitative radioligand binding assay. *Analytical biochemistry*, 338(2), 284–293. <https://doi.org/10.1016/j.ab.2004.12.026>.
- 19 Salazar, M.D.A., & Ratnam, M. (2007). The folate receptor: what does it promise in tissue-targeted therapeutics? *Cancer and Metastasis Reviews*, 26(1), 141–152. <https://doi.org/10.1007/s10555-007-9048-0>.
- 20 Tochowicz, A., Dalziel, S., Eidam, O., O'Connell III, J.D., Griner, S., Finer-Moore, J.S., & Stroud, R.M. (2013). Development and Binding Mode Assessment of N-[4-[2-Propyn-1-yl] [(6 S)-4, 6, 7, 8-tetrahydro-2-(hydroxymethyl)-4-oxo-3 H-cyclopenta [g] quinazolin-6-yl] amino] benzoyl]-l- γ -glutamyl-d-glutamic Acid (BGC 945), a Novel Thymidylate Synthase Inhibitor That Targets Tumor Cells. *Journal of medicinal chemistry*, 56(13), 5446–5455. <https://doi.org/10.1021/jm400490e>.
- 21 Bhole R., Bonde .C, Kadam P., & Wavhale R. (2021). A Comprehensive Review on Photodynamic Therapy (PDT) and Photothermal Therapy (PTT) for Cancer Treatment. *Turkish Journal of Oncology*, 36(1). <https://doi.org/10.5505/tjo.2020.2400>.
- 22 Hou, Z., & Matherly, L.H. (2014). Biology of the major facilitative folate transporters SLC19A1 and SLC46A1. *Current topics in membranes*, 73, 175–204. <https://doi.org/10.1016/b9780-12-800223-0.00004-9>.
- 23 Weitman, S.D., Lark, R.H., Coney, L.R., Fort, D.W., Frasca, V., Zurawski, V.R., & Kamen, B.A. (1992). Distribution of the folate receptor GP38 in normal and malignant cell lines and tissues. *Cancer research*, 52(12), 3396–3401.
- 24 Bhole, R.P., Jadhav, S., Zambare, Y.B., Chikhale, R.V., & Bonde, C.G. (2020). Vitamin-anticancer drug conjugates: a new era for cancer therapy. *Journal of the Faculty of Pharmacy of Istanbul University*, 50(3), 312–323. <https://doi.org/10.26650/istanbulpharm.2019.0078>.
- 25 Ross, J.F., Chaudhuri, P.K., & Ratnam, M. (1994). Differential regulation of folate receptor isoforms in normal and malignant tissues in vivo and in established cell lines. *Physiologic and clinical implications. Cancer*, 73(9), 2432–2443.
- 26 Toffoli, G., Cernigoi, C., Russo, A., Gallo, A., Bagnoli, M., & Boiocchi, M. (1997). Overexpression of folate binding protein in ovarian cancers. *International journal of cancer*, 74(2), 193–198.
- 27 Bhole, R.P., & Bhusari, K.P. (2011). Synthesis and antitumor activity of (4-hydroxyphenyl) [5-substituted alkyl/aryl]-2-thioxo-1, 3, 4-thiadiazol-3-yl] methanone and [(3, 4-disubstituted)-1, 3-thiazol-2-ylidene]-4-hydroxybenzohydrazide. *Medicinal Chemistry Research*, 20(6), 695–704. <https://doi.org/10.1007/s00044-010-9371-9>.
- 28 Zhao, R., Min, S.H., Wang, Y., Campanella, E., Low, P.S., & Goldman, I.D. (2009). A role for the proton-coupled folate transporter (PCFT-SLC46A1) in folate receptor-mediated endocytosis. *J. Biol. Chem.* 284, 4267–4274. <https://doi.org/10.1074/jbc.m807665200>.
- 29
- Nair K.L., Jagadeeshan, S., Nair, S.A., & Kumar, G.V. (2013). Folic acid conjugated δ -valerolactone-poly (ethylene glycol) based triblock copolymer as a promising carrier for targeted doxorubicin delivery. *PLoS one*, 8(8), e70697. <https://doi.org/10.1371/journal.pone.0070697>.
- 31 Trindade, A.F., Frade, R.F., Maçôas, E.M., Graça, C., Rodrigues, C.A., Martinho, J.M., & Afonso, C.A. (2014). “Click and go”: simple and fast folic acid conjugation. *Organic & biomolecular chemistry*, 12(20), 3181–3190. <https://doi.org/10.1039/c4ob00150h>.
- 32 Cheung, A., Bax, H.J., Josephs, D.H., Ilieva, K.M., Pellizzari, G., Opzoomer, J., ... & Karagiannis, S.N. (2016). Targeting folate receptor alpha for cancer treatment. *Oncotarget*, 7(32), 52553. <https://doi.org/10.18632/oncotarget.9651>.

- 33 Bhole, R.P., Jadhav, S., Chikhale, R., Shinde, Y., & Bonde, C.G. (2021) Synthesis and evaluation of vitamin-drug conjugate for its anticancer activity. *Bulletin of the University of Karaganda – Chemistry*, 103(3), 21–26. <https://doi.org/10.31489/2021Ch3/21-26>
- 34 Bhole, R.P., Yogita, S., Bonde, C.G., & Wavhale, R.D. (2021). Vitamin Drug conjugate: a systematic review of pharmacological potential. *Bulletin of the University of Karaganda – Chemistry*, (1), 27–52. <https://doi.org/10.31489/2021Ch1/27-52>
- 35 Marverti, G., Marraccini, C., Martello, A., D'Arca, D., Pacifico, S., Guerrini, R., ... & Costi, M.P. (2021). Folic Acid–Peptide Conjugates Combine Selective Cancer Cell Internalization with Thymidylate Synthase Dimer Interface Targeting. *Journal of medicinal chemistry*, 64(6), 3204–3221. <https://dx.doi.org/10.1021/acs.jmedchem.0c02107>

Р.П. Бhole, М. Свами, Р. Вавхейл, К.Г. Бонде, Р. Чихэйл

Қатерлісікке қарсы белсенділікті арттыру үшін потенциалды витамин-дәрілік конъюгаттың дизайны

5-Фторурацил, қатерлісіктің әртүрлі сатыларын емдеуде кеңінен қолданылатын біріншілік молекула, белсенді емес түрге, атап айтқанда 5,6-дигидро-5-ФУ-ға дейін тез метаболизденеді және химиотерапия кезінде әртүрлі мутациялық өзгерістерге ұшырайды. Фолий қышқылы конъюгатын алу үшін карбодимидті катализатор қолданылған. Фолий қышқылының рецепторлары ісік тіндерінде шамадан тыс экспрессияланғандықтан, бұл 5-ФУ биожетімділігін арттырады. Бұл жұмыс ісікке қарсы белсенділікті күшейтетін жаңа витамин-дәрілік конъюгатты алу мен синтездеу болып табылады. 5-Фторурацил сүт безі, тоқ ішек, асқазан және тері ісігі тіндеріне күшті әсер етеді. Фолий қышқылы рақ клеткаларының FR α рецепторларына селективті әсер етуге көмектеседі. Конъюгацияны растау үшін 5-FUFA қосылысына спектрлік сипаттама жасалады. Молекулалық динамикалық модельдеу Schrodinger пакетінде зерттелді және CRPPTRAJ бағдарламалық құралында молекулалық траекториямен расталды. Конъюгат одан әрі молекулалық модельдеу әдістерімен зерттелді және конъюгаттың қондыру индексі 5-FU-пен салыстырғанда жоғары байланысу шамасын көрсетті, атап айтқанда -8,0 ккал/моль шамасына тең болды. Препараттың рецептормен өзара әрекеттесуі Schrodinger пакетіндегі молекулалық динамикалық модельдеу және 100 нс молекулалық траекторияға арналған CRPPTRAJ бағдарламалық құралының көмегімен дәлелденді. Молекулалық динамикалық модельдеу нәтижелері 25 нс ішінде 2-ден 4 Å-ге дейін аздаған конформациялық өзгерістер болатынын, ал жалпы жағдайда тұрақты болатынын көрсетті.

Кілт сөздер: 5-фторурацил, фолий қышқылы, синтетикалық конъюгат, молекулалық қондыру, молекулалық динамика, дәрілік конструкция, химиотерапевтік агент, адамның тимидилатсинтазасы.

Р.П. Бhole, М. Свами, Р. Вавхейл, К.Г. Бонде, Р. Чихэйл

Дизайн потенциального конъюгата «витамин–лекарство» для усиления противораковой активности

5-Фторурацил, первичная молекула, широко используемая при лечении различных стадий рака, быстро метаболизируется до неактивной формы, а именно до 5,6-дигидро-5-ФУ, и подвергается различным мутационным изменениям в ходе химиотерапии. Авторами статьи использован карбодимидный катализатор для образования конъюгата с фолиевой кислотой. Поскольку рецепторы фолиевой кислоты сверхэкспрессированы в раковых тканях, это увеличивает биодоступность 5-ФУ. Данная работа представляет собой разработку и синтез нового конъюгата «витамин–лекарство», потенциально усиливающего противораковую активность. 5-Фторурацил обладает мощным действием на ткани рака молочной железы, толстой кишки, желудка и кожи. Фолиевая кислота помогает избирательно воздействовать на рецепторы FR α раковых клеток. 5-FUFA подвергали спектральной характеристике для подтверждения успешной конъюгации. Молекулярно-динамическое моделирование было изучено в пакете Schrodinger и подтверждено молекулярной траекторией в программном обеспечении CRPPTRAJ. Конъюгат был дополнительно изучен с помощью исследований молекулярного моделирования, и показатель стыковки конъюгата представлял собой более высокий показатель связывания, чем у 5-ФУ, а именно 8,0 ккал/моль. Взаимодействие лекарственного препарата с рецептором было дополнительно подтверждено с помощью молекулярно-динамического моделирования в пакете Schrodinger и программного обеспечения CRPPTRAJ для молекулярной траектории в течение 100 нс. Было обнаружено, что результаты молекулярно-динамического моделирования стабильны с небольшим конформационным изменением в течение 25 нс от 2 до 4 Å.

Ключевые слова: 5-Фторурацил, фолиевая кислота, синтетический конъюгат, молекулярный докинг, молекулярная динамика, дизайн препарата, химиотерапевтический агент, тимидилатсинтаза человека.

Information about authors

Bhole, Ritesh Prakash — PhD, Associate Professor, Dr. D.Y. Patil Institute of Pharmaceutical Sciences and Research, Sant Tukaram Nagar, Pimpri, Pune-411018, India; e-mail ritesh.bhole@dypvp.edu.in; <https://orcid.org/0000-0003-4088-7470>;

Bonde, Chandrakant Ghansham — PhD, Professor, SPTM, NMIMS, School of Pharmacy, Shirpur, Dist: Dhule, India. e-mail: chandrakant.bonde@nmims.edu; <https://orcid.org/0000-0001-5712-1119>;

Swamy, Mahadevan Raju — M. Pharm, Research Scholar, Dr. D.Y. Patil Institute of Pharmaceutical Sciences and Research, Sant Tukaram Nagar, Pimpri, Pune-411018, India; e-mail: mahadevan.swamy11@gmail.com; <https://orcid.org/0000-0003-1399-1176>;

Wavhale, Ravindra — PhD, Assistant Professor, Dr. D.Y. Patil Institute of Pharmaceutical Sciences and Research, Sant Tukaram Nagar, Pimpri, Pune-411018; India; e-mail: ravindra.wavhale@dypvp.edu.in; <https://orcid.org/0000-0003-1614-9742>;

Chikhale, Rupesh — PhD, Research Fellow, UCL school of Pharmacy, London, UK; e-mail: R.Chikhale@ucl.ac.in, <https://orcid.org/0000-0001-5622-3981>

M.Zh. Burkeyev¹, M.S. Zhunissova^{1*}, J. Plocek²,
A.T. Kazhmuratova¹, T.S. Zhumagalieva¹

¹Karagandy University of the name of academician E.A. Buketov, Kazakhstan;

²Institute of Inorganic Chemistry of the Czech Academy of Sciences, Husinec-Rez, Czech Republic

(*Corresponding author's e-mail: meruert_zhunissova@mail.ru)

Properties of cross-linked copolymers of polypropylene glycol maleate with acrylic acid obtained at various concentrations of the RAFT agent

The initial polypropylene glycol maleate has been obtained by the polycondensation reaction of maleic anhydride and propylene glycol. The molecular weight of the synthesized unsaturated polyester resin has been determined. The copolymers under study have been obtained by radical copolymerization of p-PGM. The possibility of synthesizing new polymers based on p-PGM with acrylic acid in the presence of a RAFT agent has been shown. The effect of RAFT agent concentration on the network density and product yield has been studied. It has been found that the yield of the cross-linked polymer decreases, its swelling capacity increases, and the yield of the linear polymer increases with an increase in the RAFT agent concentration. The effect of organic solvents, pH, and low-molecular-weight salts on the swelling degree of the synthesized copolymers has been investigated. The research results demonstrate that the susceptibility of polymer hydrogels to organic solvents and changes in pH, and low molecular weight salts, is affected by the amount of RAFT agent in the polymer. The synthesized objects have been characterized by infrared spectroscopy. Scanning electron microscopy has estimated the polymer surface morphology and pore sizes.

Keywords: unsaturated polyester resin, polypropylene glycol maleate, RAFT-polymerization, swelling, collapse.

Introduction

Currently, the search for materials with controllable properties and sensitivity to environmental changes is one of the key issues in macromolecular compound chemistry [1, 2]. Such polymers' ability feature is to sorb a huge amount of water and bind low molecular weight substances dissolved in it [3, 4]. Unsaturated polyesters are among promising co-monomers for synthesizing these materials [5].

Unsaturated polyester resins (UPRs) are increasingly being used. They occupy leading positions among composite materials due to the ease of production the availability of raw materials [6]. Prior to our research, a literature-patent search showed [7] the absence of data on radical copolymerization of UPRs with ionic monomers, which opens prospects for the synthesis of new "smart-systems" [8].

As practice shows, when UPRs interact with vinyl monomers, the reaction is not controllable and leads to an insoluble product with a chaotic network arrangement in space. The solution to this problem becomes possible due to the creation of a general concept of macromolecules controlled synthesis [9]. "Pseudo-living" radical polymerization is of considerable interest from this point of view. This assists in replacing uncontrolled chain termination reactions with reversible reactions by adding RAFT agents, allowing regulation of the quadratic chain termination [10].

Using radical polymerization reactions under such conditions makes it possible to design a macromolecule as part of a polymer matrix to obtain (co-)polymers with a given molecular weight, block, and graft copolymers with a controlled length, predictable properties [11].

In this regard, an attempt was made to change the copolymerization reaction of polypropylene glycol maleate (p-PGM) with acrylic acid (AA) in the presence of a RAFT agent at various concentrations. The sorption properties of new polymers were analyzed as a function of changes in the pH of the medium, the concentration of low molecular weight salts, and the choice of organic solvents.

Experimental

The following reagents were used: Propylene glycol, maleic anhydride, acrylic acid, benzoyl peroxide, zinc chloride, 1,4-dioxane, RAFT-agent (2-Cyano-2-propyl dodecyl trithiocarbonate/CPDT) from Sigma-Aldrich.

According to the standard procedure [12], initial p-PGM was obtained by the polycondensation reaction of maleic anhydride and propylene glycol at 423–453 K. The molecular mass of the synthesized p-PGM was determined indirectly by the amount of released water and the content of acid and hydroxyl numbers by the titrimetric method. The p-PGM molecular mass obtained by these methods averaged 2442 a.m.u.

Radical copolymerization of p-PGM with AA was carried out under the following conditions: 50:50 mol% co-monomer ratio, 333 K. Dioxane (1:1 weight ratio) was used as a solvent, and benzoyl peroxide was used as an initiator. After purging with an inert gas for 30 minutes, the radical copolymerization was carried out for 52 hours. The resulting copolymers were washed with dioxane and dried to constant weight in a vacuum drying oven.

Controlled polymerization was carried out similarly to the synthesis of p-PGM-AA, but with the addition of the calculated amount of the RAFT agent (2-Cyano-2-propyl dodecyl trithiocarbonate CPDT) in dioxane solution to initiate the “fluid” polymerization process. The reaction mixtures were poured into ampoules, degassed in a vacuum unit, and sealed. Then the ampoules were placed in a thermostat and incubated for 52 hours at a temperature of 70 °C. The ampoules were cooled at the end of the polymerization and opened. The resulting reaction products were separated quantitatively, and then the cross-linked copolymers filtered from the mother liquor were dried in a vacuum drying oven until a constant weight was established.

The composition of the synthesized copolymers was determined on a Shimadzu chromatograph (Japan) using HPLC by the number of unreacted monomers.

IR spectra of these samples were recorded in KBr pellets on a FSM 1201 spectrometer. Samples for IR spectroscopy were prepared by long-term grinding of 2 ± 0.1 mg of a sample with 200 ± 0.1 mg of dry KBr. The samples were pressed at 200 atm. The IR spectra of the obtained materials were recorded on a device with the best possible resolution of 1 cm^{-1} to measure the relative transmittance. The number of re-scans was increased to a maximum of 50.

The surface morphology of the samples was investigated on a scanning electron microscope MIRA3 (TESCAN, Czech Republic).

Equilibrium swelling of the obtained copolymers was achieved within 1-2 days. The swelling degree α (%) of the polymers was measured gravimetrically. The calculation of α (%) was performed as the ratio of the absolute mass of the swollen hydrogel at the point of equilibrium swelling to its initial mass in the dry state.

Aqueous solutions of low molecular weight salts (LMWS) CuSO_4 , FeCl_3 , $\text{Pb}(\text{NO}_3)_2$ were prepared in calculated amounts from 0.001 to 1 volume fraction to determine the swelling of copolymers in solutions. Buffer solutions of working ethanol pH of the third category ST-pH-04.3 were used to determine the swelling ability of the synthesized copolymers with a change in the pH of the medium.

The following solvent mixtures were chosen as model systems: water – ethanol, water – DMF, water – DMSO, the content of which varied from 0 to 1 volume fractions.

Results and Discussion

As already noted [8, 9], refractory spatially cross-linked copolymers are formed during copolymerization of unsaturated polyester resins at all ratios of the monomer mixture. In this regard, it seemed interesting to follow the change during the copolymerization reaction to the addition of a RAFT agent. Data on the synthesis of copolymers, as well as with the addition of CPDT various concentrations, are shown in Table 1.

Table 1

Influence of the RAFT agent concentration on the mechanism of copolymerization of p-PGM with AA in dioxane solution, $T = 343 \text{ K}$, $[I] = 8 \cdot 10^{-3} \text{ mol/L}$, $[M_1+M_2]=49.9:50.1 \text{ mol.}\%$, the solvent ratio $[M_1+M_2]=1:1$ by weight

| $[\text{RAFT}] \cdot 10^3, \text{ mol/L}$ | Cross-linked polymer yield, % | Swelling of the cross-linked polymer, α , % | Linear polymer yield, % |
|---|-------------------------------|--|-------------------------|
| – | 96.93 ± 1.78 | 187.12 ± 6.56 | – |
| 10.02 | 94.15 ± 6.24 | 201.16 ± 3.70 | 3.87 ± 1.59 |
| 30.01 | 78.21 ± 6.62 | 267.21 ± 4.96 | 13.52 ± 1.65 |
| 50.01 | 49.42 ± 2.72 | 314.17 ± 4.92 | 47.45 ± 2.51 |
| 80.03 | 4.96 ± 3.24 | 385.11 ± 6.44 | 92.26 ± 6.11 |

Data in Table 1 demonstrate that the copolymerization reaction proceeds in two directions with the formation of spatially cross-linked and linear copolymers. Each obtained product swells or dissolves in polar solvents, respectively, while antibaticity is observed in the product yield. It should be noted that there is an increase in the swelling degree of the copolymers obtained at high concentrations of RAFT agent. This phenomenon can be explained by a reduction in the network density due to a decrease in the reaction of bimolecular chain termination with the addition of the chain transfer agent.

IR spectral analysis of the copolymers (Fig. 1a) shows absorption band in the region of 775 cm^{-1} caused by pendulum vibrations of $-\text{CH}_2-$ bonds, as well as an absorption band at 1153 cm^{-1} , confirming the presence of $-\text{C}-\text{O}-\text{C}-$ ester bonds. An intense peak at 1300 cm^{-1} in the spectrum indicates the presence of the $-\text{C}=\text{C}-$ polyester group. Absorption bands at 1736 cm^{-1} and 2986 cm^{-1} are characteristic of the presence of $-\text{C}=\text{O}$ and symmetrically located $-\text{CH}$ bonds in the CH_2 and COOH groups, respectively. It should also be noted the presence of signals at 2866 cm^{-1} indicates the presence of the $=\text{C}-\text{H}$ group of the aromatic hydrocarbon.

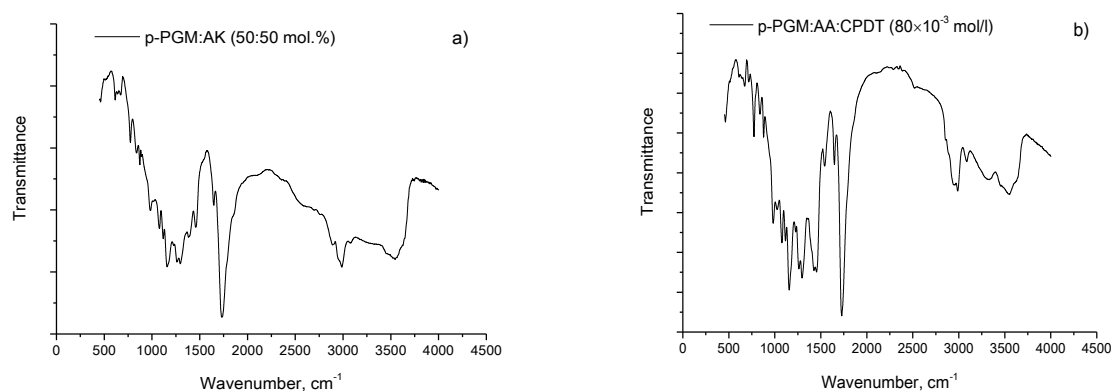


Figure 1. IR spectra of copolymers of the p-PGM-AA (a); p-PGM-AA-[CPDT] = $80 \cdot 10^{-3}$ mol/L (b)

Furthermore, the obtained IR spectra (Fig. 1b) of the p-PGM-AA-CPDT copolymers have been analyzed. There is an absorption band in the region of 3545 cm^{-1} , which is characteristic of the $\text{O}-\text{H}$ bonds. There is an absorption band in the region of 3082 cm^{-1} , which is responsible for the stretching vibration of the $=\text{C}-\text{H}$ bond of the aromatic compound, and a weak stretching vibrations band of the $\text{C}-\text{H}$ groups of the aliphatic hydrocarbon in the region of 2997 cm^{-1} . In addition, there is the manifestation of symmetrical vibrations of CH_3 groups in the region of 1381 cm^{-1} and scissor bending vibrations of CH_2 groups in the region of 1466 cm^{-1} and 1454 cm^{-1} , which indicates the presence of branched hydrocarbons. In the spectra of copolymers with an increased RAFT agent concentration, signals are observed at 2244 cm^{-1} , which indicates the presence of CN . The data was exported in the form of tables for processing in third-party software.

The spectra were inverted by subtracting the relative transmittance from unity. The positions of the absorption maxima were detected by the program, after which the amplitudes of the maxima were refined by approximating the Gaussian contours (Fig. 2 a, b).

The polymer's surface morphology was determined by scanning electron microscopy. As shown in Figure 3, the surface of the p-PGM-AA polymer particles (a) has cleavage points characteristic of hard, brittle materials.

The predominance of a layered, loose structure and the appearance of pores are seen in the image for samples containing p-PGM-AA-CPDT (b). The chipping of particles is more plastic in comparison with the p-PGM-AA polymer. The results of electron microscopy confirm that an increase in the CPDT content in the composition of the polymer-monomer mixture affects the distribution and size of the formed pores, which causes a high swelling degree.

The presence of functional units in the hydrogel structure, which is capable of ionization, increases their sensitivity to various changes in the parameters of the external environment.

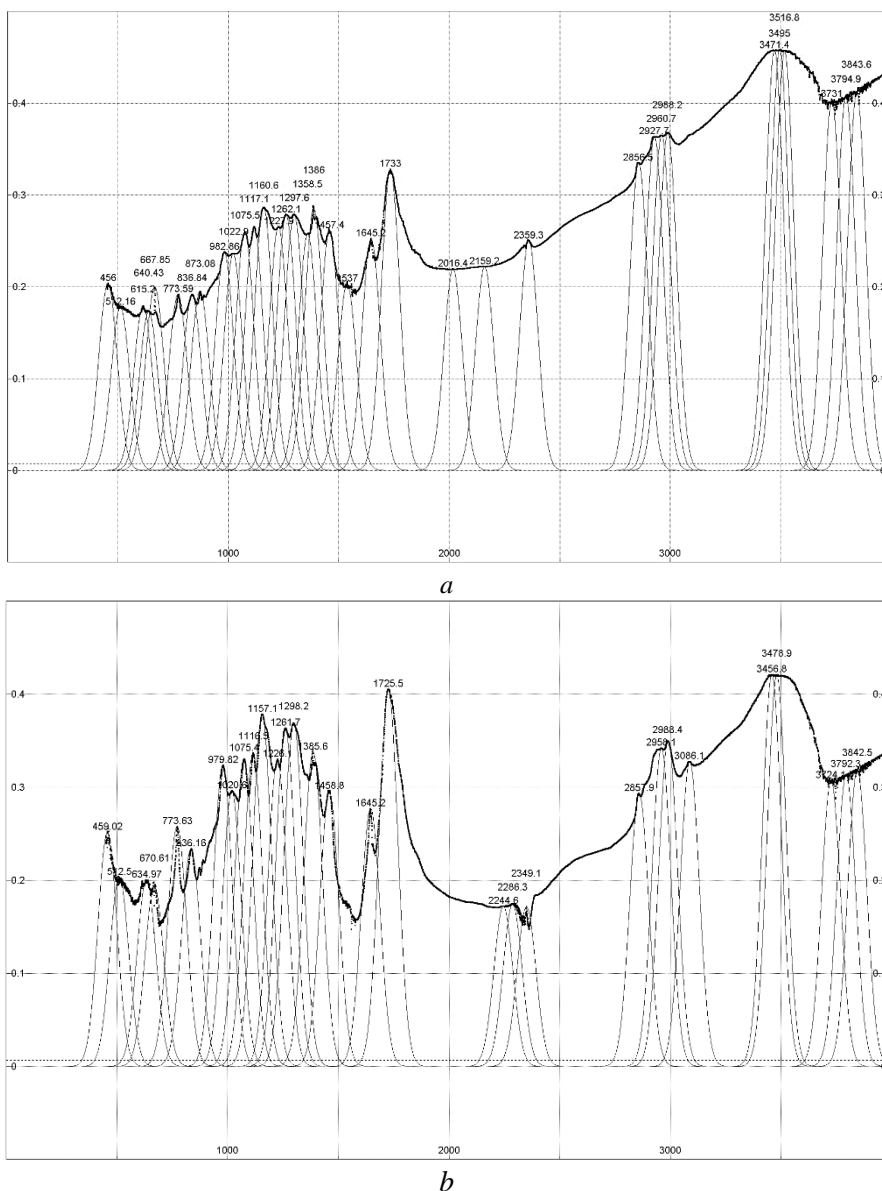


Figure 2. IR spectra of copolymers of p-PGM-AA (a); p-PGM-AA-[CPDT] = $80 \cdot 10^{-3}$ mol/L (b)

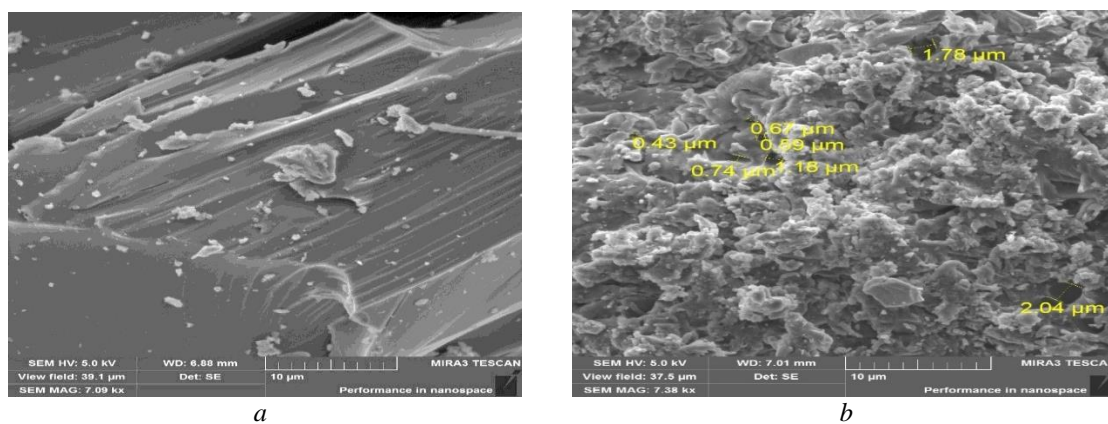
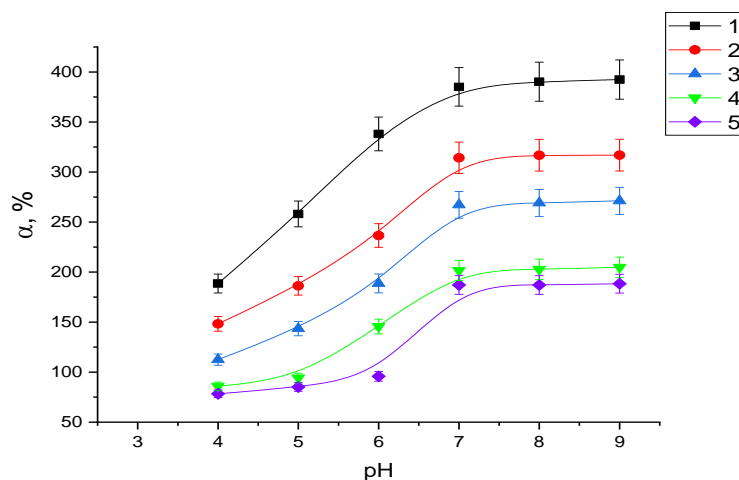


Figure 3. Surface morphology of the polymer p-PGM-AA (a); surface morphology of the polymer p-PGM-AA-[CPDT]= $80 \cdot 10^{-3}$ mol/L (b)

The pH of the medium is one of the external environment parameters that can significantly affect the polymer gels properties. In this section, the swelling ability of the synthesized copolymers based on p-PGM:AA and p-PGM-AA-CPDT was evaluated with a change in the pH of the medium (Fig. 4).



1 — p-PGM-AA-[CPDT] = $80 \cdot 10^{-3}$ mol/L; 2 — p-PGM-AA-[CPDT] = $50 \cdot 10^{-3}$ mol/L;
3 — p-PGM-AA-[CPDT] = $30 \cdot 10^{-3}$ mol/L; 4 — p-PGM-AA-[CPDT] = $10 \cdot 10^{-3}$ mol/L; 5 — p-PGM-AA

Figure 4. Effect of the medium pH on the volume of hydrogels based on p-PGM-AA and p-PGM-AA-CPDT copolymers

In Figure 4, the shape of the swelling curves of p-PGM-AA copolymer samples is similar to the networks containing a chain transfer agent. However, lower sensitivity to changes in the pH of the medium appears with an increase in the RAFT agent content in the composition of the initial polymer-monomer mixture at the same content of p-PGM-AA. The network density fundamentally affects the pH dependence of the swelling of p-PGM-AA and p-PGM-AA-CPDT.

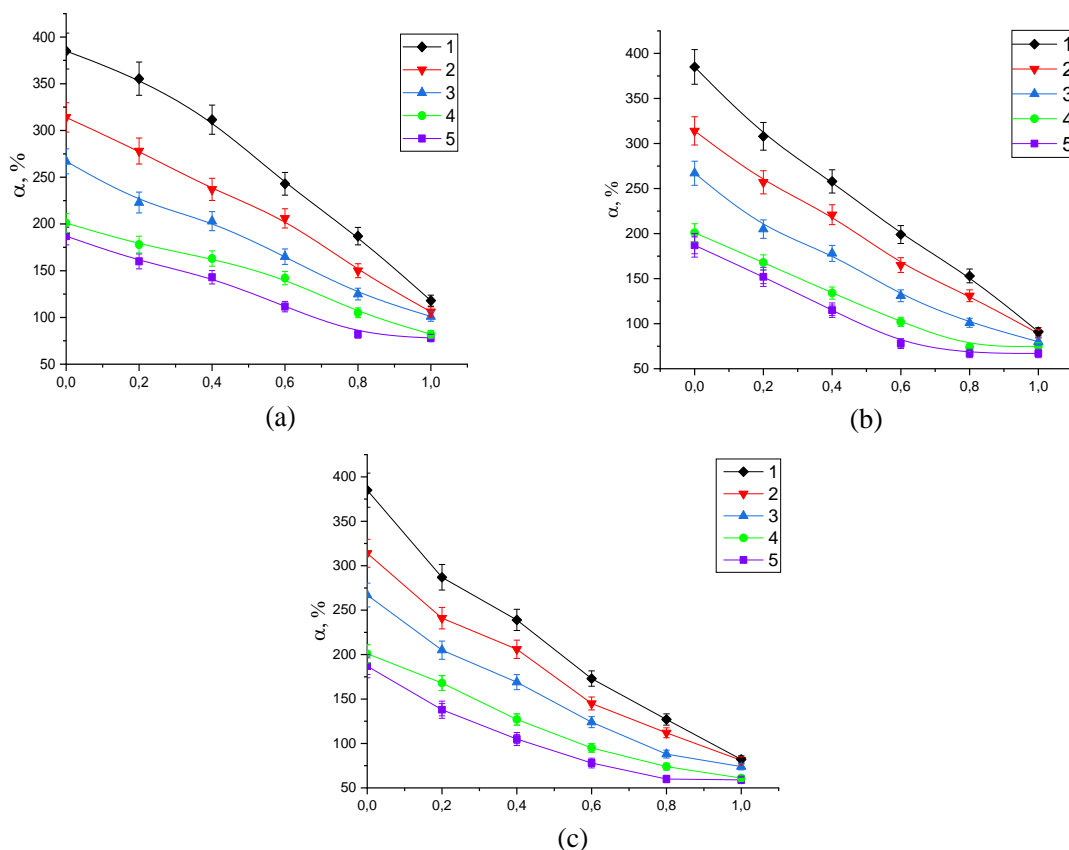
The chain of the non-dissociated p-PGM-AA macromolecule tends to curl up at low pH values compared to p-PGM-AA-CPDT. As the pH rises, the dissociation of ionogenic groups ($-\text{COOH} \dots \text{HOOC}-$) of the p-PGM-AA macromolecule increases, which contributes to the straightening of the folded chain as an effect of mutual repulsion, resulting in smooth polymer swelling. A further shift of the solution pH to an alkaline region has no significant effect on the polymer macromolecules conformation.

The swelling degree in the acidic region does not change noticeably when the RAFT agent concentration is up to $30 \cdot 10^{-3}$ mol/L. However, a more significant change in the swelling degree depends on the pH when the RAFT agent content is over $30 \cdot 10^{-3}$ mol/L.

Thus, the data presented shows that hydrogels based on copolymers p-PGM-AA and p-PGM-AA-CPDT behave as typical polyelectrolytes containing ionized acid groups covalently attached the main chain. Furthermore, we studied the effect of the presence of solvents binary mixtures (DMSO, DMF, and ethanol) on the sorption properties of the synthesized polymers (Figure 5).

Figure 5 demonstrates p-PGM-AA and p-PGM-AA-CPDT-based gels in the fraction range of 0.2 to 0.8 vol. in the water — DMSO mixture are gradually compressed. This may be because carboxyl groups' dissociation degree, providing electrostatic repulsion of the subchains from each other, decreases, and a collapse occurs. When DMF and ethanol are added to the system, the volume-phase transition occurs at lower values of the added solvent, which is associated with a lower dielectric constant of the last one.

The smallest swelling degree of the p-PGM-AA and p-PGM-AA-CPDT copolymers is observed in the case of ethanol as the least polar solvent in the DMSO>DMF>ethanol series. It should be noted that the copolymers swelling degree, depending on the solvent concentration, reduces with a decrease in the RAFT agent concentration. It follows from the above that practically all hydrogels are characterized by a high degree of sensitivity to the quality of the solvents used and behave in the same manner.



1 — p-PGM-AA-[CPDT] = $80 \cdot 10^{-3}$ mol/L; 2 — p-PGM-AA-[CPDT] = $50 \cdot 10^{-3}$ mol/L;
 3 — p-PGM-AA-[CPDT] = $30 \cdot 10^{-3}$ mol/L; 4 — p-PGM-AA-[CPDT] = $10 \cdot 10^{-3}$ mol/L; 5 — p-PGM-AA

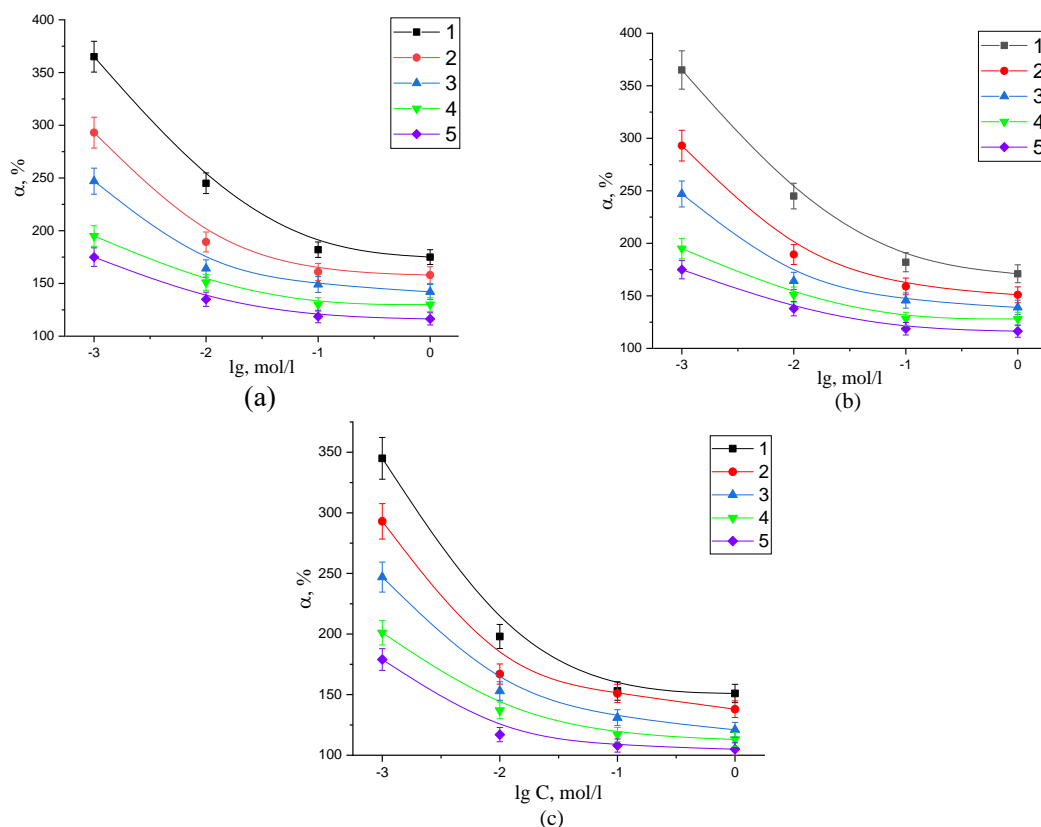
Figure 5. Effect of the volume fraction of DMSO (a), DMF (b), ethanol (c) on the hydrogels swelling based on p-PGM-AA and p-PGM-AA-CPDT copolymers

The study of the metal ions interaction processes with cross-linked polymers is of interest to researchers in this field, and many works of both foreign and domestic scientists are devoted to them [13]. According to the literature [14–17], polymer networks can both swell and undergo collapse in solutions of low molecular weight salts (LMWS). Previously, we carried out experiments to determine the influence of external factors on the behavior of hydrogels in inorganic salts solutions [18, 19]. However, the obtained results do not allow for creating a unified theory of the interaction of low molecular weight compounds with polymer macromolecules. In this regard, in the continuation of research in this direction, it seemed interesting to study the behavior of RAFT polymers based on p-PGM-AA in solutions with an increase in the concentration of mono-, bi- and trivalent salts (Figure 6).

Figure 6 (a, b, c) shows the swelling behavior of p-PGM-AA and p-PGM-AA-CPDT copolymers depending on the concentration of added low molecular weight electrolytes, namely $\text{Pb}(\text{NO}_3)_2$, CuSO_4 , and FeCl_3 .

The graphical dependence shows that an increase in the salt concentration to a certain value (about 10^{-3} mol/L) does not have a significant effect on the size of hydrogel. A further increase in the ionic strength has practically no effect on the α value. It can be seen that with an increase in the salt concentration (from 10^{-2} mol/L), the ions osmotic pressure in the solution increases, resulting in the contraction of the polyelectrolyte hydrogel.

The contraction of hydrogels in LMWS solutions during the alteration from trivalent to bivalent is observed at high values of the salt concentration, respectively. Thus, an increase in the LMWS content in the network leads to the contraction of the copolymer. This may be due to several reasons: first, an increase in the concentration of salts in the solution worsens the thermodynamic quality of water, and secondly, the polyelectrolyte effect may be suppressed by the addition of low molecular weight substrates in the surrounding solution.



1 — p-PGM-AA-[CPDT] = $80 \cdot 10^{-3}$ mol/L; 2 — p-PGM-AA-[CPDT] = $50 \cdot 10^{-3}$ mol/L;
 3 — p-PGM-AA-[CPDT] = $30 \cdot 10^{-3}$ mol/L; 4 — p-PGM-AA-[CPDT] = $10 \cdot 10^{-3}$ mol/L; 5 — p-PGM-AA

Figure 6. Effect of the volume fraction of CuSO_4 (a), $\text{Pb}(\text{NO}_3)_2$ (b), FeCl_3 (c) on the swelling of hydrogels based on p-PGM-AA and p-PGM-AA-CPDT copolymers

Conclusions

For the first time, copolymers based on p-PGM-AA with the addition of a RAFT agent (CPDT) in various concentrations were obtained by the method of controlled radical polymerization.

The study of the copolymerization reactions of unsaturated polyester resin, namely polypropylene glycol maleate with acrylic acid, showed that the addition of small amounts of RAFT agents significantly affected not only the network density but also the product yield.

Based on the results of scanning electron microscopy, it was found that copolymer samples with the addition of a RAFT agent have a loose, porous surface with average pore size in the range from 0.39 nm to 2.04 nm.

The gravimetric method for determining the swelling degree of the synthesized hydrogels proves that an increase in the CPDT content in the initial polymer-monomer mixture at the same p-PGM-AA content makes it possible to obtain a product capable of absorbing a significantly larger volume of water.

The effect of external factors (pH of the medium, quality of the organic solvent, and the solution ionic strength) on the swelling ability of copolymers without the addition of a chain transfer agent and samples containing various concentrations of the RAFT agent has been established.

Thus, understanding the dependence of the density and the network range on the RAFT-agent concentration makes it possible to “regulate” the structure of the copolymers, thereby avoiding chaos in the structure. Besides, varying the concentration of the RAFT agent will allow purposefully synthesizing copolymers with desired properties based on experimental and mathematical methods, as well as to control the cross-linking degree and the swelling degree of polymers.

Considering the fact that the concentration of the RAFT agent contributes to a decrease in the polymer network density, it is possible to obtain new “smart” systems with desired properties that can change the swelling capacity under the influence of various external factors.

References

- 1 Mesquita R.G. de A. Polyester Composites Reinforced with Corona-Treated Fibers from Pine, Eucalyptus and Sugarcane Bagasse / R. G. de A. Mesquita., A. A. da S. César, R.F. Mendes, L.M. Mendes, J.M. Marconcini, G. Glenn, G. H.D. Tonoli // *Journal of Polymers and the Environment*, 2016. — Vol. 25, No. 3. — P. 800–811. <https://doi.org/10.1007/s10924-016-0864-6>
- 2 Kang M.K. Swell-induced surface instability of confined hydrogel layers on substrates / M.K. Kang, R. Huang // *Journal of the Mechanics and Physics of Solids*, 2010. — Vol. 58, No. 10. — P. 1582–1598. <https://doi.org/10.1016/j.jmps.2010.07.008>
- 3 Kandelbauer A. Unsaturated Polyesters and Vinyl Esters [Electronic resource] / A. Kandelbauer, G. Tondi, O.C. Zaske, S.H. Goodman // *Handbook of Thermoset Plastics*, 2014. — P. 111–172. <https://doi.org/10.1016/b978-1-4557-3107-7.00006-3>
- 4 He S. Injectable biodegradable polymer composites based on poly(propylene fumarate) crosslinked with poly(ethylene glycol)-dimethacrylate / S. He, M.J. Yaszemski, A.W. Yasko, P.S. Engel, A.G. Mikos // *Biomaterials*, 2000. — Vol. 21, No. 23. — P. 2389–2394. [https://doi.org/10.1016/s0142-9612\(00\)00106-x](https://doi.org/10.1016/s0142-9612(00)00106-x)
- 5 Павлюченко В.Н. Композиционные полимерные гидрогели / В.Н. Павлюченко, С.С. Иванчев // *Высокомолекулярные соединения*. — 2009. — Т. 51, № 7. — P. 1075–1095.
- 6 Sadler J.M. Unsaturated polyester resins for thermoset applications using renewable isosorbide as a component for property improvement / J.M. Sadler, F.R. Toulan, G.R. Palmese, J. La Scala // *J. Appl. Polym. Sci.*, 2015. — Vol. 132, Iss. 30. — P. 1–11. <https://doi.org/10.1002/app.42315>
- 7 Буркеев М.Ж. Синтез и исследование свойств сополимеров на основе полипропиленгликольmaleинатфталата с акриловой кислотой / М.Ж. Буркеев, А.К. Ковалева, Е.М. Тажбаев, Э.Ж. Жакупбекова, А.А. Копбосынова // *Вестн. Караганд. ун-та. Сер. Химия*. — 2015. — № 1 (77). — P. 31–35. URI: <http://rep.ksu.kz:80/handle/data/4012>
- 8 Burkeev M.Zh. Nanocatalytic systems based on poly(ethylene glycol maleate)-acrylamide copolymers / M.Zh. Burkeev, A.K. Kovaleva, E.M. Tazhbaev, G.K. Burkeeva, S.Zh. Davrenbekov, A.A. Kopbosynovaa, A.V. Omashevaa, M.M. Mataev // *Russian Journal of Applied Chemistry*, 2015. — Vol. 88, No. 2. — P. 314–319. <https://doi.org/10.1134/s107042721502020>
- 9 Burkeev M.Zh. Effect of external factors on the swelling of hydrogels based on poly(ethylene glycol) maleate with some vinyl monomers / M.Zh. Burkeev, A.K. Magzumovaa, E.M. Tazhbaeva, G.K. Burkeevaa, A.K. Kovalevaa, T.O. Khamitovaa, M.M. Mataev // *Russian Journal of Applied Chemistry*, 2013. — Vol. 86, No. 1. — P. 63–68. <https://doi.org/10.1134/s1070427213010114>
- 10 D'Agosto F. Handbook of RAFT Polymerization / F. D'Agosto // *Macromolecular Rapid Communications*, 2008. — Vol. 29, No. 11. — P. 934, 935. <https://doi.org/10.1002/marc.200800209>
- 11 Moad C.L. Fundamentals of reversible addition–fragmentation chain transfer (RAFT) / C.L. Moad, G. Moad // *Chemistry Teacher International*, 2020. — Vol. 3, No. 2. — P. 3–17. <https://doi.org/10.1515/cti-2020-0026>
- 12 Burkeev M.Zh. Polypropylene glycol maleate phthalate terpolymerization with acrylamide and acrylic acid / M.Zh. Burkeev, A.K. Kovaleva, G.K. Burkeyeva, J. Plocek, et.al. // *Polym. Korea*, 2020. — Vol. 44, No. 22. — P. 123–131. <https://doi.org/10.7317/pk.2020.44.2.123>
- 13 Katayama S. Phase transition of a cationic gel / S. Katayama, A. Ohata // *Macromolecules*, 1985. — Vol. 18, No. 12. — P. 2781, 2782. <https://doi.org/10.1021/ma00154a074>
- 14 Kudo S. Volume-phase transitions of cationic polyelectrolyte gels / S. Kudo, N. Kosaka, M. Konno, S. Saito // *Polymer*, 1992. — Vol. 33, No. 23. — P. 5040–5043. [https://doi.org/10.1016/0032-3861\(92\)90055-2](https://doi.org/10.1016/0032-3861(92)90055-2)
- 15 Siegel R. A. pH-dependent equilibrium swelling properties of hydrophobic polyelectrolyte copolymer gels / R.A. Siegel, B.A. Firestone // *Macromolecules*, 1993. — Vol. 21. — No. 11. — P. 3254–3259. <https://doi.org/10.1021/ma00189a021>
- 16 Shibayama M. pH and salt concentration dependence of the microstructure of poly(N-isopropylacrylamide-co-acrylic acid) gels / M. Shibayama, F. Ikkai, S. Inamoto, S. Nomura, C.C. Han // *The Journal of Chemical Physics*, 1996. — Vol. 105, No. 10. — P. 4358–4366. <https://doi.org/10.1063/1.472252>
- 17 Amiya T. Reentrant phase transition of N-isopropylacrylamide gels in mixed solvents / T. Amiya, Y. Hirokawa, Y. Li, Y. Hirose, T. Tanaka // *The Journal of Chemical Physics*, 1987. — Vol. 86, No. 4. — P. 2375–2379. <https://doi.org/10.1063/1.452740>
- 18 Burkeev M.Zh. Research of the influence of external factors on copolymers based on unsaturated polyester resins / M.Zh. Burkeev, G.M. Zhumanazarova, G.K. Kudaibergen, E.M. Tazhbayev, G.A. Turlybek // *Bulletin of the University of Karaganda – Chemistry*, 2018. — Vol. 98, No. 2. — P. 51–57. <https://doi.org/10.31489/2020Ch2/51-57>
- 19 Burkeev M.Zh. Synthesis and investigation of copolymer properties on the basis of poly(ethylene glycol) fumarate and methacrylic acid / M.Zh. Burkeev, G.K. Kudaibergen, Ye.M. Tazhbayev, J. Hranicek, G.K. Burkeyeva, A.Zh. Sarsenbekova // *Bulletin of the University of Karaganda – Chemistry*, 2019. — Vol. 93, No. 1. — P. 32–38. <https://doi.org/10.31489/2019ch1/32-38>

М.Ж. Бүркеев, М.С. Жүнісова, Ю. Плоцек, А.Т. Қажымұратова, Т.С. Жұмағалиева

РАФТ агентінің әртүрлі концентрацияларында алынған акрил қышқылымен полипропиленгликольмалеинатының тігілген сополимерлерінің қасиеттері

Бастапқы полипропиленгликольмалеинаты малеин ангидридi мен пропиленгликольдiн поликонденсациялану реакциясы арқылы алынды. Синтезделген қанықпаған полиэфир шайырының молекулалық салмағы анықталды. Зерттелетiн сополимерлер радикалды сополимерлену реакциясы арқылы п-ПГМ пен қанықпаған карбон қышқылының негiзiнде алынды. RAFT-агентiнiң әртүрлi концентрациясының қатысуымен п-ПГМ мен акрил қышқылы негiзiнде жаңа полимерлердi синтездеу мүмкiндiгi көрсетiлдi. RAFT-агентiнiң концентрациясы полимер торының тығыздығына және өнiм шығымына әсерi зерттелдi. RAFT-агентiнiң концентрациясының жоғарылауымен тігілген полимердiң шығымы төмендейтiнi және оның ісiну қабілеті жоғарылайтыны, сонымен қатар сызықты полимердiң шығымы жоғарылайтыны анықталды. Синтезделген сополимерлердiң ісiну дәрежесiне органикалық ерiткіштердiң, рН ортаның және төмен молекулалы тұздардың әсерi зерттелдi. Зерттеу нәтижелерi полимерлi гидрогельдердiң органикалық ерiткіштердiң концентрациясының өзгеруiне және рН ортаның өзгеруiне, сондай-ақ төмен молекулалық тұздар ерiтiндiлерiнiң сезiмталдығына полимердегi RAFT-агенттiң мөлшерi әсер ететiндiгiн көрсеттi. Полипропиленгликольмалеинат пен акрил қышқылы негiзiндегi объектілер инфрақызыл спектроскопиясы арқылы сипатталады. Сканерлеушi электронды микроскоптың көмегiмен полимерлердiң беткi морфологиясы зерттелген, сонымен қатар тор өлшемдерi бағаланған.

Кілт сөздер: қанықпаған полиэфир шайыры, полипропиленгликольмалеинат, RAFT-полимеризация, ісiну, коллапс.

М.Ж. Буркеев, М.С. Жунисова, Ю. Плоцек, А.Т. Қажымұратова, Т.С. Жұмағалиева

Свойства сетчатых сополимеров полипропиленгликольмалеината с акриловой кислотой, полученных при различных концентрациях RAFT-агента

Реакцией поликонденсации малеинового ангидрида и пропиленгликоля получен исходный полипропиленгликольмалеинат. Определена молекулярная масса синтезированной ненасыщенной полиэфирной смолы. Путем радикальной сополимеризации п-ПГМ с ненасыщенной карбоновой кислотой получены исследуемые сополимеры. Показана возможность синтеза новых полимеров на основе п-ПГМ с акриловой кислотой в присутствии RAFT-агента. Изучено влияние концентрации RAFT-агента на плотность сетки и выход продукта. Установлено, что с увеличением концентрации RAFT-агента уменьшается выход сетчатого полимера, увеличивается его набухающая способность, а выход линейного полимера возрастает. Исследовано влияние органических растворителей, рН среды, низкомолекулярных солей на степень набухания синтезированных сополимеров. Результаты исследований показали, что на восприимчивость полимерных гидрогелей к присутствию органических растворителей и к изменению рН среды, а также низкомолекулярных солей влияет количество RAFT-агента в полимерном мономерной смеси. Синтезированные объекты охарактеризованы методами инфракрасной спектроскопии. Посредством сканирующей электронной микроскопии исследована морфология поверхности полимера и оценены размеры пор.

Ключевые слова: ненасыщенная полиэфирная смола, полипропиленгликольмалеинат, RAFT-полимеризация, набухание, коллапс.

References

- 1 Mesquita, R.G. de A., César, A.A. da S., & Tonoli, G.H.D. et al. (2016). Polyester Composites Reinforced with Corona-Treated Fibers from Pine, Eucalyptus and Sugarcane Bagasse. *Journal of Polymers and the Environment*, 25(3), 800–811. <https://doi:10.1007/s10924-016-0864-6>
- 2 Kang, M.K., & Huang, R. (2010). Swell-induced surface instability of confined hydrogel layers on substrates. *Journal of the Mechanics and Physics of Solids*, 58(10), 1582–1598. <https://doi:10.1016/j.jmps.2010.07.008>
- 3 Kandelbauer, A., Tondi, G., Zasko, O.C., & Goodman, S.H. (2014). Unsaturated Polyesters and Vinyl Esters. *Handbook of Thermoset Plastics*, 111–172. <https://doi.org/10.1016/B978-1-4557-3107-7.00006-3>
- 4 He, S., Yaszemski, M.J., Yasko, A.W., Engel, P.S., & Mikos, A.G. (2000). Injectable biodegradable polymer composites based on poly(propylene fumarate) crosslinked with poly(ethylene glycol)-dimethacrylate. *Biomaterials*, 21(23), 2389–2394. [https://doi.org/10.1016/S0142-9612\(00\)00106-X](https://doi.org/10.1016/S0142-9612(00)00106-X)

- 5 Pavlyuchenko, V.N., & Ivanchev, S.S. (2009). Kompozitsionnye polimernye gidrogeli [Composite polymer hydrogels]. *Vysokomolekuliarnye soedineniya — High molecular weight compounds*, Vol. 51, 7, 1075–1095 [in Russian].
- 6 Sadler, J.M., Toulan, F.R., Palmese, G.R., & La Scala, J.J. (2015). Unsaturated polyester resins for thermoset applications using renewable isosorbide as a component for property improvement. *Journal of Applied Polymer Science*, 132(30) <https://doi.org/10.1002/app.42315>
- 7 Burkeyev, M.Zh., Kovaleva, A.K., Tazhbayev, E.M., Zhakupbekova, E.Zh., & Kopbosynova, A.A. (2015). Sintez i issledovanie svoystv sopolimerov na osnove polipropilenglikolmaleinatftalata s akrilovoi kislotoi [Synthesis and investigation of the properties of copolymers based on polypropylene glycol maleate ftalate with acrylic acid]. *Vestnik Karagandinskogo universiteta. Seriya Khimiia — Bulletin of the University of Karaganda – Chemistry*, 1 (77), 31–36 [in Russian]. <http://rep.ksu.kz:80/handle/data/4012>
- 8 Burkeyev, M.Z., Kovaleva, A.K., Tazhbaev, E.M., Burkeeva, G.K., Davrenbekov, S.Z., & Kopbosynova, A.A., et al. (2015). Nanocatalytic systems based on poly(ethylene glycol maleate)-acrylamide copolymers. *Russian Journal of Applied Chemistry*, 88(2), 314–319. <http://doi:10.1134/s1070427215020202>
- 9 Burkeyev, M.Z., Magzumova, A.K., Tazhbaev, E.M., Burkeeva, G.K., Kovaleva, A.K., & Khamitova, T.O., et al. (2013). Effect of external factors on the swelling of hydrogels based on poly(ethylene glycol) maleate with some vinyl monomers. *Russian Journal of Applied Chemistry*, 86(1), 63–68. <http://doi:10.1134/s1070427213010114>
- 10 D'Agosto, F. (2008). Handbook of RAFT Polymerization. *Macromolecular Rapid Communications*, 29(11), 934–935. <https://doi:10.1002/marc.200800209>
- 11 Moad, C.L., & Moad, G. (2020). Fundamentals of reversible addition–fragmentation chain transfer (RAFT). *Chemistry Teacher International*, 3(2), 3–17. <https://doi:10.1515/cti-2020-0026>
- 12 Burkeyev, M.Zh., Kovaleva, A.K., Burkeyeva, G.K., Tazhbayev, Ye.M., & Plocek, J., et al. (2020). Polypropylene glycol maleate phthalate terpolymerization with acrylamide and acrylic acid. *Polym. Korea*, 44(22), 123–131. <https://doi:10.7317/pk.2020.44.2.123>
- 13 Katayama, S., & Ohata, A. (1985). Phase transition of a cationic gel. *Macromolecules*, 18(12), 2781–2782. <https://doi.org/10.1021/ma00154a074>
- 14 Kudo, S., Kosaka, N., Konno, M., & Saito, S. (1992). Volume-phase transitions of cationic polyelectrolyte gels. *Polymer*, 33(23), 5040–5043. [https://doi.org/10.1016/0032-3861\(92\)90055-2](https://doi.org/10.1016/0032-3861(92)90055-2)
- 15 Siegel, R.A., & Firestone, B.A. (1988). pH-dependent equilibrium swelling properties of hydrophobic polyelectrolyte copolymer gels. *Macromolecules*, 21(11), 3254–3259. <https://doi.org/10.1021/ma00189a021>
- 16 Shibayama, M., Ikkai, F., Inamoto, S., Nomura, S., & Han, C.C. (1996). pH and salt concentration dependence of the microstructure of poly(N-isopropylacrylamide-co-acrylic acid) gels. *The Journal of Chemical Physics*, 105(10), 4358–4366. <https://doi.org/10.1063/1.472252>
- 17 Amiya, T., Hirokawa, Y., Hirose, Y., Li, Y., & Tanaka, T. (1987). Reentrant phase transition of N-isopropylacrylamide gels in mixed solvents. *The Journal of Chemical Physics*, 86(4), 2375–2379. <https://doi.org/10.1063/1.452740>
- 18 Burkeyev, M.Zh., Zhumanazarova, G.M., Kudaibergen, G.K., Tazhbayev, E.M., & Turlybek, G.A., et al. (2018). Research of the influence of external factors on copolymers based on unsaturated polyester resins. *Bulletin of the University of Karaganda – Chemistry*, 98(2), 51–57. <https://doi:10.31489/2020Ch2/51-57>
- 19 Burkeyev, M.Zh., Kudaibergen, G.K., Tazhbayev, E.M., Hranicek, J., & Burkeyeva, G.K., et al. (2019). Synthesis and investigation of copolymer properties on the basis of poly(ethylene glycol)fumarate and methacrylic acid. *Bulletin of the University of Karaganda – Chemistry*, 93(1), 32–38. <https://doi:10.31489/2019ch1/32-38>

Information about authors

Burkeyev, Meyram Zhunusovich — Full Professor, Doctor of Chemical Sciences, Karagandy University of the name of academician E.A. Buketov, Universitetskaya street, 28, 100024, Karaganda, Kazakhstan; e-mail: m_burkeyev@mail.ru; <https://orcid.org/0000-0001-8084-4825>;

Zhunissova, Meruyert Serikhanovna — 2nd year PhD student, Karagandy University of the name of academician E.A. Buketov, Universitetskaya street, 28, 100024, Karaganda, Kazakhstan; e-mail: meruert_zhunissova@mail.ru; <https://orcid.org/0000-0001-6376-8955>;

Plocek, Jiri — PhD., CSc. Institute of Inorganic Chemistry of the Czech Academy of Sciences, Czech Republic, Husinec-Rez 1001 25068 Rez; e-mail: plocek@iic.cas.cz; <https://orcid.org/0000-0001-6082-5766>;

Kazhuratova, Akerke Temirgalievna — Candidate of chemical sciences, Karagandy University of the name of academician E.A. Buketov, Universitetskaya street, 28, 100024, Karaganda, Kazakhstan; e-mail: kazhuratova@mail.ru; <https://orcid.org/0000-0003-4044-8419>;

Zhumagalieva, Tolkyn Sergazyevna — Candidate of chemical sciences, Professor, Karagandy University of the name of academician E.A. Buketov, Universitetskaya street, 28, 100024, Karaganda, Kazakhstan; e-mail: Zhumagalieva79@mail.ru; <https://orcid.org/0000-0003-1765-752X>

A.Zh. Kassanova^{1, 2*}, M.T. Yestayeva¹, M.O. Turtubayeva^{1, 3}

¹Toraighyrov University, Pavlodar, Kazakhstan;

²National Research Tomsk Polytechnic University, Tomsk, Russia;

³S.D. Asfendiyarov Kazakh National Medical University, Almaty, Kazakhstan

(*Corresponding author's e-mail: asiyakass@mail.ru)

Arenediazonium sulfonates: synthesis, comparison of structural and physicochemical properties

Aromatic diazonium salts are important building blocks in organic synthesis. The present review is concerned with such aromatic diazonium sulfonates as tosylates, dodecylbenzenesulfonates, triflates, camphorsulfonates, silica sulfates. The first part of the review provides information on the synthesis and application of these diazonium salts. It is shown that these diazonium compounds are easily synthesized by diazotization of anilines with sodium nitrite or alkyl nitrites in the presence of corresponding sulfonic acids with high yields. These diazonium salts have found wide application in the synthesis of aromatic azides, halides, triazenes, azo dyes, stilbenes, biaryls, etc. The second part of the article presents information on the comparison of the results of X-ray analysis, infrared spectroscopy and thermal analysis. The structure of diazonium sulfonate salts corresponds to the structure of classical diazonium salts (chlorides, sulfates, tetrafluoroborates). A significant difference between arenediazonium sulfonates and other diazonium salts is their explosion safety and stability in an individual form. Arenediazonium tosylates, triflates and camphorsulfonates are easily soluble both in water and in polar organic solvents. Arenediazonium dodecylbenzenesulfonates are soluble in nonpolar organic media. These features of sulfonate salts are paramount for distinguishing characteristics of the effect of the acid anion on the stability, solubility and reactivity of diazonium salts.

Keywords: diazonium salts, diazotization, sulfonates, tosylate, triflate, camphorsulfonate, silica-sulfate, dodecylbenzenesulfonate, X-Ray.

Content

List of abbreviations

Review Plan

Introduction

1 Diazotization in the presence of sulfonic acids

1.1 Synthesis of arenediazonium tosylates, triflates, mesylates and dodecylbenzenesulfonates

1.2 Synthesis of arenediazonium camphorsulfonates, silicasulfates, biodegradable cellulose-sulfonate, o-benzenedisulfonimides

1.3 Diazotization of aminopyridines in the presence of sulfonic acids

2 Comparison of spectral and thermal characteristics of arenediazonium sulfonates

Conclusions

List of abbreviations

KI: potassium iodide

NaNO₂: sodium nitrite

DSC: differential scanning calorimetry

DTA: differential thermal analysis

TGA: thermal gravimetric analysis

ADT: arenediazonium tosylates

EtOH: ethanol

MeOH: methanol

AcOH: acetic acid

DMSO: dimethyl sulfoxide

IR: infrared spectroscopy

NMR: nuclear magnetic resonance

CCl_4 : carbon tetrachloride
 Et_2O : diethyl ether
 $\text{ArN}_2^+\text{Cl}^-$: arenediazonium chloride
 $\text{ArN}_2^+\text{BF}_4^-$: arenediazonium tetrafluoroborate
 $\text{ArN}_2^+\text{OTf}^-$: arenediazonium trifluoromethanesulfonate (triflate)
 $\text{ArN}_2^+\text{OTs}^-$: arenediazonium p-toluenesulfonate (tosylate)
 $\text{ArN}_2^+\text{p-C}_{12}\text{H}_{25}\text{C}_6\text{H}_4\text{SO}_3^-$: arenediazonium dodecylbenzenesulfonate
 $\text{ArN}_2^+\text{OSO}_2\text{Camph}$: arenediazonium camphorsulfonate
 $\text{ArN}_2^+\text{OSO}_3\text{-SiO}_2$: arenediazonium silicosulfate
 $\text{ArN}_2^+\text{N}(\text{SO}_2)_2\text{Ph}$: arenediazonium o-benzenedisulfonimides
 MeCN : acetonitrile
 THF : tetrahydrofuran
 CH_2Cl_2 : dichloromethane
 CHCl_3 : chloroform
 H_2O : water
 HCO_2H : formic acid

Review Plan

Inclusion and Exclusion Criteria: The present review is concerned with such aromatic diazonium sulfonates as tosylates, dodecylbenzenesulfonates, triflates, camphorsulfonates, silicosulfates, their synthesis and comparison of their structural characteristics.

The review data are based on scientific publications from 1936 to 2021. Some old literature sources (1936–1980) provide information about the first attempts to synthesize diazonium sulfonate salts. A large-scale study of diazonium sulfonate salts began with the work of Barbero (1998) and continues now. We searched and analyzed articles from Scopus, Web of Science, Reaxys, Sci-Finder. The keywords used for the search were ‘arenediazonium salts’, ‘sulfonates’, ‘diazotization’, ‘sulfonic acid’, etc. The resultant data were described in this article. No statistical methods were used.

Introduction

Aromatic diazonium salts are of undoubted interest in modern organic synthesis. A huge number of reviews, monographs and articles in highly rated journals have been published on the synthesis of arenediazonium salts and the study of their chemical properties. The salts discovered by Griss in 1858 [1] became a huge impetus for the development of organic synthesis: The production of azo dyes, medicines, the synthesis of halogen and azide-derived benzenes, stilbenes, diaryls, the immobilization of biodegradable polymers, nanoparticles, etc. Approximately every 10–20 years, scientists discovered new transformations of diazonium salts (Figure 1) [1]:

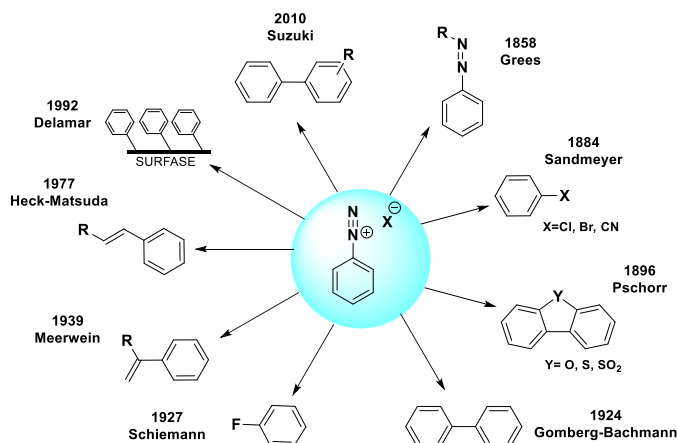


Figure 1. Transformations of diazonium salts [1]

Despite the widespread application of diazonium salts in modern organic synthesis, significant problems of their usage on an industrial scale are instability, explosiveness, non-selectivity of transformations

and poor solubility in water or organic solvents. Many diazonium salts are thermally unstable and sensitive to friction and shock. Most diazonium salts are known for their violent decomposition hazard in the solid-state. This group of chemicals causes many industrial and laboratory incidents. For solving this problem, scientists are developing new types of arenediazonium salts that differ in structure only by the nature of the diazo-anion (residues of mineral or organic acids). In recent decades, obtaining and using aromatic diazonium salts of the sulfonate type devoid of most of the disadvantages of classical diazonium salts has been actively developing. This review aims to study synthesis methods of arenediazonium sulfonates and compare their physicochemical properties.

1 Diazotization in the presence of sulfonic acids

The addition of aryl sulfonic acids has a significant effect on the stability of diazonium ions [2]. This influence has been described in many patents [3]. It has been shown that the addition of α - and β -naphthalenesulfonic acids to a solution of bisdiazotized benzidine and *p*-nitrodiazobenzene leads to the formation of precipitates, which can be filtered off and dried without any danger. These products easily dissolve in water and enter reactions characteristic of diazonium ions after long-term storage.

In later works, one-stage diazotization-iodination reactions of a wide range of aromatic and heterocyclic amines under the action of the system KI/NaNO₂, *p*-toluenesulfonic acid in acetonitrile [4], and aqueous paste [5] were demonstrated. These methods provided high yields of the target aryl iodides and were widely used [6–9]. Before these works [5, 6], individual representatives of arenediazonium sulfonates were known, namely arenediazonium naphthalenesulfonates [10], *p*-toluenesulfonates (tosylates) [11, 12], trifluoromethanesulfonates (triflates) [13–15]; arenediazonium methanesulfonates (mesylates obtained in solution but not isolated individually) [16] (Figure 2).

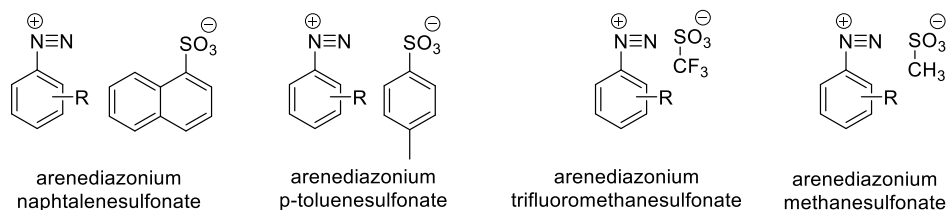


Figure 2. Some examples of diazonium sulfonate salts

1.1 Synthesis of arenediazonium tosylates, triflates, mesylates and dodecylbenzenesulfonates

Historically, the first method for preparing arenediazonium sulfonates was the decomposition reaction of arenediazonium chlorides in the presence of aromatic sulfonic acids [3]. In this case, it was necessary to resort to rubbing unsafe dry arenediazonium chlorides. This method was used to obtain some benzenediazonium salts of α -, β -naphthalene and α -, β -anthraquinone sulfonic acids [17].

Later, this approach was used to obtain some tosylates (Figure 3) [17] and 2-(trifluoromethoxy) biphenyl-2'-diazonium triflate (Figure 4) [18].

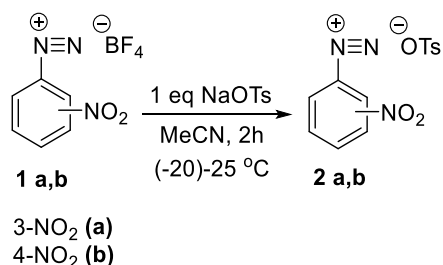


Figure 3. Obtaining arenediazonium tosylates

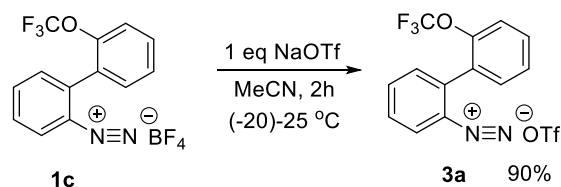


Figure 4. Obtaining arenediazonium triflate

Some arenediazonium tosylates and triflates were obtained by direct diazotization of anilines with alkyl nitrites in the presence of *p*-toluenesulfonic acid [19–21] and trifluoromethanesulfonic acid [19] in a solution of acetic acid or a mixture of tetrahydrofuran-acetic acid, respectively (Figure 5).

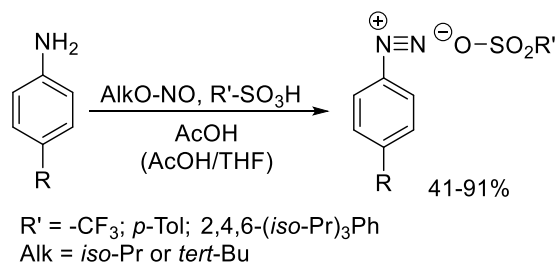
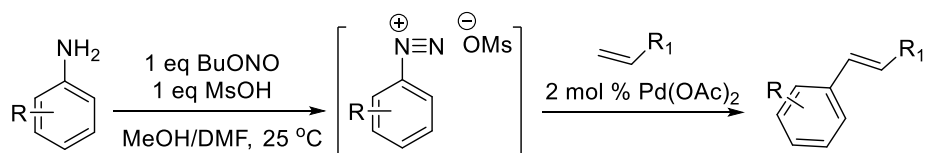
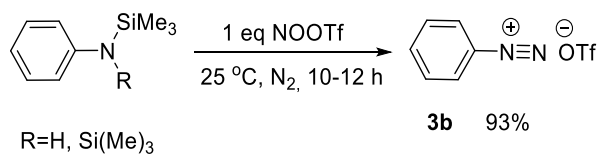


Figure 5. Preparation of arenediazonium tosylate and triflate in the presence of alkyl nitrites

Arenediazonium mesylates were obtained *in situ* with the use of methanesulfonic acid [16] and used as a solution in further transformations (Figure 6).

Figure 6. Preparation and transformation of arenediazonium mesylates *in situ*

Some examples of arenediazonium triflates were obtained by indirect methods [13, 14]. These methods were based on N-substituted aniline azodesilylation under the action of $\text{NO}^+\text{CF}_3\text{SO}_3^-$ and led to the formation of benzenediazonium trifluoromethanesulfonate in 93 % yield [13] (Figure 7).

Figure 7. Azodesilylation of N-substituted aniline under the action of $\text{NO}^+\text{CF}_3\text{SO}_3^-$

Para-substituted benzenediazonium trifluoromethanesulfonates were synthesized by treating the corresponding triazenes with 2 trifluoromethanesulfonic acid [14] (Figure 8).

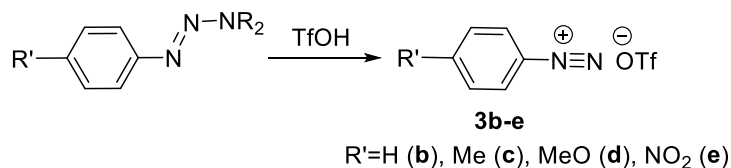


Figure 8. Synthesis of benzenediazonium trifluoromethanesulfonates via the corresponding triazenes

It should be noted that none of these works [10–21] set the task of a detailed study of the structure and physicochemical properties of arenediazonium sulfonates. This problem was partially solved in the study conducted by Filimonov V.D. et al. [21]. They developed an efficient method for the preparation of arenediazonium tosylates [21] using a new diazotizing agent with a polymer structure (Figure 9). Diazotization proceeded in acetic acid at room temperature; the formed diazonium salt was precipitated with diethyl ether. Initially, cheap sodium nitrite was used as a diazotizing agent [22]; however, in this case, the target products were contaminated with an admixture of the sodium salt of *p*-toluenesulfonic acid. The method provided the synthesis of a wide range of arenediazonium tosylates, which made it possible to conduct a detailed study of their physicochemical properties.

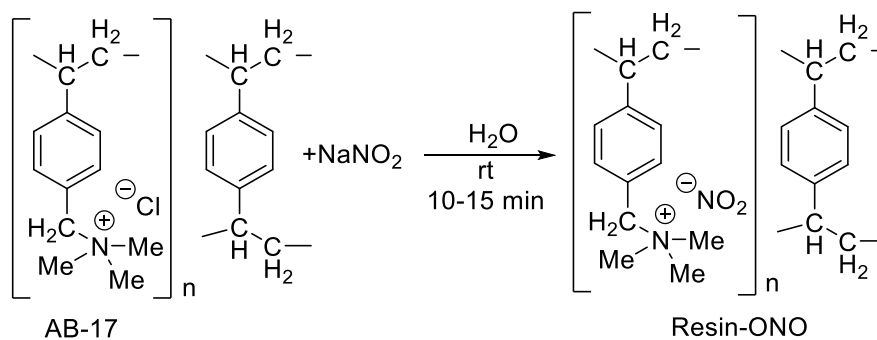
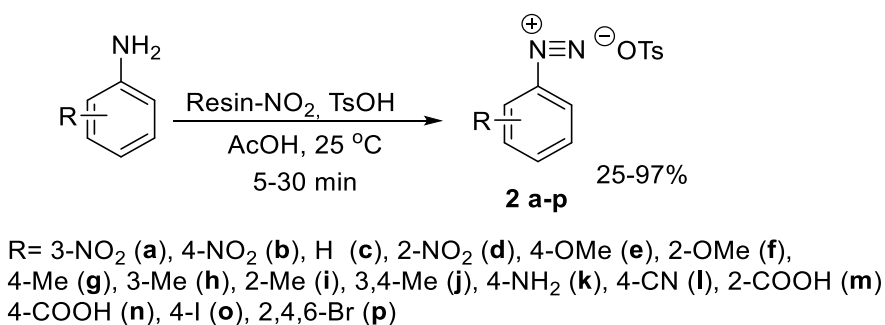


Figure 9. Preparation of arenediazonium tosylates using a new diazotizing agent with a polymer structure

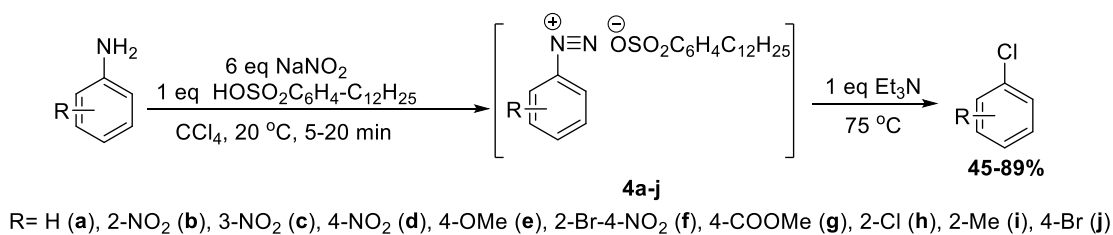
It turned out that all synthesized arenediazonium tosylates are explosion-proof and have storage stability that is unique for diazonium salts (established using DSC/DTA/TGA). In contrast to the known arenediazonium chlorides, sulfates, and tetrafluoroborates, ADT have good solubility both in water and in organic solvents (EtOH, MeOH, AcOH, and DMSO). Furthermore, the structure of all salts was investigated and reliably established by modern physicochemical methods (X-Ray, IR, NMR spectroscopy). Thus, new unique representatives of the class of aromatic diazonium salts, namely arenediazonium tosylates, were obtained. These salts immediately found wide application in organic synthesis: preparation of aromatic iodides [5, 22], arenes containing radioisotope of fluorine [23], aryltriethylsilanes [20], aromatic azides [24], in the synthesis of heterocyclic systems [25], modification of nanosurfaces [26, 27], in the Heck reaction [28].

Later, this scientific group synthesized unique in their properties arenediazonium dodecylbenzenesulfonates [29]. The synthesis was based on the diazotization of anilines with *tert*-butyl nitrite and dodecylbenzenesulfonic acid in diethyl ether at room temperature.



Figure 10. Preparation of arenediazonium dodecylbenzenesulfonates

IR and NMR spectroscopy proved the structures of the synthesized salts. All synthesized salts turned out to be explosion-proof (DSC/DTA/TGA), stable during storage and having an “abnormally” high solubility for diazonium salts: Not only in water and polar organic solvents (EtOH, MeOH, AcOH, DMSO) but also in low-polarity chloroform and CCl₄. The latter circumstance provided a specific feature of the chemical behavior of these salts. Along with the reactions typical of aromatic diazonium salts (interaction with KI, combination with 2-naphthol), a previously unknown reduction to chlorobenzenes in a CCl₄ solution in the presence of a base was observed [30]. One-pot diazotization-dediazotization reaction was carried out in a CCl₄ solution under the action of sodium nitrite (Figure 11).

Figure 11. Reduction of arenediazonium dodecylbenzenesulfonates to chlorobenzenes in a CCl₄

The authors of the work [31] proposed a convenient method for the synthesis of a wide range of arenediazonium triflates by diazotization of aromatic amines with butyl nitrite in the presence of trifluoromethanesulfonic acid in acetic acid (Figure 12). A detailed study of the physicochemical characteristics of the obtained diazonium salts and their chemical transformations were carried out in the work.

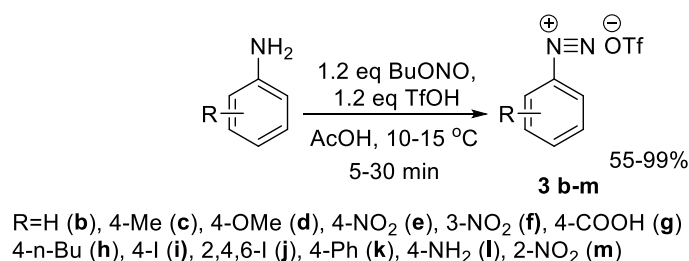


Figure 12. Synthesis of arenediazonium triflates

The authors have shown that arenediazonium triflates are highly soluble both in water and in polar and low-polar organic media, explosion-proof, and stable at room temperature.

1.2 Synthesis of arenediazonium camphorsulfonates, silicasulfates, biodegradable cellulose-sulfonate, o-benzenedisulfonimides

In work [32], it has recently been described the preparation of a wide range of arenediazonium camphorsulfonates through diazotization of anilines under the action of NaNO₂ in the presence of camphor sulfonic acid in AcOH solution at room temperature (Figure 13). It has been shown that arenediazonium camphorsulfonates can be successfully used for the preparation of aryl halides (chlorides, bromides, iodides), while the authors propose a one-stage diazotization-halogenation method both in solution (acetic acid or acetonitrile) and in the absence of a solvent.

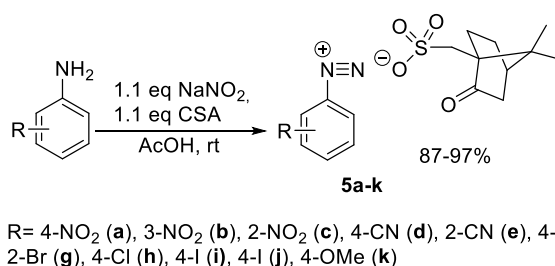
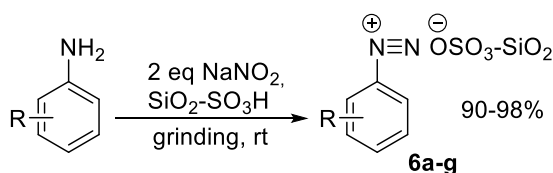


Figure 13. Preparation of arenediazonium camphorsulfonates

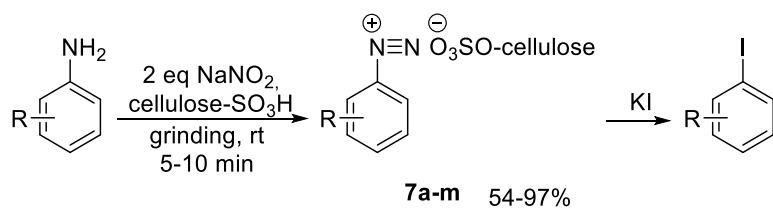
A number of works were devoted to the preparation and usage of arenediazonium silicosulfates in organic synthesis [33–38]. According to [34], diazotization of anilines with sodium nitrite in the presence of silica sulfonic acid at room temperature gave stable diazonium salts (Figure 14). These salts can be used to obtain azo dyes [34] (a method corresponding to the principles of Green Chemistry), iodoarene [33], aromatic azides [35, 36], in the reactions of C-C-coupling of Suzuki-Miyaura [37], Matsuda-Heck [38].



R=H (**a**), 2-NO₂ (**b**), 4-NO₂ (**c**), 4-SO₃Na (**d**), 2-Cl (**e**), 3-Cl (**f**), 2-Me (**g**)

Figure 14. Preparation of arenediazonium silicosulfates

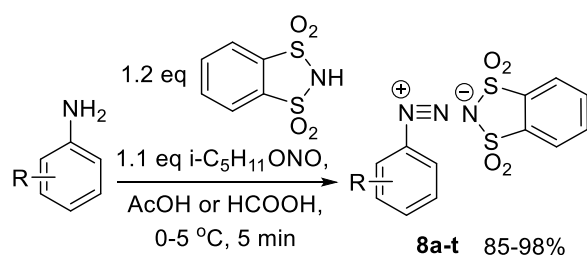
Stable aromatic diazonium salts can be synthesized by using biodegradable sulfonated cellulose (Figure 15) [39]. Diazotization proceeds mildly for 5–10 minutes at room temperature, while sulfonated cellulose can be recycled at the end of the synthesis and reused. The diazonium salts obtained easily gave the corresponding iodides and azides with quantitative yields.



R=H (**a**), 2-I (**b**), 2-COOH (**c**), 3-COOH (**d**), 4-COOH (**e**), 2,4-Cl (**f**), 3,4-Cl (**g**)
4-Cl (**h**), 4-Br (**i**), 4-OMe (**j**), 4-Me (**k**), 4-NO₂ (**l**), 2-NO₂ (**m**)

Figure 15. Using biodegradable sulfonated cellulose for diazotization

The preparation of dry arenediazonium *o*-benzenedisulfonimides was easily carried out by diazotization of aromatic amines with *i*-pentyl nitrite in the presence of *o*-benzenedisulfonimide in glacial acetic acid or in formic acid at 0–5 °C [40] (Figure 16). Using acetic acid as a solvent allows obtaining quickly a product by simple precipitation with diethyl ether. Formic acid as a solvent dissolved the diazonium salt well. Therefore, a large amount of diethyl ether was necessary for its isolation. In both solvents salts were obtained dry in high purity and excellent yields.



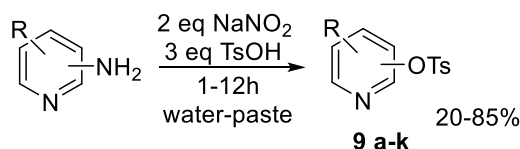
R=H (**a**), 2-Me (**b**), 3-Me (**c**), 4-Me (**d**), 2-OMe (**e**), 3-OMe (**f**), 4-OMe (**g**), 2-Cl (**h**), 3-Cl (**i**), 4-Cl (**j**),
3-Br (**k**), 4-Br (**l**), 2-NO₂ (**m**), 3-NO₂ (**n**), 4-NO₂ (**o**), 4-NMe₂ (**p**), 2,6-Me (**q**), 2-OMe-5-Cl (**r**), 2,6-Cl (**s**),
1-naphthyl (**t**)

Figure 16. Preparation of arenediazonium *o*-benzenedisulfonimides

1.3 Diazotization of aminopyridines in the presence of sulfonic acids

An attempt to use the method described above to obtain heteroaromatic diazonium salts, in particular, from aminopyridines, was unsuccessful: diazotization proceeded slowly and the corresponding hydroxypyridines were the only reaction products [41].

However, diazotization of aminopyridines under the action of sodium nitrite in the presence of *p*-toluenesulfonic acid in an aqueous paste [41] radically changed the result of the reaction. Pyridyl tosylates were isolated as the main products (Figure 17).

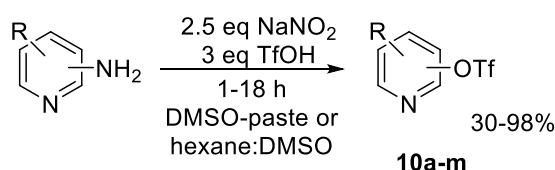


R=H, 2-NH₂ (**a**), 3-NH₂ (**b**), 4-NH₂ (**c**), R=5-Br, 2-NH₂ (**d**), R=5-I, 2-NH₂ (**e**),
 R= 3,5-Br, 2-NH₂ (**f**), R=3-Me, 2-NH₂ (**g**), R=4-Me, 2-NH₂ (**h**), R= 6-Me, 2-NH₂ (**i**)
 R= 4-Me, 5-I, 2-NH₂ (**j**), R= 2,6-NH₂ (**k**)

Figure 17. Preparation of pyridyl tosylates by direct diazotization of aminopyridines

This was the first example of the preparation of pyridyl tosylates — important intermediates in organic synthesis — by direct diazotization of aminopyridines.

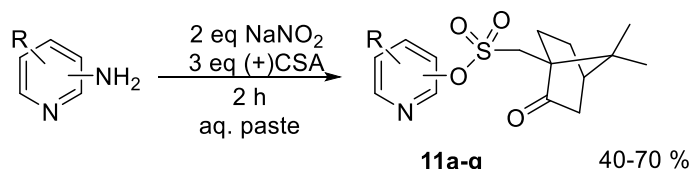
Direct diazotization of aminopyridines in the presence of trifluoromethanesulfonic acid in a DMSO-paste [42] or a mixture of solvents DMSO: hexane [43] (Figure 18) made it possible to obtain more valuable pyridyl triflates widely used in modern synthesis [44].



R=H, 2-NH₂ (**a**), 3-NH₂ (**b**), 4-NH₂ (**c**), R=5-Cl, 2-NH₂ (**d**), R=6-Me, 2-NH₂ (**e**),
 R=5-Br, 2-NH₂ (**f**), R=5-NO₂, 2-NH₂ (**g**), R=4-Me, 2-NH₂ (**h**), R= 2-Cl, 3-NH₂ (**i**)
 R= 3,5-Br, 2-NH₂ (**j**), R= 5-I, 2-NH₂ (**k**), R=H, 2,6-NH₂ (**l**), R= 3,5-I, 2,6-NH₂ (**m**)

Figure 18. Preparation of pyridyl triflates by direct diazotization of aminopyridines

Recently, a method has been proposed for the synthesis of pyridyl camphorsulfonates, which are of interest as biologically active substances [45]. The synthesis was based on the diazotization of aminopyridines in the presence of camphor sulfonic acid in an aqueous paste (Figure 19).



R=H, 2-NH₂ (**a**), 3-NH₂ (**b**), 4-NH₂ (**c**), R=5-Cl, 2-NH₂ (**d**), R=6-Me, 2-NH₂ (**e**),
 R=5-Br, 2-NH₂ (**f**), R=5-NO₂, 2-NH₂ (**g**)

Figure 19. Preparation of pyridyl camphorsulfonates

This difference between aminopyridines and anilines in the diazotization reaction is due to the fact that the resulting pyridinediazonium sulfonates are thermodynamically unstable and short-lived, unlike arenediazonium sulfonates. The pyridinediazonium cations decay with the loss of nitrogen and the formation of pyridyl cations, which are highly reactive and easily interact with all nucleophiles in solution (Figure 20). This fact has been confirmed both experimentally [41, 42] and by computational methods [46].

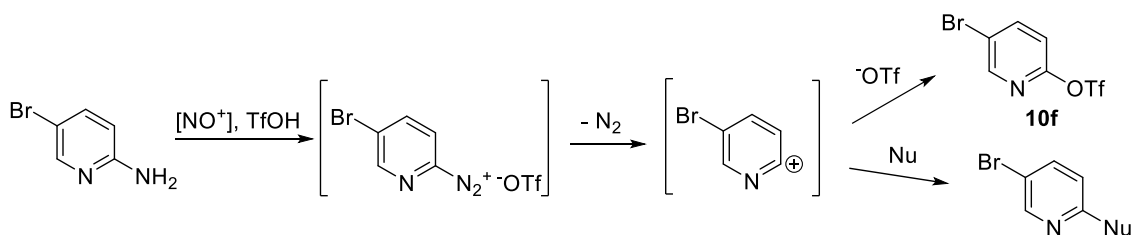


Figure 20. Plausible reaction pathways for the diazotization of 5-bromo-2-aminopyridine

Thus, arenediazonium sulfonates are easily synthesized by diazotization with sodium nitrite or alkyl nitrites in the presence of corresponding sulfonic acids with high yields. These diazonium salts have found wide application in the synthesis of aromatic azides, halides, triazenes, azo dyes, stilbenes, biaryls, etc.

2 Comparison of spectral and thermal characteristics of arenediazonium sulfonates

Comparison of the structure of aromatic diazonium salts is based on the valence oscillation of the N≡N bond in IR, the chemical shift of C_{ipso} in NMR and the results of X-ray diffraction analysis. The chemical shift of C_{ipso} carbon for all diazonium salts is in close ranges and does not correlate with the type of anion. In the IR spectrum, the valence oscillation of the diazonium group N≡N is in the characteristic region of 2100–2300 cm⁻¹.

In this review, the comparison of arenediazonium sulfonates is based on their solubility, the results of X-ray and thermal analysis. Table 1 shows the key geometric parameters, the crystallographic data, and the results of thermal analysis and information about solubility.

Table 1

The properties of some diazonium salts

| No. | Name of the diazo compound | Distance C-N | Distance N-N | Angle C-N-N | Decomposition energy, kJ/mol | The solubility | Ref. |
|-----|---|--|--------------|-------------|--|--|------|
| 1 | ArN ₂ ⁺ Cl ⁻ | 1.385 ¹ | 1.097 | 180 | No information. Explosive | Soluble in water | [2] |
| 2 | ArN ⁺ BF ₄ ⁻ | 1.415 ² | 1.083 | 179.5 | -229.2 (at 146.5 °C) explosive | Slightly soluble in water and organic compounds | [47] |
| 3 | ArN ₂ ⁺ OTf ⁻ | 1.405 ³ | 1.089 | 178.99 | From -136.1 to -840.4 non-explosive | Soluble in water, EtOH, MeOH, AcOH, DMSO, MeCN, THF; during heating in CH ₂ Cl ₂ , CHCl ₃ , CCl ₄ | [31] |
| 4 | ArN ₂ ⁺ OTs ⁻ | 1.371 ⁴ | 1.104 | 177.7 | From -60 to -885.2 non-explosive | soluble in H ₂ O, EtOH, MeOH, AcOH, DMSO, MeCN, acetone | [21] |
| 5 | ArN ₂ ⁺ p-C ₁₂ H ₂₅ C ₆ H ₄ SO ₃ ⁻ | Crystals cannot be grown for X-ray (oil) | | | From -118 to -410 non-explosive | Soluble in high and medium polarity solvents (water, DMSO, alcohols, ketones, acetic acid, chloroform) and non-polar (hexane, benzene, CCl ₄) solvents | [29] |
| 6 | ArN ₂ ⁺ OSO ₂ Camph ⁻ | 1.41 ⁵ | 1.09 | 177 | Stable and could be stored at room temperature under anhydrous conditions. No information about results of thermal analysis | Soluble in protic as well as aprotic solvents | [32] |
| 7 | ArN ₂ ⁺ OSO ₃ ⁻ SiO ₂ | Crystals cannot be grown for X-ray | | | Stability was proved indirectly through the azo combination reaction after 6, 24, 48 and 72 hours. The diazotization and diazo coupling method was found to be safe and the grinding of these aryldiazonium salts was not found to be hazardous. | Insoluble in aqueous media | [34] |
| 8 | ArN ₂ ⁺ N(SO ₂) ₂ Ph ⁻ | 1.387 ⁶ | 1.088 | 178.6 | Stored at 0 °C and at room temperature for two months underwent no decomposition | Soluble in water, HCO ₂ H, MeOH, DMSO, MeCN | [40] |

Notes:

¹Crystallographic info for PhN₂⁺Cl⁻.²Crystallographic info for PhN⁺BF₄⁻.³Crystallographic info for p-IC₆H₄N₂⁺OTf⁻.⁴Crystallographic info for p-IC₆H₄N₂⁺OTs⁻.⁵Crystallographic info for p-BrC₆H₄N₂⁺OSO₂Camph⁻.⁶Crystallographic info for 2,6-ClC₆H₃N₂⁺N(SO₂)₂Ph⁻.

The X-ray data show that the bond lengths $N\equiv N$ are in the same range and differ not significantly. The length of the C-N bond is of interest from the point of view of predicting reactivity, since that participates in the process of *de-diazotization*. The length of this bond is higher in arenediazonium tetrafluoroborates, triflates and camphorasulfonates, which indicates their greater reactivity in contrast to diazonium salts.

C-N-N bond angle in diazonium sulfonate salts differs from the bond angle in classical diazonium salts by 1–3°, which may cause greater stability of these salts. At the C-N-N bond angle equal 180°, the salt forms an easily destroyed layered crystal lattice. Changing the bond angle leads to better coordination with the anion and the formation of more complex structure (Figure 21).

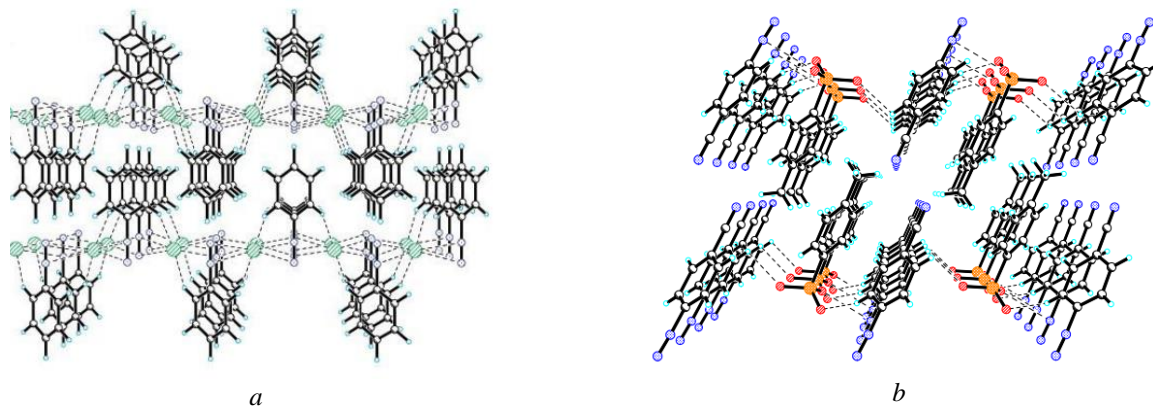


Figure 21. Crystalline networks of arenediazonium chloride (a) [48] and arenediazonium tosylate (b) [21]

The proof of stability for the diazonium salts was preserving chemical properties during the shelf life. Stability of arenediazonium silica-sulfate was proved indirectly through the azo combination reaction after 6, 24, 48, and 72 hours. Arenediazonium silica sulfates with electron-withdrawing groups on aromatic rings are more stable than those with electron-donating groups because of the instability of the resulting aryl cation. The diazotization and diazo coupling method was found to be safe and the grinding of these arenediazonium salts was not hazardous. At the same time, the authors of works recommend storing the obtained salts at 0 °C.

The stability of diazonium salts usually is compared by TGA-DSC methods. This method determines the temperature and energy of decomposition. According to the UNICEF international standard, the substance having decomposition energies of less than 800 kJ/mol is explosion-proof and can be transported. Among the considered salts, analysis was carried out only for arenediazonium tosylates, triflates, and dodecylbenzenesulfonates by TGA-DSC methods. All the studied salts are explosion-proof; the exception is *m*-nitro derivatives.

In work [49], for the first time, using isothermal flow calorimetry and DSC/TGA, authors determined the thermal decomposition energies of arenediazonium triflates, 4-nitrobenzene tosylate, and 4-nitrobenzenetetrafluoroborate. The authors calculated the decomposition energies of salts accurately. 4-Nitrobenzenediazonium triflate of all the studied diazonium salts has increased stability stored under normal conditions. The experimental and theoretical results demonstrated that, compared to DSC/TGA, isothermal flow calorimetry more adequately reflected the energetics of the thermal decomposition of DSs and their storage stability under normal conditions.

Arenediazonium sulfonates have high solubility in water and in organic solvents, which opens up more areas for their usage in contrast to arenediazonium tetrafluoroborates and chlorides.

Conclusions

Arenediazonium sulfonates are easily synthesized by diazotization with sodium nitrite or alkyl nitrites in the presence of corresponding sulfonic acids with high yields. These diazonium salts have found wide application in the synthesis of aromatic azides, halides, triazenes, azo dyes, stilbenes, biaryls, etc. The structure of diazonium sulfonate salts corresponds to the structure of classical diazonium salts (chlorides, sulfates, tetrafluoroborates). A significant difference between arenediazonium sulfonates and other diazonium salts is their explosion safety and stability in an individual form. Arenediazonium tosylate, triflates, and camphorasulfonates are easily soluble both in water and in polar organic solvents. Arenediazonium dodecylbenzenesulfonates are dissolved in nonpolar organic media. These features of sulfonate salts are paramount for dis-

tinguishing characteristics of the effect of the acid anion on the stability, solubility, and reactivity of diazonium salts.

Acknowledgments

The review was written with the financial support of the Ministry of Education and Science of the Republic of Kazakhstan, project AP 08856049.

References

- 1 Trusova, M.E., Kutonova, K.V., Kurtukov, V.V., Filimonov, V. D., & Postnikov, P.S. (2016). Arenediazonium salts transformations in water media: Coming round to origins. *Resource-Efficient Technologies, Issue 1*, 36–42. <https://doi.org/10.1016/j.reffit.2016.01.001>
- 2 Zollinger, H. (1994). *Diazo Chemistry*. Weinheim. New York. Basel. Cambridge. Tokyo.
- 3 Saunders, K.H. (1936). *The aromatic diazo-compounds and their technical applications*. London.
- 4 Krasnokutskaya, E.A., Semenischeva, N.I., Filimonov, V.D., & Knochel, P. (2007). A new, one-step, effective protocol for the iodination of aromatic and heterocyclic compounds via aprotic diazotization of amines. *Synthesis No. 1*, 81–84. <https://doi.org/10.1055/s-2006-958936>
- 5 Gorlushko, D.A., Filimonov, V.D., Krasnokutskaya, E.A., Semenischeva, N.I., Go, B.S., Hwang, H.Y., & Chi, K.-W. (2008). Iodination of arylamines in a water-paste form via stable aryl diazonium tosylates. *Tetrahedron Letters. Vol. 49. No. 6*, 1080–1082. <https://doi.org/10.1016/j.tetlet.2007.11.192>
- 6 Gregor, R.W., & Goj, L.A. (2011). Solvent-free synthesis of 2,2' — dinitrobiphenyl: an Ullmann coupling in the introductory organic laboratory. *Journal of Chemical Education*, 88, 331–333. <https://doi.org/10.1021/ed900024u>
- 7 Park, J.Y., Park, H.J., Im, W.B., Yoon, S.H., Kim, S.W., & Lee, J.K. (2012). Synthesis and antioxidant effect of caffeic acid analogues bearing a carboxy and hydroxymethyl group. *Korean Chemical Society, 12*, 3860–3863. <https://doi.org/10.5012/bkcs.2010.31.12.3860>
- 8 Puterová, Z.A., Andicsová, A., Moncol, J., Rabong, C., & Végh, D. (2009). Facile synthesis of α -substituted thiophenes from a functionalized 2-aminothiophene by homo- and cross-coupling reactions. *Tetrahedron Letters, 5*, 4670–4673. <https://doi.org/10.1016/j.tetlet.2009.06.006>
- 9 Heinrich, P., & Schuler, W. (1947). Stabilisierte Diazoniumsalze als Reagenzien zur Bestimmung von Dioxybenzolderivaten. I. Darstellung und Eigenschaften einiger naphthalinsulfosaurer Diazoniumsalze. *Helvetica Chimica Acta, 30*, 886–891. <https://doi.org/10.1002/hlca.19470300326>
- 10 Kozlov, V.V. (1950). Reports on scientific works of D.I. Mendeleev named Union Chemical Society. Academy of Sciences of the USSR, 3, 17 [in Russian].
- 11 Brown, D.M., & Shell, P. (1961). The reaction of hydroxylamine with cytosine and related compounds. *Journal of Molecular Biology, 3*, 709. [https://doi.org/10.1016/S0022-2836\(61\)80038-7](https://doi.org/10.1016/S0022-2836(61)80038-7)
- 12 Weiss, R., Wagner, K.-G., & Hertel, M. (1984). Azodesilylierung — eine neue aprotische Diazotierungstechnik. *Chemische Berichte, 117*, 1965–1972. <https://doi.org/10.1002/cber.19841170525>
- 13 Sigeeva, A.S., Beletskaya, I.P., Petrovskii, P.V., & Peregudov, A.S. (2012). Cu(I)/Cu(II)/TMEDA, New Effective Available Catalyst of Sandmeyer Reaction. *Russian Journal of Organic Chemistry* 8, 1059–1062. <https://doi.org/10.1134/S1070428012080040>
- 14 Picherit, C. (2004). The sequel to a carbocyclic nucleoside synthesis: a divergent access to both arenediazonium ions and aryl triflates / Picherit C., Wagner F., Uguen D. *Tetrahedron Letters, 45*, 2579–2583. <https://doi.org/10.1016/j.tetlet.2004.01.147>
- 15 Nalivela, K.S., Tilley, M., McGuire, M.A., & Organ, M.G. (2014). Multicomponent, flow diazotization Muzoroki-Heck coupling protocol: dispelling myths about working with diazonium salts. *Chemistry — A European Journal, 20*, 1–6. <https://doi.org/10.1002/chem.201402092>
- 16 Kikot, B.S., & Kolesnik, Yu.A. (1963). O diazonievnykh soliakh arilsulfokislota [About diazonium salts of arenesulfonic acids] // Journal organicheskoi khimii — *Journal of Organic Chemistry*, 33, 997–1001 [in Russian].
- 17 Umamoto, T., Adachi, K., & Ishihara, S.J. (2007). CF₃ oxonium salts, O-(trifluoromethyl)dibenzofuranium salts: in situ synthesis, properties, and application as a real CF₃⁺ species reagent. *The Journal of Organic Chemistry* 72, 6905. <https://doi.org/10.1021/jo070896r>
- 18 Knöchel, A.O., & Zwernemann, O. (1986). Development of a NO-carrier added method for ¹⁸F — labeling of aromatic compounds by fluorodediazotization. *Journal of Labelled Compounds and Radiopharmaceuticals* 38, 325–335. [https://doi.org/10.1002/\(SICI\)1099-1344\(199604\)38:4%3C325::AID-JLCR843%3E3.0.CO;2-9](https://doi.org/10.1002/(SICI)1099-1344(199604)38:4%3C325::AID-JLCR843%3E3.0.CO;2-9)
- 19 Nazaretyan, V.P., Volkov, N.D., & Liptuga, N.I. (2006). Benzothiazol-2-yl(difluoro)methanesulfonic acid: Synthesis and reactions. *Russian Journal of Organic Chemistry*, 42, 1188. <https://doi.org/10.1134/S1070428006080148>
- 20 Tang, Z.Y., Zhang, Yu., Wang, T., & Wang, W. (2010). Rhodium (I)-catalyzed synthesis of aryltriethoxysilanes from arenediazonium tosylate with triethoxysilane. *Synlett, 5*, 804–808. <https://doi.org/10.1055/s-0029-1219090>

- 21 Filimonov, V.D., Trusova, M., Postnikov, P., Krasnokutskaya E.A., Lee, Y.M., Hwang, H.Y., Kim, H., & Chi, K.-W. (2008). Unusually stable, versatile, and pure arenediazonium tosylates: their preparation, structures, and synthetic applicability. *Organic Letters*, Vol. 10, 18, 3961–3964. <https://doi.org/10.1021/ol8013528>
- 22 Trusova, M.A., Krasnokutskaya, E.A., Postnikov, P., Choi, Y., Chi, K.-W., & Filimonov, V.D. (2011). Green Procedure for the Diazotization-Iodination of Aromatic Amines under Aqueous, Strong-Acid-Free Conditions. *Synthesis*, 13, 2154–2158. <https://doi.org/10.1055/s-0030-1260046>
- 23 Riss, P.J., Kuschel, S., & Aigbirhio, F. (2012). No carrier-added nucleophilic aromatic radio fluorination using solid phase supported arenediazonium sulfonates and 1-(aryldiazenyl)pipeazines. *Tetrahedron Letters*, 53, 1717–1719. <https://doi.org/10.1016/j.tetlet.2012.01.082>
- 24 Kutonova, K.V., Trusova, M.E., Postnikov, P.S., Filimonov, V.D., & Parello, J.A. (2013). Simple and Effective Synthesis of Aryl Azides via Arenediazonium Tosylates. *Synthesis*, 45, 2706–2710. <https://doi.org/10.1055/s-0033-1339648>
- 25 Velikorodov A.V. Ionova, V.A., Temirbulatova, S.I., & Suvorova, M.A. (2013). Somechemical transformations of alkyl (4-aminophenyl)carbamates. *Russian Journal Organic Chemistry*, Vol. 49, 7, 1007–1008. <https://doi.org/10.1134/S1070428013070087>
- 26 Postnikov, P.S., Trusova, M.E., Feduchak, T.A., Uimin, M.A., Ermakov, A.E., & Filimonov, V.D. (2010). Arenediazonium tosylates as new effective agents of covalent grafting of aromatic groups to carbon shells of metal nanoparticles. *Russian Nanotechnologies in Russia*, 78, 15–16. <https://doi.org/10.1134/S1995078010070037>
- 27 Min, M., Seo, S., Lee, Ju., Lee, S. M., Hwang, E., & Lee, H. (2013). Changes in major charge transport by molecular spatial orientation in graphene channel field effect transistors. *Chemical Communications*, 49, 6289–6291. <https://doi.org/10.1039/C3CC42591F>
- 28 Kutonova, K.V., Trusova, M.E., Stankevich, A.V., Postnikov, P.S., & Filimonov, V.D. (2015). Matsuda–Heck reaction with arenediazonium tosylates in water. *Beilstein Journal Organic Chemistry*, 11, 358–362. <https://doi.org/10.3762/bjoc.11.41>
- 29 Gusel'nikova, O.A., Kutonova, K.V., Trusova M.E., Postnikov, P.S., & Filimonov, V.D. (2014). Synthesis and characterization of the first representatives of arenediazonium dodecylbenzenesulfonates. *Russian Chemical Bulletin*, 1, 289–230. <https://doi.org/10.1007/s11172-014-0427-8>
- 30 Kutonova, K.V., Trusova, M.E., Postnikov, P.S., & Filimonov, V.D. (2012). The first example of the copper-free chloro- and hydrodediazotization of aromatic amines using sodium nitrite, CCl₄, and CHCl₃. *Russian Chemical Bulletin*, 61, 206–208. <https://doi.org/10.1007/s11172-012-0029-2>
- 31 Filimonov, V.D., Kassanova, A.Zh., Krasnokutskaya, E.A., Fedorova, V.A., Stankevich, K.S., Naumov, N.G., Bondarev, A.A., & Kataeva, V.A. (2019). Structure, and Synthetic Potential of Arenediazonium Trifluoromethanesulfonates as Stable and Safe Diazonium Salts. *European Journal Organic Chemistry*, 665–674. <https://doi.org/10.1002/ejoc.201800887>
- 32 Vajpayee, V. Moon, M.E., Lee, S., Ravikumar, S., Kim, H., Ahn, B., Choi, S., Hong, S.H., & Chi, K. -W. (2013). Halogenation and DNA cleavage via thermally stable arenediazonium camphorsulfonate salts. *Tetrahedron*, 69, 3511–3517. <https://doi.org/10.1016/j.tet.2013.02.016>
- 33 Zarei, A.A., Hajipour, A.R., & Khazdooz, L. (2009). One-pot method for the iodination of aryl amines via stable aryl diazonium silica sulfates under solvent-free conditions. *Synthesis*, 941–944. <https://doi.org/10.1055/s-0028-1087981>
- 34 Zarei A., Hajipour, A.R., Khazdooz, L., Mirjalili, B.F., & Najafi, C.A. (2009). Rapid and efficient diazotization and diazo coupling reactions on silica sulfuric acid under solvent-free conditions. *Dyes and Pigments*, 81, 240–244. <https://doi.org/10.1016/j.dyepig.2008.10.011>
- 35 Zarei A., Hajipour A.R., Khazdooz, L., & Aghaei, H. (2009). A fast and efficient method for the preparation of aryl azides using stable aryl diazonium silica sulfates under mild conditions. *Tetrahedron Letters*, 50, 4443–4445. <https://doi.org/10.1016/j.tetlet.2009.05.049>
- 36 Zarei, A., Khazdooz, L., Hajipour, A.R., Aghaei, H., & Azizi, G. (2012). Microwave-assisted click chemistry synthesis of 1,2,3-triazoles from aryldiazonium silica sulfates in water. *Synthesis*, 44, 21, 3353–3360. <https://doi.org/10.1055/s-0032-1316783>
- 37 Zarei, A., Khazdooz, L., Hajipour, A.R., Rafiee F., Azizi, G., & Abrishami, F. (2012). Suzuki-Miyaura cross-coupling of aryldiazonium silica sulfates under mild and heterogeneous conditions. *Tetrahedron Letters*, 53, 406–408. <https://doi.org/10.1016/j.tetlet.2011.11.053>
- 38 Zarei, A., Khazdooz, L., Pirisedigh, A., Hajipour, A.R., Seyedjamali, H., & Aghaei, H. (2011). Aryldiazonium silica sulfates as efficient reagents for Heck-type arylation reactions under mild conditions. *Tetrahedron Letters Vol.* 52, 35, 4554–4557. <https://doi.org/10.1016/j.tetlet.2011.06.095>
- 39 Nemati, F., & Elhampour, A. (2012). Green and efficient diazotization-iodination of aryl amines using cellulose sulfuric acid as a biodegradable and recyclable proton source under solvent-free condition. *Scientia Iranica*, Vol. 19, 6, 1594–1596. <https://doi.org/10.1016/j.scient.2012.10.015>
- 40 Barbero, M., Crisma, M., Degani, I., Fochi, R., & Perracino, P. (1998). New Dry Arenediazonium Salts, Stabilized to an Exceptionally High Degree by the Anion of o-Benzenedisulfonimide. *Synthesis*; 8, 1171–1175. <https://doi.org/10.1055/s-1998-2132>
- 41 Tretyakov, A.N., Krasnokutskaya, E.A., Gorlushko, D.A., Ogorodnikov, V.D., & Filimonov, V.D. (2011). A new one-pot solvent-free synthesis of pyridinyl tosylates via diazotization of aminopyridines. *Tetrahedron Letters*, 52, 85–87. <https://doi.org/10.1016/j.tetlet.2010.10.163>
- 42 Krasnokutskaya, E.A., Kassanova, A.Zh., Estaeva, M.T., & Filimonov, V.D. (2014). A new synthesis of pyridinyl trifluoromethanesulfonates via one-pot diazotization of aminopyridines in the presence of trifluoromethanesulfonic acid. *Tetrahedron Letters*, 55(28), 3771–3773. <https://doi.org/10.1016/j.tetlet.2014.05.052>

- 43 Krasnokutskaya, E.A., Kassanova, A.Zh., Beisembai, P.S., & Filimonov, V.D. (2016). A novel convenient synthesis of pyridinyl and quinolinyltriflates and tosylates via one-pot diazotization of aminopyridines and aminoquinolines in solutions. *Synthesis*, 48, 256–262. <https://doi.org/10.1055/s-0035-1560392>
- 44 Kassanova, A.Zh., Krasnokutskaya, E.A., & Filimonov, V.D. (2016). Pyridinyl trifluoromethanesulfonates: preparation methods and use in organic synthesis. *Russian Chemical Bulletin*, 65(2), 2559–2567. <https://doi.org/10.1007/s11172-016-1619-1>
- 45 Sanzhiev, A.N., Krasnokutskaya, E.A., Erina, K.D., & Filimonov, V.D. (2021). Diazotization of Aminopyridines in the Presence of Camphorsulfonic Acid. Synthesis and Some Properties of Pyridinyl Camphorsulfonates. *Russian Journal of Organic Chemistry*, Vol.57, 6, 922–929. <https://doi.org/10.1134/S1070428021060063>
- 46 Breton, G.W. (2018). DFT study of ortho, meta and para-pyridyl cations. Pyridinium found? *Computational and Theoretical Chemistry*, 1133, 51–58. <https://doi.org/10.1016/j.comptc.2018.04.013>
- 47 Cygler, M., & Przybylska, M. (1982). The crystal structure of benzenediazonium tetrafluoroborate, $C_6H_5N_2^+ \cdot BF_4^-$. *Canadian Journal of Chemistry*, 60, 2852. <https://doi.org/10.1139/v82-407>
- 48 Linderman, S.V., & Kochi, J.K. (2004). Arenediazonium Salts as Versatile (meso-Ionic) Tectons. Charge-Transfer Intercalates and Clathrates in Unusual Crystalline Networks Self-Assembled with Neutral Aromatic π -Donors. *Crystal Growth and Design*, 4 (3), 563–571. <https://doi.org/10.1021/cg034218j>
- 49 Bondarev, A.A., Naumov, E.V., Kassanova, A.Zh., Krasnokutskaya, E.A., Stankevich, K.S., & Filimonov, V.D. (2019). First Study of the Thermal and Storage Stability of Arenediazonium Triflates Comparing to 4-Nitrobenzenediazonium Tosylate and Tetrafluoroborate by Calorimetric Methods. *Organic Process Research & Development*, 23 (11), 2405–2415. <https://doi.org/10.1021/acs.oprd.9b00307>

А.Ж. Касанова, М.Т. Естаева, М.О. Туртубаева

Арендiazоний сульфонаттары: синтездеу, құрылымдық және физика-химиялық қасиеттерін салыстыру

Хош иісті diaзоний тұздары органикалық синтезде маңызды құрылыс материалы болып табылады. Әр түрлі аниондары бар diaзоний тұздарының көп мөлшері белгілі. Мақалада хош иісті diaзоний сульфонаттары қарастырылған: тозилаттар, додецилбензолсульфонаттар, трифлаттар, камфорасульфонаттар, силикатсульфаттар. Мақаланың бірінші бөлімінде осы diaзоний тұздарын синтездеу және қолдану туралы ақпарат берілген. Әдетте, diaзоний тұздарын анилиндерді натрий нитритімен немесе алкил нитритімен тиісті сульфокислоттардың қатысуымен diaзоттау арқылы оңай синтездеуге болады. Бұл diaзоний тұздары хош иісті азидтер, галогендер, триазендер, азо-бояғыштары, стилбендер, биарилдер және т.б. синтездерінде кеңінен қолданылады. Жұмыстың екінші бөлімінде рентгендік талдау, инфрақызыл спектроскопия және термиялық талдау нәтижелерін салыстыру туралы ақпарат келтірілген. Diaзонийдің сульфонат тұздарының құрылымы негізінен классикалық diaзоний тұздарының (хлоридтер, сульфаттар, тетрафторбораттар) құрылымына сәйкес келеді. Сульфонаттардың арендиязонийі мен басқа diaзоний тұздарының арасындағы маңызды айырмашылық олардың жарылыс қауіпсіздігі мен тұрақтылығы болып табылады. Арендiazоний тозилаттар, трифлаттар және камфорасульфонаттар суда да, полярлы органикалық еріткіштерде де оңай ериді. Арендiazоний додецилбензолсульфонаттары липофильді анионға байланысты полярлы емес органикалық ортада ериді. Арендiazоний сульфонат тұздарының бұл ерекшеліктері қышқыл анионының diaзоний тұздарының тұрақтылығына, ерігіштігіне және реактивтілігіне әсер ету ерекшеліктерін түсіну үшін өте маңызды.

Кілт сөздер: diaзоний тұздары, diaзоттау, сульфонаттар, тозилаттар, трифлаттар, камфорасульфонаттар, силика-сульфаттар, додецилбензолсульфонаттар, рентген-құрылымдық талдау.

А.Ж. Касанова, М.Т. Естаева, М.О. Туртубаева

Арендiazоний сульфонаты: синтез, сравнение структурных и физико-химических свойств

Ароматические соли diaзония являются важными строительными блоками в органическом синтезе. Известно большое количество солей diaзония с разными анионами-остатками. В данном обзоре рассмотрены ароматические diaзоний сульфонаты: тозилаты, додецилбензолсульфонаты, трифлаты, камфорасульфонаты, силика-сульфаты. В первой части статьи представлены сведения по синтезу и применению данных солей diaзония. Показано, что, как правило, указанные соли diaзония легко синтезируются diaзотированием анилинов нитритом натрия или алкилнитритами в присутствии соответствующих сульфокислот с высокими выходами. Данные соли diaзония нашли широкое применение в синтезе ароматических азидов, галогенидов, триазенов, азокрасителей, стильбенов, биариллов и т.д. Аминопиридины diaзотируются в присутствии сульфокислот с образованием других важных полу-

продуктов органического синтеза — пиридинилсульфонатов. Во второй части обзора дана информация по сравнению результатов рентгеноструктурного анализа, инфракрасной спектроскопии и термического анализа. Строение сульфонатных солей диазония в основном соответствует строению классических солей диазония (хлориды, сульфаты, тетрафторбораты). Существенным отличием арендиазоний сульфонатов от других солей диазония являются их взрывобезопасность и стабильность в индивидуальном виде. Арендиазоний тозилаты, трифлаты и камфорасульфонаты легко растворяются как в воде, так и в полярных органических растворителях. Арендиазоний додецилбензолсульфонаты, благодаря липофильному аниону, растворимы в неполярных органических средах. Эти особенности сульфонатных солей очень важны для понимания влияния аниона кислоты на устойчивость, растворимость и реакционную способность диазониевых солей.

Ключевые слова: соли диазония, диазотирование, сульфонаты, тозилаты, трифлаты, камфорасульфонаты, силика-сульфаты, додецилбензолсульфонаты, рентгеноструктурный анализ.

Information about authors

Kassanova, Assiya Zhursunovna (corresponding author) — Candidate of chemical sciences, Associate Professor, Toraighyrov University, Lomov street, 64, 140008, Pavlodar, Kazakhstan; National Research Tomsk Polytechnic University, Tomsk, Russia; e-mail: asiyakass@mail.ru; <http://orcid.org/0000-0002-9563-5521>;

Yestayeva, Makpal Tlemisovna — Senior Lecturer, Researcher, Toraighyrov University, Lomov street, 64, 140008, Pavlodar, Kazakhstan; e-mail: estaeva_makpal@mail.ru; <http://orcid.org/0000-0003-2127-3465>;

Turtubaeva, Meruyert Orazgalievna — PhD, Senior Researcher, S.D. Asfendiyarov Kazakh National Medical University, Almaty, Tole bi street, 94, 050012; Toraighyrov University, Lomov street, 64, 140008, Pavlodar, Kazakhstan; e-mail: azat-2000@bk.ru; <http://orcid.org/0000-0001-7932-5075>.

S.S. Mendigalieva¹, D.A. Birimzhanova¹, I.S. Irgibaeva^{1*},
N.N. Barashkov², Y.E. Sakhno³

¹*L.N. Gumilyov Eurasian National University, Nur-Sultan, Kazakhstan;*

²*Micro Tracers, Inc., San Francisco, California, USA;*

³*University of Delaware, Newark, Delaware, USA*

(*Corresponding author's e-mail: irgsm@mail.ru)

Aggregation-induced emission of 5-(benzylidene)pyrimidine-2,4,6-triones

5-(Benzylidene)pyrimidine-2,4,6-triones with different substituents on the phenyl rings: 5-(4'-dimethylaminobenzylidene) barbituric acid and 5-(4'-methoxybenzylidene) barbituric acid were synthesized, and their spectral-luminescent properties were investigated. A decreasing fluorescence efficiency in the solid-state is general and is mainly attributed to the intermolecular vibronic interactions, which induce the nonradiative deactivation process. Whereas the isolated dye molecules are virtually non-luminescent in dilute solutions, they become highly emissive upon solution thickening or aggregation in poor solvents or in the solid-state, show an increase of luminescence intensity, the phenomenon of the aggregation-induced emission (AIE phenomenon). The development of efficient luminescent materials is a topic of great current interest. The emission color is changed from red (maximum at 630 nm) to green (maximum at 540 nm) by varying the substituent on the phenyl ring from dimethylamino to the methoxy group. Theoretical calculation shows that the dye molecules' aggregation-induced emission characteristics result from intermolecular interactions. Utilizing such features, the molecules can be employed as fluorescent probes for the detection of the ethanol content in aqueous solutions.

Keywords: aggregation-induced emission, barbituric acid, fluorescent probes, fluorescence peak intensities, luminophore, dye molecules, substituent phenyl ring, solid state, intramolecular rotations.

Introduction

Whereas light emissions of luminophores are normally investigated in the solution state, they are practically used as materials commonly in the solid-state [1]. The formation of aggregates with an ordered or random structure in the solid-state is facilitated by the close proximity of molecules that experience strong π - π stacking interactions. The nonradiative decay of the excited state of molecules is often caused by aggregation-caused quenching (ACQ) of light radiation in the condensed phase.

Various chemical, physical, and engineering approaches and processes have been developed to eliminate the effect of ACQ, but attempts have met with only limited success [2].

It would be good if a system can be developed in which light emission is enhanced, rather than quenched, by aggregation because no additional effect will need to be placed to artificially interrupt the very natural process of luminophore aggregation.

Recently, Tang and co-workers found that the fluorescence of some molecules was weak in dilute solutions but became strong when they were in aggregate states [2–4]. The restriction of intramolecular rotation is responsible for such effects. This effect is called Aggregation-Induced Emission (AIE). Utilizing the AIE characteristics, many authors explored potential applications of the AIE luminogens as chemical sensors [5], biological probes [6, 7], smart nanomaterials [8–10], and solid-state emitters [11–15].

We are interested in expanding the AIE system to cover the whole visible spectral region. In this work, we designed and synthesized two derivatives of barbituric acid (Figure 1) and reported their AIE effect. Firstly, the AIE in derivatives of barbituric acid was reported by Barashkov, Bolotin, and Tang in 2004 [16]. Later, these derivatives became the subjects of the number of publications [17, 18]. By changing the substituent on the phenyl group, the conjugation and hence the emission color of the luminophore can be varied. The molecules can be employed as fluorescent probes and can detect the ethanol contents in ethanol-water mixtures [19–23].

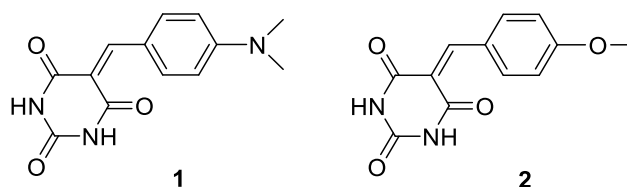


Figure 1. Molecular structures of the pyrimidine-2,4,6-triones derivatives 1 and 2

Experimental

Materials and Instrumentation. Tetrahydrofuran (THF; Labscan), methanol (RDH), *N,N*-dimethylformamide (DMF, Labscan), and other solvents were used as received without further purification. Barbituric acid (pyrimidine-2,4,6-trione), 4-dimethylaminobenzaldehyde, 4-methoxybenzaldehyde were purchased from Aldrich and used without further treatment.

UV absorption spectra were measured on a Milton Roy Spectronic 3000 Array spectrophotometer. Photoluminescence (PL) spectra were recorded on Perkin Elmer LS 55 Fluorescence spectrometer or Hitachi Fluorescence Spectrophotometer F-2000. Particle size measurements were performed on a Beckman Coulter Delsa 440SX Zeta potential analyzer. Scanning electron microscope (SEM) image was taken on a JEOL JSM-7500F electron microscope.

Synthesis. Dye **1** and **2**, namely 5-[(4-dimethylamino)benzylidene]pyrimidine-2,4,6-trione and 5-[(4-methoxy)benzylidene]pyrimidine-2,4,6-trione, were prepared by coupling reaction of barbituric acid with 4-dimethylaminobenzaldehyde and 4-methoxybenzaldehyde in an ethanol solution of sodium hydroxide (Scheme 1). A typical procedure for the synthesis of **1** is given below.

8.96 g (0.07 mol) barbituric acid, 120 mL ethanol, 11.92 g (0.08 mol) 4-dimethylaminobenzaldehyde and 1.2 mL 10 % aqueous solution of sodium hydroxide were added into a 250 mL round-bottom flask. After stirring for 4 h at 80–85 °C, the solution was filtered. The residue was washed with hot water and then ethanol, and dried in vacuum. Dye **1** was obtained as red powder with a yield of 88 %. ¹H NMR (400 MHz, DMSO-*d*₆), δ (ppm): 3.12 (s, 6H), 6.80 (d, 2H), 8.15 (s, 1H), 8.42 (d, 2H), 10.92 (s, 1H), 11.03 (s, 1H). ¹³C NMR (100 MHz, DMSO-*d*₆), δ (ppm): 39.71, 109.53, 111.20, 119.98, 139.05, 150.31, 154.18, 155.48, 162.70, 164.70. Dye **2** was prepared similarly from 8.96 g (0.07 mol) of barbituric acid and 10.88 g (0.08 mol) of 4-methoxybenzaldehyde and isolated as yellow-green powder with a yield of 86 %. ¹H NMR (400 MHz, DMSO-*d*₆), δ (ppm): 3.86 (s, 3H), 7.15 (d, 2H), 8.43 (d, 2H), 8.24 (s, 1H), 11.04 (s, 1H), 11.17 (s, 1H). ¹³C NMR (100 MHz, DMSO-*d*₆), δ (ppm): 55.70, 113.95, 115.54, 125.16, 137.48, 150.20, 154.98, 162.17, 163.46, 163.92.

Results and Discussion

Synthesis and Absorption. To enrich the family of AIE-active molecules, we obtained two pyrimidine-2,4,6-triones (**1** and **2**) with different substituents on the phenyl rings according to Figure 1. While the dye-containing dimethylamino group appears red, that with methoxy substituent is greenish-yellow.

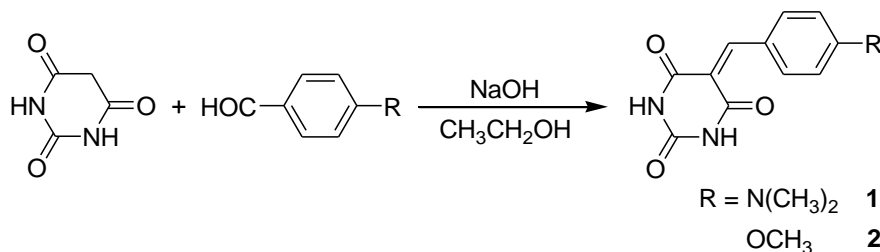
Figure 1. Synthesis of dye **1** and **2**

Figure 2 shows the absorption spectra of **1** and **2** in different solvents. In chloroform, **1** absorbs at 468 nm. The spectrum shifts to shorter wavelengths when the solvent is changed to ethyl acetate and THF. In methanol, the absorption maximum (λ_{ab}) is located at a wavelength similar to that in chloroform. To correlate the position of the λ_{ab} with the solvent, we performed additional measurements and checked the orientation polarizabilities (Δf) of the solvents. The results are summarized in Table 1. In solvents with “lower” and

“higher” polarities, such as chloroform and methanol, **1** shows redder absorption. Since **1** has a high dipole moment, it can be better solvated in highly polar solvents. The good solvation of the molecule enables better planarity and hence shifts the λ_{ab} to the longer wavelengths. On the contrary, the solvating ability of chloroform is comparatively less, but it disturbs little the hydrogen bonding between molecules of **1**. Thus, the λ_{ab} is found in the redder region. A similar change in the absorption behavior with the solvent polarity is also observed in **2**. The λ_{ab} is located at much shorter wavelengths because the electron-donating ability of the methoxy group of **2** is weaker than the dimethylamino moiety in **1**, which has thus lowered its conjugation.

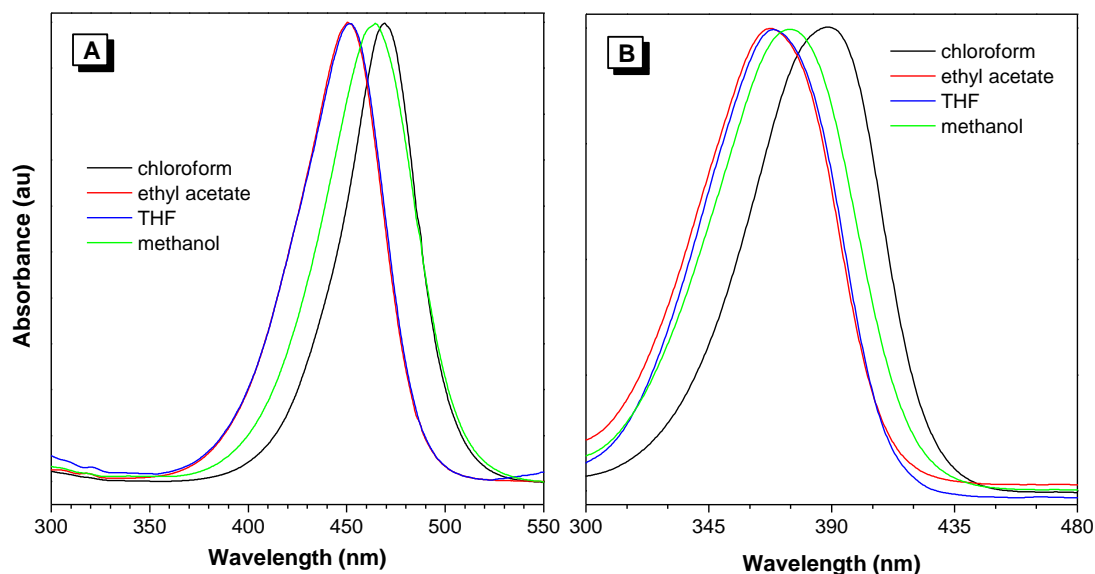


Figure 2. UV spectra of (A) **1** and (B) **2** in different solvents. Concentration: 25 μ M.

Table 1

Absorption of 1 and 2 in Nonhalogenated and Chlorinated Solvents with Different Polarities^a

| Solvent | Δf | λ_{ab} (nm) | |
|---------------|------------|---------------------|----------|
| | | 1 | 2 |
| Ethyl acetate | 0.199 | 450 | 367 |
| THF | 0.210 | 452 | 368 |
| DMF | 0.275 | 460 | 370 |
| Acetonitrile | 0.305 | 461 | 372 |
| Methanol | 0.308 | 465 | 375 |
| Chloroform | 0.148 | 468 | 388 |

Note: ^a In solutions with a dye concentration of 25 μ M.

Abbreviation: λ_{ab} = absorption maximum, Δf = orientation polarizability = $[(\epsilon - 1)/(2\epsilon + 1)]/[(\eta^2 - 1)/(2\eta^2 + 1)]$ (ϵ and η are the dielectric constant and refractive index of the solvent) [16, 17].

Light Emission. We then investigated the photoluminescence (PL) of **1** in different organic solvents. In chloroform, **1** exhibits a weak emission at 535 and 630 nm, which can hardly be observed (Figure 3). In more polar solvents, such as THF and methanol, the PL spectrum varies little but displays only broadband at 507 and 539 nm, respectively. The small influence of solvent polarity on the luminescence of **1** suggests that its dipole is too small and leads to a normal π - π^* instead of an intramolecular charge transfer singlet-excited state observed in highly polarized molecules.

The peak at 630 nm in chloroform is due to the aggregate emission of **1** because it is intensified when the solution is concentrated (Figure 2B). The absence of such emission in THF and methanol suggests that **1** is still molecularly dissolved in the solutions. A much higher dye concentration is required for aggregate formation in these solvents.

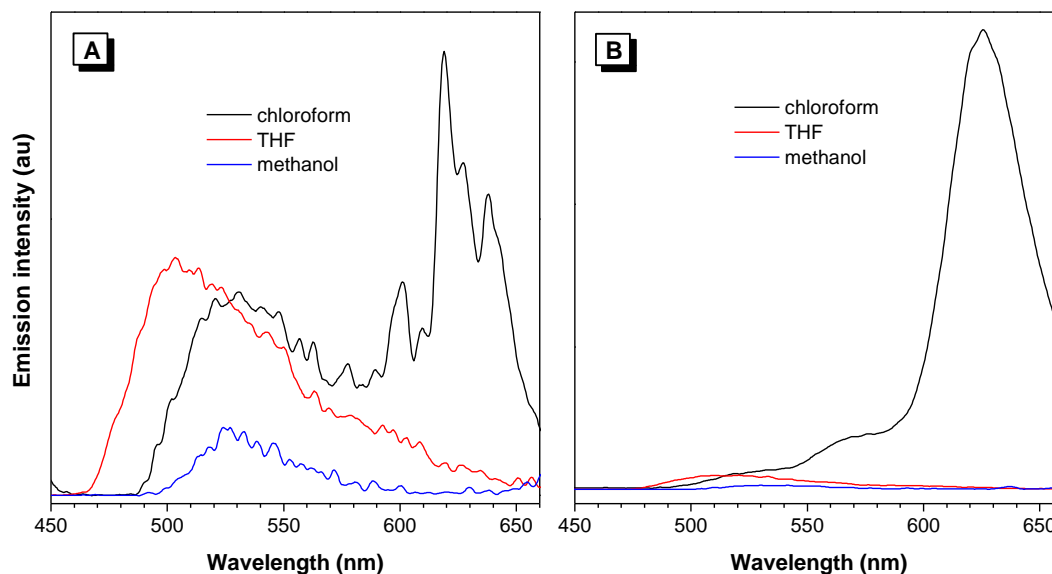


Figure 3. Photoluminescence spectra of **1** in different solvents.
Concentration (μM): (A) 5 and (B) 10. Excitation wavelength: 350 nm

To have a more detailed investigation, we prepared solutions of **1** in THF with different concentrations and measured the PL change (Figure 4). When the solution concentration becomes higher, the broad peak centered at ~ 500 nm is intensified and progressively shifts to the longer wavelengths. At a concentration of $250 \mu\text{M}$, the PL is located at 628 nm, which is 100 nm red-shift from that at $100 \mu\text{M}$. The peak intensity is 10-fold higher, revealing that the emission of **1** is enhanced instead of quenched by aggregate formation. In other words, **1** displays a phenomenon of aggregation-induced emission (AIE). Dye **2** is also AIE-active. In chloroform, it emits at 552 nm, which intensifies when the solution concentration is increased (Figure 5).

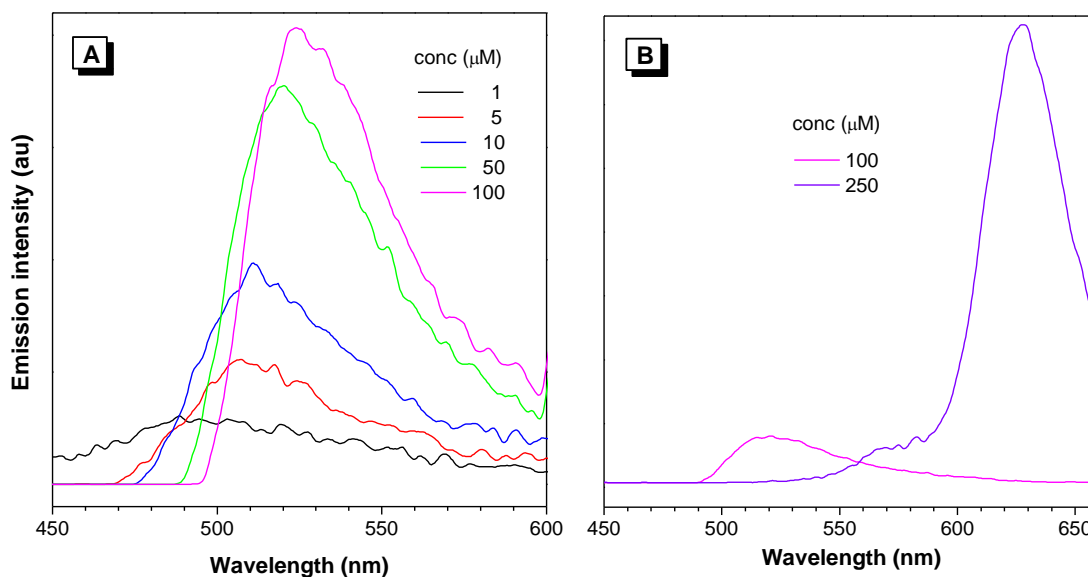


Figure 4. Photoluminescence spectra of THF solutions of **1** with different concentrations.
Excitation wavelength: 350 nm

All the above data indicate that **1** and **2** emit weakly in the dilute solutions but become strong emitters upon aggregation in concentrated solutions [24, 25]. If so, they should also emit intensely in the solid state, since the molecules are in close vicinity in the condensed phase. As expected, powders **1** and **2** give strong red and green lights upon photoexcitation, whose emission maxima are located at the same wavelengths as in concentrated solutions (Figure 6).

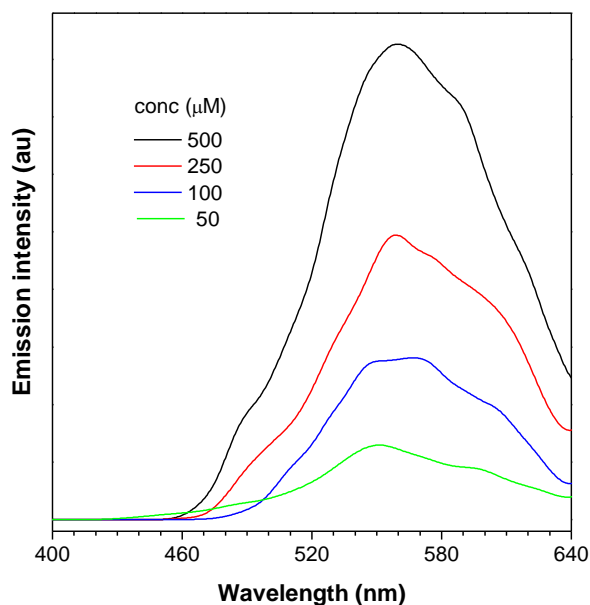


Figure 5. Photoluminescence spectra of chloroform solutions of **2** with different concentrations. Excitation wavelength: 330 nm

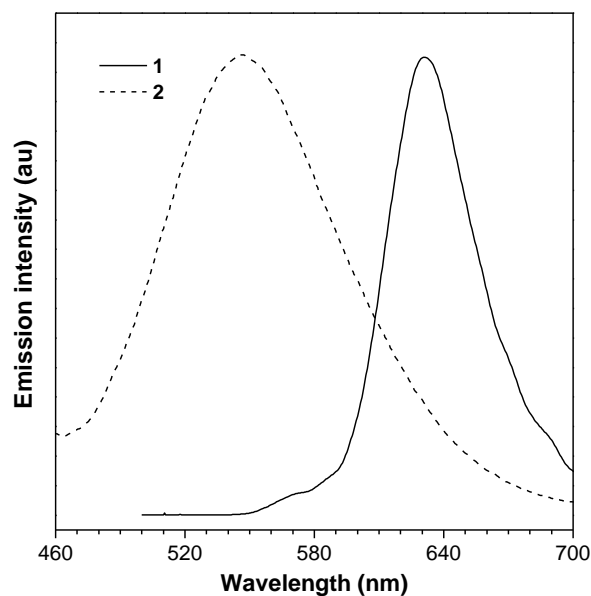


Figure 6. Emission spectra of solid powders of **1** and **2**. Excitation wavelength (nm): 452 (**1**), 368 (**2**)

Figure 7 shows the visual observations of THF solutions and solid powders of **1** and **2** under UV irradiation. Whereas the THF solutions of **1** and **2** are transparent, strong red and green emissions are observed in their solid powders.

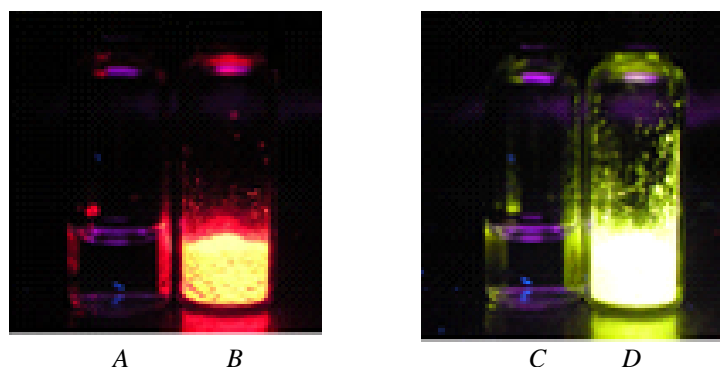


Figure 7. Photographs of (A and C) dilute THF solutions and (B and D) solid powders of **1** (left) and **2** (right) taken under UV light

To determine **1** and **2** are AIE-active, we added water into their THF solutions and studied their PL. Since water does not dissolve **1** and **2**, the dye molecules should be aggregated in THF/water mixtures with high water fractions. Figure 8A depicts the PL spectra of **1** in THF/water mixtures with different water contents. The emission of the solution is enhanced in water and reaches its maximum intensity at 60 % water content (Figure 8B). However, a further increase in the amount of water led to a decrease in the PL intensity, probably due to the change in the packing order of the aggregates from a crystalline to an amorphous state. In the mixture with “lower” water content, the molecules of **1** can slowly assemble in an ordered manner to form more emissive crystalline clusters. In contrast, the dye molecules can abruptly agglomerate in the mixture with a very high water fraction to form less emissive amorphous powders.

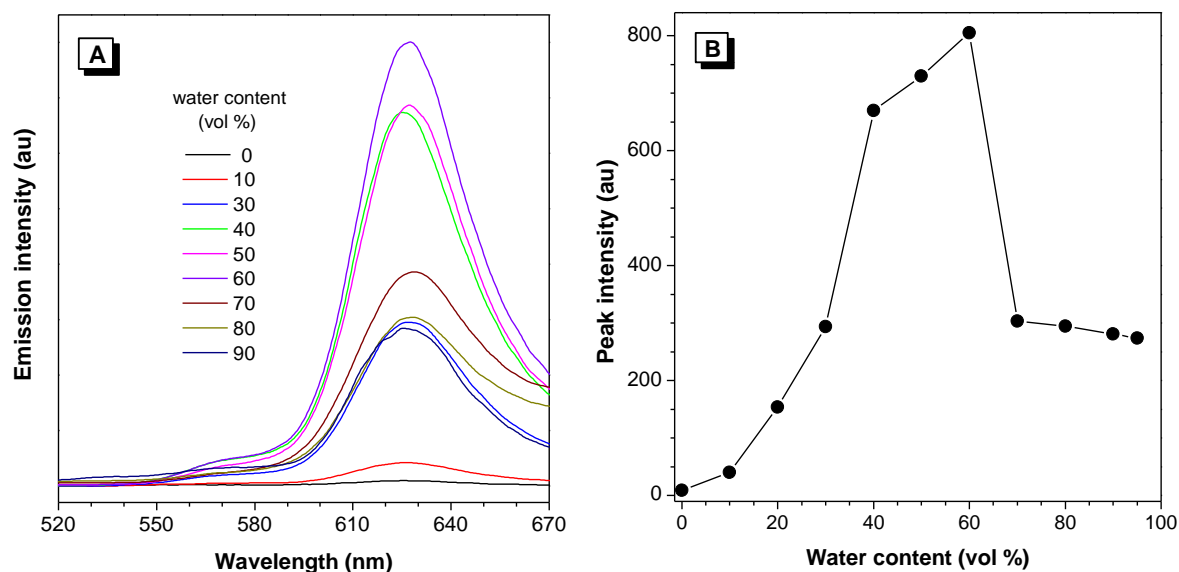


Figure 8. (A) Photoluminescence spectra of **1** in THF/water mixtures with different water contents. (B) Plot of fluorescence peak intensities versus water contents in THF/water mixtures. Concentration: 2.5×10^{-3} M; excitation wavelength: 350 nm

The PL of **2** in THF also becomes stronger when water is added. The peak intensity remains almost unchanged in the presence of up to 70 % water in the solvent mixture, but after that, it starts to increase rapidly (Figure 9). At 90 % water content, the intensity is more than 800 times higher than that of a pure THF solution. Similar to **1**, the emission becomes weaker as more water is added.

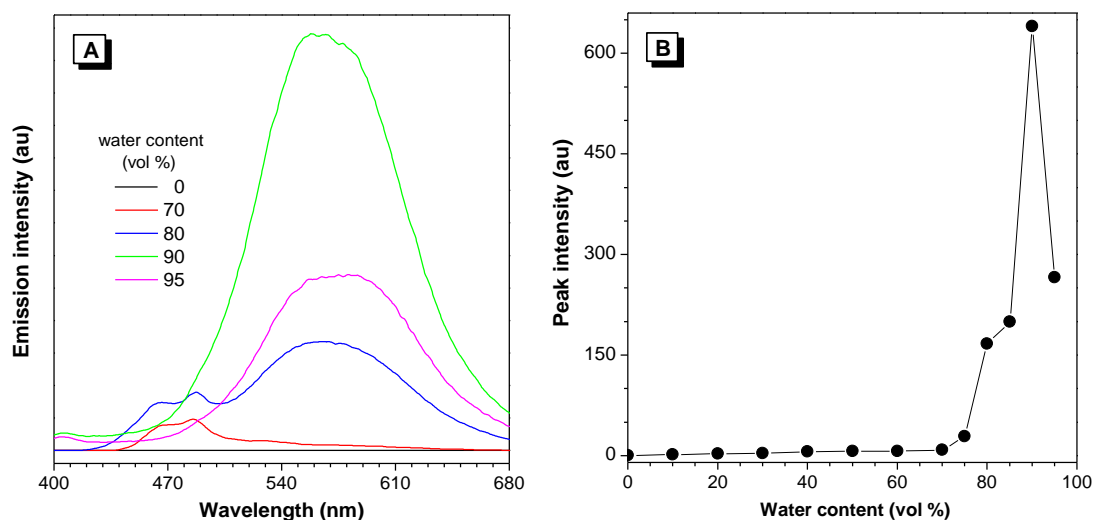


Figure 9. (A) PL spectra of **2** in THF/water mixtures with different water fractions. (B) Plot of fluorescence peak intensities versus water contents in THF/water mixtures. Concentration: 5×10^{-3} M; excitation wavelength: 368 nm

As shown in Figures 8, 9, the emission intensity of solutions **1** and **2** rises with an increase in the concentration of the non-solvent, while the wavelength of the maximum of the luminescence remains unchanged. This is the main difference between the AEE effect and the solvatochromism effect, in which the luminescence wavelength changes with an increase in the concentration of the non-solvent [26, 27].

It should be noted that even at water content as high as 90 %, the THF/water mixtures **1** and **2** remain visually transparent and macroscopically homogeneous. This suggests that the aggregates of molecules should be nanosized. Indeed, we measured the aggregate sizes and found that the particles of **1** and **2** in THF/water mixtures with 90 % water are in the range of 140–200 nm (Figure 10).

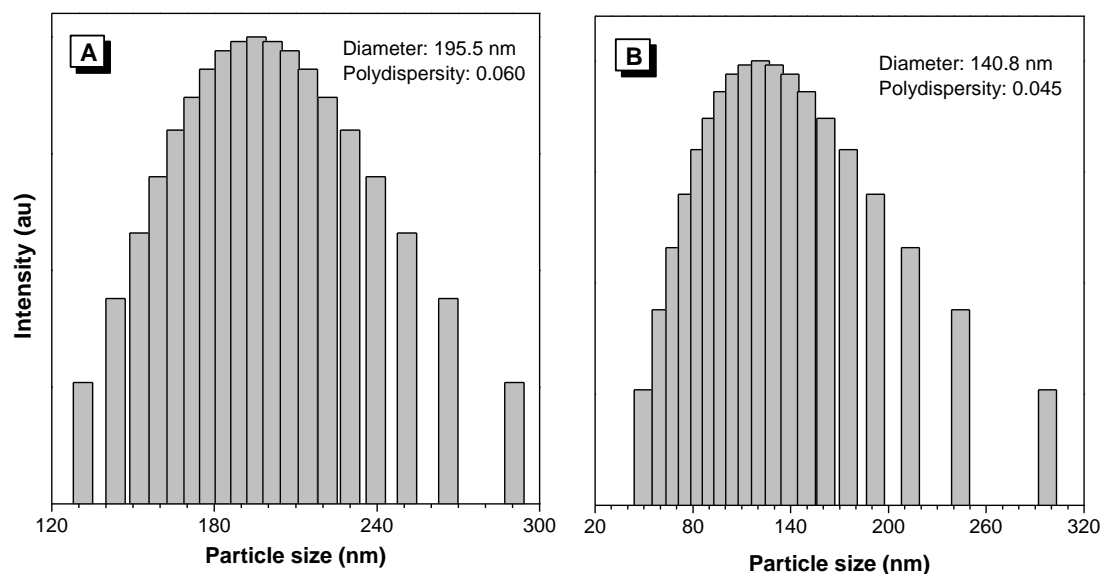


Figure 10. Particle distributions of (A) **1** and (B) **2** in THF/water mixtures with 90 % water. Concentration: 10^{-3} M

Mechanism. For some molecules, such as siloles, the AIE feature is believed to be the result of intramolecular rotation restriction, which shuts down nonradiative relaxation processes and thus boosts their PL emissions. To evaluate this possibility, we doped **1** and **2** into poly(methyl methacrylate) films (1 %), which function as a kind of solid solvent to separate the dye molecules and impede molecular motions at the same time. PL signals cannot be captured from the doped films. Thus, in contrast to their silole congeners, the AIE feature of **1** and **2** should result from intermolecular interactions rather than the restriction of intramolecular rotations.

We carried out quantum chemical calculations using the ZINDO method to further study the structures and optical properties of the dye molecules. Figure 11 shows a sandwich model of an aggregate of **1** formed by intermolecular hydrogen bonds and donor-acceptor interactions. The preferred distance between molecules of **1** in the same plane is 2.6 Å, indicating the existence of strong edge-to-edge interaction or *J*-aggregation. The HOMO is mainly located on the dimethylamino group, while the LUMO is situated on the pyrimidine-2,4,6-trione ring. The absorption band undergoes a bathochromic shift when more molecules are clustered together. For instance, the aggregate formed by 10 molecules of **1** absorbs at 442 nm, close to its experimental value.

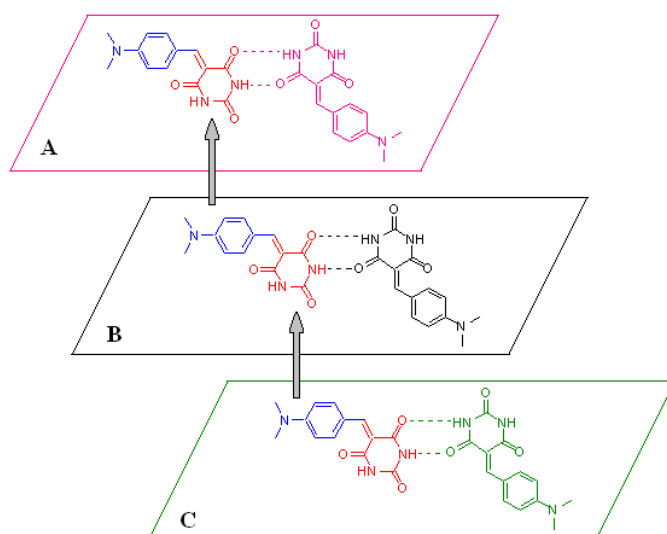


Figure 11. Aggregate formation of molecules **1** via intermolecular hydrogen bonds and D-A interactions in different planes (A, B, and C)

Fluorescence probe. The AIE characteristic has encouraged us to use it as a fluorescent probe to detect the ethanol content in water solution [16]. Since **1** is slightly soluble in ethanol, we prepared a solution of **1** in *N*-methylpyrrolidone and investigated the PL change by adding ethanol/water mixtures with varying ethanol content. The emission intensity increases when the mixture's ethanol fraction is changed from 67 to 40 % (Figure 12). This is understandable since the solvation of the solution becomes poorer progressively, which encourages the aggregation of the molecules of **1**. Through such measurements, a linear dependence of the fluorescence intensity on the ethanol content was established (Figure 12B).

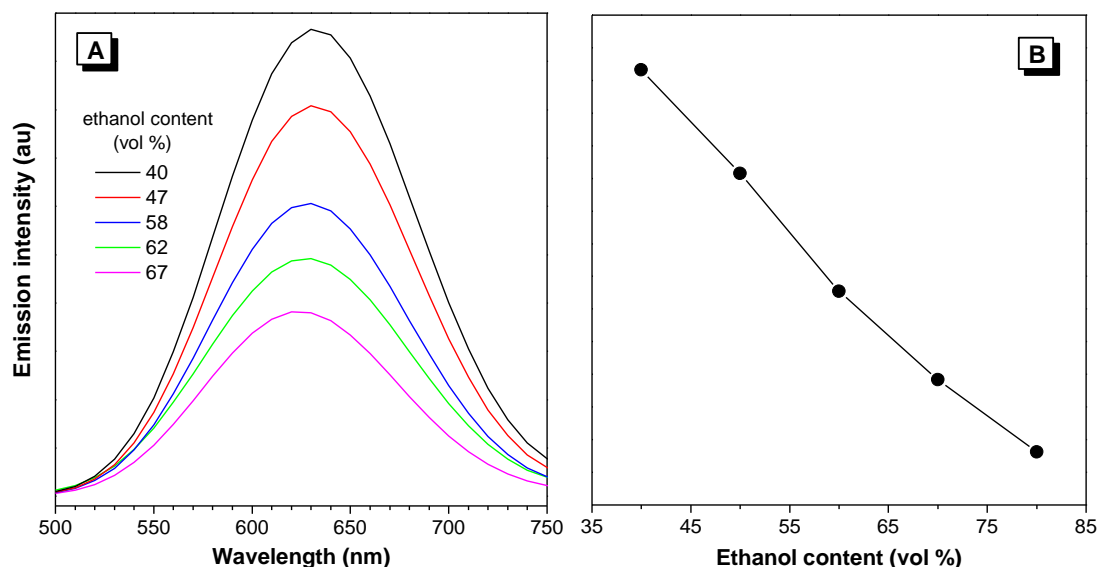


Figure 12. (A) Change in photoluminescence of **1** in *N*-methylpyrrolidone solution upon addition of ethanol/water mixtures with different ethanol contents. Concentration of **1**: 0.13 %; excitation wavelength: 405 nm. The ratio between *N*-methylpyrrolidone and ethanol/water mixture was kept at 3:1 by weight in all measurements. (B) Dependence of fluorescence intensity at 644 nm on the ethanol contents for ethanol/water mixtures

Conclusions

In this work, 5-(benzylidene)pyrimidine-2,4,6-triones with different substituents on the phenyl rings were synthesized, and their optical properties were investigated. Whereas the isolated molecules of **1** and **2** are virtually non-luminescent in dilute solutions, they become highly emissive upon solution thickening or aggregation in poor solvents or the solid-state, demonstrating the AIE phenomenon. The color of the AIE of the dye molecules can be varied by changing the substituent on the phenyl ring. While **1** with a dimethylamino group exhibits red emission, the molecule substituted with methoxy functionality (i.e., **2**) emits green light upon photoexcitation. Analysis by theoretical calculation reveals the strong dependence of the emission of **1** and **2** on their molecular packing. The dye molecules can act as a fluorescent probe and determine the ethanol content in an aqueous solution.

Acknowledgments

The author are grateful to Professor Ben Zhong Tang and his colleagues from the Department of Chemistry, Hong Kong University of Science & Technology for their help in performing this study.

References

- 1 Birks, J.B. (1970). *Photophysics of Aromatic Molecules*. Wiley-VCH Verlag GmbH & Co. KGaA, Vol. 74, 704 pp. <https://doi.org/10.1002/bbpc.19700741223>
- 2 Luo, J., Xie, Z., Lam, J.W.Y., Cheng, L., Chen, H., Qiu, C., Kwok, H.S., Zhan, X., Liu, Y., Zhu, D., & Tang, B.Z. (2001). Aggregation-induced emission of 1-methyl-1,2,3,4,5-pentaphenylsilole. *Chem. Commun.* 2001, 18, 1740–1741. <https://doi.org/10.1039/B105159H>

- 3 Hong, Y., Lam, J.W.Y., & Tang, B.Z. (2011). Aggregation-induced emission. *Chem. Soc. Rev.*, 40 (11), 5361–5388. <https://doi.org/10.1039/C1CS15113D>
- 4 Liu, Y., Tang, Y., Barashkov, N.N., Irgibaeva, I.S., Lam, J.W.Y., Hu, R., Birimzhanova, D., Yu, Y., & Tang, B.Z. (2010). Fluorescent chemosensor for detection and quantitation of carbon dioxide gas. *J. Am. Chem. Soc.*, 132, 13951–13953. <https://doi.org/10.1021/ja103947j>
- 5 Shi, W., Zhao, S., Su, Y., Hui, Y., & Xie, Z. (2016). Barbituric acid-triphenylamine adduct as an AIEE-type molecule and optical probe for mercury (II). *New J. Chem.*, 40 (9), 7814–7820. <https://doi.org/10.1039/C6NJ00894A>
- 6 Korneev, O.V., Sakhno, T.V., & Korotkova, I.V. (2019). Nanoparticles-based photosensitizers with effect of aggregation-induced emission. *Biopolymers and Cell. Vol. 35. N 4.* 249–267 doi: <http://dx.doi.org/10.7124/bc.000A08>
- 7 Zhang, H., Guo, L., Xie, Z., Xin, X., Sun, D., & Yuan, S. (2016). Tunable aggregation-induced emission of polyoxometalates via amino acid-directed self-assembly and their application in detecting dopamine. *Langmuir*, 32 (51), 13736–13745. <https://doi.org/10.1021/acs.langmuir.6b03709>
- 8 Liang, G.D., Weng, L.-T., Lam, J.W.Y., Qin, W., & Tang, B.Z. (2014). Crystallization-induced hybrid nano-sheets of fluorescent polymers with aggregation-induced emission characteristics for sensitive explosive detection. *ACS Macro Lett.*, 3 (1), 21–25. <https://doi.org/10.1021/mz4005887>
- 9 Wang, X., Song, P., Peng, L., Tong, A., & Xiang, Y. (2016). Aggregation-induced emission luminogen-embedded silica nanoparticles containing DNA aptamers for targeted cell imaging. *ACS Appl. Mater. Interfaces*, 8 (1), 609–616. <https://doi.org/10.1021/acsami.5b09644>
- 10 Goswami, N., Yao, Q., Luo, Z., Li, J., Chen, T., & Xie, J. (2016). Luminescent metal nanoclusters with aggregation-induced emission. *J. Phys. Chem. Lett.*, 7 (6), 962–975. <https://doi.org/10.1021/acs.jpcclett.5b02765>
- 11 Mei, Ju., Leung, Nelson Lik Ching., Kwok, Tsz Kin., Lam, Wing Yip., & Tang, Benzong (2015). Aggregation-Induced Emission: Together We Shine, United We Soar! *Chemical Reviews*, 115, (21), 11718–11940. <https://doi.org/10.1021/acs.chemrev.5b00263>
- 12 Yuan, W.Z., Yu, Z.-Q., Tang, Y., Lam, J.W.Y., Xie, N., Lu, P., Chen, E.-Q., & Tang, B.Z. (2011). High solid-state efficiency fluorescent main chain liquid crystalline polytriazoles with aggregation-induced emission characteristics. *Macromolecules*, 44 (24), 9618–9628. <https://doi.org/10.1021/ma2021979>
- 13 Marafie, J.A., Bradley, D.D.C., & Williams, C.K. (2017). Thermally stable zinc disalphen macrocycles showing solid-state and aggregation-induced enhanced emission. (2017). *Inorg. Chem.*, 56 (10), 5688–5695. <https://doi.org/10.1021/acs.inorgchem.7b00300>
- 14 An, P., Shi, Z.-F., Dou, W., Cao, X.-P., & Zhang, H.-L. (2010). Synthesis of 1,4-bis[2,2-bis(4-alkoxyphenyl)vinyl]benzenes and side chain modulation of their solid-state emission. *Org. Lett.*, 12 (19), 4364–4367. <https://doi.org/10.1021/ol101847w>
- 15 Zhang, P., Liu, W., Niu, G., Xiao, H., Wang, M., Ge, J., Wu, J., Zhang, H., Li, Y., & Wang, P. (2017). Coumarin-based boron complexes with aggregation-induced emission. *J. Org. Chem.*, 82 (7), 3456–3462. <https://doi.org/10.1021/acs.joc.6b02852>
- 16 Barashkov, N., Bolotin, B., Tang, B., Peng, H., & Chen, J. (2004). *U.S. Patent No. 20040157334 (A1)*.
- 17 Wang, E., Lam, J.W.Y., Hu, R., Zhang, C., Zhao, Y.S., & Tang, B.Z. (2014). Twisted intramolecular charge transfer, aggregation-induced emission, supramolecular self-assembly and the optical waveguide of barbituric acid-functionalized tetraphenylethene. *J. Mater. Chem. C*, 2 (10), 1801–1807. <https://doi.org/10.1039/C3TC32161D>
- 18 Zhu, Z., Qian, J., Zhao, X., Qin, W., Hu, R., Zhang, H., Li, D., Xu, Z., Tang, B.Z., & He, S. (2016). Stable and size-tunable aggregation-induced emission nanoparticles encapsulated with nanographene oxide and applications in three-photon fluorescence bioimaging. *ACS Nano*, 10 (1), 588–597. <https://doi.org/10.1021/acs.nano.5b05606>
- 19 Loboda, O., Minaev, B., Vahtras, O., Schimmelpfennig, B., Ågren, H., & Ruud, K. (2003). Ab initio calculations of zero-field splitting parameters in linear polyacenes. *Chemical physics*, 286 (1), 127–137. DOI: [10.1016/S0301-0104\(02\)00914-X](https://doi.org/10.1016/S0301-0104(02)00914-X)
- 20 Dong, Y., Lam, J.W.Y., Qin, A., Sun, J., Liu, J., Li, Z., Sun, J., Sung, H.H.Y., Williams, I.D., Kwok, H.S., & Tang, B.Z. (2007). Aggregation-induced and crystallization-enhanced emissions of 1,2-diphenyl-3,4-bis(diphenylmethylene)-1-cyclobutene. *Chem. Commun.*, 31, 3255–3257. <https://doi.org/10.1039/B704794K>
- 21 Qin, A., Jim, C.K.W., Lu, W., Lam, J.W.Y., Häußler, M., Dong, Y., Sung, H.H.Y., Williams, I.D., Wong, G.K.L., & Tang, B.Z. (2007). Click polymerization: facile synthesis of functional poly(aryltriazole)s by metal-free, regioselective 1,3-dipolar polycycloaddition. *Macromolecules*, 40 (7), 2308–2317. <https://doi.org/10.1021/ma062859s>
- 22 Minaev, B., Knuts, S., Ågren, H., & Vahtras, O. (1993). The vibronically induced phosphorescence in benzene. *Chemical physics*, 175 (2-3), 245–254.
- 23 Xu, J., Liu, X., Lv, J., Zhu, M., Huang, C., Zhou, W., Yin, X., Liu, H., Li, Y., & Ye, J. (2008). Morphology transition and aggregation-induced emission of an intramolecular charge-transfer compound. *Langmuir*, 24 (8), 4231–4237. <https://doi.org/10.1021/la703662w>
- 24 Zhang, H.-J., Tian, Y., Tao, F., Yu, W., You, K.-Y., Zhou, L.-R., Su, X., Li, T., & Cui, Y.-Z. (2019). Detection of nitroaromatics based on aggregation induced emission of barbituric acid derivatives. *Spectrochimica Acta Part A: Molecular and Biomolecular Spectroscopy*, 222, 117168. <https://doi.org/10.1016/j.saa.2019.117168>
- 25 Xi, J., Zhang, H., Xu, Z., Tao, F., & Cui, Y. (2021). Wavelength tuneable barbituric acid derivatives: Synthesis, aggregation-induced emission and nitroaromatic detection. *Journal of Luminescence*, 232, 117865. doi:10.1016/j.jlumin.2020.117865. <https://doi.org/10.1016/j.jlumin.2020.117865>

26 Hu, R., Gómez-Durán, C.F.A., Lam, J.W.Y., Belmonte-Vázquez, J.L., Deng, C., Chen, S., Ye, R., Peña-Cabrera, E., Zhong, Y., Wong, K.S., & Tang, B.Z. (2012). Synthesis, solvatochromism, aggregation-induced emission and cell imaging of tetraphenylethene-containing BODIPY derivatives with large Stokes shifts. *Chem. Commun.*, 48 (81), 10099–10101. <https://doi.org/10.1039/C2CC35188A>

27 Liu, B., Luo, Z., Si, S., Zhou, X., Pan, C., & Wang, L. (2017). A photostable triphenylamine-based flavonoid dye: solvatochromism, aggregation-induced emission enhancement, fabrication of organic nanodots, and cell imaging applications. *Dye. Pigment.*, 142, 32–38. <https://doi.org/10.1016/j.dyepig.2017.03.023>

С.С. Мендигалиева, Д.А. Биримжанова, И.С. Иргибаетова, Н.Н. Барашков, Ю. Сахно

5-(Бензилиден)пиримидин-2,4,6-триондарының агрегаттық-индукцияланған эмиссиясы

Фенил сақиналарында әртүрлі алмастырғыштары бар 5-(бензилиден)пиримидин-2,4,6-триондардың спектрлік-люминесценттік қасиеттері синтезделді және зерттелді: 5-(4'-диметиламинобензилиден) барбитур қышқылы және 5-(4'-метоксибензилиден) барбитур қышқылы. Қатты күйдегі флуоресценция тиімділігінің төмендеуі өте жалпы сипатқа ие сияқты радиациялық емес дезактивация процестерін тудыратын молекулааралық тербеліс әсерлесуімен түсіндіріледі. Оқшауланған бояғыш молекулалар сұйылтылған ерітінділерде іс жүзінде люминесценцияланбайды, олар ерітінді концентрациясының жоғарылауымен немесе нашар еріткіштерде немесе қатты күйде агрегатталуымен қатты сәуле шығарады, люминесценция қарқындылығының жоғарылауын, агрегаттық-индукцияланған эмиссия құбылысын көрсетеді (АИЭ құбылысы). Тиімді люминесцентті материалдарды әзірлеу өзекті тақырып болып табылады. Фенил сақинасындағы орынбасар диметиламинодан метокситопқа өзгерген кезде сәулелену түсі қызылдан (максимум 630 нм) жасылға (максимум 540 нм) өзгереді. Теориялық есептеу бояғыш молекулалардың агрегаттық-индукцияланған эмиссиясының сипаттамалары молекулааралық өзара әрекеттесудің нәтижесі екенін көрсетеді. Осы қасиеттің арқасында молекулаларды флуоресцентті зондтар ретінде қолдануға болады және сулы ерітінділердегі этанол құрамын анықтауға болады.

Кілт сөздер: агрегаттық-индукцияланған эмиссия, барбитур қышқылы, флуоресцентті зондтар, флуоресценцияның ең жоғары қарқындылығы, фосфор, бояғыш молекулалары, фенил сақинасын алмастырғыш, қатты күй, молекулаішілік айналымдар.

С.С. Мендигалиева, Д.А. Биримжанова, И.С. Иргибаетова, Н.Н. Барашков, Ю.Е. Сахно

Агрегационно-индуцированная эмиссия 5-(бензилиден)пиримидин-2,4,6-трионов

Синтезированы и исследованы спектрально-люминесцентные свойства 5-(бензилиден)пиримидин-2,4,6-трионов с различными заместителями в фенильных кольцах: 5-(4'-диметиламинобензилиден) барбитуровая кислота и 5-(4'-метоксибензилиден) барбитуровая кислота. Снижение эффективности флуоресценции в твердом состоянии носит довольно общий характер и, в основном, объясняется межмолекулярными колебательными взаимодействиями, которые индуцируют процессы безызлучательной дезактивации. Тогда как изолированные молекулы красителя практически не люминесцируют в разбавленных растворах, они становятся сильно излучающими при увеличении концентрации раствора или агрегации в плохих растворителях или в твердом состоянии, проявляют увеличение интенсивности люминесценции, явление агрегационно-индуцированной эмиссии (явление АИЭ). Разработка эффективных люминесцентных материалов является актуальной темой. При изменении заместителя в фенильном кольце с диметиламино- на метоксигруппу цвет излучения меняется с красного (максимум при 630 нм) на зеленый (максимум при 540 нм). Теоретический расчет показывает, что характеристики агрегационно-индуцированной эмиссии молекул красителя являются результатом межмолекулярных взаимодействий. Благодаря этому свойству молекулы можно использовать в качестве флуоресцентных зондов и определять содержание этанола в водных растворах.

Ключевые слова: агрегационно-индуцированная эмиссия, барбитуровая кислота, флуоресцентные зонды, интенсивности пиков флуоресценции, люминофор, молекулы красителя, заместитель фенильного кольца, твердое состояние, внутримолекулярные вращения.

Information about authors

Mendigaliyeva, Svetlana Samigulliyena — 3rd year PhD student, Chemistry Department, L.N. Gumilyov Eurasian National University, Satpayev street, 2, 010000, Nur-Sultan, Kazakhstan; e-mail: svet_men@mail.ru; <https://orcid.org/0000-0002-2737-7188>;

Birimzhanova, Dinara Asylbekovna — PhD in Chemical Sciences, Senior Lecturer, L.N. Gumilyov Eurasian National University, Satpayev street, 2, 010000, Nur-Sultan, Kazakhstan; e-mail: dinarabirimzhanova@gmail.com; <https://orcid.org/0000-0002-5572-9339>;

Irgibaeva, Irina Smailovna (corresponding author) — Doctor of science in chemistry, Professor of Chemistry Department, L.N. Gumilyov Eurasian National University, Satpayev street, 2, 010000, Nur-Sultan, Kazakhstan; e-mail: irgsm@mail.ru; <https://orcid.org/0000-0003-2408-8935>;

Barazhkov, Nikolay Nikolayevich — Doctor of science in chemistry, Director of R&D and Technical Services, Micro-Tracers, Inc. 1370 Van Dyke Avenue San Francisco, CA 94124, USA; e-mail: nikolay@microtracers.com; <https://orcid.org/0000-0003-2494-9248>;

Sakhno, Yuriy Eduardovich — Dr., Postdoctoral Fellow, Department of Plant and Soil Sciences, 154a Townsend Hall, 531 S. College Avenue Newark, DE 19713; University of Delaware, Delaware, USA; e-mail: ysakhno@udel.edu; <https://orcid.org/0000-0001-8115-739X>

PHYSICAL AND ANALYTICAL CHEMISTRY

Article

UDC 544.42+519.242.7

<https://doi.org/10.31489/2022Ch1/50-59>

T. Annavarapu¹, S. Kamepalli¹, S.K. Kondala², V. Kotra³,
S.R. Challa⁴, M. Rudrapal^{5*}, A.R. Bendale⁶

¹Acharya Nagarjuna University College of Pharmaceutical Sciences, Guntur, Andhra Pradesh, India;

²School of Pharmaceutical Sciences, Vignan's Foundation for Science, Technology and Research, Guntur, Andhra Pradesh, India;

³Faculty of Pharmacy, Quest International University Perak (QIUP), Perak, Malaysia;

⁴Department of Cancer Biology and Pharmacology, College of Medicine, University of Illinois, Peoria, Illinois, USA;

⁵Rasiklal M. Dhariwal Institute of Pharmaceutical Education & Research, Pune, Maharashtra, India;

⁶Sandip Institute of Pharmaceutical Sciences, Nashik, Maharashtra, India

(*Corresponding author's e-mail: rsmrpal@gmail.com)

Anti-inflammatory and antioxidant activities of 4-allylpyrocatechol and its derivatives with molecular docking and ADMET investigations

Abnormal production of pro-inflammatory mediators and generation of reactive oxygen species (ROS) play a key role in the development and progression of various human disorders. The study aims to investigate the *in vitro* anti-inflammatory and antioxidant activity of 4-allyl pyrocatechol (4-APC) and its derivatives (APC-1 and APC-2) by albumin denaturation and 1,1-Diphenyl-2-picrylhydrazyl (DPPH) methods, respectively. Also, the test compounds are studied *in silico* for their inhibitory potential against the pro-inflammatory and oxidative markers (calpain, FAAH, and TNF- α) via molecular docking. The compounds have exhibited appreciable *in vitro* anti-inflammatory and antioxidant activities. The APC-2 compound has demonstrated significant anti-inflammatory and antioxidant activity (percentage inhibition = 69 ± 0.76 and 77.05 ± 0.92 , respectively, at 100 $\mu\text{g/ml}$) compared to the standard drugs, aspirin and ascorbic acid (percentage inhibition = 82 ± 0.83 and 92.35 ± 0.75 , respectively, at 100 $\mu\text{g/ml}$). The docking study has showed that APC-2 significantly inhibited calpain (PDB ID: 2R9C), FAAH (2WJ1) and TNF- α (2AZ5) inflammatory markers. The drug-likeness, bioactivities, ADME profile (pharmacokinetic) and toxicity properties have also been determined using online tools (Molinspiration, pkCSM, SwissADME, PreADMET). The test compounds have showed acceptable drug-likeness, bioactivity score, ADME and toxicity properties. Finally, we conclude that the 4-allylpyrocatechol and its derivatives can be used as lead molecules for their further development as therapeutically useful anti-inflammatory agents.

Keywords: pyrocatechol, anti-inflammatory, antioxidant, lead molecule, inflammatory markers, calpain, FAAH, TNF- α , docking, ADMET.

Introduction

Chronic anti-inflammatory diseases, including rheumatoid arthritis, are still one of the major health problems of the world's population. Chronic inflammation may lead to considerable tissue damage in human diseases [1, 2]. Inflammation can cause damage to body tissues (endothelial cells, muscle cells, nerve cells) through the production of an array of pro-inflammatory and inflammatory mediators, such as prostaglandins (PGEs), interleukins (ILs), tumor necrosis factor-alpha (TNF), etc. [3]. The abnormal production of pro-inflammatory mediators and the generation of reactive oxygen species (ROS) play a key role in the development of inflammations and associated human illness [4, 5]. ROS are free oxygen radicals that can rapidly react with biological molecules (lipids, DNA, and proteins), resulting in oxidative stress (OS) and consequently cellular damage [6]. The production of free radicals and pro-inflammatory/ inflammatory mediators

is believed to be the underlying cause of inflammatory diseases [6–9]. The anti-inflammatory, antioxidant, antimicrobial, antifungal activities of 4-allylpyrocatechol (APC) have already been reported [10, 11]. As continuation of our work [12], this work aims to study the anti-inflammatory and antioxidant activity of previously synthesized 4-allylpyrocatechol and its derivatives by using *in vitro* methods. Further, molecular docking was carried out by *in silico* method to investigate the inhibitory potential of test compounds against oxidative (calpain), fatty acid amide hydrolase (FAAH), and pro-inflammatory (TNF- α) markers. To evaluate the overall drug-likeness, drug-likeness parameters, bioactivities, ADME profile (pharmacokinetic) and toxicity properties were also determined using online tools.

Experimental

Chemicals: 1,1-Diphenyl-2-picrylhydrazyl (DPPH), DMSO, ethanol, ascorbic acid, bovine albumin were purchased from National Scientific Products, Guntur, A.P. India. All other chemical reagents and chemicals used were of analytical grade.

In vitro anti-inflammatory activity: The protein denaturation method was used to determine the anti-inflammatory activity of the synthesized molecules according to the previously reported technique [8] with some minor modifications. The final volume of the reaction mixture was 5 ml and comprised 0.2 ml bovine albumin (1 %), 0.70 ml phosphate buffer saline (PBS, pH 6.4), and 0.1 ml test compound (sample). The pH was adjusted to 1N HCl. The reaction mixture was incubated in water bath for 15 min at 37 °C, and then it was heated to 70 °C for 5 min. The absorbance of the turbid solution was determined at 660 nm by using a UV-Visible Spectrophotometer (Elico, India). The phosphate buffer was used as a control, and aspirin was used as a standard reference drug. The percentage inhibition of protein denature was calculated using the following formula:

$$\text{Percentage inhibition of denaturation} = ([1 - (A_s/A_c)] \times 100),$$

where A_c — the absorbance of a control; A_s — the absorbance of a sample.

In vitro antioxidant activity: The antioxidant activity was assessed by DPPH radical scavenging assay according to the previously published method [13] with some modifications. The 1 mg/ml stock solution was prepared by mixing the test compound using DMSO as a solvent. The DPPH radical solution (0.5 mM) was prepared using ethanol. The stock solution was used to prepare different concentrations (100 μ g/ml, 50 μ g/ml, and 25 μ g/ml) of the test compound with DMSO. The standard solution of ascorbic acid was also prepared in the same way as mentioned above. The different final test solutions consisted of 0.5 ml sample solution, 3 ml absolute ethanol and 0.3 ml 0.5 mM DPPH solution in ethanol. The blank consisted of 3.3 ml ethanol and 0.5 ml sample solution. The control solution was prepared by mixing 3.5 ml ethanol and 0.3 ml DPPH solution. Test solutions were incubated for 30 min at room temperature. The change in color (from deep violet to light yellow) was measured at 517 nm using a UV-Visible Spectrophotometer against the blank. The radical scavenging activity was measured in percentage using the following formula:

$$\text{Percentage of scavenging activity} = ([1 - (Ab_s/Ab_c)] \times 100),$$

where Ab_c — the absorbance of a control; Ab_s — the absorbance of a sample.

Statistical analysis: The statistical analysis was performed using GraphPad Prism 8.0, and values were expressed in mean \pm SEM. The statistical comparison was made using ANOVA, where $p < 0.05$ was considered statistically significant.

Molecular docking study: The docking study was performed for 4-allyl pyrocatechol (4-APC) and its two derivatives, APC-1 and APC-2, against the oxidative and pro-inflammatory markers such as calpain, FAAH, and TNF- α . The protein-ligand docking was conducted in PyRx Virtual Screening software 0.8 [14–16].

The X-ray crystal structures of calpain (PDB ID: 2R9C), FAAH (PDB ID: 2WJ1, FAAH) and TNF- α (PDB ID: 2AZ5) were retrieved from Protein Data Bank [17–20]. The water molecules were removed, hydrogen atoms were added, and co-crystal ligands were extracted using PyMOL 2.3.4 and saved in .mol2 format. The mol2 file of protein was loaded converted to .pdbqt format through AutoDock module Macromolecule tool in PyRx Virtual Screening software 0.8.

The 2D structures of ligands (4-APC, APC-1, and APC-2), which were previously characterized by $^1\text{H-NMR}$, $^{13}\text{C-NMR}$, and high-resolution mass spectrophotometry [12], were drawn using ChemSketch v14.00 and saved as .sdf file. The ligand files were subjected to energy minimization (force field-off) through the Open babel tool and then conformers for the selected ligands were generated through AutoDock .pdbqt files in PyRx Virtual screening software 0.8. The 2D structures of 4-APC and its derivatives (APC-1 and APC-2) are presented in Figure 1.

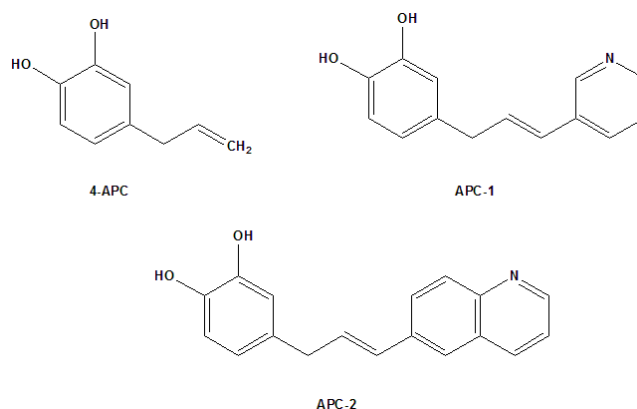


Figure 1. Structures of 4-APC and its derivatives (APC-1 and APC-2)

Drug-likeness, bioactivities, ADME and toxicity prediction: The 2D structures of 4-APC, APC-1, and APC-2 were used for assessing drug-likeness, bioactivities, ADME and toxicity properties [21–23]. Various online tools such as Molinspiration, pkCSM, SwissADME and PreADMET [24, 25] were used to calculate the abovementioned properties.

Results and Discussion

Anti-inflammatory activity: The results of *in vitro* anti-inflammatory activity of the test compounds are shown in Figure 2. The compound APC-2 showed maximum inhibitory activity of 69 ± 0.76 % at $100 \mu\text{g/ml}$. The standard anti-inflammatory drug aspirin exhibited 74 ± 0.83 % inhibition of protein denaturation at $100 \mu\text{g/ml}$. The other two compounds, 4-APC and APC-1 also exhibited anti-inflammatory activity with 47 ± 0.96 % and 56 ± 0.45 % inhibition of protein denaturation at $100 \mu\text{g/ml}$, respectively.

Antioxidant activity: Figure 3 presents the results of *in vitro* antioxidant activity. Test compounds, 4-APC, APC-1, and APC-2 showed significant DPPH radical scavenging activity compared with the standard drug, ascorbic acid. The decrease in absorbance of DPPH radicals was observed with increase in the concentration of test compounds due to the scavenging of radicals by hydrogen donation. This was easily observed with change in color from purple to yellow. Among the test samples, APC-2 exhibited a significant percentage inhibition (77.05 ± 0.92 %, $100 \mu\text{g/ml}$) compared with standard ascorbic acid (92.35 ± 0.75 %, $100 \mu\text{g/ml}$). The other two compounds (4-APC and APC-1) showed considerable DPPH radical scavenging activity.

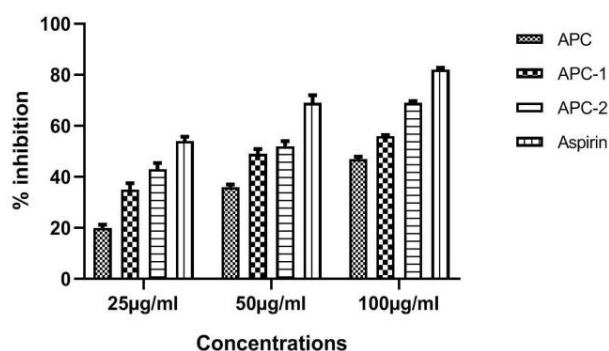


Figure 2. Protein denaturation activity of 4-APC and its derivatives (APC-1 and APC-2)

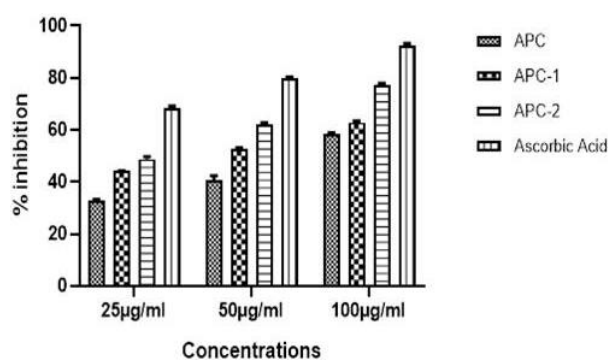


Figure 3. DPPH radical scavenging activity of 4-APC and its derivatives (APC-1 and APC-2)

Docking study: A molecular docking study substantiated the anti-inflammatory and antioxidant activities of 4-APC, APC-1, and APC-2. Three oxidative and pro-inflammatory markers, such as calpain, FAAH, and TNF- α , were used as target proteins in the docking study. Results of protein-ligand docking are expressed as binding energies (kcal/mol) of protein-ligand interaction and are presented in Tables 1, 2, 3. From docking results, the compound APC-2 showed the lowest binding energies against all three different proteins. The other two compounds (4-APC and APC-1) exhibited comparatively more binding energies than the compound APC-2. However, the binding energies of internal ligands (co-crystal ligands) were found over the test compounds. From binding energies, it is clear that APC-2 possesses more binding affinity than

the other two compounds (4-APC and APC-1) against all the three target proteins (calpain, FAAH, and TNF- α).

Table 1

Binding energies and interacting amino acids of 4-APC, APC-1, and APC-2 against calpain

| Sl. No. | Compound | Binding energy (kcal/mol) | Interaction(s) | Interacting amino acids |
|---------|-----------------------|---------------------------|--------------------|---|
| 1 | 4-APC | -4.7 | H bond pi-alkyl | Gly110 Trp298, Val301 |
| 2 | APC-1 | -5.8 | H bond | Ser251, Glu349 |
| 3 | APC-2 | -6.8 | H bond pi-alkyl | Arg270, His272, Glu300 Ala262 |
| 4 | Internal ligand (GRD) | -8.2 | H bond | Glu109, Leu112, Cys115, Gly208, Thr210, Trp298, Glu349 |

Table 2

Binding energies and interacting amino acids of 4-APC, APC-1, and APC-2 against FAAH

| Sl. No. | Compound | Binding energy (kcal/mol) | Interaction(s) | Interacting amino acids |
|---------|-----------------------|---------------------------|--------------------------------|--|
| 1 | 4-APC | -6.5 | pi-sigma Pi-alkyl | Phe192 Ser193 |
| 2 | APC-1 | -8.6 | H bond pi-alkyl | Tyr194, Gly216, Ser241, Leu404, Val491 |
| 3 | APC-2 | -9.1 | H bond pi-sigma pi-alkyl | Lys142, Thr236, Ser241, Gln273 Ile238, Met191 Val270, Leu278 |
| 4 | Internal ligand (S99) | -8.6 | H bond pi-sigma pi-alkyl | Cys269, Val270 Ile238 Leu278, Leu380 |

Table 3

Binding energies and interacting amino acids of 4-APC, APC-1, and APC-2 against TNF- α

| Sl. No. | Compound | Binding energy (kcal/mol) | Interaction(s) | Interacting amino acids |
|---------|-----------------------|---------------------------|-------------------------------------|--|
| 1 | 4-APC | -4.7 | H bond pi-alkyl pi-pi staking | Leu120, Gly121 Ile155 Tyr59 |
| 2 | APC-1 | -5.6 | H bond pi-alkyl pi-pi staking | Ser60, Leu120 Leu57 Tyr59 |
| 3 | APC-2 | -6.6 | H bond pi-alkyl pi-pi staking | Gln61 His15, Tyr59, Tyr151 Tyr59, Tyr119 |
| 4 | Internal ligand (307) | -6.8 | H-bond pi-alkyl pi-pi staking | Leu120 Gln61, Tyr119 Tyr59, Tyr119, Tyr151 |

Upon analysis of protein-ligand interactions, various non-bonding interactions exist between ligands (4-APC, APC-1, and APC-2) and proteins (calpain, FAAH, and TNF- α). Non-bonding interactions like H bond, pi-alkyl and pi-pi staking are involved between ligand and protein molecules. Various amino acid residues, such as Tyr59, Ser60, Gln61, Tyr119, Leu120, Gly121, Ile155, Tyr194, Gly216, Ser241, Leu404, Val491, and so on, are involved in the interactions from the active binding sites of calpain, FAAH, and

TNF- α . Binding poses (3D) and protein-ligand interaction diagrams (2D) of protein-ligand are presented in Figures 4, 5, 6.

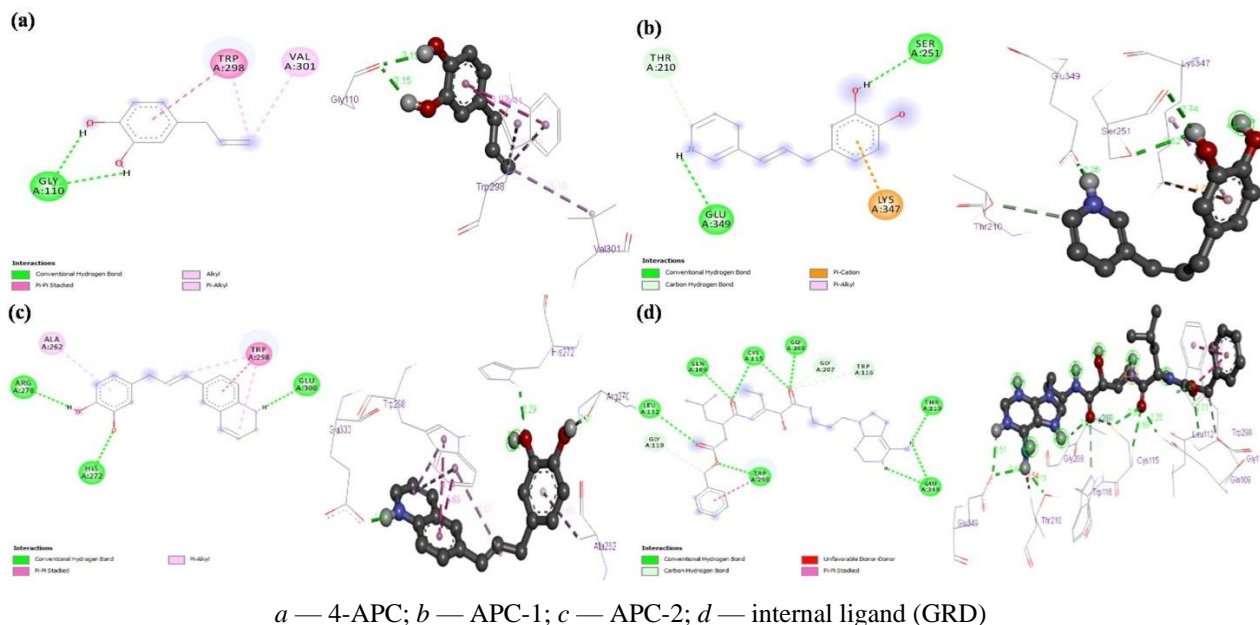


Figure 4. Binding poses (3D) and interaction diagrams (2D) of protein-ligand docking against calpain

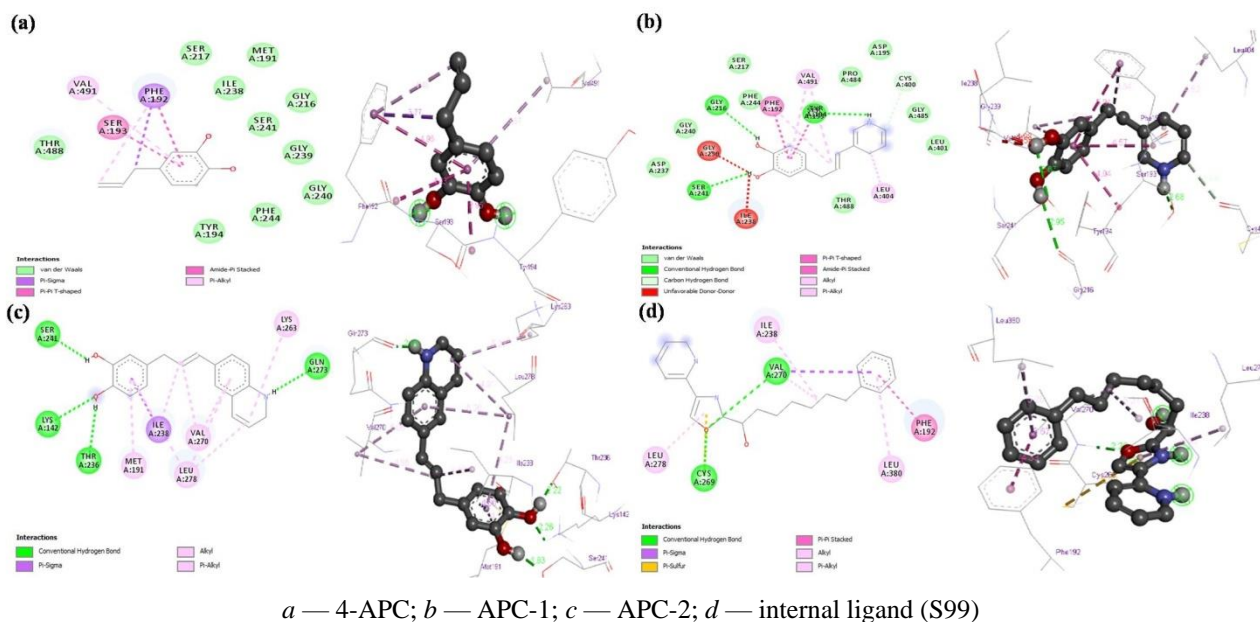


Figure 5. Binding poses (3D) and interaction diagrams (2D) of protein-ligand docking against FAAH

Drug-likeness, bioactivities, ADME and toxicity profile: The results of drug-likeness, bioactivities, ADME and toxicity profile are given in Tables 4, 5, 6 and 7. Three compounds, such as 4-APC, APC-1, and APC-2, possess acceptable drug-likeness parameters (molecular weight, LogP, H bond acceptors, H bond donors etc.), bioactivities (GPCR ligand, ion channel modulator, kinase inhibitor, nuclear receptor ligand, protease or enzyme inhibitor etc.), pharmacokinetics (ADME), and toxic properties. All the compounds were found to be drug-like molecules, biologically active, water/lipid soluble, non-toxic or non-mutagenic.

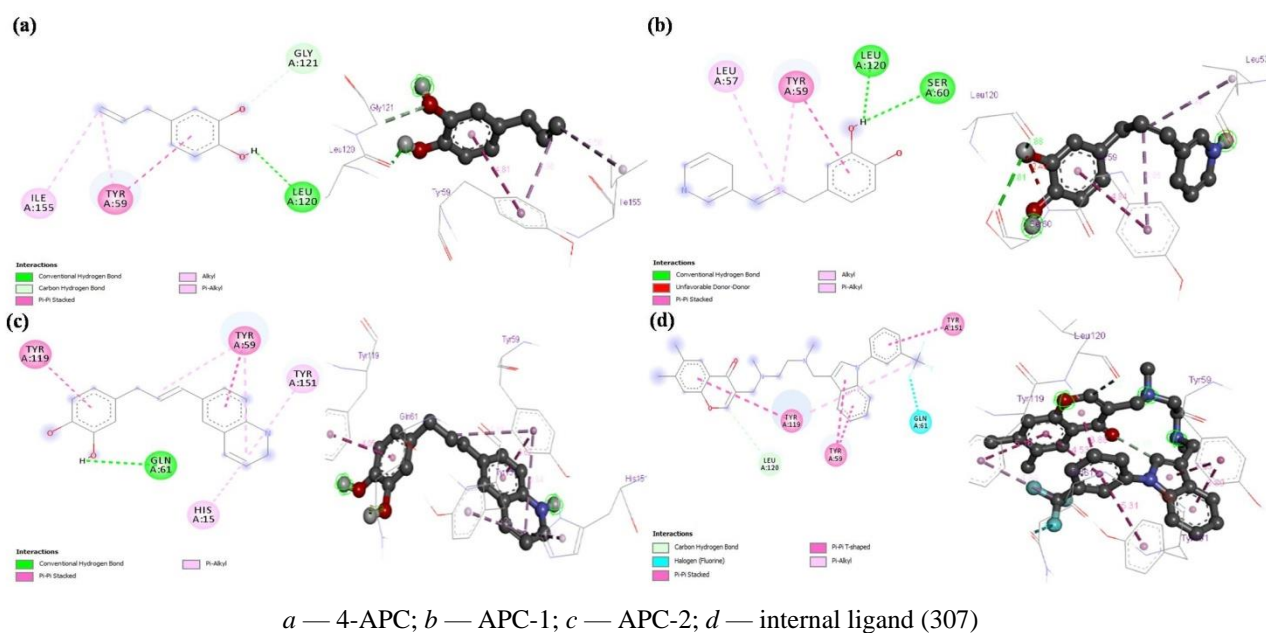
Figure 6. Binding poses (3D) and interaction diagrams (2D) of protein-ligand docking against TNF- α

Table 4

Predicted drug-likeness properties of 4-APC, APC-1, and APC-2

| Sl. No. | Descriptor | 4-APC | APC-1 | APC-2 |
|---------|------------------|---------|---------|---------|
| 1 | Molecular weight | 150.177 | 227.263 | 277.323 |
| 2 | LogP | 1.8263 | 2.7487 | 3.9019 |
| 3 | H bond acceptors | 2 | 3 | 3 |
| 4 | H bond donors | 2 | 2 | 3 |
| 5 | Surface area | 65.425 | 99.702 | 122.384 |

Table 5

Predicted Bioactivity of 4-APC, APC-1, and APC-2

| Sl. No. | Bioactivity | Bioactivity score | | |
|---------|-------------------------|-------------------|-------|-------|
| | | 4-APC | APC-1 | APC-2 |
| 1 | GPCR ligand | -0.88 | 0.11 | 0.28 |
| 2 | Ion channel modulator | -0.28 | 0.33 | 0.25 |
| 3 | Kinase inhibitor | -1.26 | -0.04 | 0.18 |
| 4 | Nuclear receptor ligand | -0.76 | 0.06 | 0.31 |
| 5 | Protease inhibitor | -1.28 | -0.48 | -0.12 |
| 6 | Enzyme inhibitor | -0.40 | 0.30 | 0.31 |

Table 6

Predicted ADME profile of 4-APC, APC-1, and APC-2

| Parameter | ADME properties | 4-APC | APC-1 | APC-2 |
|------------|--|--------|--------|--------|
| 1 | 2 | 3 | 4 | 5 |
| Absorption | Water solubility (log mol/L) | -0.974 | -2.511 | -4.428 |
| | Caco2 permeability (log Papp in 10 ⁻⁶ cm/s) | 1.596 | 1.298 | 1.342 |
| | Intestinal absorption (human) (% Absorbed) | 90.171 | 91.252 | 92.235 |
| | Skin permeability (log Kp) | -2.278 | -2.612 | -2.766 |
| | P-glycoprotein substrate (Yes/No) | No | Yes | Yes |
| | P-glycoprotein I inhibitor (Yes/No) | No | No | No |

Continuation of Table 6

| 1 | 2 | 3 | 4 | 5 |
|--------------|--------------------------------------|--------|--------|--------|
| | P-glycoprotein II inhibitor (Yes/No) | No | No | No |
| Distribution | VDss (human) (log L/kg) | 0.31 | 0.196 | 0.133 |
| | Fraction unbound (human) (Fu) | 0.448 | 0.198 | 0.033 |
| | BBB permeability (log BB) | 0.166 | 0.118 | 0.057 |
| | CNS permeability (log PS) | -2.075 | -2.164 | -1.864 |
| Metabolism | CYP2D6 substrate (Yes/No) | No | No | No |
| | CYP3A4 substrate (Yes/No) | No | Yes | Yes |
| | CYP1A2 inhibitor (Yes/No) | Yes | Yes | Yes |
| | CYP2C19 inhibition(Yes/No) | No | Yes | Yes |
| | CYP2C9 inhibitor (Yes/No) | No | No | Yes |
| | CYP2D6 inhibitor (Yes/No) | No | No | No |
| | CYP3A4 inhibitor (Yes/No) | No | No | Yes |
| Excretion | Total clearance (log ml/min/kg) | 0.214 | 0.175 | 0.164 |
| | Renal OCT2 substrate (Yes/No) | No | No | No |

Table 7

Predicted drug toxicity for 4-APC, APC-1, and APC-2

| Sl. No. | Toxicity parameter | 4-APC | APC-1 | APC-2 |
|---------|---|-------------|-------------|-------------|
| 1 | AMES toxicity | Yes | Yes | No |
| 2 | Max. tolerated dose (human) (log mg/kg/day) | 0.696 | 0.484 | 0.049 |
| 3 | hERG I inhibitor | No | No | No |
| 4 | hERG II inhibitor | No | No | Yes |
| 5 | Oral rat acute toxicity (LD ₅₀) (mol/kg) | 2.079 | 2.021 | 2.082 |
| 6 | Oral rat chronic toxicity (log mg/kg_bw/day) | 2.204 | 1.721 | 1.795 |
| 7 | Hepatotoxicity | No | No | Yes |
| 8 | Skin sensitisation | Yes | No | No |
| 9 | Tetrahymena pyriformis toxicity (log ug/L) | 0.166 | 1.211 | 1.067 |
| 10 | Minnow toxicity (log mM) | 1.724 | 1.062 | -0.114 |
| 11 | Acute algae toxicity | 0.05680 | 0.06064 | 0.02052 |
| 12 | 2 years carcinogenicity bioassay in mouse | Positive | Negative | Negative |
| 13 | 2 years carcinogenicity bioassay in rat | Negative | Negative | Negative |
| 14 | Acute daphnia toxicity | 0.12609 | 0.16367 | 0.04595 |
| 15 | <i>In vitro</i> Human ether-a-go-go related gene channel inhibition | Medium Risk | Medium Risk | Medium Risk |
| 16 | Acute fish toxicity (medaka) | 0.02144 | 0.03946 | 0.00407 |
| 17 | Acute fish toxicity (minnow) | 0.01102 | 0.03670 | 0.00812 |
| 18 | <i>In vitro</i> Ames test results in TA100 strain (Metabolic activation by rat liver homogenate) | Negative | Positive | Positive |
| 19 | <i>In vitro</i> Ames test results in TA100 strain (No metabolic activation) | Negative | Negative | Negative |
| 20 | <i>In vitro</i> Ames test results in TA1535 strain (Metabolic activation by rat liver homogenate) | Positive | Positive | Negative |
| 21 | <i>In vitro</i> Ames test results in TA1535 strain (No metabolic activation) | Positive | Positive | Negative |

Conclusions

In conclusion, we conclude that the pyrocatechol and its derivatives possess appreciable *in vitro* anti-inflammatory and antioxidant activities. The pyrocatechol derivative 2 (APC-2) has a better activity profile among the three compounds. The *in silico* studies revealed a significant inhibitory potential of the compounds, especially the compound APC-2, against the oxidative and pro-inflammatory markers with an acceptable level of drug-likeness, ADME profile, and toxicities. Finally, it was suggested that the 4-allylpyrocatechol and its derivatives can be used as lead molecules for their further development as therapeutically useful anti-inflammatory agents.

References

- 1 Hussain, N., Kakoti, B.B., Rudrapal, M., & Sarwa, K.K. (2020). Anti-inflammatory and Antioxidant Activities of *Cordia dichotoma* Forst. Bark. *Biomedicine and Pharmacology Journal*, 13(4), 2093–2099. <https://dx.doi.org/10.13005/bpj/2090>
- 2 Junejo, J.A., Zaman, K., & Rudrapal, M. (2022). Hepatoprotective and Anti-inflammatory Activities of Hydro-alcoholic Extract of *Oxalis debilis* Kunth. *Leaves Letters in Applied NanoBioScience*, 11(3), 3626–3633. <https://dx.doi.org/10.33263/LIANBS113.36263633>
- 3 Jongejan, A., de Graaf, C., Vermeulen, N.P., Leurs, R., & de Esch, I.J. (2005). The role and application of *in silico* docking in chemical genomics research. *Methods in Molecular Biology*, 310, 63–91. https://dx.doi.org/10.1007/978-1-59259-948-6_5
- 4 Morphy, R., Kay, C., & Rankovic, Z. (2004). From magic bullets to designed multiple ligands. *Drug discovery today*, 9(15), 641–651. [https://dx.doi.org/10.1016/S1359-6446\(04\)03163-0](https://dx.doi.org/10.1016/S1359-6446(04)03163-0)
- 5 Sharom, J.R., Bellows, D.S., & Tyers, M. (2004). From large networks to small molecules. *Current Opinion in Chemical Biology*, 8(1), 81–90. <https://dx.doi.org/10.1016/j.cbpa.2003.12.007>
- 6 Ekins, S., Mestres, J., & Testa, B. (2007). *In silico* pharmacology for drug discovery: applications to targets and beyond. *British Journal of Pharmacology*, 152(1), 21–37. <https://dx.doi.org/10.1038/sj.bjp.0707306>
- 7 Jeong, D., Yang, W.S., Yang, Y., Nam, G., Kim, J.H., & Yoon, D.H. et al. (2013). *In vitro* and *in vivo* anti-inflammatory effect of *Rhodomlyrtus tomentosa* methanol extract. *Journal of Ethnopharmacology*, 146(1), 205–213. <https://dx.doi.org/10.1016/j.jep.2012.12.034>
- 8 Wang, Q., Kuang, H., Su, Y., Sun, Y., Feng, J., Guo, R., & Chan, K. (2013). Naturally derived anti-inflammatory compounds from Chinese medicinal plants. *Journal of Ethnopharmacology*, 146(1), 9–39. <https://dx.doi.org/10.1016/j.jep.2012.12.013>
- 9 Lushchak V.I. (2014). Free radicals, reactive oxygen species, oxidative stress and its classification. *Chemico-biological Interactions*, 224, 164–175. <https://dx.doi.org/10.1016/j.cbi.2014.10.016>
- 10 Rathee, J.S., Patro, B.S., Mula, S., Gamre, S., Chattopadhyay, S. (2006). Antioxidant activity of piper betel leaf extract and its constituents. *Journal of Agricultural and Food Chemistry*, 54(24), 9046–9054. <https://doi.org/10.1021/jf061679e>
- 11 Sarkar, D., Saha, P., Gamre, S., Bhattacharjee, S., Hariharan, C., & Ganguly, S. et al. (2008). Anti-inflammatory effect of allylpyrocatechol in LPS-induced macrophages is mediated by suppression of iNOS and COX-2 via the NF-kappaB pathway. *International Immunopharmacology*, 8(9), 1264–1271. <https://doi.org/10.1016/j.intimp.2008.05.003>
- 12 Annavarapu, T.R., Kamepalli, S., Kotra, V., & Rao, V.G. (2021). Neuroprotective Propensity of 4-Allylpyrocatechol Derivatives against Oxaliplatin Induced Peripheral Neuropathy. *Journal of Pharmaceutical Research International*, 33(24A), 92–100. <https://dx.doi.org/10.9734/jpri/2021/v33i24A31436>
- 13 Salla, S., Sunkara, R., Ogutu, S., Walker, L.T. and Verghese, M. (2016) Antioxidant Activity of Papaya Seed Extracts against H₂O₂ Induced Oxidative Stress in HepG2 Cells. *LWT—Food Science and Technology*, 66, 293–297. <http://dx.doi.org/10.1016/j.lwt.2015.09.008>
- 14 Kumar, P., Choonara, Y.E., & Pillay, V. (2014). *In silico* affinity profiling of neuroactive polyphenols for post-traumatic calpain inactivation: a molecular docking and atomistic simulation sensitivity analysis. *Molecules*, 20(1), 135–168. <https://doi.org/10.3390/molecules20010135>
- 15 Criscuolo, E., De Sciscio, M.L., Fezza, F., & Maccarrone, M. (2020). *In Silico* and *In Vitro* Analysis of Major Cannabis-Derived Compounds as Fatty Acid Amide Hydrolase Inhibitors. *Molecules*, 26(1), 48. <https://doi.org/10.3390/molecules26010048>
- 16 Saddala, M.S., Huang, H. (2019). Identification of novel inhibitors for TNF α , TNFR1 and TNF α -TNFR1 complex using pharmacophore-based approaches. *Journal of Translational Medicine*, 17, 215. <https://doi.org/10.1186/s12967-019-1965-5>
- 17 Rathinavel, T., Ammasi, S., & Shanmugam, G. (2021). Analgesic and anti-inflammatory potential of Lupeol isolated from Indian traditional medicinal plant *Crateva adansonii* screened through *in vivo* and *in silico* approaches. *Journal of Genetic Engineering & Biotechnology*, 19(1), 62. <https://doi.org/10.1186/s43141-021-00167-6>
- 18 Pires, D.E., Blundell, T.L., & Ascher, D.B. (2015). pkCSM: Predicting Small-Molecule Pharmacokinetic and Toxicity Properties Using Graph-Based Signatures. *Journal of Medicinal Chemistry*, 58(9), 4066–4072. <https://doi.org/10.1021/acs.jmedchem.5b00104>
- 19 Han, Y., Zhang, J., Hu, C. Q., Zhang, X., Ma, B., & Zhang, P. (2019). *In silico* ADME and Toxicity Prediction of Ceftazidime and Its Impurities. *Frontiers in Pharmacology*, 10, 434. <https://doi.org/10.3389/fphar.2019.00434>
- 20 Brand-Williams, W., Cuvelier, M.E., & Berset, C. (1995). Use of a free radical method to evaluate antioxidant activity. *Food Science and Technology*, 28(1), 25–30. [https://doi.org/10.1016/S0023-6438\(95\)80008-5](https://doi.org/10.1016/S0023-6438(95)80008-5)
- 21 Mandal, G., Chatterjee, C., & Chatterjee, M. (2015). Evaluation of anti-inflammatory activity of methanolic extract of leaves of *Bougainvillea spectabilis* in experimental animal models. *Pharmacognosy Research*, 7(1), 18–22. <https://doi.org/10.4103/0974-8490.147194>
- 22 Ghosh, S., Chetia, D., Gogoi, N., & Rudrapal, M. (2021). Design, Molecular Docking, Drug-likeness and Molecular Dynamics Studies of 1,2,4-Trioxane Derivatives as Novel *P. falciparum* Falcipain-2 (FP-2) Inhibitors. *Biotechnologia*, 102(3), 257–275. <https://doi.org/10.5114/bta.2021.108722>
- 23 Rudrapal, M., Rashid, I.A., Agoni, C., Bendale, A.R., Nagar, A., Soliman, M.E.S., & Lokwani, D. (2021). *In Silico* screening of phytopolyphenolics for the identification of bioactive compounds as novel protease inhibitors effective against SARS-CoV-2. *Journal of Biomolecular Structure and Dynamics*. <https://doi.org/10.1080/07391102.2021.1944909>

24 Othman, I.M.M., Mahross, M.H., Gad-Elkareem, M.A.M., Rudrapal, M., Gogoi, N., & Chetia, D., et al. (2021). Toward a treatment of antibacterial and antifungal infections: Design, synthesis and *in vitro* activity of novel arylhydrazothiazolylsulphonamide analogues and their insight of DFT, docking and molecular dynamics simulations. *Journal of Molecular Structure*, 1243, 130862. <https://doi.org/10.1016/j.molstruc.2021.130862>

25 Hussain, N., Kakoti, B.B., Rudrapal, M., Sarwa, K.K., Celik, I., & Attah, E.I. et al. (2021). Bioactive Antidiabetic Flavonoids from the Stem Bark of *Cordia dichotoma* Forst.: Identification, Docking and ADMET Studies. *Molbank*, 2021, M1234. <https://doi.org/10.3390/M1234>

Т. Аннаварapu, С. Камепалли, С.К. Кондала, В. Котра,
С.Р. Чалла, М. Рудрапал, А.Р. Бендейл

4-Аллилпирокатехиннің қабынуға қарсы және антиоксиданттық белсенділігін және оның туындыларын молекулалық докинг пен ADMET арқылы зерттеу

Қабынуға қарсы медиаторлардың аномальды өнімдері және оттегінің белсенді түрлерінің генерациясы (ОБТ) адамның әртүрлі ауруларының дамуы мен өршуінде шешуші рөл атқарады. Осы зерттеудің мақсаты альбумин денатурациясы мен DPPH (1,1-дифенил-2-пикрилгидразил) әдісі арқылы 4-аллилпирокатехиннің (4-APC) және оның туындыларының (APC-1 және APC-2) қабынуға қарсы және антиоксиданттық белсенділігін *in vitro* зерттеу. Сонымен қатар, сыналған қосылыстар *in silico*-да қабынуға қарсы және тотықтырғыш маркерлерге (кальпаин, FAAH және TNF- α) қатысты ингибиторлық потенциалы үшін молекулалық докинг әдісімен зерттелді. Қосылыстар *in vitro* жағдайында қабынуға қарсы және антиоксиданттық айқын белсенділікті көрсетті. APC-2 қосындысы аспирин және аскорбин қышқылы сияқты стандартты препараттармен салыстырғанда (пайыздық тежелу = 100 мкг/мл кезінде сәйкесінше $82 \pm 0,83$ және $92,35 \pm 0,75$) айтарлықтай қабынуға қарсы және антиоксиданттық белсенділікті көрсетті (пайыздық тежелу = 100 мкг/мл кезінде сәйкесінше $69 \pm 0,76$ және $77,05 \pm 0,92$). Молекулалық докинг әдісі APC-2 кальпаиннің қабыну белгілерін (PDB ID: 2R9C), FAAH (2WJ1) және TNF- α (2AZ5) айтарлықтай тежейтінін көрсетті. Онлайн құралдардың көмегімен (Molinspiration, pkCSM, Swiss ADME, PreADMET) дәрілік заттардың ұқсастығы, биологиялық белсенділігінің көрсеткіші, ADME профилі (фармакокинетикасы) және ұйттылық қасиеттері сияқты параметрлер анықталды. Сонымен қатар, сыналған қосылыстар дәріге жақын ұқсастығын, биологиялық белсенділік көрсеткішін, ADME қасиеттерін және ұйттылық қасиеттерін көрсеткен. Қорытындыда 4-аллилпирокатехин және оның туындыларын терапевтік пайдалы қабынуға қарсы құрал ретінде одан әрі дамыту үшін жетекші молекула ретінде пайдалануға болады деген тұжырым жасалған.

Кілт сөздер: пирокатехин, қабынуға қарсы әрекет, антиоксидант, қорғасын молекуласы, қабыну маркерлері, кальпаин, FAAH, TNF- α , докинг, ADMET.

Т. Аннаварapu, С. Камепалли, С.К. Кондала, В. Котра,
С.Р. Чалла, М. Рудрапал, А.Р. Бендейл

Исследование противовоспалительной и антиоксидантной активности 4-аллилпирокатехина и его производных методами молекулярного докинга и ADMET

Аномальная продукция провоспалительных медиаторов и генерация активных форм кислорода (АФК) играют ключевую роль в развитии и прогрессировании различных заболеваний человека. Целью настоящего исследования было изучение *in vitro* противовоспалительной и антиоксидантной активности 4-аллилпирокатехина (4-APC) и его производных (APC-1 и APC-2) путем денатурации альбумина и DPPH (1,1-дифенил-2-пикрилгидразил) методом. Тестируемые соединения также были изучены *in silico* на предмет их ингибирующего потенциала в отношении провоспалительных и окислительных маркеров (кальпаин, FAAH и TNF- α) методом молекулярного докинга. Соединения показали *in vitro* заметную противовоспалительную и антиоксидантную активность. Соединение APC-2 продемонстрировало значительную противовоспалительную и антиоксидантную активность (процентное ингибирование = $69 \pm 0,76$ и $77,05 \pm 0,92$ соответственно при 100 мкг/мл) по сравнению с такими стандартными препаратами, как аспирин и аскорбиновая кислота (процентное ингибирование = $82 \pm 0,83$ и $92,35 \pm 0,75$ соответственно при 100 мкг/мл). Методом молекулярного докинга было показано, что APC-2 значительно ингибирует воспалительные маркеры кальпаина (PDB ID: 2R9C), FAAH (2WJ1) и TNF- α (2AZ5). С помощью онлайн-инструментов (Molinspiration, pkCSM, Swiss ADME, PreADMET) также

были определены такие параметры, как сходство с лекарством, биологическая активность, ADME профиль (фармакокинетика) и свойства токсичности. Испытываемые соединения показали приемлемое сходство с лекарством, показатель биологической активности, ADME свойства и свойства токсичности. В заключение был сделан вывод, что 4-аллилпирокатехин и его производные могут быть использованы в качестве ведущих молекул для их дальнейшего развития в качестве терапевтически полезных противовоспалительных средств.

Ключевые слова: пирокатехин, противовоспалительное действие, антиоксидант, молекула свинца, маркеры воспаления, кальпаин, FAAH, TNF- α , докинг, ADMET.

Information about authors

Annavarapu, Tirupathirao — Research Scholar, Acharya Nagarjuna University College of Pharmaceutical Sciences, Guntur-522508, Andhra Pradesh, India; e-mail: tirupathionline@gmail.com; <https://orcid.org/0000-0001-5311-689X>;

Kamepalli, Sujana — Assistant Professor, Acharya Nagarjuna University College of Pharmaceutical Sciences, Guntur-522508, Andhra Pradesh, India; e-mail: drksujana36@gmail.com;

Kondala, Sathish Kumar — Assistant Professor, School of Pharmaceutical Sciences, Vignan's Foundation for Science, Technology and Research, Guntur-522213, Andhra Pradesh, India; e-mail: sathishkonidala@gmail.com; <https://orcid.org/0000-0002-8250-3570>;

Kotra, Vijay — Associate Professor, Faculty of Pharmacy, Quest International University Perak (QIUP), Perak, Malaysia; e-mail: vijai.kotra@gmail.com; <https://orcid.org/0000-0002-2043-4928>;

Challa, Siva Reddy — Research Collaborator, Department of Cancer Biology and Pharmacology, College of Medicine, University of Illinois, Peoria-61605, Illinois, USA; e-mail: sivareddypharma@gmail.com; <https://orcid.org/0000-0003-0487-2757>;

Rudrapal, Mithun (corresponding author) — Associate Professor and HoD, Department of Pharmaceutical Chemistry, Rasiklal M. Dhariwal Institute of Pharmaceutical Education & Research, Pune-411019, Maharashtra, India; email: rsmrpal@gmail.com; <https://orcid.org/0000-0002-8172-6633>;

Bendale, Atul R. — Associate Professor, Sandip Institute of Pharmaceutical Sciences, Nashik-422213, Maharashtra, India; e-mail: atulbendale123@gmail.com; <https://orcid.org/0000-0002-3219-0377>

K.D. Asgaonkar*, S.M. Patil, T.S. Chitre, S.D. Wani, M.T. Singh

AISSMS College of Pharmacy, Pune, Maharashtra, India
(*Corresponding author's e-mail: kalyani_a@aissmscop.com)

QSAR tool for optimization of nitrobenzamide pharmacophore for antitubercular activity

Tuberculosis (TB) is a leading cause of death worldwide from a single infectious agent, *Mycobacterium tuberculosis* (MTB), especially due to the development of resistant strains and its co-infections in HIV. Quantitative-structure activity relationship (QSAR) studies aid rapid drug discovery. In this work, 2D and 3D QSAR studies were carried out on a series of nitrobenzamide derivatives to design newer analogues for antitubercular activity. 2D QSAR was performed using MLR on a data set showing antitubercular activity. The 3D-QSAR studies were performed by kNN-MFA using simulated annealing variable selection method. Alignment of given set of molecules was carried out by the template-based alignment method and then was used to build the 3D-QSAR model. Robustness and predictive ability of the models were evaluated by using various traditional validating parameters. Different physicochemical, alignment-based, topological, electrostatic, and steric descriptors were generated, which indicated the key structural requirements for optimizing the pharmacophore for better antitubercular activity. For 2D QSAR, the best statistical model was generated using SA-MLR method ($r^2 = 0.892$, $q^2 = 0.819$) while 3D QSAR model was derived using the SA KNN method ($q^2 = 0.722$). The positively contributing descriptors can be incorporated to design new chemical entities for future study.

Keywords: tuberculosis, 2D QSAR, 3D QSAR, nitrobenzamide, SA-MLR, SA-kNN, pharmacophore, antitubercular activity.

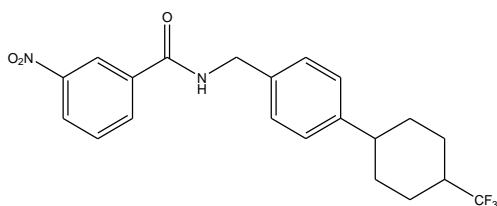
Introduction

Tuberculosis (TB) is an infectious disease caused by *Mycobacterium tuberculosis* (MTB). It has emerged as a global health menace due to drug resistance strains, such as multidrug-resistant, totally drug-resistant, and extremely drug-resistant TB. Also, its co-existence with HIV makes it even more challenging to treat [1]. Moreover, COVID-19 pandemic threatens the progress in reducing the global burden of TB disease [2]. This necessitates rapid drug development in this area. One way to achieve this is by applying statistical analytical methods as quantitative structure-activity relationship (QSAR). This technique is valuable as it helps to narrow down a library of molecules to effective potential inhibitors by predicting biological activities [3-5]. In the present study, 2D and 3D QSAR studies were carried out on nitrobenzamide derivatives to optimise the pharmacophore for antitubercular activity.

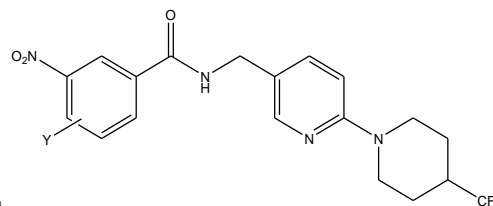
Experimental

All QSAR studies were performed using V-Life sciences MDS Version 4.3 [6].

Data set: A data set of 24 nitrobenzamide derivatives with chemical and biological variation processing antitubercular activity reported by Wang H. et al. was used for the QSAR study (Table 1) [7]. Biological activity expressed as Minimum Inhibitory concentration (MIC, μM) values was converted into pMIC values [$\text{pMIC} = -\log(\text{MIC})$]. QSAR structures of the compounds were drawn using the ChemDraw tool and converted into 3D structures (.mol2) using the V life MDS software. Geometry optimisation of the structures was carried out using the standard Merck Molecular Force Field (MMFF).



Compound 1-2



Compound 7-8

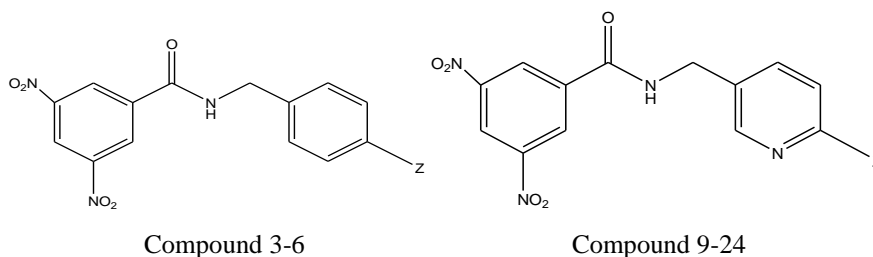


Table 1

Data set of 24 nitrobenzamide derivatives for the QSAR study

| Compound No. | Y- | Z- | MIC(μ M) | pMIC |
|--------------|-------------------|-------------------|---------------|--------|
| 1 | 5-F | - | 1.357 | -0.599 |
| 2* | 5-Br | - | 0.459 | 0.055 |
| 3 | - | | 0.060 | 0.903 |
| 4* | - | -F | 0.120 | -0.574 |
| 5 | - | -CF ₃ | 0.059 | -0.201 |
| 6 | - | -OCF ₃ | 0.033 | -1.346 |
| 7 | 5-NO ₂ | - | 0.059 | 0.886 |
| 8 | 5-Br | - | 0.944 | -0.288 |
| 9 | - | | 0.094 | 0.632 |
| 10 | - | | 0.030 | 1.146 |
| 11 | - | | 0.030 | 1.189 |
| 12 | - | | 0.108 | 0.591 |
| 13* | - | | 0.059 | 0.835 |
| 14 | - | | 0.119 | 0.603 |
| 15 | - | | 0.452 | 0.040 |
| 16 | - | | 0.235 | 0.361 |
| 17 | - | | 0.480 | 0.042 |
| 18 | - | | 1.255 | -0.361 |
| 19 | - | | 0.210 | 0.359 |
| 20 | - | | 0.178 | 0.446 |
| 21* | - | | 0.233 | 0.366 |
| 22* | - | | 0.491 | 0.033 |
| 23 | - | | 0.973 | -0.250 |
| 24 | - | | 0.143 | 0.542 |

*Test set

Generation of training and test set: Entire data set of 24 compounds was distributed as training set (19 molecules) and test set (5 molecules) using the sphere exclusion method. The selection of the test compounds was made based on their biological activity, structural diversity, and activity distribution plot. Unicolumn statistics for both training and test set was applied to check rightness of selection criteria for training and test set molecules. The mean of the test set was higher than the mean in the training set, indicating the presence of relatively more active molecules than inactive ones. A higher standard deviation in the training set indicated a wide distribution of the molecules' activity compared to the test set molecules.

QSAR studies: 2D and 3D QSAR were computed using various statistical models. Robustness and predictive ability of the models was evaluated by using various traditional validating parameters for internal validation—correlation coefficient (r^2), cross-validated correlation coefficient (q^2) and external validation (pred_r^2) [3,4,5,8-11].

2D QSAR studies: V life MDS software can calculate various 2D descriptors such as physicochemical and alignment-based. While calculating the physicochemical descriptors, dipole moment, distance-based topological indices, electrostatic, hydrophobic descriptors were deselected as they are 3D descriptors. A molecular descriptor based upon a counting statistic of the topological distance matrix is used in QSAR studies. Thus Baumann alignment independent topological descriptors with attributes 2, T, C, N, O, F, S, and Cl, were selected. These topological descriptors provide an idea about the desired 2D pharmacophoric features. Correlation matrix was applied to select the predominant descriptors influencing the antitubercular activity of the analogues taking each descriptor as independent and pMIC as dependent variable. Descriptors showing the highest correlation with pMIC were selected for generation of the QSAR model using multiple linear regression (MLR), Partial Least Square (PLS), Principal component regression (PCR). Regression methods were performed by selecting Set Cross-Correlation Limit as 0.5, Number of variables in final Equation as 10, Term Selection criteria as r^2 . Various models were generated and were analysed using the fitness plot, contribution plot, and statistical parameter compliance.

3D QSAR Studies: The 3D-QSAR studies were performed by kNN–MFA using simulated annealing variable selection method. KNN–MFA method requires suitable alignment of a given set of molecules. After optimization, alignment was carried out by the template-based alignment method. This was followed by generating common rectangular grid around the molecules (Figure 1). The resulting set of aligned molecules was then used to build 3D-QSAR models and information generated was used to predict activity of those designed molecules that have a similar template or set of atoms. Steric, hydrophobic and electrostatic interaction energies were computed at the lattice points of the grid.

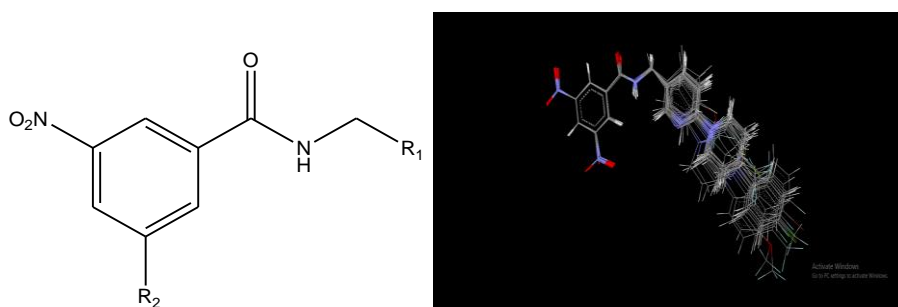


Figure 1. Common template used and alignment of nitrobenzamide derivatives

Results and Discussion

2D QSAR: Amongst the various 2D QSAR methods developed, SA-MLR method demonstrated the best results as given in Equation (1):

$$\text{pMIC} = -0.2140 (\pm 0.0249) (\text{T_T_F_5}) + 0.3571 (\pm 0.0455) (\text{SssCH2count}) - 0.2377 (\pm 0.0455) (\text{SaasCE-index}) \quad (1)$$

This model produced a correlation coefficient $r^2=0.8922$, cross-validated correlation coefficient $q^2=0.8197$ and $\text{pred}_r^2=0.7356$ (Table 2). The observed and predicted activities of the test and training sets are shown in Table 3. Contribution plot of descriptors is depicted in Figure 2. This plot describes the extent (percentage) to which different descriptors influence biological activity. Also, the plot of actual versus predicted activity of training set and test set is shown in Figure 3. Positive descriptors favor biological activity,

whereas negative descriptors would have a detrimental effect on biological activity. Hence while designing new chemical entities, positively contributing descriptors are favored, and negative descriptors should be avoided. In the present study, the positively contributing descriptors SssCH2count indicated that a total number of $-CH_2$ group connected with two single bonds would increase activity. Negatively contributing descriptors T_T_F_5 indicated that any atom separated from fluorine by five bond distance would result in decrease of activity. Negative Saas CE-index indicated electrotopological state indices for a number of carbon atoms connected with one single bond along with two aromatic bonds would decrease the antitubercular activity.

Table 2

Statistical parameters of 2D-QSAR model

| Statistical parameter | Regression method SA-MLR |
|-----------------------|---|
| N | 19 |
| r^2 | 0.892 |
| q^2 | 0.819 |
| Pred $_r^2$ | 0.735 |
| Pred $_r^2_{se}$ | 0.336 |
| F test | 0.336 |
| r^2_{se} | 0.225 |
| q^2_{se} | 0.292 |
| Best Rand r^2 | 0.447 |
| Best Rand q^2 | 0.227 |
| Z score R^2 | 8.317 |
| Z score Q^2 | 5.618 |
| Alpha Rand R^2 | 0.000 |
| Alpha Rand Q^2 | 0.000 |
| Descriptors | T_T_F_5 SssCH2count SaasCE-index |
| Coefficients | -0.214(\pm 0.024) 0.357(\pm 0.045) -0.237(\pm 0.045) |

Table 3

Observed, predicted and residual values for training set and test set

| Compound no. | Observed activity (pMIC) | Predicted activity | Residual activity |
|--------------|--------------------------|--------------------|-------------------|
| | 2 | 3 | 4 |
| 1 | -0.599 | 0.049 | -0.648 |
| 2* | 0.055 | -0.507 | 0.562 |
| 3 | 0.903 | 0.514 | 0.388 |
| 4* | -0.574 | -0.521 | -0.052 |
| 5 | -0.201 | 0.493 | 0.694 |
| 6 | -1.346 | 0.0507 | -1.853 |
| 7 | 0.886 | 0.814 | 0.071 |
| 8 | -0.288 | -0.371 | 0.083 |
| 9 | 0.632 | 0.496 | 0.139 |
| 10 | 1.146 | 0.915 | 0.231 |
| 11 | 1.189 | 0.958 | 0.230 |
| 12 | 0.591 | 0.664 | -0.072 |
| 13* | 0.835 | -0.156 | 0.991 |
| 14 | 0.603 | 0.559 | 0.442 |
| 15 | 0.040 | 0.593 | -0.553 |
| 16 | 0.361 | 0.456 | -0.094 |

Continuation of Table 3

| | | | |
|-----|--------|--------|--------|
| 1 | 2 | 3 | 4 |
| 17 | 0.042 | 0.335 | -0.293 |
| 18 | -0.361 | 0.226 | -0.587 |
| 19 | 0.359 | 0.443 | -0.084 |
| 20 | 0.446 | 0.411 | 0.035 |
| 21* | 0.366 | 0.226 | 0.139 |
| 22* | 0.033 | -0.452 | 0.485 |
| 23 | -0.250 | 0.336 | -0.586 |
| 24 | 0.542 | 0.522 | 0.02 |
| | | RMSE | 0.558 |

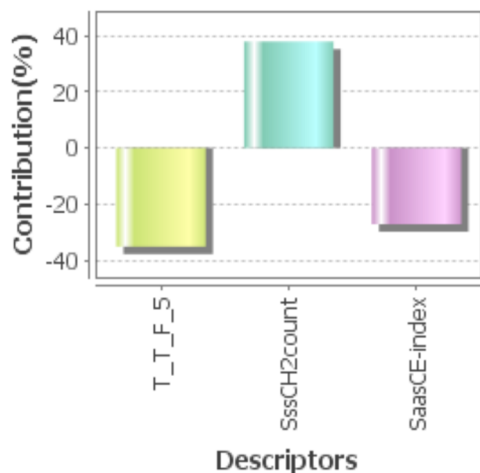


Figure 2. Contribution of descriptors

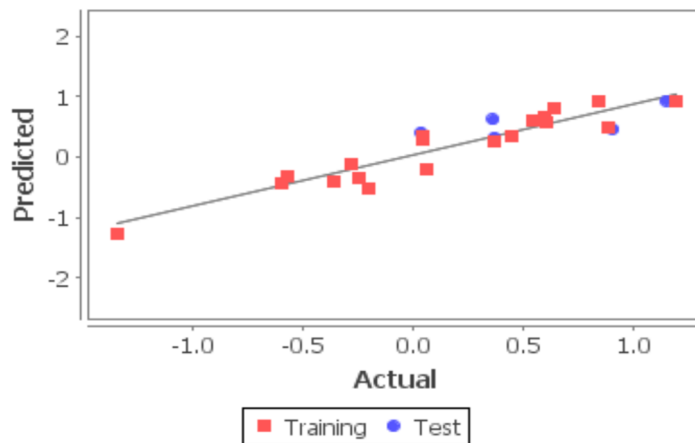


Figure 3. Plot of actual versus predicted Activity of training set and test set of SA-MLR method

3D QSAR: In continuation to 2D QSAR studies, 3D QSAR SA kNN MFA models were also commuted. The statistical results generated by SA-kNN MFA methods are depicted in Table 4. The q^2 , $pred_r^2$, $pred_r^2\ se$ and K values of model were found to be statistically significant hence model was considered for designing of NCE's. The 3D data point descriptors were generated in rectangular grid according to the range of contribution mentioned in parenthesis using SA kNN-MFA are depicted in Figure 4. Experimental and predicted activities are shown in Table 5. In model, residuals obtained are near to zero indicating a good predicting ability of the model. The plots of observed vs. predicted activity for the optimal cross-validated kNN-QSAR model are depicted in Figure 5.

Table 4

Statistical results of 3D QSAR generated by SA kNN-MFA methods

| Statistical Parameters | SA-kNN MFA |
|--------------------------|--|
| k Nearest Neighbour | 4 |
| N | 19 |
| Degree of freedom | 14 |
| q^2 | 0.722 |
| $q^2\ se$ | 0.330 |
| $pred\ r^2$ | 0.879 |
| $pred\ r^2\ se$ | 0.227 |
| Contributing descriptors | E_671 -0.0228 -0.0198 S_943 -6.0242 -3.0694 E_580 1.1626 4.0054 S_901 -0.8031 -0.4015 |

To visualise the information contained in the 3D-QSAR models, grid was generated. The electrostatic and steric descriptors are shown in Figure 4. Points generated in SA kNN-MFA 3D-QSAR model were E_671 (-0.0228-0.0198), S_943(-6.0242-3.0694), E_580 (1.1626 4.0054), S_901(-0.8031 -0.4015) i.e., electrostatic and steric interaction at lattice points 671,580 and 943,901, respectively. Negative values in electrostatic field descriptors indicated that negative electronic potential is required to increase activity and more electronegative substituent is preferred on the aryl group. Similarly, negative values of steric descriptors revealed that less sterically bulky aryl groups are favorable for maximum activity.

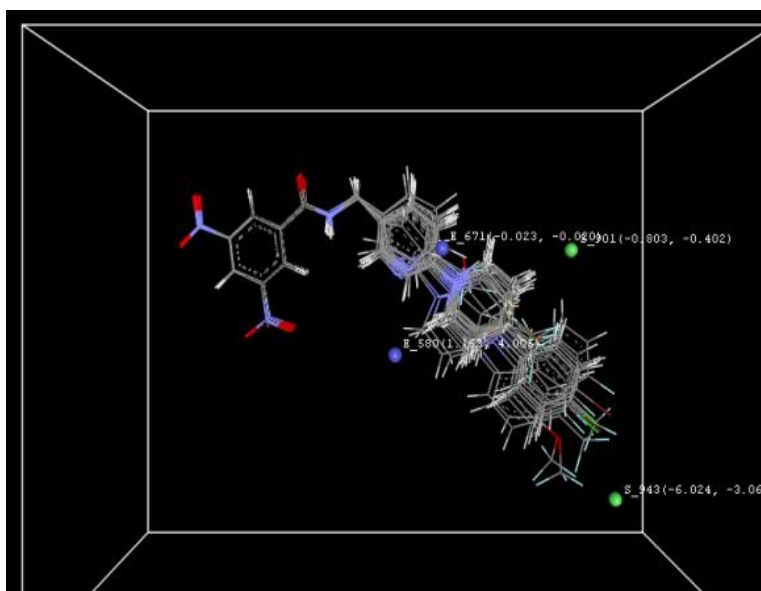


Figure 4. Generated data point

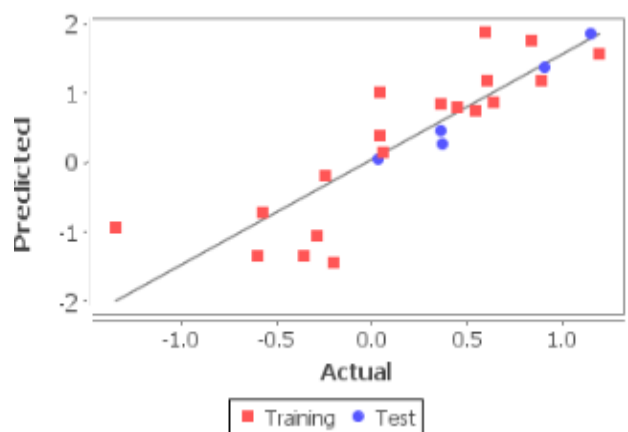


Figure 5. Plot of actual versus predicted activity of training set and test set of SA-kNN MFA

Table 5

Experimental and predicted activities

| Compound no. | Actual activity (pMIC) | Model | |
|--------------|------------------------|--------------------|-------------------|
| | | Predicted activity | Residual activity |
| 1 | 2 | 3 | 4 |
| 1 | -0.599 | -0.609 | 0.010 |
| 2 | 0.055 | -0.529 | 0.585 |
| 3* | 0.903 | 0.780 | 0.122 |
| 4 | -0.574 | -0.625 | 0.151 |
| 5 | -0.201 | -0.215 | 0.014 |

| 1 | 2 | 3 | 4 |
|-----|--------|--------|--------|
| 6 | -1.346 | -1.001 | -0.344 |
| 7 | 0.886 | 0.165 | 0.720 |
| 8 | -0.288 | 0.529 | -0.817 |
| 9 | 0.632 | 0.448 | 0.184 |
| 10* | 1.146 | 1.137 | 0.009 |
| 11 | 1.189 | 1.132 | 0.057 |
| 12 | 0.591 | -0.184 | 0.775 |
| 13 | 0.835 | 1.239 | -0.404 |
| 14 | 0.603 | 0.443 | 0.160 |
| 15 | 0.040 | 0.586 | -0.546 |
| 16 | 0.361 | 0.588 | -0.227 |
| 17 | 0.042 | 0.259 | -0.217 |
| 18 | -0.361 | -0.648 | 0.287 |
| 19* | 0.359 | 0.043 | 0.315 |
| 20 | 0.446 | 0.187 | 0.258 |
| 21* | 0.366 | 0.189 | 0.176 |
| 22* | 0.0330 | -0.140 | 0.173 |
| 23 | -0.250 | -1.179 | 0.929 |
| 24 | 0.542 | -0.195 | 0.737 |
| | | RMSE | 0.438 |

Conclusions

In order to optimise pharmacophore for antitubercular activity, a data set of nitrobenzamide derivatives was selected to perform QSAR studies. 2D and 3D QSAR were performed using MLR and SA kNN methods, respectively. Statistically significant models were used for interpretation. The study indicated a positive contribution of 2D descriptors (SssCH2count), 3D descriptors (more electronegative substituent on the aryl group and less sterically bulky aryl groups) are favorable for maximum antitubercular activity (Fig. 6). Considering different descriptors generated from 2D and 3D QSAR, new chemical entities can be designed for further studies.

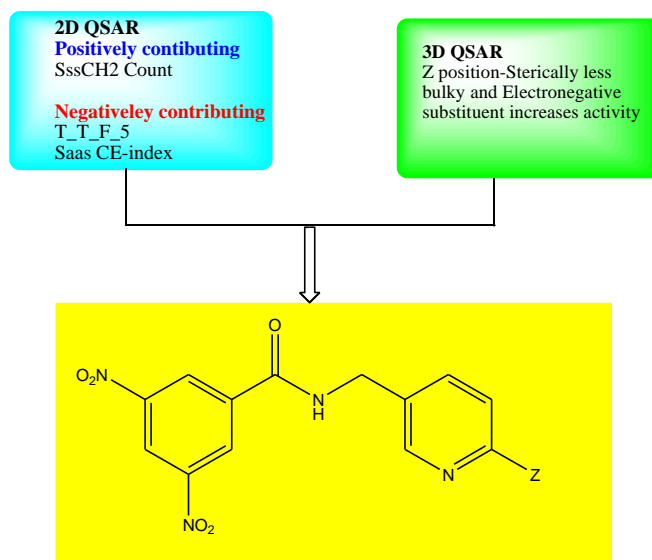


Figure 6. Optimised Pharmacophore

Acknowledgments

The authors are grateful to Dr. Ashwini R. Madgulkar, Principal of AISSMS College of Pharmacy, for continuous motivation, support, and providing the necessary infrastructure to carry out this work.

References

- 1 Bhat, Z.S., Rather, M.A., Maqbool, M., & Ahmad, Z. (2018). Drug Targets Exploited in Mycobacterium Tuberculosis: Pitfalls and Promises on the Horizon. *Biomedicine & Pharmacotherapy*, 103, 1733–1747. <https://doi.org/10.1016/j.biopha.2018.04.176>
- 2 Global Tuberculosis Report 2020. World Health Organization <https://www.who.int/publications/i/item/9789240013131>
- 3 Yuanita, E., Sudirman, Dharmayani NKT., Ulfa, M., & Syahri, J. (2020). Quantitative structure–activity relationship (QSAR) and molecular docking of xanthone derivatives as anti-tuberculosis agents. *Journal of Clinical Tuberculosis and Other Mycobacterial Diseases*, 21, 100203. <https://doi.org/10.1016/j.jctube.2020.100203>
- 4 Bhadoriya, K.S., Kumawata, N.K., Bhavthankara, S.V., Avchara, M.H., Dhumala, D.M., Patil, S.D. et al. (2016). Exploring 2D and 3D QSARs of benzimidazole derivatives as transient receptor potential melastatin 8 (TRPM8) antagonists using MLR and kNN-MFA methodology. *Journal of Saudi Chemical Society*, 20, S256–S270. <https://doi.org/10.1016/j.jscs.2012.11.001>
- 5 Qiao, K., Fu, W., Jiang, Y., Chen, L., Li, S., Ye, Q., & Gui W. (2020). QSAR models for the acute toxicity of 1,2,4-triazole fungicides to zebrafish (*Danio rerio*) embryos. *Environmental Pollution*, 265, 114837. <https://doi.org/10.1016/j.envpol.2020.114837>
- 6 Vlife MDS SUITS manual version 4.3
- 7 Wang, H., Lva, K., Lia, X., Wang, B., Wang, A., Tao, A et al. (2018). Design, synthesis and antimycobacterial activity of novel nitrobenzamide derivatives. *Chinese Chemical Letters*; 30(2): <https://doi.org/10.1016/j.ccl.2018.08.005>
- 8 Zambre, V.P., Patil, R.B., Rajesh, B., Sangshetti, J.N., & Sawant, S.D. (2019). Comprehensive QSAR studies reveal structural insights into the NR2B subtype selective benzazepine derivatives as N-Methyl-D-Aspartate receptor antagonists. *Journal of Molecular Structure*, 1197, 617–627. <https://doi.org/10.1016/j.molstruc.2019.07.068>
- 9 Kumar, A., Narasimhan, B., & Kumar, D. (2007). Synthesis, antimicrobial, and QSAR studies of substituted benzamides. *Bioorganic & Medicinal Chemistry*, 15 (12), 4113–4124.
- 10 Chitre, T.S., Asgaonkar, K.D., Patil, S.M., Kumar, S., Khedkar, V.M., & Garud, D.R. (2017). QSAR, docking studies of 1,3-thiazinan-3-yl isonicotinamide derivatives for antitubercular activity. *Computational Biology and Chemistry*, 68, 211–218. <https://doi.org/10.1016/j.compbiolchem.2017.03.015>
- 11 Chen, J.C., Qian, L., Wu, W.J., Chen, L.M., & Zheng, K.C. (2005). QSAR study of substituted benzophenazines as potential anticancer agents. *Journal of Molecular Structure THEOCHEM*, 756, 167–172. <https://doi.org/10.1016/j.theochem.2005.09.010>

К.Д. Асгаонкар, С.М. Патил, Т.С. Читре, С.Д. Вани, М.Т. Сингх

Туберкулезгекарсы белсенділік үшін нитробензамид фармакофорасының QSAR оңтайландыруы

Туберкулез (ТБ) бүкіл әлемде *Mycobacterium tuberculosis* (MTB) сияқты инфекциялық агенттен, әсіресе төзімді штамдардың дамуына және оның АИТВ-мен бірге жұқтыруына байланысты жұқпалы қоздырғышынан өлімнің негізгі себебі болып табылады. Химиялық қосылыстардың құрылымы мен белсенділігі (QSAR) арасындағы байланысты сандық зерттеу жаңа препараттың даму процесін едәуір жылдамдатуға көмектеседі. Осы жұмыста туберкулезгекарсы белсенділігі бар жаңа аналогтарды әзірлеу мақсатында нитробензамид туындыларының бірқатарына 2D және 3D QSAR-зерттеулер жүргізілді. 2D QSAR туберкулезгекарсы белсенділікті көрсететін мәліметтер жиынтығында MLR әдісін қолдану арқылы жасалды. 3D-QSAR зерттеулері kNN-MFA алгоритмін қолданып, күйдіру процесін модельдейтін айнымалыларды таңдау әдісі арқылы орындалды. Берілген молекулалар жиынтығын тегістеу шаблонға негізделген тегістеу алгоритмі арқылы жүргізілді, содан кейін 3D-QSAR моделін құру үшін қолданылды. Модельдердің сенімділігі мен болжау қабілеті әртүрлі дәстүрлі тексеру параметрлерін қолдана отырып бағаланды. Теңестіруге негізделген әртүрлі физика-химиялық, топологиялық, электростатикалық және стерильді дескрипторлар анықталды, олар туберкулезгекарсы белсенділігі жоғарылаған фармакофорды оңтайландыру үшін негізгі құрылымдық талаптарды көрсетті. 2D QSAR үшін ең жақсы статистикалық модель SA-MLR ($r^2 = 0.892$, $q^2 = 0.819$) әдісін қолдана отырып жасалды, ал 3D qsaг моделі SA KNN ($q^2 = 0.722$) алгоритмін қолдана отырып алынды. Анықталған дескрипторларды әрі қарайғы зерттеулерде жаңа химиялық туындыларды әзірлеу үшін пайдалануға болады.

Кілт сөздер: туберкулез, 2D QSAR, 3D QSAR, нитробензамид, SA-MLR, SA-kNN, фармакофор, туберкулезгекарсы белсенділік.

К.Д. Асгаонкар, С.М. Патил, Т.С. Читре, С.Д. Вани, М.Т. Сингх

QSAR-оптимизации фармакофора нитробензамида для противотуберкулезной активности

Туберкулез является ведущей причиной смерти во всем мире от такого инфекционного агента, как *Mycobacterium tuberculosis*, особенно вследствие развития резистентных штаммов и его коинфекции при ВИЧ. Количественные исследования взаимосвязи структуры и активности (QSAR) химических соединений помогают значительно ускорить процесс разработки нового лекарства. В статье проведены 2D и 3D QSAR-исследования ряда производных нитробензамида с целью разработки новых аналогов с противотуберкулезной активностью. 2D QSAR был выполнен с использованием MLR-метода на наборе данных, показывающих противотуберкулезную активность. Исследования 3D-QSAR были выполнены с помощью kNN-MFA-алгоритма с использованием метода выбора переменных, моделирующих отжиг. Выравнивание заданного набора молекул проводилось с помощью алгоритма выравнивания на основе шаблона, а затем использовалось для построения модели 3D-QSAR. Надежность и прогностическая способность моделей оценивались с помощью различных традиционных параметров проверки. Были выделены различные физико-химические, основанные на выравнивании, топологические, электростатические и стерические дескрипторы, которые указывали на ключевые структурные требования для оптимизации фармакофора с повышенной противотуберкулезной активностью. Для 2D QSAR наилучшая статистическая модель была создана с использованием метода SA-MLR ($r^2 = 0,892$, $q^2 = 0,819$), тогда как модель 3D QSAR была получена с применением алгоритма SA KNN ($q^2 = 0,722$). Выявленные дескрипторы могут быть полезны для разработки новых химических производных в дальнейших исследованиях.

Ключевые слова: туберкулез, 2D QSAR, 3D QSAR, нитробензамид, SA-MLR, SA-kNN, фармакофор, противотуберкулезная активность.

Information about authors

Asgaonkar, Kalyani D. — Assistant Professor in Dept. of Pharmaceutical chemistry, AISSMS College of Pharmacy, Kennedy Road, Pune, Maharashtra, India. e-mail: kalyani_a@aiissmscop.com. <https://orcid.org/0000-0003-3780-5323>

Patil, Shital M. — Assistant Professor in Dept. of Pharmaceutical chemistry, AISSMS College of Pharmacy, Kennedy Road, Pune, Maharashtra, India. e-mail: shital_patil@aiissmscop.com. <https://orcid.org/0000-0003-2692-2380>

Chitre, Trupti S. — Associate Professor in Dept. of Pharmaceutical chemistry, AISSMS College of Pharmacy, Kennedy Road, Pune, Maharashtra, India. e-mail: drugdesign2@gmail.com. <https://orcid.org/0000-0002-1722-7215>

Wani, Sadeecha D. — M.Pharm student, Dept. of Pharmaceutical chemistry, AISSMS College of Pharmacy, Kennedy Road, Pune, Maharashtra, India. e-mail: sadeecha.wani@gmail.com. <https://orcid.org/0000-0003-2568-2338>

Singh, Muskan T. — M.Pharm student, Dept. of Pharmaceutical chemistry, AISSMS College of Pharmacy, Kennedy Road, Pune, Maharashtra, India. e-mail: muskansingh5735@gmail.com. <https://orcid.org/0000-0002-8130-6401>

A.R. Galiyeva*, Ye.M. Tazhbayev, T.S. Zhumagaliyeva, D.T. Sadyrbekov,
D.A. Kaikenov, B.N. Karimova, S.S. Shokenova

¹Karagandy University of the name of academician E.A. Buketov, Karaganda, Kazakhstan
(*Corresponding author's e-mail: aldana_karaganda@mail.ru)

Poly lactide-co-glycolide nanoparticles immobilized with isoniazid: optimization using the experimental Taguchi method

The research aims to optimize and minimize the number of experiments to obtain poly lactide-co-glycolide (PLGA) nanoparticles (NPs) immobilized with anti-tuberculosis (anti-TB) drug — isoniazid (INH) by applying the Taguchi method and Design Expert statistical software. Several experiments were performed with varying parameters, namely polymer/drug ratio, polyvinyl alcohol (PVA) concentration, the ratio of organic solvent to the aqueous phase, and solvent type. Three different levels and a fractional factorial design were derived for each parameter, particularly the standard orthogonal array (OA) L9. Drug-loaded nanoparticles were prepared by the double emulsion method. The results were obtained from 9 runs indicated particle sizes ranging from 152.2±6.4 nm to 496.4±9.5 nm. These results were used to predict the optimum conditions for synthesizing INH-PLGA particles. The calculated data correlate well with the experimental data. INH-PLGA NPs were obtained with a mean size and polydispersity of nanoparticles of 152.2±2.25 nm and 0.279±0.03, respectively. Scanning electron microscopy, thermogravimetric analysis, and differential scanning calorimetry were carried out to characterize the obtained nanoparticles. The degree of drug release from PLGA NPs was studied, and the results showed that PLGA prolonged the release of INH from the polymer matrix.

Keywords: isoniazid, nanoparticles, Taguchi method, poly lactide-co-glycolide, double emulsion, anti-TB drug, experimental design, biopolymers.

Introduction

Nanoparticles (NPs) based on polymers have drawn a major interest in biomedical research, in particular for drug delivery applications of anti-tuberculosis (anti-TB) drugs. Drug delivery based on polymeric NPs has shown perspective for addressing poor bioavailability, toxicity, and long-term treatment of tuberculosis or overcoming the side effects of anti-TB drugs. It has been successfully used in various preclinical studies [1]. Polymeric materials, namely polylactide, poly butyl cyanoacrylate, and poly lactide-co-glycolide (PLGA), have generated considerable interest in encapsulating various therapeutic agents [2–4]. Nanoparticles prepared from these and other polymers have been investigated and used as delivery systems for anti-TB drugs [5–7]. PLGA is one of the promising carriers. It is one of the few polymers that the Food and Drug Administration (FDA) has approved for use in humans due to its biocompatibility and biodegradability [8, 9]. In this study, we used PLGA as a carrier to prepare isoniazid (INH) loaded NPs.

There are different methods to produce PLGA-based nanoparticles: Simple emulsion, double emulsion, salting-out, nanoprecipitation, microfluidic technology, flow focusing, and membrane emulsification [8, 11]. All these methods for the production of PLGA NPs share a common feature of mixing a PLGA dispersed organic phase with a non-solvent. Evaporation, extraction, and/or combinations are commonly used for solvent removal [8, 10, 11].

Physicochemical properties of the obtained NPs, such as particle size, polydispersity, encapsulation efficiency (EE) and NPs' yield, play an important role. In addition, particle size is an important characteristic when passively targeting macrophages since it affects the success of internalization in these cells. In this respect, particles with a diameter of approximately 500 nm are ideal for phagocytosis by alveolar macrophages [7, 12]. Therefore, this work aims to develop and optimize the conditions for obtaining PLGA nanoparticles and immobilizing INH in them. A controlled INH delivery system with high drug loading and EE, as well as NPs' yield should be obtained. Polymeric nanoparticles containing INH were prepared using the double emulsion (W/O/W) method. The Taguchi design method was used to optimize the nanoparticle preparation method. The Taguchi design method is a fractional factorial design that uses an orthogonal array (OA), which can considerably reduce the number of experiments. The effects of the proposed experiments on the

responses were analyzed using Design Expert (test version 13, Stat-Ease, Minneapolis, USA) to independently obtain the main effects of these factors. Then an analysis of variance (ANOVA) was performed to determine the statistically significant factors [12–14]. In this way, various parameters such as ratio and type of organic solvent, surfactant concentration, and polymer/anti-TB drug ratio were investigated. A selection function determined the optimal conditions. The resulting formulation was characterized by analysis of variance (ANOVA), which can be used to estimate the influence of factors on the characteristic properties. In addition, we investigated the release kinetics of the INH drug in vitro.

Experimental

Isoniazid (INH) with indicated purity over 99 %, polyvinyl alcohol (PVA) (hydrolyzed, MW 9000-10000) and polylactide-co-glycolide (PLGA 50:50, MW 24,000-38,000) were purchased from Sigma Aldrich (Germany). Ethyl acetate (EA) and dichloromethane (DCM), sodium phosphate dibasic and potassium phosphate monobasic were obtained from Component Reagent (Russia).

Preparation of polylactide-co-glycolide nanoparticles immobilized with isoniazid.

INH-loaded PLGA NPs were prepared by a double emulsion method [12]. 1 mL of an aqueous INH solution was first emulsified in 5 mL of solvent (EA, DCM, or mixture of EA/DCM 50/50) containing PLGA (INH/PLGA ratio: 1/1-1/5 by weight) for 2 min using a homogenizer (Ultra-Turrax T-10, IKA, Germany). The resulting primary emulsion was added to 0.5-2 % PVA (at an organic /aqueous phase ratio from 1/1 to 1/10); the mixture was then homogenized using a homogenizer for 3 min to form a secondary emulsion. The secondary emulsion was stirred continuously for 6 hours on a magnetic stirrer to completely remove solvent at room temperature. INH-loaded PLGA NPs were extracted by centrifugation (MiniSpi, Eppendorf, Hamburg, Germany) (14,000 rpm, 20 min). The resulting nanoparticle suspension was rinsed with distilled water using three centrifugation steps at 14,000 rpm for 15 min each to remove dissolved solids and organic solvent from the mixture.

Determination of particle size, polydispersity (PDI)

Particle size and PDI of nanoparticles were determined using photon correlation spectroscopy (PCS) on a Zetasizer Nano S90 from Malvern (Malvern Instruments Ltd., Malvern, UK). Samples were diluted in distilled water. Each dimensional analysis lasted 120 seconds and was carried out at 298 K with a 90° angle determination. Measurements were conducted in triplicate ($n = 3$). The surface morphology of INH-PLGA NPs was analysed with a scanning electron microscope (SEM) (MIRA 3 LM TESCAN, Czech Republic).

Encapsulation efficiency and yield of PLGA NPs

The amount of isoniazid encapsulated in PLGA NPs was quantified by measuring the amount of unencapsulated isoniazid in the supernatant after centrifugation and particle washing. The amount of free INH was determined using a UV spectrophotometer at 262 nm. The EE and NPs yields were calculated as below:

$$\text{Encapsulation efficiency (EE\%)} = \frac{\text{Mass of the total drug} - \text{Mass of free drug}}{\text{Mass of total drug}} \times 100 \%;$$

$$\text{Nanoparticles yield (\%)} = \frac{\text{Mass of total nanoparticles}}{\text{Mass of the total drug} + \text{Mass of total PLGA}} \times 100 \%.$$

In vitro study of drug release from PLGA NPs

In vitro drug release experiments were carried out to determine the extent of INH release from PLGA NPs. NPs (24 mg) were re-dispersed in 14 mL of phosphate-buffered saline (PBS, pH 7.4) and kept at 335 K with stirring. Periodically, samples of the dialysates were taken (3 mL at a time). The amount of released drug was recorded on a UV-spectrophotometer (Promekolab, Russia) at wavelength $\lambda_{\text{max}} = 262$ nm for the drug compared to the pure PBS.

Thermogravimetric analysis and differential scanning calorimetry

Thermogravimetric and differential thermal analysis were performed on a LabSYS evo TGA/DTA/DSC analyser (Setaram, France) in the temperature range of 30-550 °C in an aluminum oxide crucible at a heating rate of 10 °C/min in nitrogen inert medium and flow rate was 30 mL/min by decomposition of a nanoparticle sample.

Results and Discussion

Optimization of Nanoparticles Preparation

In our research work, the Taguchi method was used to optimize the immobilization of the biologically active substance isoniazid into PLGA nanoparticles. Four important factors influencing nanoparticle size and polydispersity (PDI) were as follows: Solvent type, INH/PLGA ratio, organic phase / aqueous phase volume ratio and PVA concentration. Three different levels and a fractional factorial design were derived for each parameter, particularly the standard OA L9 (Table 1).

Table 1

Selected process parameters and corresponding levels in the Taguchi experimental design

| Process parameters | Level 1 | Level 2 | Level 3 |
|-----------------------------------|---------|---------|---------|
| Solvent type | DCM | EA/DCM | EA |
| INH/PLGA ratio | 1/1 | 1/2.5 | 1/5 |
| Organic solvent/water phase ratio | 1/1 | 1/5 | 1/10 |
| PVA concentration (%) | 0.5 | 1 | 2 |

Taguchi's design was used to determine the significant factors that affect the size of INH-PLGA NPs. Considering four factors to be investigated, non-usage of an experimental design would have resulted in $3^4 = 81$ separate experiments, which would have been difficult and inefficient. Instead, the Taguchi OA L9 design allowed nine experiments to determine the optimum conditions for each factor in achieving the smallest size of INH-PLGA NPs. By using these optimal results, PLGA nanoparticles immobilized with drug were synthesized. The results are shown in Table 2.

Table 2

Structure of the Taguchi OA L9, corresponding particle size and polydispersity

| No. | Solvent type | INH/PLGA ratio | Organic solvent/water phase ratio | PVA concentration (%) | Size (nm) | PDI |
|-----|--------------|----------------|-----------------------------------|-----------------------|------------|------------|
| 1 | EA | 1/1 | 1/5 | 1 | 282.6±16.6 | 0.485±0.02 |
| 2 | EA | 1/2.5 | 1/1 | 0.5 | 160.2±32 | 0.101±0.05 |
| 3 | EA | 1/5 | 1/10 | 2 | 403.6±15.7 | 0.654±0.06 |
| 4 | DCM | 1/1 | 1/1 | 0.5 | 496.4±9.5 | 0.837±0.08 |
| 5 | DCM | 1/5 | 1/5 | 2 | 265.7±18.5 | 0.681±0.03 |
| 6 | DCM/EA | 1/1 | 1/5 | 0.5 | 365.8±4.4 | 0.8±0.03 |
| 7 | DCM/EA | 1/1 | 1/10 | 1 | 422.6±8.4 | 0.678±0.05 |
| 8 | DCM/EA | 1/2.5 | 1/1 | 1 | 189.6±18.4 | 0.518±0.02 |
| 9 | DCM/EA | 1/5 | 1/5 | 2 | 152.2±6.4 | 0.285±0.02 |

Table 2 shows the results for the diameters of PLGA nanoparticles obtained by PCS. It can be seen from the above numbers that PLGA nanoparticles have satisfactory physicochemical characteristics. The results obtained from 9 runs showed that the particle size ranged from 152.2±6.4 nm to 496.4±9.5 nm.

After these indicators, the experiments results were analyzed. Design-Expert software developed to independently obtain the main effects of these factors and then analysis of variance to determine the statistically significant factors was developed using ANOVA table [12–14]. The ANOVA tables for mean size and PDI are presented in Table 3. When the raw data were analyzed by ANOVA, the results showed that solvent type had no effect on mean particle size and PDI. Therefore, this parameter does not appear in the ANOVA analysis. For the mean particle size (Table 3a), the “P-value” for the model is below 0.05, indicating that the model is significant. The ratios of INH/PLGA and organic solvent/aqueous phase are significant conditions of the model, while the concentration of PVA can be considered as not significant. By removing the non-significant variable, the model can be improved. Although PVA concentration has a “P-value” of 0.4, this variable was still included in the model because the model becomes significant when this parameter is retained.

The PDI values were analyzed similarly to the mean particle size. In the ANOVA table (Table 3b), the “P-value” for the model is greater than 0.05, indicating that the model is not significant. The “F-value” of the model is 1.14, indicating that the model is not significant with respect to noise. The probability that such a

large “F-value” could arise due to noise is 48.83 %. In this case, the concentrations of INH/PLGA ratio, organic solvent/water phase ratio, and PVA concentration are all significant conditions to support the model structure since we did not consider the effect of noise (stirrer speed and sonication time) on the PDI values in the nanoparticle preparation process.

Table 3

ANOVA for selected factorial model

| Source | Sum of Squares | Degrees of freedom | Mean Square | F-value | P-value | |
|---------------------------------------|----------------|--------------------|-------------|---------|---------|-----------------|
| (a) Size (nm) | | | | | | |
| Model | 97158.79 | 5 | 19431.76 | 17.28 | 0.0203 | Significant |
| B — INH/PLGA ratio | 59358.26 | 2 | 29679.13 | 26.39 | 0.0125 | |
| C — Organic solvent/water phase ratio | 31538.13 | 2 | 15769.07 | 14.02 | 0.0300 | |
| D — PVA concentration (%) | 1032.32 | 1 | 1032.32 | 0.9178 | 0.4087 | |
| Residual | 3374.50 | 3 | 1124.83 | | | |
| Cor Total | 1.005E+05 | 8 | | | | |
| (b) PDI | | | | | | |
| Model | 0.2533 | 5 | 0.0507 | 1.14 | 0.4883 | Not significant |
| B — INH/PLGA ratio | 0.1851 | 2 | 0.0925 | 2.08 | 0.2712 | |
| C — Organic solvent/water phase ratio | 0.0257 | 2 | 0.0129 | 0.2889 | 0.7678 | |
| D — PVA concentration (%) | 0.0029 | 1 | 0.0029 | 0.0643 | 0.8162 | |
| Residual | 0.1335 | 3 | 0.0445 | | | |
| Cor Total | 0.3868 | 8 | | | | |

Figure 1 shows the different effect of the independent variables on the average nanoparticle size and PDI. The smallest size and PDI of nanoparticles are observed with INH/PLGA ratios of 1/2.5 and organic solvent/water phase of 1/5. With increasing PVA concentration, the particle size decreases and the PDI increases.

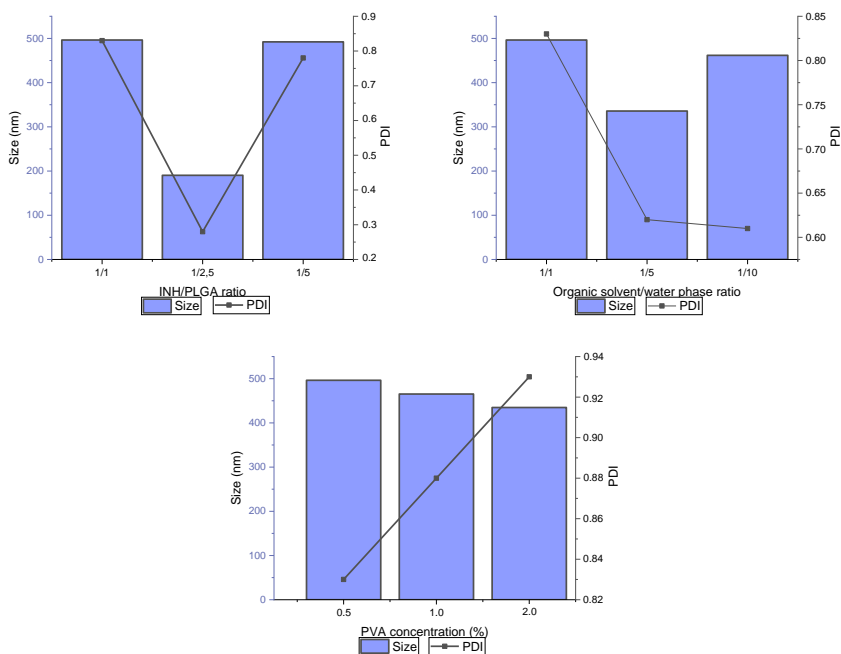


Figure 1. Influence of parameters on particle size and polydispersity

After processing the data by ANOVA, parameters were selected to optimize the process to obtain particles with minimum size and PDI (Table 4).

Table 4

Optimum solutions for synthesis of INH-PLGA NPs

| Name | Goal | Lower Limit | Upper Limit | Lower Weight | Upper Weight | Importance |
|---------------------------------------|-----------------|-------------|-------------|--------------|--------------|------------|
| A — Solvent type | is in range | DCM | EA | 1 | 1 | 3 |
| B — INH/PLGA ratio | is in range | 1/1 | 1/5 | 1 | 1 | 3 |
| C — Organic solvent/water phase ratio | is equal to 1/5 | 1/1 | 1/10 | 1 | 1 | 3 |
| D — PVA concentration (%) | is in range | 0.5 | 2 | 1 | 1 | 3 |
| Size | Minimize | 152.2 | 496.4 | 1 | 1 | 3 |
| PDI | Minimize | 0.101 | 0.83 | 1 | 1 | 3 |

The best parameters for obtaining INH-PLGA NPs were as follows: solvent type — DCM and EA mixture, INH/PLGA ratio 1/5, PVA concentration 1 %, and organic solvent to aqueous phase ratio 1/5. Under these conditions, the software estimated a nanoparticle size of 150.65 nm, while the nanoparticle size obtained from the experiment was 152.2 ± 2.25 nm, as shown in Figure 2. Experiments were carried out to confirm the optimum parameters obtained by the Taguchi method. A good agreement was observed between the predicted particle size and the experimental particle size (Table 5). Consequently, the size of the synthesized isoniazid-loaded polylactide-co-glycolide nanoparticles can be improved using the Taguchi method.

Table 5

Predicted and experimental results for INH-PLGA NPs

| | Size (nm) | PDI |
|--------------|------------------|------------------|
| Predicted | 150.65 | 0.232 |
| Experimental | 152.2 ± 2.25 | 0.279 ± 0.03 |
| Error % | 1.03 | 20.3 |

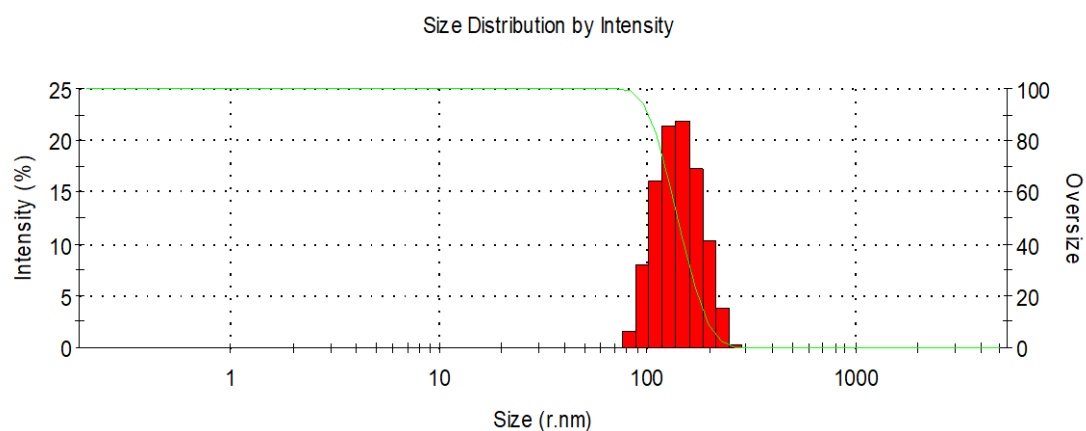


Figure 2. Histogram of particle size distribution of INH-PLGA NPs obtained under optimum conditions

Physicochemical characteristics of PLGA NPs immobilized with isoniazid

Morphological analysis of the polymeric nanoparticles was performed using a scanning electron microscope (SEM) MIRA 3 LM TESCAN (Czech Republic). The obtained images are shown in Figure 3. Micrographs of nanoparticle samples show both single particles and their agglomerates. The systems mainly consist of particles of the same size in the range of 100–250 nm, but larger particles (over 300 nm) are also present. We suggest that they are formed in combining nanoparticles by evaporation of the organic solvent.

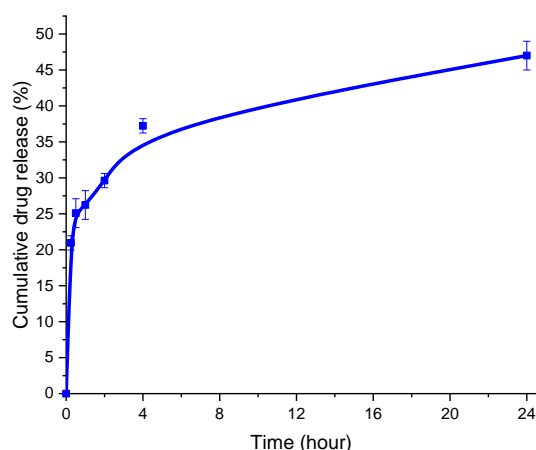


Figure 5. Release rate of isoniazid from polylactide-co-glycolide nanoparticles

Conclusions

This study has shown that the size of polylactide-co-glycolide nanoparticles with isoniazid synthesized by the double emulsion method can be controlled by changing the process conditions. The smallest size and PDI of nanoparticles are observed with INH/PLGA ratios of 1/2.5 and an organic solvent/water phase of 1/5. The particle size decreases with increasing PVA concentration, and the PDI increases. Using the Taguchi method, it has been found that the INH/PLGA ratio has the most significant effect on the size of polylactide-co-glycolide nanoparticles. The Taguchi method is one of the most suitable methods for optimizing the experimental conditions to achieve the minimum PLGA nanoparticle size for drug delivery systems. The obtained nanoparticles have been characterized by PCS, which shows that the system consists of rather small particles of 152.2 ± 2.25 nm. The obtained particles have a narrow particle size distribution (PDI = 0.279 ± 0.03). The drug loading and encapsulation efficiency are 67 and 83 %, respectively. The yield of INH-PLGA NPs is 45 %. The synthesized NPs have a spherical morphology and average size of less than 300 nm. The results of in vitro study show that PLGA prolongs the release of INH from the polymer matrix. The obtained INH-PLGA NPs have satisfactory physicochemical parameters for further application as targeted drug transport systems.

References

- Nabi, B., Rehman, S., Aggarwal, S., Baboota, S., & Ali, J. (2020). Nano-based anti-tubercular drug delivery: an emerging paradigm for improved therapeutic intervention. *Drug Delivery and Translational Research*, 10(4), 1111–1121. <https://doi.org/10.1007/s13346-020-00786-5>
- Katata, L., Tshweu, L., Naidoo, S., Kalombo, L., & Swai, H. (2012). Design and formulation of nano-sized spray dried efavirenz-part I: influence of formulation parameters. *Journal of Nanoparticle Research*, 14(11). <https://doi.org/10.1007/s11051-012-1247-0>
- Tazhbayev, Y.M., Galiyeva, A.R., Zhumagalieva, T.S., Burkeyev, M.Z., & Kazhmuratova, A.T. (2021). Synthesis and characterization of isoniazid immobilized polylactide-co-glycolide nanoparticles. *Bulletin of the University of Karaganda — Chemistry*, 101(1), 61–70. <https://doi.org/10.31489/2021ch1/61-70>
- Tazhbayev, Y.M., Zhumagalieva, T.S., Zhaparova, L.Z., Agdarbek, A.A., & Zhakupbekova, E.Z. (2020). Synthesis and investigation of PLGA-based nanoparticles as a modern tool for the drug delivery. *Bulletin of the University of Karaganda — Chemistry*, 98(2), 97–104. <https://doi.org/10.31489/2020ch2/97-104>
- Liang, Q., Xiang, H., Li, X., Luo, C., Ma, X., Zhao, W., & Song, X. (2020). Development of Rifapentine-Loaded PLGA-Based Nanoparticles: In vitro Characterisation and in vivo Study in Mice. *International Journal of Nanomedicine*, Vol. 15, 7491–7507. <https://doi.org/10.2147/ijn.s257758>
- Loiko, O.P., Herk, A.M. van, Ali, S.I., Burkeyev, M.Z., Tazhbayev, Y.M., & Zhaparova, L.Z. (2013). Controlled release of Capreomycin sulfate from pH responsive nanocapsules. *e-Polymers*, 13(1). <https://doi.org/10.1515/epoly-2013-0118>
- Costa, A., Pinheiro, M., Magalhães, J., Ribeiro, R., Seabra, V., Reis, S., & Sarmento, B. (2016). The formulation of nano-medicines for treating tuberculosis. *Advanced Drug Delivery Reviews*, 102, 102–115. <https://doi.org/10.1016/j.addr.2016.04.012>
- Sah, E., & Sah, H. (2015). Recent Trends in Preparation of Poly(lactide-co-glycolide) Nanoparticles by Mixing Polymeric Organic Solution with Antisolvent. *Journal of Nanomaterials*, 2015, 1–22. <https://doi.org/10.1155/2015/794601>

- 9 Hernández-Giottonini, K.Y., Rodríguez-Córdova, R.J., Gutiérrez-Valenzuela, C.A., Peñuñuri-Miranda, O., Zavala-Rivera, P., Guerrero-Germán, P., & Lucero-Acuña, A. (2020). PLGA nanoparticle preparations by emulsification and nanoprecipitation techniques: effects of formulation parameters. *RSC Advances*, 10(8), 4218–4231. <https://doi.org/10.1039/c9ra10857b>
- 10 Tazhbayev, Ye.M., Burkeyev, M.Zh., Zhaparova, L.Zh., Zhumagalieva, T.S., & Arystanova, Zh.T. (2018). Nanoparticles on the basis of polylactic acid and polylactic-co-glycolic acids loaded with drugs. *Bulletin of the University of Karaganda — Chemistry*, 2(90), 31–39. <https://doi.org/10.31489/2018Ch2/31-39>
- 11 Muttill, P., Wang, C., & Hickey, A.J. (2009). Inhaled Drug Delivery for Tuberculosis Therapy. *Pharmaceutical Research*, 26(11), 2401–2416. <https://doi.org/10.1007/s11095-009-9957-4>
- 12 Pham, D.-D., Fattal, E., & Tsapis, N. (2015). Pyrazinamide-loaded poly(lactide-co-glycolide) nanoparticles: Optimization by experimental design. *Journal of Drug Delivery Science and Technology*, 30, 384–390. <https://doi.org/10.1016/j.jddst.2015.07.006>
- 13 Tazhbayev, Y., Galiyeva, A., Zhumagalieva, T., Burkeyev, M., Karimova, B. Isoniazid—Loaded Albumin Nanoparticles: Taguchi Optimization Method. *Polymers* 2021, 13, 3808. <https://doi.org/10.3390/polym13213808>
- 14 Mensah, R.A., Kirton, S.B., Cook, M.T., Styliari, I.D., Hutter, V., & Chau, D.Y.S. (2019). Optimising poly(lactic-co-glycolic acid) microparticle fabrication using a Taguchi orthogonal array design-of-experiment approach. *PLOS ONE*, 14(9), e0222858. <https://doi.org/10.1371/journal.pone.0222858>
- 15 Maksimenko, O.O., Vanchugova, L.V., Shipulo, E.V., Shandryuk, G.A., Bondarenko, G.N., Gel'perina, S.É., & Shvets, V.I. (2010). Effects of technical parameters on the physicochemical properties of rifampicin-containing polylactide nanoparticles. *Pharmaceutical Chemistry Journal*, 44(3), 151–156. <https://doi.org/10.1007/s11094-010-0420-y>
- 16 Burkeev, M.Zh., Kreuter, J., Tazhbayev, Ye.M., Zhaparova, L.Zh., Zhumagalieva, T.S., & Mukhanova, D.A. (2017). Preparation, characterization and investigation of in vitro release of anti-tuberculosis drug p-amino salicylic acid based on human serum albumin. *Bulletin of the University of Karaganda — Chemistry*, 87(3), 38–44. <https://doi.org/10.31489/2017ch3/38-44>
- 17 Zhaparova, L.Z., Tazhbayev, Y.M., Burkeev, M.Z., Kazhmuratova, A.T., Zhumagalieva, T.S., Ali, S.I., & van Herk, A.M. (2012). Synthesis and characterization of polyethyl cyanoacrylate nanoparticles loaded with capreomycin sulfate. *Pharmaceutical Chemistry Journal*, 46(1), 6–9. <https://doi.org/10.1007/s11094-012-0724-1>

А.Р. Галиева, Е.М. Тажбаев, Т.С. Жұмағалиева, Д.Т. Садырбеков,
Д.А. Кайкенов, Б.Н. Каримова, С.С. Шокенова

Изониазидпен иммобилизацияланған полилактид-со-гликолид нанобөлшектері: Тагучи эксперименттік әдісінің көмегімен оңтайландыру

Зерттеудің мақсаты изониазидпен (INH) иммобилизацияланған полилактид-со-гликолидін (PLGA) нанобөлшектерін (НБ) алу үшін Тагучи әдісі мен Design Expert статистикалық бағдарламаны қолдану арқылы оңтайландыру және эксперименттер санын азайту болып табылады. Полимер мен дәрілік заттың қатынасы, поливинил спиртінің (ПВС) концентрациясы, органикалық еріткіш пен су фазасының қатынасы және еріткіштің түрі сияқты параметрлерді түрлендіру кезінде бірқатар эксперименттер жүргізілді. Өрбір параметр үшін үш түрлі деңгей және бөлшек факторлық конструкция, атап айтқанда, стандартты ортогональды матрица L9 алынды. Дәрілік препаратпен жүктелген нанобөлшектер қос эмульсия әдісімен алынды. 9 эксперимент барысында алынған нәтижелерге сүйене отырып, бөлшектердің көлемі 152,2±6,4 нм-нен 496,4±9,5 нм-ге дейін болғаны анықталды. Бұл нәтижелер PLGA– INH бөлшектері синтезінің оңтайлы жағдайларын болжау үшін пайдаланылды. Есептелген деректер эксперименттік мәліметтермен сәйкес келеді. PLGA — INH НБ—нің орташа мөлшері мен полидисперстілігі тиісінше 152,2±2,25 нм және 0,279±0,03 алынды. Алынған нанобөлшектерді сипаттау үшін мына физика-химиялық талдаулар жүргізілді: сканерлеуші электрондық микроскопия, термогравиметрлік талдау, дифференциалды сканерлеуші калориметрия. PLGA нанобөлшектерінен дәрілік заттың босап шығу дәрежесі зерттелді және алынған нәтижелер PLGA полимерлік матрицадан INH босату мерзімін ұзартатыны анықталды.

Кілт сөздер: изониазид, нанобөлшектер, Тагучи әдісі, полилактид-со-гликолид, қос эмульсия, туберкулезгеарсы дәрілік зат, тәжірибелік дизайн, биополимерлер.

А.Р. Галиева, Е.М. Тажбаев, Т.С. Жұмағалиева, Д.Т. Садырбеков,
Д.А. Кайкенов, Б.Н. Каримова, С.С. Шокенова

Наночастицы полилактид со-гликолида, иммобилизованные изониазидом: оптимизация с помощью экспериментального метода Тагучи

Целью настоящего исследования была оптимизация и минимизация количества экспериментов для получения наночастиц (НЧ) полилактид со-гликолида (PLGA), иммобилизованных изониазидом

(INH), путем применения метода Тагучи и статистического программного обеспечения Design Expert. Проведен ряд экспериментов при варьировании параметров: соотношение полимера и лекарственного препарата, концентрация поливинилового спирта, соотношение органического растворителя и водной фазы и тип растворителя. Для каждого параметра были получены три различных уровня и дробная факторная конструкция, в частности, стандартная ортогональная матрица L9. Наночастицы, загруженные лекарственным препаратом, были получены методом двойной эмульсии. Результаты, полученные в ходе 9-ти экспериментов, показали, что размер частиц варьировался от $152,2 \pm 6,4$ до $496,4 \pm 9,5$ нм. Полученные данные были использованы для прогнозирования оптимальных условий синтеза частиц PLGA–INH. Рассчитанные результаты хорошо коррелируют с экспериментальными. Получены НЧ PLGA–INH со средним размером и полидисперсностью наночастиц $152,2 \pm 2,25$ нм и $0,279 \pm 0,03$, соответственно. Для характеристики полученных наночастиц были проведены следующие физико-химические анализы: сканирующая электронная микроскопия, термогравиметрический анализ, дифференциальная сканирующая калориметрия. Была изучена степень высвобождения лекарства из НЧ PLGA, и результаты показали, что PLGA пролонгирует высвобождение INH из полимерной матрицы.

Ключевые слова: изониазид, наночастицы, метод Тагучи, полилактид со-гликолид, двойная эмульсия, противотуберкулезный препарат, экспериментальный дизайн, биополимеры.

Information about authors

Galiyeva, Aldana Rymzhanovna — 3rd year PhD student, Department of organic chemistry and polymers, Karagandy University of the name of academician E.A. Buketov, Universitetskaya street, 28, 100024, Karaganda, Kazakhstan.; e-mail: aldana_karaganda@mail.ru. <https://orcid.org/0000-0002-8551-6297>

Kaikenov, Daulet Khan Asanovich — PhD, Leading Researcher of the laboratory of the engineering profile “Physical and chemical methods of research”, Karagandy University of the name of academician E.A. Buketov, Universitetskaya street, 28, 100024, Karaganda, Kazakhstan; e-mail: krg.daykai@mail.ru. <https://orcid.org/0000-0003-4621-7603>

Karimova, Bakhytgul Nurlanovna — Candidate of chemical sciences, Assistant Professor, Karagandy University of the name of academician E.A. Buketov, Universitetskaya street, 28, 100024, Karaganda, Kazakhstan; e-mail: b.karimova2011@mail.ru. <https://orcid.org/0000-0001-6548-3179>

Sadyrbekov, Daniyar Tleuzhanovich — Candidate of chemical sciences, Researcher of the laboratory of the engineering profile “Physical and chemical methods of research”, Karagandy University of the name of academician E.A. Buketov, Universitetskaya street, 28, 100024, Karaganda, Kazakhstan.; e-mail: acidbear@mail.ru. <https://orcid.org/0000-0002-3047-9142>

Shokenova, Senim Serikovna — 2nd year Master student, Department of organic chemistry and polymers, Karagandy University of the name of academician E.A. Buketov, Universitetskaya street, 28, 100024, Karaganda, Kazakhstan; e-mail: shokenova9696@mail.ru.

Tazhbayev, Yerkeblan Muratovich — Full Professor, Doctor of Chemical Sciences, Karagandy University of the name of academician E.A. Buketov, Universitetskaya street, 28, 100024, Karaganda, Kazakhstan; e-mail: tazhbayev@mail.ru. <https://orcid.org/0000-0003-4828-2521>

Zhumagaliyeva, Tolky n Sergazyevna — Candidate of chemical sciences, Assoc. Professor, Karagandy University of the name of academician E.A. Buketov, Universitetskaya street, 28, 100024, Karaganda, Kazakhstan; e-mail: zhumagaliyeva79@mail.ru. <https://orcid.org/0000-0003-1765-752X>

R.I. Jalmakhanbetova^{1,2}, Ye.M. Suleimen^{2,3*}, N. Abe⁴, M. Oyama⁴,
A.M. Metwaly⁵, I.H. Eissa⁵, M.Yu. Ishmuratova⁶, Zh.A. Ibatayev^{2,7}

¹L.N. Gumilyov Eurasian National University, Nur-Sultan, Kazakhstan;

²Republican Collection of Microorganisms, Nur-Sultan, Kazakhstan;

³Sh. Ualikhanov Kokshetau University, Kokshetau, Kazakhstan;

⁴Gifu Pharmaceutical University, Gifu, Japan;

⁵Al-Azhar University, Cairo, Egypt;

⁶Karagandy University of the name of academician E.A. Buketov, Karaganda, Kazakhstan;

⁷S. Seifullin Kazakh Agricultural Technical University, Nur-Sultan, Kazakhstan

(*Corresponding author's e-mail: syerlan75@yandex.kz)

Isolation and *in silico* SARS-CoV-2 main protease inhibition potential of chrysoeriol from *Chondrilla brevirostris* Fisch. & C.A. Mey.

The genus *Chondrilla* L. comprises 22 species on the CIS territory. 16 species of them grow in Kazakhstan. All species of the genus *Chondrilla* L. are rubber-bearing herbaceous plants that belong to the *Asteraceae* family. We picked *Chondrilla brevirostris* Fisch. & C.A. Mey. for the chemical study. It is a perennial herb that grows in desert steppes and forest meadows. The aboveground parts of *Ch. brevirostris* were extracted with ethanol at room temperature. Several fractions were obtained by separating ethanol extract on column chromatography. Rechromatography and preparative thin-layer chromatography were used to further study the obtained fractions and the isolation of flavonoids. As a result of preparative thin-layer chromatography, the flavonoid 5,7,4'-trihydroxy-3'-methoxyflavone (compound **1**) was isolated. The chemical structure of **1** was established by spectroscopic data. Compound **1** was isolated for the first time from the species of *Chondrilla*. Compound **1** was subjected to a molecular docking study against COVID-19 main protease (M^{pro}) to investigate its expected activity against SARS-CoV-2. In this case, the substance showed a good binding mode with a free energy of -6.22 kcal/mol, while the binding energy of the co-crystallized ligand was -7.83 kcal/mol.

Keywords: *Chondrilla brevirostris*, Asteraceae, extraction, column chromatography, PTLC, isolation, flavonoid, structure, spectroscopy, molecular docking study.

Introduction

Chondrilla L. is a genus of plants in the *Asteraceae* family. *Chondrilla brevirostris* Fisch. & C.A. Mey. is the most well-known species from this genus. It widely grows in Kazakhstan, China, Kyrgyzstan and Russia. Synonyms of the plant are *Chondrilla filifolia* Iljin and *Chondrilla juncea* Ledeb. [1].

Previously, four flavonoids, including luteolin, luteolin-7-glucoside, luteolin-7-galactosylglucuronide and quercetin-3-galactoside, were reported from this plant [2].

Plant material is still important in finding new and bioactive compounds that are of practical interest as a source of new drugs. This indicates the relevance of this research. This work aims to isolate and identify, as well as to study the molecular docking of the isolated flavonoid from a plant source.

Recently, several scientific records reported the use of molecular docking studies to prove the biological activities of natural compounds [3–6]. Accordingly, we applied the isolated compound to *in silico* studies aiming at exploring its biological importance.

Experimental

General experimental procedures. Column chromatography separations (CC) were performed on glass columns packed with silica gel (230–400 mesh ASTM, Merck, LTD, Japan). Thin layer chromatography (analytical and preparative thin layer chromatography (TLC) was performed on silica gel 60 F 254 Glass plates (Merck, LTD, Japan). Spots were visualized under a UV light (254 and 366 nm) and by spraying with 10 % sulfuric acid reagent followed by heating. Isolated compound was identified by NMR analysis (¹H 500 MHz) acquired on the Jeol Delta. TMS was an internal standard. DMSO-d₆ was a solvent. Coupling constants are given in Hertz. The chemical shifts are expressed in δ ppm.

Plant Material. The aerial parts of *Ch. brevirostris* were collected in the steppe, 200 km from Zhezkazgan city, Kazakhstan, in August 2019, stage flowering — fruiting. The plant material was examined by Professor M. Ishmuratova, Department of Botany, Karagandy University of the name of academician E.A. Buketov (Republic of Kazakhstan), and classified as belonging to the *Ch. brevirostris* group and deposited in the herbarium of the faculty of biology and geography.

Extraction and Isolation. Dry finely ground raw materials (aboveground part) of *Ch. brevirostris* (1.0 kg) were extracted three times with ethanol by standing for 1 day at room temperature. The ethanol extracts were combined and evaporated under reduced pressure to yield a crude extract of 68 g. Chromatographic separation of the crude extract was carried out on a silica gel column using the system hexane — acetone with a gradient increase of the latter and then with methanol. The fractions were studied on TLC, and similar fractions were combined. Compound (**1**) (4 mg) was separated by using PTLC in the system of chloroform-methanol (200+10 mL).

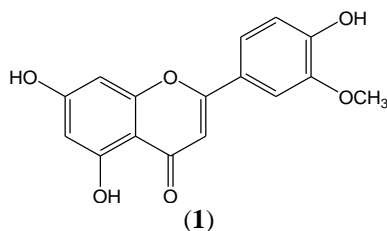
Compound identification. 5,7,4'-Trihydroxy-3'-methoxyflavone (*chrysoeriol*) (**1**) [7]: Pale yellow powder, C₁₆H₁₂O₆, Yield is 4 mg. ¹H NMR (DMSO-d₆, 500 MHz) δ (ppm): 12.97 (s, 5-OH), 6.87 (s, H-3), 6.15 (d, *J* = 2.0 Hz, H-6), 6.46 (d, *J* = 2.0 Hz, H-8), 7.55 (d, *J* = 2.0 Hz, H-2'), 6.92 (d, *J* = 9.0 Hz, H-5'), 7.55 (dd, *J* = 2.0, 9.0 Hz, H-6'), 3.89 (s, 3'-OCH₃).

Molecular docking study. The crystal structures of the target enzymes COVID-19 main protease (M^{Pro}) (PDB ID: 6lu7, resolution: 2.16 Å) were downloaded from Protein Data Bank (<http://www.pdb.org>). Molecular Operating Environment (MOE) was used for the docking analysis [8, 9]. The free energies and binding modes of the examined molecules against M^{Pro} were determined. At first, water molecules were removed from the crystal structure of M^{Pro}, retaining only one chain, which was essential for binding. The Co-crystallized ligand (PRD-002214) was used as a reference ligand. Then, the protein structure was protonated and the hydrogen atoms were hidden. Next, the energy was minimized and the binding pocket of the protein was determined [10, 11].

The structure of the examined compound and the co-crystallized ligand were drawn using Chem Bio Draw Ultra 14.0 and saved as SDF format. Then, the saved file was opened using MOE software and 3D structures were protonated. Next, the energy of the molecules was minimized. A validation process was performed for the target receptor by running the docking process for only the co-crystallized ligand. Low RMSD values between docked and crystal conformations indicated valid performance. The docking procedures were carried out utilizing a default protocol. In each case, 30 docked structures were generated using genetic algorithm searches. The output from MOE software was analyzed further and visualized using Discovery Studio 4.0 software [12, 13].

Results and Discussion

The aerial parts of *Ch. brevirostris* were extracted with ethanol. The EtOH solutions were combined and evaporated under reduced pressure. As a result of chromatography (rechromatography, PTLC), a pale yellow powder (**1**) was obtained. The yield was 4 mg. Analysis of spectral (¹H NMR) characteristics suggested that the isolated substance (**1**) was flavonoid chrysoeriol (5,7,4'-Trihydroxy-3'-methoxyflavone).



The compound (**1**) structure was established based on ¹H NMR spectrum data. Characteristic proton signal at C-3 was detected in the form of a singlet at 6.87 ppm. Proton signals at C-6 and C-8 resonate as doublets at 6.15 and 6.46 ppm, respectively, with *J* = 2 Hz. Proton signals at C-2' and C-5' appear in the form of doublets in the area of 7.55 and 6.92 ppm with *J* = 2 and *J* = 9 Hz, respectively. A proton signal appears in the form of a doublet-doublets at 7.55 ppm with the *J* = 9 Hz. The signal of protons of the methoxy group appears in the spectrum at 3.89 ppm in the form of a singlet. The presence of a hydroxyl group at C-5 is confirmed by the presence of a single-proton singlet signal in the ¹H NMR spectra spectrum at 12.97 ppm.

A docking study was carried out for compound (1) against the COVID-19 main protease (M^{pro}) (PDB ID: 6lu7, resolution: 2.16 Å) to examine the mode of binding with the proposed target. The co-crystallized ligand (PRD-002214) was used as a reference molecule. The docking studies revealed that the docked compound had good binding affinities against COVID-19 main protease with binding free energies.

The crystallized ligand (PRD-002214) showed binding energy of -7.83 kcal/mol. The detailed binding mode of the crystallized ligand was as follows: The 2-oxopyrrolidin-3-yl moiety occupied the first pocket of M^{pro} , forming three hydrogen bonds with Phe140, His163, and Glu166. Additionally, *tert*-butyl carbamate moiety occupied the second pocket of M^{pro} . Furthermore, the phenyl ring of phenylalanine moiety occupied the third pocket of the receptor forming hydrophobic interaction with His41. Moreover, ethyl propionate moiety was incorporated in the fourth pocket (Figures 1–3).

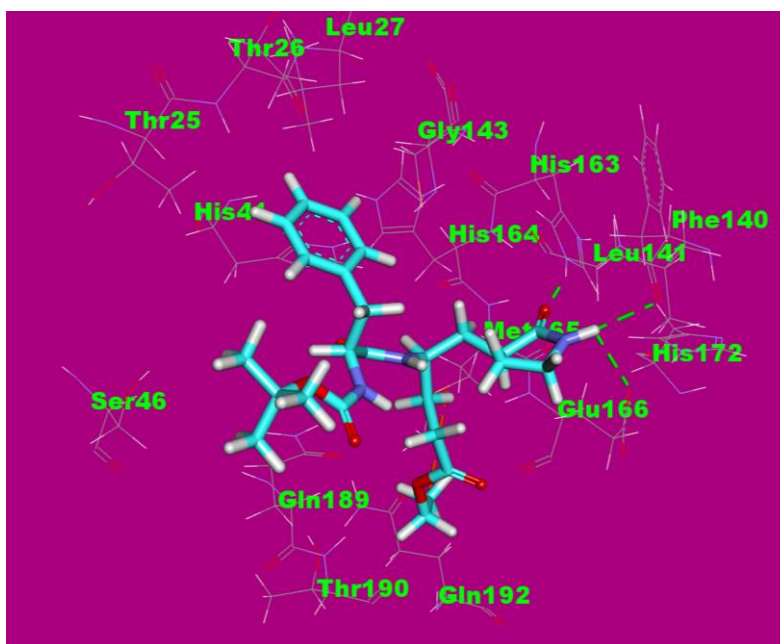


Figure 1. Co-crystallized ligand (PRD-002214) docked into the active site of the COVID-19 main protease, the hydrogen bonds are represented in green dashed lines and the hydrophobic interactions are represented in orange dashed lines

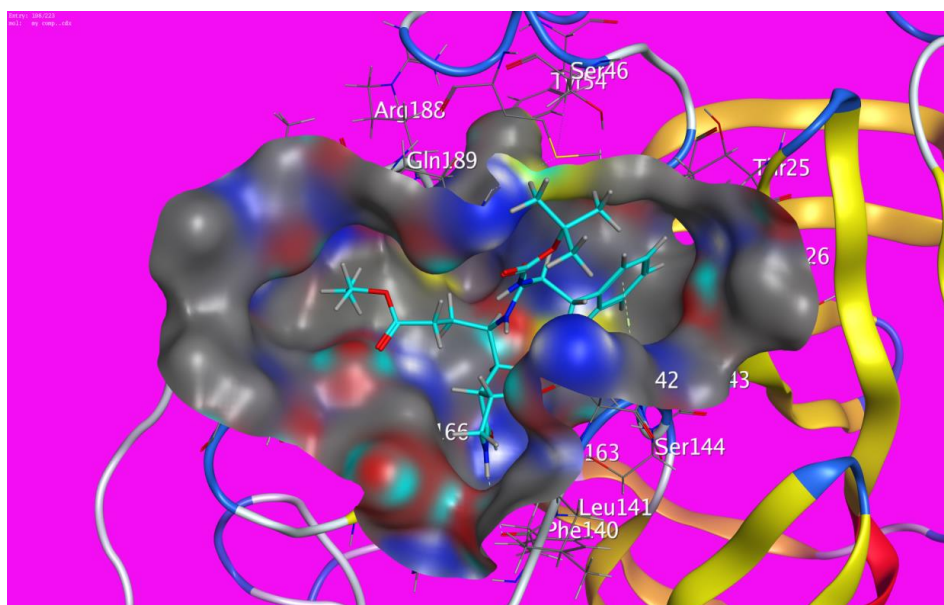


Figure 2. Mapping surface showing the co-crystallized ligand (PRD-002214) occupying the active pocket of the COVID-19 main protease

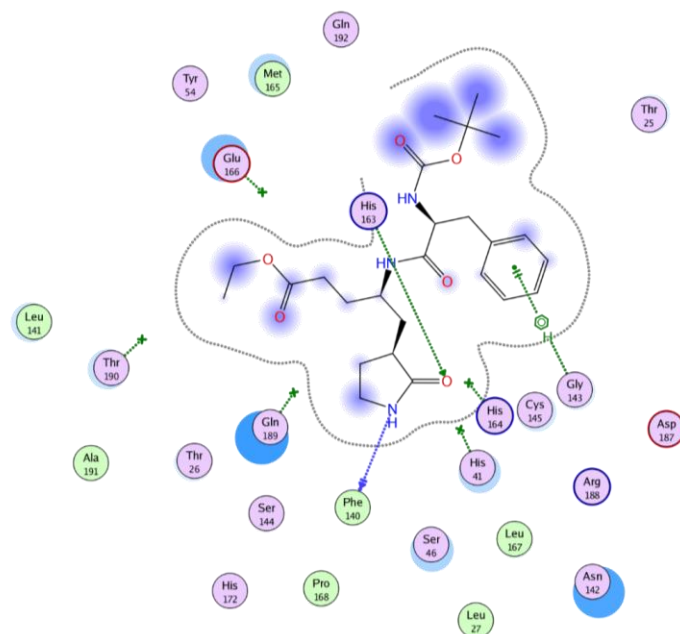


Figure 3. 2D interaction of the co-crystallized ligand (PRD-002214) in the active site of the COVID-19 main protease

Compound (**1**) showed good binding mode with energy of -6.22 kcal/mol (Tab. 1) occupying three pockets of M^{pro} . The detailed binding mode was as follows: The 2-methoxyphenol moiety occupied the first pocket of M^{pro} forming two hydrogen bonds with Gly143 and Leu141. Additionally, it showed one electrostatic attraction with Cys145. The 4H-pyran-4-one moiety occupied the second pocket of M^{pro} forming one hydrophobic interaction with Met165. Furthermore, the 1,3-dihydroxybenzen moiety occupied the third pocket of the receptor forming one hydrogen bond with Gln192 (Figures 4–6).

Table 1

The docking binding free energies of compounds, simeprevir and the co-crystallized ligand (PRD-002214) against COVID-19 main protease

| Compounds | Binding free energy (kcal/mol) |
|-------------------------------------|--------------------------------|
| (1) | -6.19 |
| Co-crystallized ligand (PRD-002214) | -7.83 |



Figure 4. Compound **1** docked into the active site of the COVID-19 main protease, the hydrogen bonds are represented in green dashed lines and the hydrophobic interactions are represented in orange dashed lines

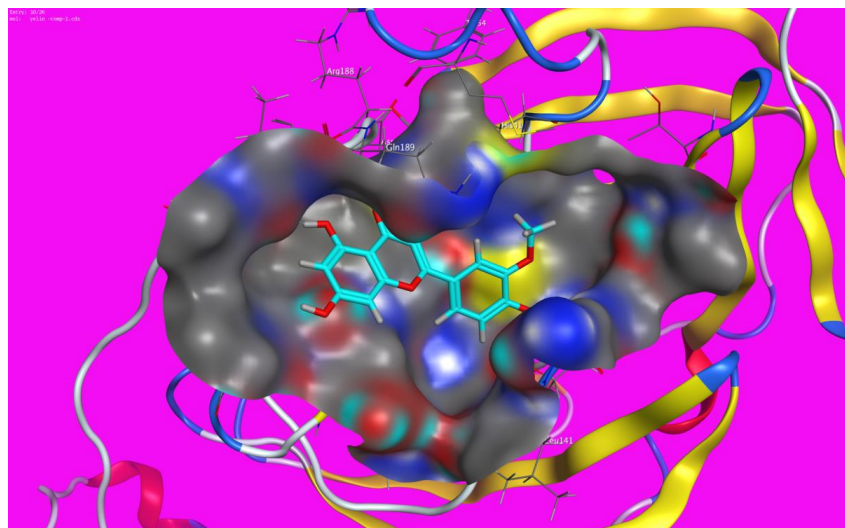


Figure 5. Mapping surface showing compound **1** occupying the active pocket of the COVID-19 main protease

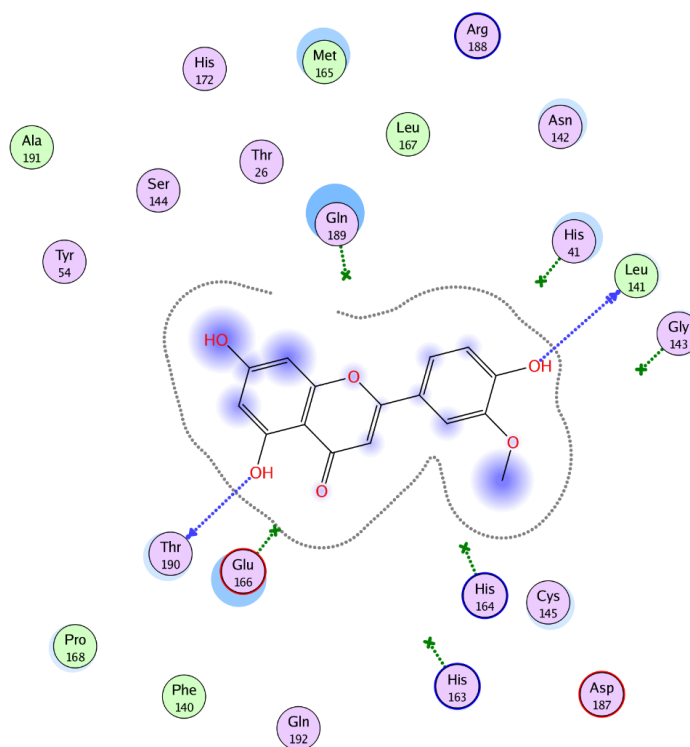


Figure 6. 2D interaction of compound **1** in the active site of the COVID–19 main protease

Conclusions

By virtue of the column chromatography, then by preparative thin-layer chromatography of the extract obtained from ethanol extraction of the aboveground parts of *Chondrilla brevirostris* Fisch. & C.A. Mey., the flavonoid 5,7,4'-trihydroxy-3'-methoxyflavone was isolated. This compound from *Ch. brevirostris* was isolated for the first time. *In silico*, molecular docking study was carried out for the isolated compound against the COVID–19 main protease. As a result, the compound showed good binding energy.

Acknowledgments

This research is funded by the Science Committee of the Ministry of Education and Science of the Republic of Kazakhstan OR11465530 “Creation and replenishment of the collection of industrially valuable microorganisms, study and preservation of their biological diversity for the needs of biotechnology, medicine

and agriculture”, Grant AP08051842 “Study of the composition and biological activity of the essential oils of plants of Central and Southeast Asia” and Matsumae International Foundation (Japan).

References

- [Электронный ресурс]. Режим доступа: <http://www.theplantlist.org> (дата обращения: 20 марта, 2021).
- Terencio M. On the occurrence of caffeoyltartronic acid and other phenolics in *Chondrilla juncea* / M. Terencio, R. Giner, M. Sanz, S. Manez, J. Rios // *Zeitschrift für Naturforschung*, 1993. — Vol. 48. — P. 417–419.
- Suleimen Y.M. Isolation, Crystal Structure, and In Silico Aromatase Inhibition Activity of Ergosta-5, 22-dien-3 β -ol from the Fungus *Gyromitra esculenta* / Y.M. Suleimen, A.M. Metwaly, A.E. Mostafa, E.B. Elkaeed, H. -W. Liu, B.B. Basnet, R.N. Suleimen, M.Y. Ishmuratova, K.M. Turdybekov, K. Van Hecke // *Journal of Chemistry*, 2021. — Article ID 5529786. <https://doi.org/10.1155/2021/5529786>
- Jalmakhanbetova R.I. Isolation and In Silico Anti-COVID-19 Main Protease (Mpro) Activities of Flavonoids and a Sesquiterpene Lactone from *Artemisia sublessingiana* / R.I. Jalmakhanbetova, Y.M. Suleimen, M. Oyama, E.B. Elkaeed, I. Eissa, R.N. Suleimen, A.M. Metwaly, M.Y. Ishmuratova // *Journal of Chemistry*, 2021. — Article ID 5547013. <https://doi.org/10.1155/2021/5547013>
- Jalmakhanbetova R. Synthesis and Molecular Docking of Some Grossgemin Amino Derivatives as Tubulin Inhibitors Targeting Colchicine Binding Site / R. Jalmakhanbetova, E.B. Elkaeed, I.H. Eissa, A.M. Metwaly, Y.M. Suleimen // *Journal of Chemistry*, 2021. — Article ID 5586515. <https://doi.org/10.1155/2021/5586515>
- Zhanzhaxina A. In vitro and in silico cytotoxic and antibacterial activities of a diterpene from *Cousinia alata* Schrenk / A. Zhanzhaxina, Y. Suleimen, A.M. Metwaly, I.H. Eissa, E.B. Elkaeed, R. Suleimen, M. Ishmuratova, K. Akatan, W. Luyten // *Journal of Chemistry*, 2021. — Article ID 5542455. <https://doi.org/10.1155/2021/5542455>
- Ninomiya M. Structure–activity relationship studies of 5, 7-dihydroxyflavones as naturally occurring inhibitors of cell proliferation in human leukemia HL-60 cells / M. Ninomiya, K. Nishida, K. Tanaka, K. Watanabe, M. Koketsu // *Journal of Natural Medicines*, 2013. — Vol. 67, Issue 3. — P. 460–467. <https://doi.org/10.1007/s11418-012-0697-0>
- Chemical Computing Group, Molecular Operating Environment (MOE). [Электронный ресурс]. Режим доступа: <http://www.chemcomp.com> (дата обращения: 23 мая 2021).
- El-Demerdash A. Comprehensive virtual screening of the antiviral potentialities of marine polycyclic guanidine alkaloids against SARS-CoV-2 (COVID-19) / A. El-Demerdash, A.M. Metwaly, A. Hassan, A. El-Aziz, T. Mohamed, E.B. Elkaeed, I.H. Eissa, R.K. Arafa, J.D. Stockand // *Biomolecules*, 2021. — Vol. 11, Iss. 4. — P. 460. <https://doi.org/10.3390/biom11030460>
- Imieje V.O. Comprehensive In Silico Screening of the Antiviral Potentialities of a New Humulene Glucoside from *Asteriscus hierochunticus* against SARS-CoV-2 / V.O. Imieje, A.A. Zaki, A.M. Metwaly, A.E. Mostafa, E.B. Elkaeed, A. Falodun // *Journal of Chemistry*, 2021. — Article ID 5541876. <https://doi.org/10.1155/2021/5541876>
- Alesawy M.S. In Silico Studies of Some Isoflavonoids as Potential Candidates against COVID-19 Targeting Human ACE2 (hACE2) and Viral Main Protease (Mpro) / M.S. Alesawy, A.E. Abdallah, M.S. Taghour, E.B. Elkaeed, I.H. Eissa, A.M. Metwaly // *Molecules*, 2021. — Vol. 26, Issue 9. — P. 2806. <https://doi.org/10.3390/molecules26092806>
- Eissa I. Molecular docking and dynamics simulation revealed the potential inhibitory activity of ACEIs against SARS-CoV-2 targeting hACE2 receptor / I. Eissa, A. Al-Karmalawy, M.A. Dahab, A.M. Metwaly, S.S. Elhady, E.B. Elkaeed, K.M. Darwish // *Frontiers in Chemistry*, 2021. — Vol. 9. — P. 227. <https://doi.org/10.3389/fchem.2021.661230>
- Imieje V.O. Antileishmanial Derivatives of Humulene from *Asteriscus hierochunticus* with in silico Tubulin Inhibition Potential / V.O. Imieje, A.A. Zaki, A.M. Metwaly, I.H. Eissa, E.B. Elkaeed, Z. Ali, I.A. Khan, A. Falodun // *Rec. Nat. Prod.*, 2022. — Vol. 16, Issue 2. — P. 150–171. <http://doi.org/10.25135/rnp.253.21.01.1945>

Р.И. Жалмаханбетова, Е.М. Сүлеймен, Н. Абе, М. Ояма,
А.М. Метуали, И.Х. Эйса, М.Ю. Ишмуратова, Ж.А. Ибатаев

***Chondrilla brevirostris* Fisch & C.A. Mey-ден хризозериолдың бөліп алынуы және *in silico* SARS-CoV-2 негізгі протеазаны ингибирлеу потенциалы**

Chondrilla L. туысының ТМД аумағында 22 түрі бар, олардың 16-сы Қазақстанда. *Chondrilla* L. туысының барлық түрлері — сағызды өсімдік, күрделі гүлділер (*Asteraceae*) тұқымдасына жататын шөптесін өсімдіктер. Химиялық зерттеу үшін *Chondrilla brevirostris* Fisch & C.A. Mey. алынды. Бұл шөпті дала мен орман шалғындарында өсетін көпжылдық шөпті өсімдік. *Ch. brevirostris*-тің өсімдік шикізатын зерттеу үшін 2019 жылдың тамыз айында Қарағанды облысының Жезқазған қаласынан 200 шақырым жерде гүлдену мен жеміс беру кезеңінде жиналды. *Ch. Brevirostris* жер үсті бөлігі бөлме температурасында этанолмен экстракцияланды. Этанол сығындысын колонкалық хроматография арқылы бөлу нәтижесінде бірнеше фракциялар алынды. Алынған фракцияларды әрі қарай зерттеу және флавоноидтарды бөліп алу үшін рехроматография және препаративті жұқа қабатты

хроматография қолданылды. Препаративті жұқа қабатты хроматографиялау нәтижесінде флавоноид 5,7,4'-тригидрокси-3'-метоксифлавоң (қосылыс 1) бөлінді. Қосылыстың 1 химиялық құрылымы спектроскопиялық мәліметтер бойынша дәлелденді. Бұл қосылыс *Chondrilla*-ның осы түрінен алғаш рет бөлініп алынды. Бөлініп алынған қосылысқа докинг зерттеулері жүргізілді. Бұл жағдайда қосылыс жақсы байланыс энергиясын $-6,22$ ккал/моль көрсетті, ал эталондық молекуланың байланыс энергиясы $-7,83$ ккал/мольді құрады.

Кілт сөздер: *Chondrilla brevirostris*, *Asteraceae*, экстракция, колонкалық хроматография, ПЖҚХ, оқшаулау, флавоноид, құрылым, спектроскопия, докинг зерттеуі.

Р.И. Джалмаханбетова, Е.М. Сүлеймен, Н. Абе, М. Ояма,
А.М. Метуали, И.Х. Эйса, М.Ю. Ишмуратова, Ж.А. Ибатаев

Выделение и *in silico* основной потенциал ингибирования протеазы SARS-CoV-2 хризозериола из *Chondrilla brevirostris* Fisch. & C.A. Mey

Род *Chondrilla* L. на территории СНГ насчитывается 22 вида, из них 16 — в Казахстане. Все виды рода *Chondrilla* L. являются каучуконосными растениями, родом травянистых растений семейства сложноцветных (*Asteraceae*). Для химического исследования использовано *Chondrilla brevirostris* Fisch. & C.A. Mey., представляющее многолетнее травянистое растение, произрастающее в пустынных степях и на лесных лугах. Растительное сырье *Ch. Brevirostris* для исследований было собрано в августе 2019 года в 200 км от г. Жезказгана Карагандинской области в фазе цветения–плодоношения. Надземную часть *Ch. brevirostris* экстрагировали этанолом при комнатной температуре. В результате разделения этанольного экстракта на колоночной хроматографии было получено несколько фракций. Для дальнейшего изучения полученных фракций и выделения флавоноидов применяли рехроматографию и препаративную тонкослойную хроматографию. В результате препаративной тонкослойной хроматографии был выделен флавоноид 5,7,4'-тригидрокси-3'-метоксифлавоң (соединение 1). Химическая структура 1 была установлена по спектральным данным. Данный флавоноид из этого вида *Chondrilla* был выделен впервые. Оно было подвергнуто докинг исследованию. При этом вещество показало хорошую энергию связи $-6,22$ ккал/моль, а энергия связи эталонной молекулы составила $-7,83$ ккал/моль.

Ключевые слова: *Chondrilla brevirostris*, *Asteraceae*, экстракция, колоночная хроматография, ПТСХ, выделение, флавоноид, структура, спектроскопия, докинг исследование.

References

- 1 Retrieved from: <http://www.theplantlist.org>. [in Russian].
- 2 Terencio, M., Giner, R., Sanz, M., Manez, S., & Rios, J. (1993). On the occurrence of caffeoyltartronic acid and other phenolics in *Chondrilla juncea*. *Zeitschrift für Naturforschung*, 48, 417–419.
- 3 Suleimen, Y.M., Metwaly, A.M., Mostafa, A.E., Elkaeed, E.B., Liu, H.-W., & Basnet, B.B., et al. (2021). Isolation, Crystal Structure, and In Silico Aromatase Inhibition Activity of Ergosta-5, 22-dien-3 β -ol from the Fungus *Gyromitra esculenta*. *Journal of Chemistry*, 5529786. <https://doi.org/10.1155/2021/5529786>
- 4 Jalmakhanbetova, R.I., Suleimen, Y.M., Oyama, M., Elkaeed, E.B., Eissa, I., Suleimen, R.N., Metwaly, A.M., & Ishmuratova, M.Y. (2021). Isolation and In Silico Anti-COVID-19 Main Protease (Mpro) Activities of Flavonoids and a Sesquiterpene Lactone from *Artemisia sublessingiana*. *Journal of Chemistry*, 5547013. <https://doi.org/10.1155/2021/5547013>
- 5 Jalmakhanbetova, R., Elkaeed, E.B., Eissa, I.H., Metwaly, A.M., & Suleimen, Y.M. (2021). Synthesis and Molecular Docking of Some Grossgemin Amino Derivatives as Tubulin Inhibitors Targeting Colchicine Binding Site. *Journal of Chemistry*, 5586515. <https://doi.org/10.1155/2021/5586515>.
- 6 Zhanzhaxina, A., Suleimen, Y., Metwaly, A.M., Eissa, I.H., Elkaeed, E.B., & Suleimen, R., et al. (2021). In vitro and in silico cytotoxic and antibacterial activities of a diterpene from *Cousinia alata* Schrenk. *Journal of Chemistry*, 5542455. <https://doi.org/10.1155/2021/5542455>
- 7 Ninomiya, M., Nishida, K., Tanaka, K., Watanabe, K., & Koketsu, M. (2013). Structure–activity relationship studies of 5,7-dihydroxyflavones as naturally occurring inhibitors of cell proliferation in human leukemia HL-60 cells. *Journal of Natural Medicines*, 67, 3; 460–467. <https://doi.org/10.1007/s11418-012-0697-0>
- 8 Chemical Computing Group, Molecular Operating Environment (MOE). (2021). Retrieved from: <http://www.chemcomp.com>.
- 9 El-Demerdash, A., Metwaly, A.M., Hassan, A., El-Aziz, A., Mohamed, T., Elkaeed, E.B., Eissa, I.H., Arafa, R.K., & Stockand, J.D. (2021). Comprehensive virtual screening of the antiviral potentialities of marine polycyclic guanidine alkaloids against SARS-CoV-2 (COVID-19). *Biomolecules*, 11, 4; 460. <https://doi.org/10.3390/biom11030460>

10 Imieje, V.O., Zaki, A.A., Metwaly, A.M., Mostafa, A.E., Elkaeed, E.B., & Falodun, A. (2021). Comprehensive *In Silico* Screening of the Antiviral Potentialities of a New Humulene Glucoside from *Asteriscus hierochunticus* against SARS-CoV-2. *Journal of Chemistry*, 5541876. <https://doi.org/10.1155/2021/5541876>

11 Alesawy, M.S., Abdallah, A.E., Taghour, M.S., Elkaeed, E.B., Eissa, I.H., & Metwaly, A.M. (2021). *In Silico* Studies of Some Isoflavonoids as Potential Candidates against COVID-19 Targeting Human ACE2 (hACE2) and Viral Main Protease (Mpro). *Molecules*, 26, 9; 2806. <https://doi.org/10.3390/molecules26092806>.

12 Eissa, I., Al-Karmalawy, A., Dahab, M.A., Metwaly, A.M., Elhady, S.S., Elkaeed, E.B., & Darwish, K.M. (2021). Molecular docking and dynamics simulation revealed the potential inhibitory activity of ACEIs against SARS-CoV-2 targeting hACE2 receptor. *Frontiers in Chemistry*, 9; 227. <https://doi.org/10.3389/fchem.2021.661230>

13 Imieje, V.O., Zaki, A.A., Metwaly, A.M., Eissa, I.H., Elkaeed, E.B., Ali, Z., Khan, I.A., & Falodun, A. (2022). Antileishmanial Derivatives of Humulene from *Asteriscus hierochunticus* with *in silico* Tubulin Inhibition Potential. *Rec. Nat. Prod.*, 16, 2; 150–171. <http://doi.org/10.25135/rnp.253.21.01.1945>

Information about the authors

Jalmakhanbetova, Roza Ilemisovna — Doctor of Chemical Sciences, Associate Professor, L.N. Gumilyov Eurasian National University, K. Munaitpasov street, 13, Z01C0X0, Nur-Sultan, Kazakhstan; International Centre for Interdisciplinary Solutions on Antibiotics and Secondary Metabolites, Republican Collection of Microorganisms, Valikhanov street, 13/1, 010000, Nur-Sultan, Kazakhstan; e-mail: rozadi-chem@mail.ru; <https://orcid.org/0000-0001-9937-275X>;

Suleimen, Yerlan Melsuly — Candidate of Chemical Sciences, PhD, Head of the International Centre for Interdisciplinary Solutions on Antibiotics and Secondary Metabolites, Republican Collection of Microorganisms, Valikhanov street, 13/1, 010000, Nur-Sultan, Kazakhstan; Sh. Ualikhanov Kokshetau University, 020000, Kokshetau, Kazakhstan; e-mail: syerlan75@yandex.kz; <https://orcid.org/0000-0002-5959-4013>;

Abe, Naohito — PhD, Associate Professor, Laboratory of Pharmacognosy, Gifu Pharmaceutical University, Gifu, Japan, e-mail: aben@gifu-pu.ac.jp; <https://orcid.org/0000-0002-2757-3736>;

Oyama, Masayoshi — PhD, Professor, Head of the Laboratory of Pharmacognosy, Gifu Pharmaceutical University, 501-1196, Gifu, Japan, e-mail: oyama@gifu-pu.ac.jp; <https://orcid.org/0000-0002-6947-5798>;

Metwaly, Ahmed Mohamed — PhD, Associate Professor, Pharmacognosy Department, Faculty of Pharmacy (Boys), Al-Azhar University, Cairo, Egypt, e-mail: ametwaly@azhar.edu.eg; <https://orcid.org/0000-0001-8566-1980>;

Eissa, Ibrahim Hassan Abd-Elgawwad — PhD, Pharmaceutical Medicinal Chemistry & Drug Design Department, Faculty of Pharmacy (Boys), Al-Azhar University, Cairo, Egypt, e-mail: Ibrahimeissa@azhar.edu.eg; <https://orcid.org/0000-0002-6955-2263>;

Ishmuratova, Margarita Yulayevna — Candidate of Biological Sciences, Professor, Botany Department, Karagandy University of the name of academician E.A. Buketov, Universitetskaya street, 28, 100024, Karaganda, Kazakhstan; e-mail: margarita.ishmur@mail.ru; <https://orcid.org/0000-0002-1735-8290>;

Ibatayev, Zharkyn Abykenovich — Candidate of chemical sciences, Head of the Department of Physics and Chemistry, S. Seifullin Kazakh Agricultural Technical University, 010011, Nur-Sultan, Kazakhstan, e-mail: zhardisser@mail.ru; <https://orcid.org/0000-0003-2261-222X>.

A.Zh. Sarsenbekova¹, A.N. Bolatbay^{1*}, V.V. Morgun¹,
D. Havlicek², S.Zh. Davrenbekov¹, E. Nasikhatuly¹

¹Karagandy University of the name of academician E.A. Buketov, Karaganda, Kazakhstan;

²Charles University, Prague, Czech Republic

(*Corresponding author's e-mail: abylai_bolatbai@mail.ru)

Study of thermal stability and determination of effective activation energy values during degradation of unsaturated polyester copolymers in the air atmosphere

The study of the kinetic parameters of copolymers based on polyethylene glycol fumarates, as well as the external and internal effects on them, is essential for production processes at various levels. This will solve a whole range of issues in the field of the shelf life of materials and storage conditions. All these point to the relevance of this research. The authors of the research attempt to test the most common thermogravimetric data processing methods and to improve them in terms of the quality of the predictive capabilities of the resulting regression equation. Both of them are important for the production of initial components and the manufacture of the final product from the studied materials. Therefore, the study and further use of the numerical data of the TG/DTA curves applies to both theoretical and practical branches of science. Thus, summarizing the experimental data on the thermal stability studies, we assume that p-EGF: AA copolymers with compositions of 21.03:78.97 and 68.96:31.04 wt.% have a relatively high degree of resistance to heating. It was found that the calculation by the FR method agreed well with the results of the KAS method. It should be noted that for the p-EGF: AA copolymer (21.03:78.97 wt.%) at heating rates of 5.0, 10.0, 20.0 °C·min⁻¹, the average activation energy data obtained for two methods increase in the following series: $\bar{E}_{KAS} = 187.34 \text{ kJ/mol} < \bar{E}_{FR} = 200.17 \text{ kJ/mol}$.

Keywords: thermogravimetry, thermal analysis, kinetic parameters, copolymers, polyethylene glycol fumarate, acrylic acid, activation energy, polyesters.

Introduction

Previously, we have developed methods for producing unsaturated polyester resins [1]. By implementing radical co- and terpolymerization of ionic monomers, a number of cross-linked polymers with a mesh structure were obtained, which can be used as hydrogels in vegetable crops. Also, the main kinetic parameters of the decomposition of some of the above copolymers were identified using differential and integral methods [2, 3]. The research result showed the practical value of this technique. It should be noted that, before our study, the process of studying the thermal stability of unsaturated polymers had not yet been considered by experts.

An integral part of the research is that no domestic or international professional literature has yet been developed that allows the most accurate prediction of the composition of polymeric materials and their kinetic properties. Determining the properties of kinetic polymers is a complex process in which many external factors have to be considered, especially thermal exposure, which requires significant time, material and physical cost. With the help of data, the prediction accuracy will increase, and the process itself will become less costly and time-consuming.

The main purpose of this work is to conduct a thermal analysis [4] of unsaturated polyester resin copolymers of various compositions in the atmosphere and to interpret the kinetic parameters obtained as a result of mathematical processing of thermogravimetric data.

Experimental

The study of the thermal decomposition of the copolymer of polyethylene glycol fumarates with acrylic acid was carried out on a differential scanning calorimeter LABSYSTM EVO 1600 °C SETARAM, (France) in dynamic mode in the temperature range of 30–1000 °C at heating rates 5.0, 10.0, 20.0 °C·min⁻¹ in the purified air environment, at a speed flow 30 mL/min. The device calibration for thermogravimetric studies and heat flux was performed according to CaCO₃ and In (Indium) standards, respectively.

As a rule, the differential kinetic equation for the thermal decomposition process can be written as follows:

$$\ln\left(\beta \frac{d\alpha}{dT}\right) = \ln[Af(\alpha)] - \frac{E}{RT} \quad (1)$$

The expression on the right side of the equation contains an exponential function and this expression cannot be represented as an analytical function. The solution can be the search for some approximation [5]. In practice, the most common way to overcome this difficulty is to use the following methods:

a) The Friedman method (FR) [6] is considered a “model-free” method, since $f(\alpha)$ is not explicitly specified.

b) The main equation of the Kissinger-Akahira-Sunose (KAS) method [7, 8] is as follows:

$$\ln(\beta/T^2) = \ln[AE/(Rg(\alpha))] - E/RT$$

The choice of methods is due to the possibility of comparing the activation energy obtained by differential and integral methods, which makes it possible to assess the validity of the assumptions made when deriving these equations. The results of the FR and KAS methods are systematized in Table 1 the graphical interpretation is shown in Figure 3.

Results and Discussion

In this work, the objects of study were previously synthesized copolymers of polyethylene glycol fumarate with acrylic acid with compositions of 21.03:78.97 and 68.96:31.04 wt.%. Figure 1 demonstrates the results of thermogravimetric analysis of these copolymers.

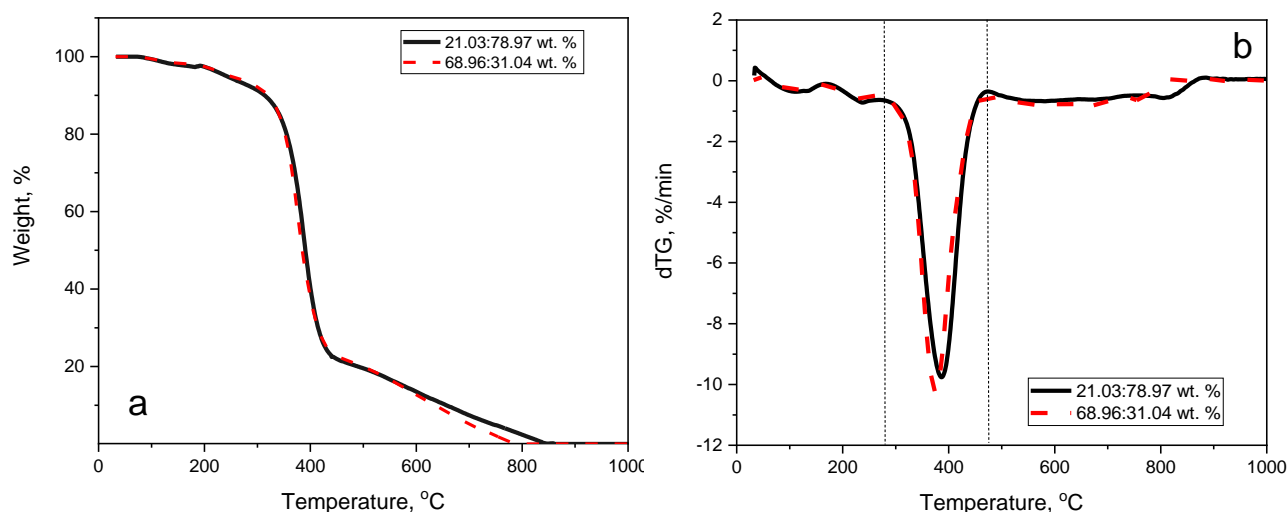


Figure 1. Dependences of samples mass on temperature (a) and mass change rate (b) of p-EGF:AA copolymers at a heating rate of 10 °C/min

Figure 1 indicates the thermograms of copolymers of p-EGF:AA composition 21.03:78.97 and 68.96:31.04 wt.%. It is shown that the copolymers of p-EGF:AA (21.03:78.97 and 68.96:31.04 of the wt.%) are resistant to 1000.0 °C, while the copolymers are observed exothermic effect $T_{\text{initial}} = 277 \pm 0.1$ °C (at 386 °C) for p-EGF:AK (21.03:78.97) and $T_{\text{initial}} = 265.0 \pm 0.1$ °C (at 375.0 °C). The low-temperature peak is associated with the cleavage of crystallization water, the second peak is explained by the destruction of the main chains, which proceeds by random rupture model. The p-EGF:AK copolymers composites 21.03:78.97 and 68.96:31.04 wt.% (Figure 1, b) are resistant at 1000.0 °C, from 10 % to 15 % weight loss at 200.0 °C. The residual weight is 58–60 %.

Table 1

Thermogravimetric data for copolymers 21.03:78.97 and 68.96:31.04 wt.%

| Copolymer | $T_{\text{initial}}(^{\circ}\text{C})$ | $T_{\text{peak}}(^{\circ}\text{C})$ | $T_{\text{final}}(^{\circ}\text{C})$ |
|------------------|--|-------------------------------------|--------------------------------------|
| 21.03:78.97 wt.% | 277 | 386 | 472 |
| 68.96:31.04 wt.% | 265 | 375 | 470 |

To determine the activation energy of the thermal decomposition process, the main stage of the copolymer decomposition was chosen (Figure 1b). Figure 2 (a, b) shows the decomposition degree.

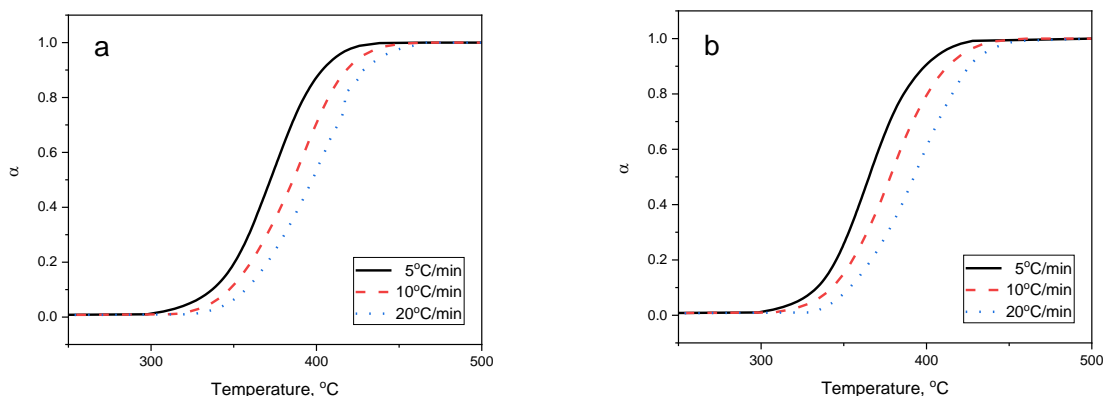


Figure 2. Dependence of conversion degree α on temperature of p-EGF:AA copolymers 21.03:78.97 (a) and 68.96:31.04 (b) at different heating rates

As can be seen from Figure 2, the calculated values of the degree [9] of transformation have a similar conversion nature. However, there is a delay in the decomposition process with an increasing heating rate. This can be seen from the shift in the initial temperature from 300 °C to 330 °C for lower and higher heating rates, respectively. Kinetic parameters obtained from the slope and intersection of the straight lines are presented in Table 1; graphical interpretation is shown in Figure 3.

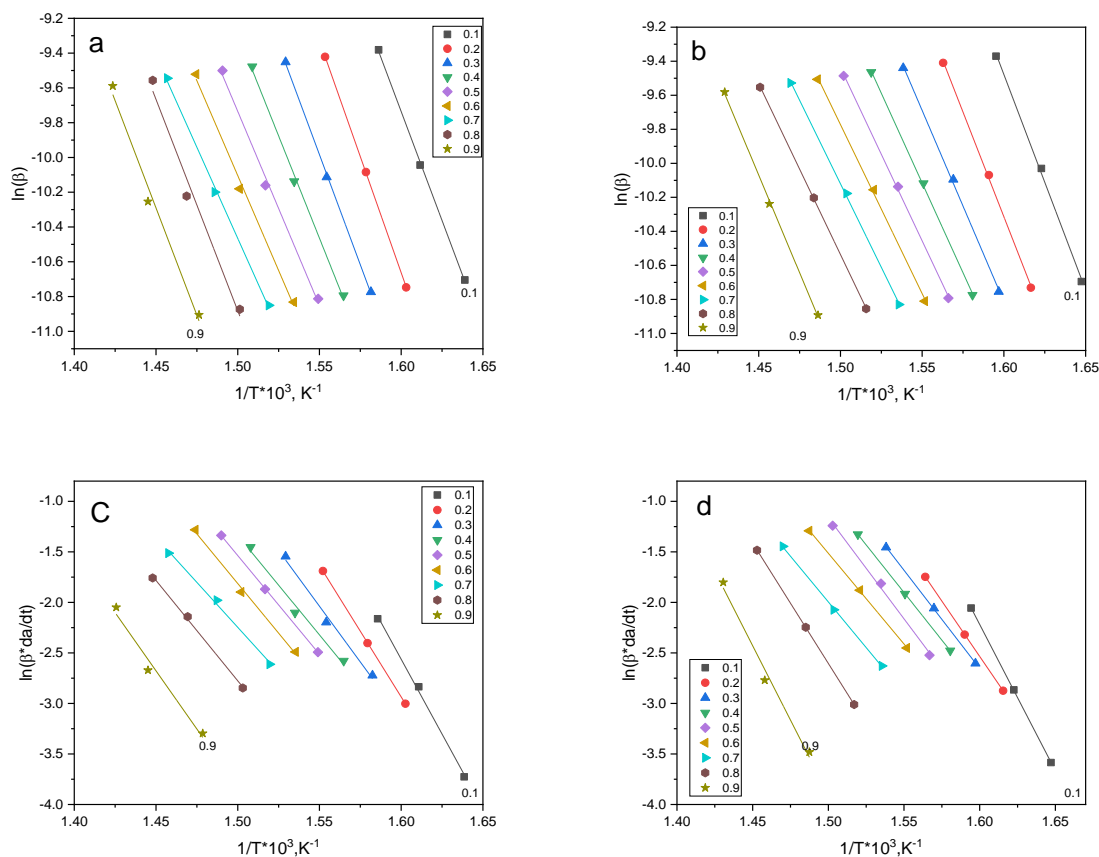


Figure 3. Graphical dependences of Kissinger-Akahira-Sunose (a, b) and Friedman (c, d) equations for the p-EGF:AK copolymer at 21.03:78.97 and 68.96:31.04 wt.% ratios

The curves (Figure 3) obtained by the KAS and FR methods for p-EGF:AA copolymers at 21.03:78.97 and 68.96:31.04 wt.% ratios are linear, which means that both methods provide reliable results regarding their thermal decomposition kinetics. The conclusion further [10] is supported by the fact that the activation energies calculated by both methods agree relatively closely (Table 1). This experimental result suggests that both the composition and, most importantly, the ability of NPS (polyethylene glycol fumarate) to form copolymers with acrylic acid (AA) play an important role in determining the thermal degradation kinetics of p-EGF: AA copolymers. The fact that in the FR method [6] (model-free analysis) $f(\alpha)$ is a constant value, while the logarithm of the conversion rate $\ln[\beta(d\alpha/dT)]$ is considered as a function of the corresponding temperature at any fixed value of α . In contrast, in the KAS method [7, 8] (integral method), the determination of kinetic triplets is based on determining the temperature (T) corresponding to a certain, derivatively chosen value of the degree of conversion (α) at various heating rates (β). Analysis of the obtained results (Figure 4) led to the conclusion that the FR and KAS methods make it possible to determine the kinetic characteristics of the decomposition of p-EGF:AA copolymers.

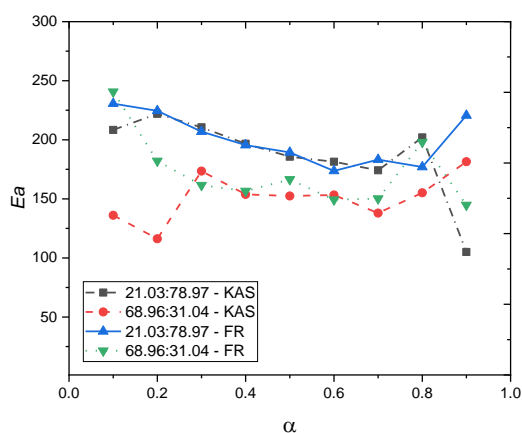


Figure 4. Activation energies according to Kissinger-Akahira-Sunose (KAS) and Friedman (FR)

Comparing the data (Figure 2) from the KAS and FR approaches, it can be noted that the results for activation energies are similar. Nevertheless, the first method (KAS) provides activation energies (\bar{E}) values which are 10 % lower than those of the FR method. This makes sense because these methods are based on relatively different approximations. However, the FR equation provides more reliable and accurate results than the KAS equation [11].

Conclusions

The thermostability and thermal decomposition kinetics of copolymers of polyethylene glycol fumarate with acrylic acid (21.03:78.97 and 68.96:31.04 wt.%) were first studied by thermogravimetric analysis (TGA) and differential thermogravimetry (DTG). A new direction of application in the identification of copolymers, as well as in the development of production technology [12] and safe disposal of macromolecular substances based on NPS (polyethylene glycol fumarate), was investigated. These parameters were determined based on FR and KAS methods, which have good convergence. It was shown that thermostability decreases in the following order: p-EGF:AA (21.03:78.97) > p-EGF:AA (68.96:31.04). Based on the study of TG/DTG curves for copolymers of polyethylene glycol fumarate with acrylic acid of two different compositions 21.03:78.97 and 68.96:31.04 wt.%, it can be assumed that these compounds have a relatively high degree of heat resistance. Under the influence of oxygen, the copolymers are completely decomposed to high temperatures without a carbon residue. It was also found that the copolymer with a high content of polyester resins exhibits less activity.

References

- 1 Burkeyev, M.Zh., Kudaibergen, G.K., Burkeyeva, G.K., & Tazhbayev Y.M., et al. (2018). The number average and mass average molar masses of polyethylene(propylene)glycol fumarates. *Bulletin of the University of Karaganda — Chemistry*, 90, 17–22. <https://doi.org/10.31489/2018ch2/17-22>
- 2 Burkeev, M.Zh., Sarsenbekova, A.Zh., & Bolatbay, A.N., et al. (2020). The use of differential calculation methods for the destruction of copolymers of polyethylene glycol fumarate with the acrylic acid. *Bulletin of the University of Karaganda – Chemistry*, 99, 4–10. <https://doi.org/10.1134/S0036024415120067>
- 3 Burkeev, M.Zh., Bolatbay, A.N., Sarsenbekova, A.Zh., Davrenbekov, S.Zh., & Nasikhatuly, E. (2021). Integral Ways of Calculating the Destruction of Copolymers of Polyethylene Glycol Fumarate with Acrylic Acid. *Russian Journal of Physical Chemistry A*, 95, 2009–2013. <https://doi.org/10.1134/s0036024421100034>
- 4 Wunderlich, B. (2005). *Thermal Analysis of Polymeric Materials*. Berlin, Heidelberg: Springer. <https://doi.org/10.1007/b137476>
- 5 Vyazovkin, S., Burnhnam, A.K., Criado, J.M., Perez-Maqueda, L.A., Popescu, C., & Sbirrazzuoli, N. (2011). ICTAC Kinetic Committee recommendation for performing kinetic computations on thermal analysis data. *Thermochimica Acta*, 520, 1–19. <https://doi.org/10.1016/j.tca.2011.03.034>
- 6 Friedman, H.L. (1964). Kinetics of thermal degradation of char-forming plastics from thermogravimetry. Application to a phenolic plastic. *Journal of Polymer Science*, 6, 183–185. <https://doi.org/10.1002/polc.5070060121>
- 7 Kissinger, H.E. (1957). Reaction kinetics in differential thermal analysis. *Analytical Chemistry*, 29, 1702–1706. <https://doi.org/10.1021/ac60131a045>
- 8 Akahira, T., & Sunose, T. (1971). Method of determining activation deterioration constant of electrical insulating materials. *Research Report Chiba Institute of Technology. Sci. Technol*, 16, 22–31. <https://doi.org/10.17221/115/2016-RAE>
- 9 Sarsenbekova, A.Z., Kudaibergen G.K., & Burkeev M.Z., et al. (2019). Comparative analysis of the thermal decomposition kinetics of polyethylene glycol fumarate-acrylic acid copolymers. *Russian Journal of Physical Chemistry A*, 93, 1252–1257. <https://doi.org/10.1134/S0044453719060281>
- 10 Ewa, K.W. (2003). Kinetics of thermal decomposition of unsaturated polyester resins with reduced flammability. *Journal of Applied Polymer Science*, 88, 2851–2857. <https://doi.org/10.1002/app.11723>
- 11 Muravyev, N.V., Pivkina, A.N., & Koga N. (2019). Critical appraisal of kinetic calculation methods applied to overlapping multistep reactions. *Molecules*, 24, 2298. <https://doi.org/10.3390/molecules24122298>
- 12 Fidanovski, B.Z., Spasojevic, P.M., Panic V.V., Seslija S.I., Spasojevic, J.P., & Popovic, I.G. (2017). Synthesis and characterization of fully bio-based unsaturated polyester resins. *Journal of Materials Science*, 53, 4635–4644. <https://doi.org/10.1007/s10853-017-1822-y>

А.Ж. Сарсенбекова, А.Н. Болатбай, В.В. Моргун,
Д. Хавличек, С.Ж. Давренбеков, Е. Насихатұлы

Ауа атмосферасындағы қанықпаған полиэфир сополимерлерінің деградациясы кезінде жылу тұрақтылығын зерттеу және активтендіру энергиясының тиімді мәндерін анықтау

Полиэтиленгликольфумарат негізіндегі сополимерлердің кинетикалық көрсеткіштері, сондай-ақ, оларға ішкі және сыртқы әсер ету саласындағы зерттеулер әр түрлі деңгейдегі өндірістік процестер үшін өте маңызды. Бұл материалдардың жарамдылық мерзімі мен оларды сақтау шарттары саласындағы бірқатар мәселелерді шешеді. Мұның бәрі осы зерттеудің өзектілігін көрсетеді. Жұмыста термогравиметриялық деректерді өңдеудің және олардан алынған регрессиялық теңдеудің болжамды мүмкіндіктерін сапасы тұрғысынан жетілдірудің кең таралған әдістерін тексеруге әрекет жасалған. Сонымен қатар, бұл көрсеткіштер бастапқы компоненттерді өндіру үшін де, зерттелетін материалдардан түпкілікті өнімді жасау үшін де өте пайдалы. Сондықтан ТГ/ДТА қисықтарының сандық деректерін зерттеу және одан әрі қарай пайдалану ғылымның теориялық және практикалық салалары үшін маңызы бар. Осылайша, термиялық тұрақтылығын зерттеу бойынша эксперименттік деректерді жинақтай отырып, құрамы 21.03:78.97 және 68.96:31.04 болатын п-ЭГФ:АК сополимерлерінің қыздыруға төзімділігін салыстырмалы түрде жоғары дәрежеге ие деп болжанады. Сондай-ақ, ФР әдісі бойынша есептеулер, КАС әдісінің есептеу нәтижелерімен жақсы сәйкесетіндігі анықталды. п-ЭГФ: АК сополимері үшін (21.03:78.97 масс. %) 5.0, 10.0, 20.00 С. мин⁻¹. қыздыру жылдамдығы кезінде активтендіру энергиясы бойынша алынған орташа деректер екі әдіс үшін де мына қатарда артады: $\bar{E}_{КАС} = 187.34$ кДж/моль $< \bar{E}_{ФР} = 200.17$ кДж/моль.

Кілт сөздер: термогравиметрия, термиялық анализ, кинетикалық параметрлер, сополимерлер, полиэтиленгликольфумарат, акрил қышқылы, активтендіру энергиясы, полиэфирлер.

А.Ж. Сарсенбекова, А.Н. Болатбай, В.В. Моргун,
Д. Хавличек, С.Ж. Давренбеков, Е. Насихатұлы

Изучение термической стабильности и определение эффективных значений энергии активации при деградации сополимеров ненасыщенных полиэфиров в атмосфере воздуха

Исследования в области кинетических показателей сополимеров на основе полиэтиленгликольфумаратов, а также внешнего и внутреннего воздействия на них очень важны для производственных процессов самого различного уровня. Это позволит решить целый спектр вопросов в области срока годности материалов и условий их хранения. Все это указывает на актуальность данного исследования. В статье предпринята попытка проверки наиболее распространенных методов обработки термогравиметрических данных и их совершенствования с точки зрения качества прогнозирующих возможностей получаемого регрессионного уравнения. В то же время данные показатели очень важны как для производства исходных компонентов, так и для изготовления конечного продукта из исследуемых материалов. Поэтому исследование и дальнейшее использование числовых данных кривых ТГ/ДТА имеет актуальное значение как для теоретической, так и для практической отраслей науки. Таким образом, обобщая экспериментальные данные по изучению термической стабильности, авторы приходят к выводу, что сополимеры п-ЭГФ: АК составом 21.03:78.97 и 68.96:31.04 масс, % обладают относительно высокой степенью устойчивости к нагреванию. Кроме того, было установлено, что, рассчитанные по методу ФР хорошо согласуются с результатами расчета с применением метода КАС. Следует отметить, что для сополимера п-ЭГФ:АК (21.03:78.97 масс, %) при скоростях нагрева 5.0, 10.0, 20.0 °С·мин⁻¹ полученные средние данные по энергии активации увеличиваются для двух методов в следующем ряду: $\bar{E}_{КАС}=187.34$ кДж/моль < $\bar{E}_{ФР}=200.17$ кДж/моль.

Ключевые слова: термогравиметрия, термический анализ, кинетические параметры, сополимеры, полиэтиленгликольфумарат, акриловая кислота, энергия активации, полиэферы.

Information about authors

Sarsenbekova, Akmaral Zhakanovna — PhD, Associate Professor, Physical and Analytical Chemistry Department, Karagandy University of the name of academician E.A. Buketov, Universitetskaya street, 28, 100024, Karaganda, Kazakhstan; e-mail: chem_akmaral@mail.ru; <https://orcid.org/0000-0002-8951-3616>

Bolatbay, Abylaikhan Nurlanuly (*corresponding author*) — Doctoral student, Karagandy University of the name of academician E.A. Buketov, Universitetskaya street, 28, 100024, Karaganda, Kazakhstan; e-mail: abylai_bolatabai@mail.ru; <https://orcid.org/0000-0001-5047-3066>

Morgun, Valeria Valerievna — Master student, Karagandy University of the name of academician E.A. Buketov, Universitetskaya street, 28, 100024, Karaganda, Kazakhstan; e-mail: morgunvaleria@yandex.ru;

Havlicek, David — RNDr., Associate Professor, Faculty of Science, Department of Inorganic Chemistry, Charles University in Prague, Prague, Czech Republic; e-mail: havlicek@natur.cuni.cz; <https://orcid.org/0000-0002-8854-6213>

Davrenbekov, Santay Zhanabilovich — Associate Professor, Karagandy University of the name of academician E.A. Buketov, Universitetskaya street, 28, 100024, Karaganda, Kazakhstan; e-mail: sdavrenbekov@mail.ru; <https://orcid.org/0000-0002-0218-7062>

Nasikhatuly, Ermauit — Master student, Karagandy University of the name of academician E.A. Buketov, Universitetskaya street, 28, 100024, Karaganda, Kazakhstan; e-mail: ermauit@gmail.com; <https://orcid.org/0000-0003-4574-0902>

INORGANIC CHEMISTRY

Article

UDC 546.2'24'87

<https://doi.org/10.31489/2022Ch1/92-98>

F.R. Aliyev^{1*}, E.N. Orujlu², D.M. Babanly³

¹Azerbaijan State Oil and Industry University, Baku, Azerbaijan;

²Institute Catalysis and Inorganic Chemistry named after M. Nagiyev, ANAS, Baku, Azerbaijan;

³French-Azerbaijani University, UFAZ, Baku, Azerbaijan

(*Corresponding author's e-mail: fariz_ar@hotmail.com)

Synthesis and study of a new mixed-layered compound GeBi_3Te_4 belonging to the $n\text{Bi}_2\text{-}m\text{GeBi}_2\text{Te}_4$ homologous series

In light of the structural properties of tetradymite-like layered chalcogenide compounds, the mixed-layered compound GeBi_3Te_4 was predicted and synthesized for the first time, which belongs to the $n\text{Bi}_2\text{-}m\text{GeBi}_2\text{Te}_4$ homologous series in the Ge-Te-Bi system. A polycrystal of a new phase was synthesized, and its single crystal was grown by the Bridgman–Stockbarger method. The obtained samples were investigated by differential thermal analysis (DTA) and powder X-ray diffraction (XRD). It was found that the compound melts peritectically at 563 °C and has a rhombohedral lattice-type structure with the following lattice parameters: $a = 4.3625$ (5) Å, $c = 31.381$ (2) Å (sp. gr R3m). The crystal structure of the layered van der Waals compound GeBi_3Te_4 consists of a repetition of seven-layer GeBi_2Te_4 packets and two-layer Bi packets in the form of -7-2-7-7-2-7-2-7- which differ from the previously discovered GeBi_4Te_4 phase, which consists of unit cells from only one seven-layer packet. The discovery of a new mixed-layered compound indicates the possibility of the formation of similar compounds in $\text{A}^{\text{IV}}\text{-B}^{\text{V}}\text{-Te}$ ($\text{A}^{\text{IV}} = \text{Ge, Sn, Pb}$; $\text{B}^{\text{V}} = \text{Sb, Bi}$) systems.

Keywords: Ge-Bi-Te ternary system, $n\text{Bi}_2\text{-}m\text{GeBi}_2\text{Te}_4$ homologous series, GeBi_3Te_4 , GeBi_4Te_4 , tetradymite-like structure, Bi-bilayers, crystal structure, topological insulators.

Introduction

In recent years, researchers have intensively studied the members of the homologous series $(\text{A}^{\text{IV}}\text{Te})_n(\text{B}_2^{\text{V}}\text{Te}_3)_m$ ($\text{A}^{\text{IV}} = \text{Ge, Sn, Pb}$; $\text{B}^{\text{V}} = \text{Sb, Bi}$) due to their extraordinary properties. These tetradymite-type layered ternary phases are potentially attractive thermoelectric materials with low thermal conductivity [1–6]. In addition, homologous members of $(\text{A}^{\text{IV}}\text{Te})_n(\text{B}_2^{\text{V}}\text{Te}_3)_m$ have been confirmed as three-dimensional topological insulators (TI) [7–11], which gave impetus to the study of the $\text{A}^{\text{IV}}\text{-B}^{\text{V}}\text{-Te}$ systems and the search for new layered compounds in the indicated systems. Since topological insulators can demonstrate many exotic properties, scientists believe that these materials have a huge perspective in the use of spintronics, quantum computers, medicine, protection systems, etc. [12–15].

An interesting feature of the $\text{Ge-B}^{\text{V}}\text{-Te}$ systems is that compounds belonging to the $n\text{GeTe} \cdot \text{B}_2^{\text{V}}\text{Te}_3$ homologous series are formed in the $\text{A}^{\text{IV}}\text{-B}^{\text{V}}\text{-Te}$ systems in addition to $\text{A}^{\text{IV}}\text{Te} \cdot m\text{B}_2^{\text{V}}\text{Te}_3$ homologous series. The crystal structure of Bi_2Te_3 -rich and GeTe -rich members of $n\text{GeTe} \cdot m\text{Bi}_2\text{Te}_3$ differ significantly from each other due to their structures [16–19]. The ternary compounds with GeTe -rich phase made up of identical slabs in which introduction of one GeTe bilayer unit to seven-layer packed increases the number of layers by two, giving 9-, 11-, and 13-layer slabs ($\text{Ge}_2\text{Bi}_2\text{Te}_5$, $\text{Ge}_3\text{Bi}_2\text{Te}_6$, and $\text{Ge}_4\text{Bi}_2\text{Te}_7$) [20]. Compounds with a high Bi_2Te_3 content are also built of two types of slabs: Seven-layer packets typical to GeBi_2Te_4 , which comprises

four anionic and three cationic layers and five-layered tetradymite. The general formula for these mixed layers can be written as $n\text{GeBi}_2\text{Te}_4 \cdot m\text{Bi}_2\text{Te}_3$, where n and m are the numbers of seven-layer and five-layer packets per unit cell, respectively. The slabs are bonded with each other by weak van der Waals forces.

The existence of another type of mix-layered compounds belonging to $n\text{B}_2^{\text{V}} \cdot m\text{B}_2^{\text{V}}\text{X}_3$ homologous series is also confirmed [21–23]. The crystal structure of this type of homologous series consists of repeating five-layered $\text{B}_2^{\text{V}}\text{X}_3$ and two-layered B_2^{V} packets connected by the van der Waals forces that are stacked along the c axes in an ordered manner.

Analysis of the literature shows that in the $\text{A}^{\text{IV}}\text{–B}^{\text{V}}\text{–Te}$ systems, along with the homologous series $(\text{A}^{\text{IV}}\text{Te})_n(\text{B}_2^{\text{V}}\text{Te}_3)_m$, there also exist ternary phases corresponding to the $n\text{B}_2^{\text{V}}\text{–}m\text{A}^{\text{IV}}\text{B}_2^{\text{V}}\text{Te}_4$ homologous series. The formation of such kinds of members is confirmed in numerous works: SnBi_4Te_4 [24], GeSb_4Te_4 [25], and GeBi_4Te_4 [26]. The existence of these compounds, in particular GeBi_4Te_4 , increases the probability of formation of other members of $n\text{Bi}_2\text{–}m\text{GeBi}_2\text{Te}_4$ homologous series in the Ge–Te–Bi system. Considering foresaid, in this paper, for the first time, a new van der Waals type of mixed-layered compound $\text{Bi}_2 \cdot 2(\text{GeBi}_2\text{Te}_4)$ was synthesized and studied, which comprises seven-layer GeBi_2Te_4 packets and two-layer Bi packets repeating along the c axis in the form of -7-2-7-7-2-7-7-2-7-.

Experimental

For synthesis GeBi_3Te_4 compound, high purity elements Ge (99.999 %, Alfa Aesar), Bi (99.999 %, Alfa Aesar), and Te (99.999 %, Alfa Aesar) (Table 1) were melted in a quartz ampoule according to stoichiometric amounts under the vacuum condition (10^{-2} Pa) at 800 °C for 3 hours and quenched in ice water. Then annealing was carried out at 450 °C for 1000 h to reach an equilibrium state. In the second part of the work, a single-crystal sample with GeBi_3Te_4 composition was grown by the vertical Bridgman–Stockbarger method. For this, a quartz ampoule with a conical bottom was sealed (10^{-2} Pa) and passed through the hot zone (650 °C) of the two-zone furnace into the cold zone (450 °C) at the 1.0 mm/h speed. As a result, bulk single-crystal ingots 2.5 cm in length and 0.8 cm in diameter were grown by the vertical Bridgman–Stockbarger method. The obtained samples were investigated by DTA and XRD methods.

X-ray diffraction analysis was performed at room temperature in the range $2\theta = 5\text{–}75$ degrees on a Bruker D2 PHASER diffractometer ($\text{CuK}_{\alpha 1}$ radiation). The “NETZSCH 404 F1 Pegasus” system was used for differential thermal analysis. DTA of the annealed alloy was carried out from room temperature to 800 °C with a heating and cooling rate of $5 \text{ }^\circ\text{C min}^{-1}$. The crystal lattice parameters were calculated using the TOPAS V3.0 program.

Table 1

Information about initial elements

| Element | CAS number | Source | Purity | Form |
|-----------|------------|------------|----------|----------------------|
| Germanium | 7440-56-4 | Alfa Aesar | 99.999 % | Pieces |
| Tellurium | 13494-80-9 | Alfa Aesar | 99.999 % | Lump |
| Bismuth | 7440-69-9 | Alfa Aesar | 99.998 % | Polycrystalline lump |

Results and Discussion

The polycrystalline sample of GeBi_3Te_4 was analyzed by powder X-ray diffraction method and obtained XRD patterns were compared with bismuth, GeBi_2Te_4 , and GeBi_4Te_4 (Figure 1). XRD pattern of GeBi_4Te_4 was taken from [26]. Comparison of diffraction lines of the synthesized polycrystalline sample with the bismuth, GeBi_2Te_4 , and GeBi_4Te_4 data shows that new diffraction lines appear on the diffraction pattern of the GeBi_3Te_4 sample. Using TOPAS V3.0 software, the XRD result of the new phase was indexed and identified as a GeBi_3Te_4 compound with a tetradymite-like layered structure and has the lattice parameter values $a = 4.3625 (5) \text{ \AA}$, $c = 31.381 (2) \text{ \AA}$ (sp. gr R3m1).

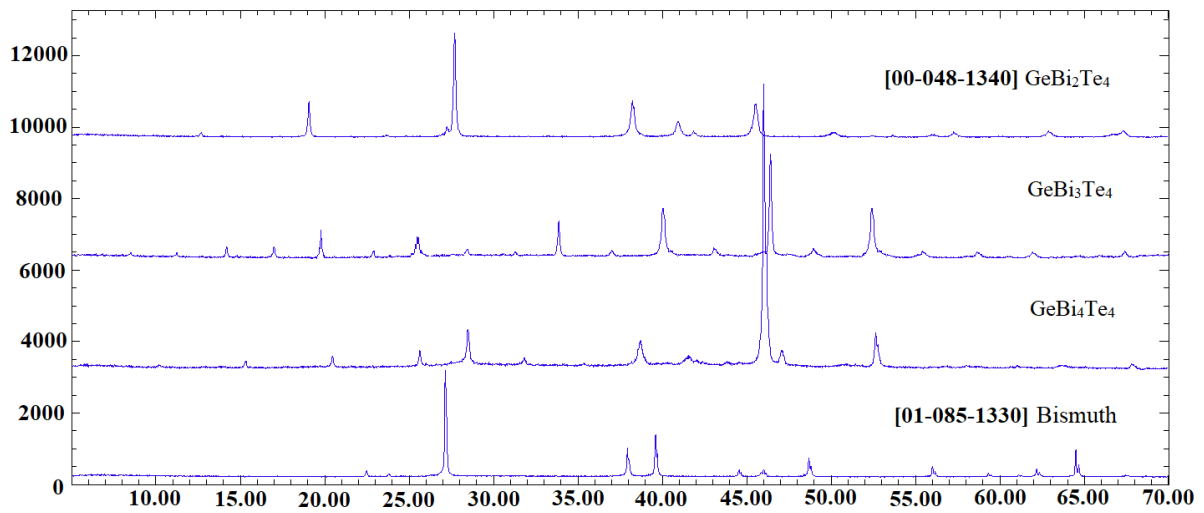


Figure 1. PXRD patterns of Bismuth, GeBi_2Te_4 , GeBi_3Te_4 , and GeBi_4Te_4

In Figure 2, the Rietveld refinement profile for the new synthesized GeBi_3Te_4 phase was shown. It is seen that all peak positions of the PXRD pattern are perfectly indexed with calculated lattice parameters.

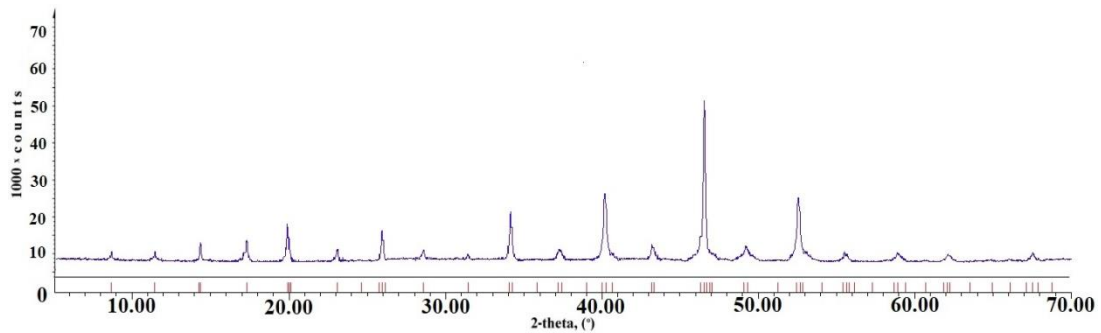
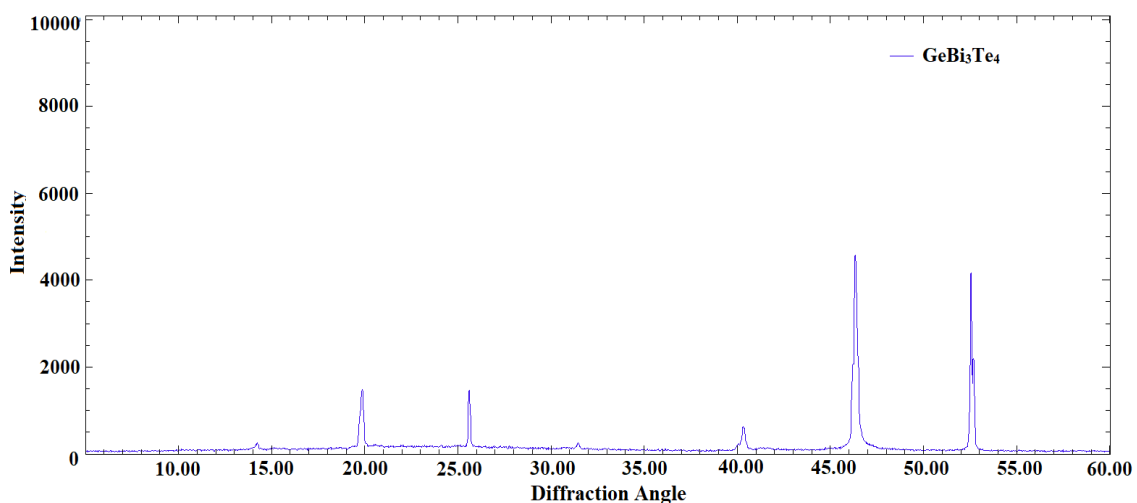


Figure 2. PXRD pattern for the GeBi_3Te_4

Analyses performed on the cleaved surface of the single-crystal sample, obtained by the Bridgman–Stockbarger method (nominal composition of GeBi_3Te_4), show that crystal comprises several phases along with the sample (Figure 3). The XRD results show that the primary crystallization phase is GeBi_3Te_4 , then comes a mix of two phases GeBi_3Te_4 and GeBi_4Te_4 , and finally pure phase of GeBi_4Te_4 . Subsequent research shows that no other ternary mixed-layered compounds were found.



a)

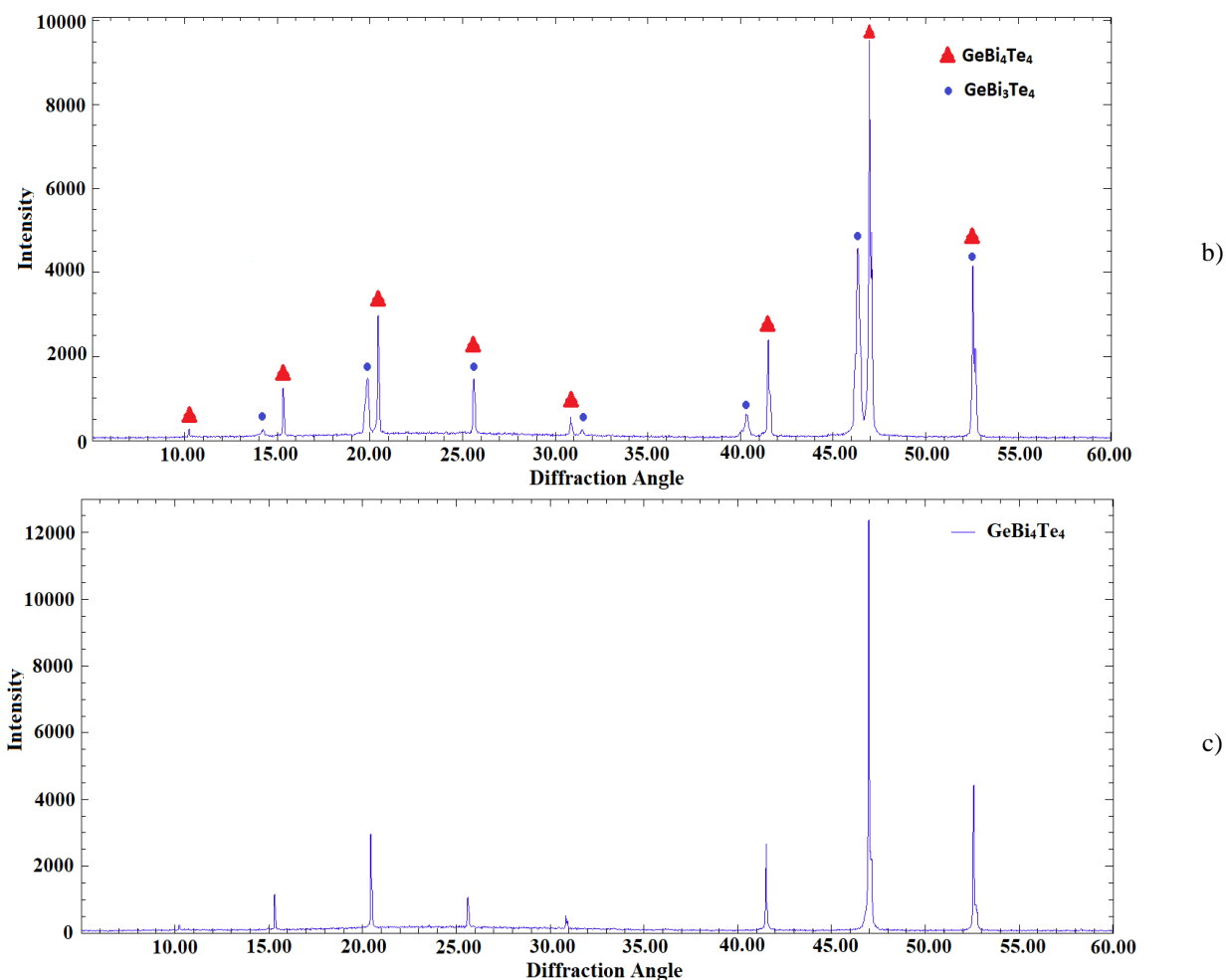


Figure 3. XRD pattern of a sample from the cleaved surface of the single-crystal a) GeBi_3Te_4 , b) $\text{GeBi}_3\text{Te}_4 + \text{GeBi}_4\text{Te}_4$, c) GeBi_4Te_4

The novel synthesized compound belongs to the tetradymite-type layered structure family where crystal structure consists of stacked together two rocksalt-type septuple blocks of Te-Bi-Te-Ge-Te-Bi-Te (GeBi_2Te_4 , sp. gr R-3m) and bismuth bilayer Bi-Bi (Figure 4) repeating along the c axis. Each atomic layer is strongly bonded with each other by covalent bonds, while weak van der Waals forces exist between blocks.

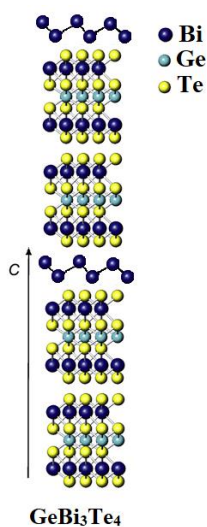


Figure 4. Crystal structure of GeBi_3Te_4

Figure 5 shows DTA results of the newly synthesized GeBi_3Te_4 phase which was analyzed from the powder sample. As can be seen, two endothermic effects are observed in the thermogram. The first and intensive endothermic effect noted at 563 °C belongs to the peritectic decomposition of the GeBi_3Te_4 compound, while the second endothermic effect at 585 °C refers to the end of melting. No additional effects are detected in DTA analysis which confirms that the synthesized sample is phase pure and does not contain any traces of other phases alongside GeBi_3Te_4 .

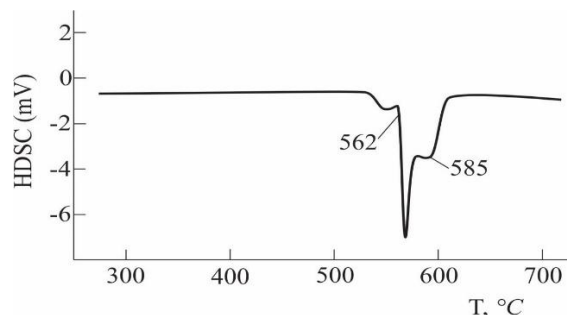


Figure 5. Heating thermogram of the GeBi_3Te_4 phase

Finding one more compound alongside GeBi_4Te_4 in $n\text{Bi}_{2-m}\text{GeBi}_2\text{Te}_4$ homologous series opens to researchers great opportunities for searching new mixed layered ternary compounds in another homologous series such as $n\text{B}_2^{\text{V}}-m\text{A}^{\text{IV}}\text{B}_4^{\text{V}}\text{Te}_7$ and $n\text{B}_2^{\text{V}}-m\text{A}_2^{\text{IV}}\text{B}_2^{\text{V}}\text{Te}_5$. New ternary materials with more complex and long-period mixed layered structures will potentially show more extraordinary properties.

Conclusions

In this paper, for the first time, the mixed-layered compound GeBi_3Te_4 was synthesized and analyzed which belongs to $n\text{Bi}_{2-m}\text{GeBi}_2\text{Te}_4$ homologous series in the Ge-Te-Bi system. Novel ternary compound melts peritectically at 563 °C and crystallizes: $a = 4.3625 (5) \text{ \AA}$, $c = 31.381 (2) \text{ \AA}$ (sp. gr R3m). The structure of the novel phase consists of a repetition of seven-layer GeBi_2Te_4 and Bi bilayer packets in the -7-7-2-7-7-2-7-7-2- form. Finding a second ternary compound in $n\text{Bi}_{2-m}\text{GeBi}_2\text{Te}_4$ increases the probability of the existence of other mixed-layered ternary compounds in $n\text{B}_2^{\text{V}}-m\text{A}^{\text{IV}}\text{B}_2^{\text{V}}\text{Te}_4$ homologous series. Synthesized novel phase has potential application as topological insulators.

Acknowledgements

This work has been carried out within the framework of the international joint research laboratory “Advanced Materials for Spintronics and Quantum Computing” (AMSQC) established between the Institute of Catalysis and Inorganic Chemistry of ANAS (Azerbaijan) and Donostia International Physics Center (Basque Country, Spain) and partially supported by the Science Development Foundation under the President of the Republic of Azerbaijan — Grant No. EIF-GAT-5-2020-3(37)-12/02/4-M-02.

References

- 1 Wu, D., Xie, L., Xu, X., He, & High, J. (2019). Thermoelectric Performance Achieved in $\text{GeTe}-\text{Bi}_2\text{Te}_3$ Pseudo-Binary via Van der Waals Gap-Induced Hierarchical Ferroelectric Domain Structure. *Adv. Funct. Mater.* 1806613. <https://doi.org/10.1002/adfm.201806613>
- 2 Madar, N., Givon, T., Mogilyansky, D., & Gelbstein, Y. (2016). High thermoelectric potential of Bi_2Te_3 alloyed GeTe-rich phases. *Journal of Applied Physics*, 120(3), [035102]. <https://doi.org/10.1063/1.4958973>
- 3 Junqin Li, Yucheng Xie, Chunxiao Zhang, Kuan Ma, Fusheng Liu, Weiqin Ao, Yu Li, & Chaohua Zhang. (2019). Stacking Fault-Induced Minimized Lattice Thermal Conductivity in the High-Performance GeTe-Based Thermoelectric Materials upon Bi_2Te_3 Alloying. *Alloying. Mater. Interfaces*. 20064–20072. <https://doi.org/10.1021/acsami.9b04984>
- 4 Di Wu, Lin Xie, Xiaolian Chao, Zupei Yang, & Jiaqing He (2019). Step-Up Thermoelectric Performance Realized in Bi_2Te_3 Alloyed GeTe via Carrier Concentration and Microstructure Modulations. *ACS Appl. Energy Mater.* 1616–1622. <https://doi.org/10.1021/acsaem.9b00057>

- 5 von Rohr, F., Schilling, A., & Cava, R.J. (2013). Single-crystal growth and thermoelectric properties of Ge(Bi,Sb)₄Te₇. *Journal of physics. Condensed matter : an Institute of Physics journal*, 25(7), 075804. <https://doi.org/10.1088/0953-8984/25/7/075804>
- 6 Omoto T., Kanaya, H., Ishibashi, H., Kubota, Y., Kifune, K., & Kosuga, A. (2016). Formation Phases and Electrical Properties of Ge-Bi-Te compounds with Homologous Structures. *Journal of electronic materials*, 45, 1478–1483. <https://doi.org/10.1007/s11664-015-4083-z>
- 7 Kampmeier, J., Weyrich, C., Lanus, M., Schall, M., Neumann, E., Mussler, G., Schäpers, T., & Grützmacher, D. (2016). Selective area growth of Bi₂Te₃ and Sb₂Te₃ topological insulator thin films. *Journal of Crystal Growth*, 443, 38–42. <https://doi.org/10.1016/j.jcrysgro.2016.03.012>
- 8 Politano, A., Caputo, M., & Nappini, S. (2014). Exploring the surface chemical reactivity of single crystals of binary and ternary bismuth chalcogenides. *J. Physical Chemistry C*, 21517–21522. <https://doi.org/10.1021/jp506444f>
- 9 Okamoto, K., Kuroda, K., & Miyahara, H. (2012). Observation of a Highly Spin-Polarized Topological Surface State in GeBi₂Te₄. *Phys. Rev. B.*, 195304. <https://doi.org/10.1103/PhysRevB.86.195304>
- 10 Nurmamat, M., Okamoto, K., Siyuan, Zhu., Menshchikova, T V., Rusinov, I.P., & Korostelev, V.O. (2020). Topologically Nontrivial Phase-Change Compound GeSb₂Te₄. *ACS nano*, 14, 9059–9065. <https://doi.org/10.1021/acsnano.0c04145>
- 11 Rabia Sultanaab, Nehac, P., Goyalab, R., Patnaikc, S., & Awanaa, V. (2017). Unusual non saturating Giant Magnetoresistance in single crystalline Bi₂Te₃ topological insulator. *Journal of Magnetism and Magnetic Materials*, 428, 213–218. <https://doi.org/10.1016/j.jmmm.2016.12.011>
- 12 Babanly, M.B., Chulkov, E.V, Aliev, Z.S., Shevelkov, A.V., & Amiraslanov, I.R. (2017). Phase Diagrams in Materials Science of Topological Insulators Based on Metal Chalcogenides. *Russian Journal of Inorganic Chemistry*, 62, 1703–1729. <https://doi.org/10.1134/S0036023617130034>
- 13 Viti, L., Coquillat, D., Politano, A., Kokh, K.A., Aliev, Z.S., & Babanly, M.B. (2016). Plasma-wave terahertz detection mediated by topological insulators surface states. *Nano Letters*, 80–87. <https://doi.org/10.1021/acs.nanolett.5b02901>
- 14 Otrokov, M.M., Klimovskikh, I.I., & Bentmann, H. (2019). Prediction and observation of the antiferromagnetic topological insulator. *Nature*, 416–422. <https://doi.org/10.1038/s41586-019-1840-9>
- 15 Papagno M., Ereemeev, S., Fujii, J., Aliev, Z.S., Babanly, M.B., Mahatha, S., Vobornik, I., & Mamedov, N. (2016). Multiple Coexisting Dirac Surface States in Three-Dimensional Topological Insulator PbBi₆Te₁₀. *ACS Nano*, 10, 3518–3524. <https://doi.org/10.1021/acsnano.5b07750>
- 16 Shelimova, L.E., Karpinskii, O.G., Kosyakov, V.I., Shestakov, V.A., & Zemskov, V.S. (2000). Homologous series of layered tetradymite-like compounds in Bi-Te and GeTe-Bi₂Te₃ systems. *Journal of Structural Chemist*, 81–87. <https://doi.org/10.1007/BF02684732>
- 17 Shelimova, L.E., Karpinskii, O.G., Zemskov, V.S, & Konstantinov P.P. (2000). Structural and Electrical Properties of Layered Tetradymite-like Compounds in the GeTe-Bi₂Te₃ and GeTe-Sb₂Te₃ Systems. *Inorganic Materials*, 36, 235–242. <https://doi.org/10.1007/BF02757928>
- 18 Shelimova, L.E., Karpinskii, O.G., Konstantinov, P.P., Avilov, E.S., & Kretova, M.A. (2004). Crystal Structures and Thermoelectric Properties of Layered Compounds in the ATe-Bi₂Te₃ (A = Ge, Sn, Pb) Systems. *Inorganic Materials*, 40, 451–460. <https://doi.org/10.1023/B:INMA.0000027590.43038.a8>
- 19 Shelimova, L.E., Karpinskii, O.G., Kretova, M.A., & Zemskov, V.S. (2000). X-ray Diffraction Study of Ge-Bi-Te Mixed-Layer Ternary Compounds. *Inorganic Materials*, 36, 1108–1113. <https://doi.org/10.1007/BF02758926>
- 20 Alakbarova, T.M., Hans-Jürgen, Meyer, Orujlu, E.N., Amiraslanov, I.R., & Babanly, M.B. (2021). Phase Transitions Phase equilibria of the GeTe-Bi₂Te₃ quasi-binary system in the range 0–50 mol% Bi₂Te₃. *Phase Transitions*, 94, 366–375. <https://doi.org/10.1080/01411594.2021.1937625>
- 21 Manisha Samanta, & Kanishka Biswas (2020). 2D Nanosheets of Topological Quantum Materials from Homologous (Bi₂)_m(Bi₂Se₃)_n Heterostructures: Synthesis and Ultralow Thermal Conductivity. *Chemistry of Materials*, 8819–8826. <https://doi.org/10.1021/acs.chemmater.0c02129>
- 22 Pierre F.P. Poudeu (2005). Mercuri G. Kanatzidis. Design in solid state chemistry based on phase homologies. Sb₄Te₃ and Sb₈Te₉ as new members of the series (Sb₂Te₃)_m(Sb₂)_n. *Chem. Commun.*, 2672–2674. <https://doi.org/10.1039/B500695C>
- 23 Govaerts, K., Sluiter, M.H.F., Partoens, B., & Lamoen, D. (2012). Stability of Sb-Te layered structures: First-principles study. *Phys. Rev. B.*, 144114. <https://doi.org/10.1103/PhysRevB.85.144114>
- 24 Orujlu, E.N., Seidzade, A.E., Aliev, Z.S., Amiraslanov, I.R., & Babanly, M.B. (2020). Synthesis and crystal structure of a new 9P-type layered Van der Waals compound SnBi₄Te₄. *Chemical Problems*, 1, 40–48. <https://doi.org/10.32737/2221-8688-2020-1-40-48>.
- 25 Matthias N. Schneider, & Oliver Oeckler Dr. (2009). GeSb₄Te₄ — a New 9P-Type Phase in the System Ge/Sb/Te. *Contributions Dedicated to Professor Arndt Simon on the Occasion of His 70th Birthday*, 137–143. <https://doi.org/10.1002/zaac.200900453>
- 26 Aliyev, F.R. (2021). Synthesis and Study of a Novel 9P-type Mixed Layered Tetradymite-Like GeBi₄Te₄ Compound in the Ge-Te-Bi System. *Physics and Chemistry of solid state*, 3, 401–406. <https://doi.org/10.15330/pcss.22.3.401-406>

Ф.Р. Алиев, Э.Н. Оруджлу, Д.М. Бабанлы

$n\text{Bi}_2-m\text{GeBi}_2\text{Te}_4$ гомологтық қатарына жататын GeBi_3Te_4 жаңа аралас-қатпарлы қосылыстарын синтездеу және зерттеу

Бұрыннан белгілі тетрадимит тәрізді қабаттасқан халькогенидті қосылыстардың құрылымдық қасиеттерін ескере отырып, Ge-Te-Vi жүйесінде $n\text{Bi}_2-m\text{GeBi}_2\text{Te}_4$ гомологтық қатарына жататын жаңа тетрадимит тәрізді аралас-қатпарлы GeBi_3Te_4 қосылысы болжанып, синтезделді. Жаңа фазалық поликристал синтезделіп, оның монокристалы Бригман–Стокбаргер әдісімен алынды. Алынған үлгілер дифференциалды термиялық талдау (ДТТ) және рентгендікфазалық талдау (РФТ) арқылы зерттелді. Қосылыс 563 °C температурада перитектикалық балкитыны анықталды және тор параметрлерінің мынадай мәндері бар: $a = 4,3625(5) \text{ \AA}$, $c = 31,381(2) \text{ \AA}$ (sp. gr R3m). GeBi_3Te_4 Ван дер Ваальс қатпарлы қосылысының кристалдық құрылымы қабатты -7-2-7-7-2-7-2-7- түріндегі GeBi_2Te_4 жеті қабатты пакеттері мен Vi екі қабатты пакеттерінің қайталануынан тұрады. Ол бұрын ашылған элементарлы ұяшықта тек бір ғана жеті қабатты пакетті бірлік ұяшықтан тұратын GeBi_4Te_4 фазасынан басқаша болады. Жаңа аралас-қабатты қосылыстың ашылуы AIV–BV–Te (AIV = Ge, Sn, Pb; BV = Sb, Bi) жүйелерінде ұқсас қосылыстардың болуы мүмкіндігін көрсетеді.

Кілт сөздер: Ge-Vi-Te үштік жүйесі, $n\text{Bi}_2-m\text{GeBi}_2\text{Te}_4$ гомологиялық қатар, GeBi_3Te_4 , GeBi_4Te_4 , тетрадимиттәрізді құрылым, Vi-бикабаттар, кристалдық құрылым, топологиялық изоляторлар.

Ф.Р. Алиев, Э.Н. Оруджлу, Д.М. Бабанлы

Синтез и исследование нового смешанно-слоистого соединения GeBi_3Te_4 , принадлежащего к $n\text{Bi}_2-m\text{GeBi}_2\text{Te}_4$ гомологическому ряду

Учитывая структурные свойства уже известных тетрадимитоподобных слоистых халькогенидных соединений, в системе Ge–Te–Vi было предсказано и синтезировано новое тетрадимитоподобное смешанно-слоистое соединение GeBi_3Te_4 , относящееся к $n\text{Bi}_2-m\text{GeBi}_2\text{Te}_4$ гомологическому ряду. Поликристал новой фазы был синтезирован, а его монокристалл выращен методом Бригмана–Стокбаргера. Полученные образцы исследовали методами дифференциального термического анализа (ДТА) и рентгенофазового анализа (РФА). Было обнаружено, что соединение плавится перитектически при температуре 563 °C и имеет следующие значения параметров решетки: $a = 4,3625(5) \text{ \AA}$, $c = 31,381(2) \text{ \AA}$ (sp. gr R3m). Кристаллическая структура слоистого соединения Ван-дер-Ваальса GeBi_3Te_4 состоит из повторения семислойных пакетов GeBi_2Te_4 и двухслойных пакетов Vi в форме -7-2-7-7-2-7-2-7-, которая отличается от обнаруженной ранее фазы GeBi_4Te_4 , состоящей в элементарной ячейке всего лишь из одного семислойного пакета. Открытие нового смешанно-слоистого соединения указывает на возможность существование подобных соединений в A^{IV}–B^V–Te (A^{IV} = Ge, Sn, Pb; B^V = Sb, Bi) системах.

Ключевые слова: тройная система Ge–Vi–Te, гомологический ряд $n\text{Bi}_2-m\text{GeBi}_2\text{Te}_4$, GeBi_3Te_4 , GeBi_4Te_4 , тетрадимитоподобная структура, Vi-бислои, кристаллическая структура, топологические изоляторы.

Information about authors

Aliyev, Fariz Ramiq — PhD student, Researcher, Azerbaijan State Oil and Industry University, 16/21 Azadliq avenue, AZ-1010 Baku, Azerbaijan; e-mail: fariz_ar@hotmail.com; <https://orcid.org/0000-0003-1709-0164>

Orujlu, Elnur Nəcəf — PhD student, Researcher, Institute of Catalysis and Inorganic Chemistry named after academician M.Nagiyevev, Azerbaijan National Academy of Sciences, 113, H. Javid avenue, Baku, AZ-1143, Baku, Azerbaijan; e-mail: elnur.oruclu@yahoo.com; <https://orcid.org/0000-0001-8955-7910>

Babanly, Dunya Mahammad — Doctor of Chemical sciences, Associate Professor. French-Azerbaijani University, UFAZ, 183 Nizami St, AZ-1010 Baku, Azerbaijan; e-mail: dunya.babanly@ufaz.az; <https://orcid.org/0000-0002-8330-7854>

CHEMICAL TECHNOLOGY

Article

UDC 66-922

<https://doi.org/10.31489/2022Ch1/99-112>

M.S. Sagyndikov^{1,2*}, I.I. Salimgarayev², E.K. Ogay²,
R.S. Seright³, S.E. Kudaibergenov⁴

¹Satbayev University, Almaty, Kazakhstan;

²KMG Engineering LLP, Kazakhstan;

³New Mexico Institute of Mining and Technology, USA;

⁴Institute of Polymer Materials and Technology, Almaty, Kazakhstan

(*Corresponding author's e-mail: sagyndikov_marat@mail.ru)

Assessing polyacrylamide solution chemical stability during a polymer flood in the Kalamkas field, Western Kazakhstan

During a polymer flood, the field operator must be convinced that significant chemical investment is not compromised at the early stages of polymer injection. Further, dissolved oxygen in the viscous polymer solution must be controlled at a safe level, where viscosity loss will be insignificant. Under anaerobic conditions, the hydrolyzed polyacrylamide (HPAM) solution is stable even if iron ions are present in the process water. Thus, in the field operation, introduced oxygen and existing iron ions will cause an enormous viscosity decline. The geochemical calculation reveals that dissolved oxygen can rapidly deplete after entering Kalamkas formation. This paper confirms this prediction through a combination of laboratory measurements and field observations. This study is based on rheology measurements of polymer solutions and produced fluid from the offset production well associated with the Kalamkas oilfield in Western Kazakhstan. Comprehensive analysis confirms no viscosity loss at the surface facilities during polymer preparation and injection at a Polymer Slicing Unit and significant viscosity loss at an Eductor-type unit caused by oxygen introduced during polymer solution preparation. However, even introduced high dissolved oxygen levels that degrade polymer at the surface can be rapidly depleted during contact with the formation, thereby promoting polymer chemical stability in the reservoir.

Keywords: polyacrylamide, polymer solution, chemical degradation, polymer flood, iron, oxygen, viscosity, injection.

Introduction

During a typical polymer flood, a high-molecular-weight partially-hydrolyzed polyacrylamide (HPAM) considerably increases viscosity for the injected water, thereby reducing the water-oil mobility ratio and improving reservoir sweep efficiency [1]. However, HPAM solutions can experience significant viscosity losses through mechanical and oxidative degradation [2–11]. Because chemical floods commonly involve a huge investment in polymers, it is critical to have confidence that the polymer is not degraded while being injected into the reservoir. Thus, any polymer degradation (and consequently reduced solution viscosity) can incur a substantial investment loss, and minimizing polymer degradation is a key to successful polymer flooding. Most Kazakhstan oil fields formation water (including the Kalamkas field) have high salinity and iron content. Commonly, those oil fields have no alternative fresh or low salinity (i.e., without iron content) water source similar to Daqing [12] or Milne Point [13]. The HPAM solution at sealed and anaerobic conditions is stable if iron ions exist in the process water [6]. Therefore, a sealing system for a polymer injection unit is crucial.

Nevertheless, in a field application, controlling dissolved oxygen content at the “zero” level is challenging. The study [6] suggested that 200 ppb oxygen is the highest value, where viscosity losses will be insignif-

icant. In contrast, [9] found that 46 ppb can lead to 10 % viscosity loss. Based on the geochemical calculation and laboratory experiment, [5] revealed that high dissolved oxygen content (which can be introduced during polymer solution preparation and injection) after entering the sandstone with 1 % pyrite (FeS_2) — as in the case of Kalamkas formation — can rapidly be depleted. On the other hand, lower dissolved oxygen content leads to higher polymer chemical stability, and the “zero” (undetectable) level is an ideal case. So how much-dissolved oxygen will be feasibly acceptable in a real field setting? A significant part of this paper is dedicated to testing and confirming those predictions in a field application at the Kalamkas polymer project. This confirmation required developing a special method to back-produce polymer solutions without further mechanical or oxidative degradation.

The Kalamkas Oilfield and Polymer Flood Review

The research in this paper is associated with the Kalamkas oilfield discovered in 1976. The field has been developed commercially since 1979 [14]. The brownfield Kalamkas oilfield has reached high water cut and non-uniform oil depletion, which is caused by a high difference in the mobility of water and oil [15]. The oil viscosity is over 16 cp at reservoir temperature (38–43 °C). Under these conditions, the application of polymer flooding is essential to increase oil recovery.

Pilot projects have been conducted in the West part since September 2014 and in the East part of the field since March 2015. These pilots use two types of polymer preparation and injection units having differences. Both units use polymer powder. The first unit uses the Polymer Slicing Unit (PSU) to dissolve polymer powder into water. This PSU reduces the polymer particle size to a uniform and allows for significantly higher polymer concentrations [16] up to 1.5 % or 15 000 ppm. In this unit, a polyacrylamide powder inlet is at the upper part to supply polymer by gravity force (positive pressure) to the screw pump and PSU. The unit is completely isolated from air by a nitrogen blanketing system (Fig. 1). The second one is the eductor-type unit. This conventional eductor works on the Venturi principle, and polymer powder is supplied by air injection. There is no action to isolate air from the unit (Fig. 2). After initial dissolution with these units, this polymer and water mixture flow to maturation tanks to achieve the mother solution’s target viscosity. The time to fully dissolve the polymer in water for the PSU is ~45 minutes and for the eductor-type is ~3 hours. The next step is mixing the mother solution with brine to achieve the target viscosity, and then it is transferred by a low-shear pump to the injection well. An individual pump was used for each injection well. The PSU was used for the two West injectors and the seven injectors’ East extension. The other four wells were supplied by the eductor-type polymer unit. Two types of commercially available HPAM were used for the West and East projects.

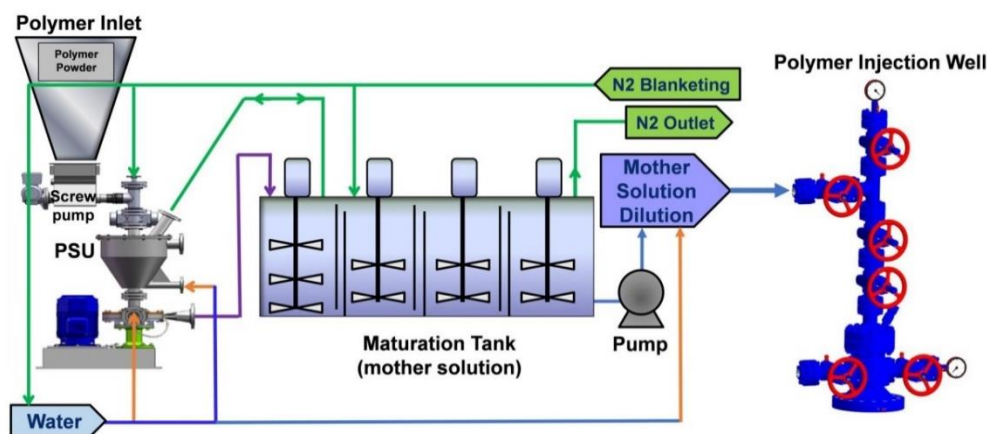


Figure 1. Main components of the polymer slicing unit (PSU)

The field oil pay zones are concentrated at Jurassic deposits, and Cretaceous deposits have massive gas and water reservoirs (Fig. 3). Cretaceous brine is used in the polymer-solution injection process (preparing the mother solution and diluting the target concentration). The brines’ physical and chemical properties (salinity, density, viscosity, pH) of the Cretaceous and Jurassic formations are similar. The main reason for using Cretaceous brine is the absence of dissolved oxygen and lower total suspended solids (TSS) content. As mentioned previously in the Kalamkas field, there is no alternative to low salinity or freshwater sources (e.g., lakes and rivers) to reduce polymer consumption.

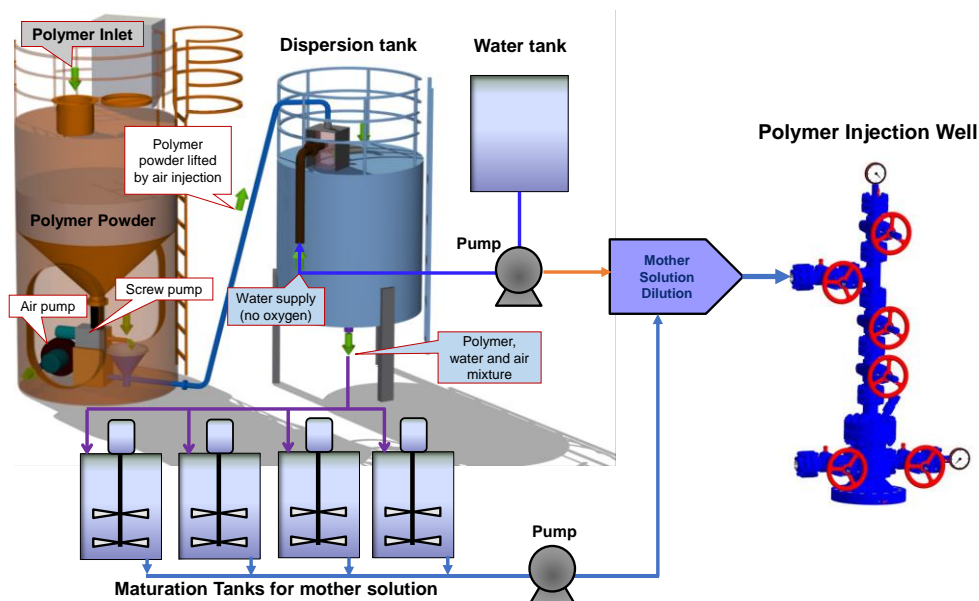


Figure 2. Main components of the eductor-type polymer unit

Cretaceous brine for polymer units is supplied from dedicated wells. The brine has high salinity (TDS 10–11.5 %) and high content of divalent cations (6 500–7 700 ppm). The field brine iron content varies between 20–40 ppm. Consistent with [6] experimental work, polymer solution viscosity losses at Kalamkas field conditions should be insignificant if the initial dissolved-oxygen concentration is 200 ppb or less. We recognize that the formation salinities are high and that HPAM provides much more cost-effective viscosity in low-salinity brine than in high-salinity brine. Nevertheless, polymer flooding with HPAM under the conditions at Kalamkas still provides a substantial economic benefit. Further, as in most current situations throughout the world, given the price and (lack of) availability of biopolymer, the use of HPAM is still more cost-effective than alternatives.

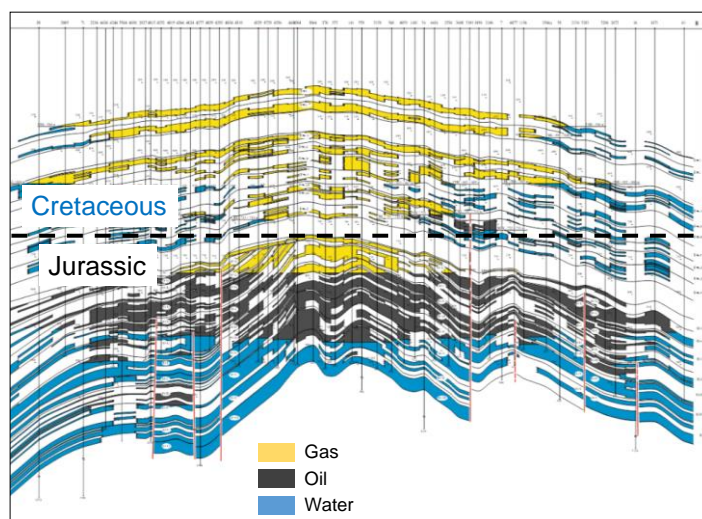


Figure 3. Geological profile of the Kalamkas field

The water's dissolved oxygen level was measured at the wellhead of production wells supplying West and East polymer projects. It was also measured in the water at storage tanks and in the mother solution from maturation tanks of the West PSU, the East PSU, and the East eductor-type polymer unit using CHEMets® express tests. The measurement results are shown in Table 1. Tests results reveal that, at the formation, brine (from the wellhead) dissolved oxygen level is undetectable (less than 0.025 ppm or 25 ppb). This finding is consistent with the fact that Kalamkas oil reservoirs have a reducing environment due to iron-containing minerals up to 2–4 % [5].

Table 1 represents that at the West polymer project, oxygen was introduced during water transportation from the production well to the storage tank, and its level was at 0.3–0.4 ppm. In contrast, this problem did not occur at the East polymer project, where the oxygen level at the storage tanks was undetectable. During the polymer dissolving process, the oxygen was introduced into the mother solution. The oxygen level was 0.3–0.4 ppm for the PSU-type system, and for the eductor-type unit was 2–3 ppm. For the PSU, the dissolved oxygen was close to the acceptable safe range, according to [6]. However, for the eductor-type, this value was over ten times higher than the acceptable level. As will be shown later, this unacceptable oxygen level resulted in 45 % viscosity loss and the equivalent of 25 % polymer concentration loss.

Table 1

The dissolved oxygen measurement results during polymer injection in the Kalamkas field

| Polymer injection unit | Dissolved oxygen content, ppm | | | |
|------------------------|-------------------------------|--------------------|-------------------------|------------------|
| | Water producer | Water storage tank | Polymer mother solution | Polymer Injector |
| West PSU | 0 | 0.2–0.3 | 0.3–0.4 | 0–0.3 |
| East PSU | 0 | 0 | 0.3–0.4 | 0.3 |
| East eductor | 0 | 0 | 2–3 | 1–2 |

Experimental

A field sampling of polymer solutions

We compared laboratory prepared and sampled polymer solutions viscosities to assess chemical stability, where polymer concentrations were the same as at the field. Mother solutions were sampled from polymer dissolving units (PSU and eductor type) and polymer solution from injectors wellhead. We used fresh polymer solution viscosities as a baseline for comparison (the methodology will be shown later in this section). Viscosities were measured using a high-precision rheometer Anton Paar MCR 502 (Austria) at a shear rate of 7.34 s^{-1} , at room temperature ($25 \text{ }^\circ\text{C}$), and aerobic conditions. A shear rate of 7.34 s^{-1} is commonly used as a standard single-point for comparison of viscosities for non-Newtonian enhanced oil recovery fluids [7; 17–19]. Because most liquids (including polymer solution) are incompressible at low or medium pressures, a considerable change in pressure from 14.5 to 4350 psi causes no significant change in viscosity [20]. Therefore, the reservoir pressure condition for polymer solution viscosity measurement is not essential. The viscosity of each sample was usually measured twice and then averaged.

Polymer solution at the wellhead was collected in pressurized cylinders (Fig. 4). Pressurized cylinders and collection procedures were specially designed for the polymer flood project to protect the solution from oxidative degradation [7; 21]. These cylinders are made of stainless steel and coated with an inert material to prevent corrosion and any iron contamination. Oxygen can be effectively excluded by carefully flushing air from the cylinder with a polymer solution while collecting the sample.



Figure 4. Pressurized cylinders for a polymer solution sampling at the wellhead

The Brine, Polymers and Concentrations

During this study, brine was collected from the dedicated production wells of the Cretaceous water reservoir (which is used for polymer dilution, as shown in Table 2). Brines (West and East Producers) have high iron content. Consequently, Fe^{2+} reacts with oxygen after exposure to the air. Therefore, to eliminate the effect of oxidized products, both brines are pumped by air to oxidize all iron from the solution and then passed through paper filters before further use.

Table 2

Cretaceous formation brine physical and chemical properties

| Parameter | Cretaceous formation brine (used for polymer dilution) | |
|---|---|-----------------|
| | West Producer | East Producer |
| pH | 5.8 | 6.0 |
| Density, g/cm^3 | 1.071 | 1.082 |
| Ca^{2+} content, ppm | 4 809.6 | 5 611.2 |
| Mg^{2+} content, ppm | 1 702.4 | 2 067.2 |
| K^+ and Na^+ content, ppm | 32 722.5 | 35 890.9 |
| Cl^- content, ppm | 63 810 | 71 254.5 |
| SO_4^{2-} content, ppm | 118.5 | 21.4 |
| CO_3^{2-} content, ppm | 0 | 0 |
| Total salinity, ppm | 103 187.4 | 114 857.4 |
| Water type by Sulin 1946* | Cl-Ca | Cl-Ca |
| Water hardness, mg-eq/l | 410 | 470 |
| Iron (Fe) content, ppm | 40.6 | 18.2 |
| Total suspended solids (TSS) content, ppm | 14.0 | 12.0 |
| Dissolved oxygen content, ppm | 0 ² | 0 ^{**} |

Notes: * [22]; **dissolved oxygen content measured with CHEMets® express tests shows the undetectable value (less than 0.025 ppm or 25 ppb).

Two powder-form partially hydrolyzed polyacrylamides (HPAM) (SNF products) were used, namely Superpusher K-129 and Polyacrylamide R-1. They had a molecular weight of 14 million Daltons and a hydrolysis degree of 16 %.

Polymer solutions were prepared by sprinkling the appropriate mass of polymer powder onto the brine vortex created by an overhead stirrer with a four-blade propeller. After mixing for several hours at a high rate, the stir rate was reduced for at least four hours, and the solution stood overnight. As in the field application, our target polymer concentrations for the three projects are in Table 3. For Superpusher K-129, we used brine from West producer (10.3 % TDS) and for Polyacrylamide R-1 — East Producer (11.5 % TDS).

Table 3

Polymer concentrations for the laboratory study

| Polymer injection unit | Polymer type | Active polymer concentration, ppm | |
|------------------------|--------------------|-----------------------------------|-------------------|
| | | Mother solution | Injector wellhead |
| West PSU | Superpusher K-129 | 9 200 | 1 600 |
| East PSU | Polyacrylamide R-1 | 15 000 | 1 700 |
| East educator | Polyacrylamide R-1 | 4 900 | 2 200 |

A sampling of producer fluid

Many polymer flood projects reported that production wells responded to polymer flooding by water cut decreases and increased produced polymer concentration [7; 23–26]. In some cases, the polymer channeled directly from an injector to a producer through a fracture, i.e., producing the same polymer concentration as injected. This circumstance occurred in Kalamkas field, where severe channeling and polymer breakthrough was observed from Injector XX37 to Producer XX87 in June 2019. Note that this polymer-channeling problem developed only once during over seven years of polymer injection (i.e., since 2014). The distance between the producer and injector was 400 m. After the breakthrough, polymer concentration in-

creased roughly from undetectable values (i.e., <1 ppm) to the injected values. Injector pressure fall-off tests (using the same method utilized later in this paper) after polymer injection revealed that injection occurred above the formation parting pressure and the fracture half-length was close to 400 m. This value is close to the well spacing (Fig. 10 and Table 7). Thus, the fracture was detrimental to sweep efficiency in this particular case because it extended from the injector to the producer. After several unsuccessful attempts to plug the fracture (both from the production and injection sides), the production well was shut down.

Figure 5 shows Injector XX37 and Producer XX87 operation history before and after polymer breakthrough. This history indicates a powerful hydrodynamic connection expressed by a quick change in producer dynamic fluid level during an injector workover and after injection. After the polymer breakthrough, the water cut increased from 87 % to 100 %. Tracer tests (Table 4 and Fig. 6) during water and polymer injection confirmed that the source of polymer breakthrough was Injector XX37.

This unusual case provided the opportunity to assess polymer solution chemical and mechanical stability that traveled from the injector to the producer through the reservoir.

Table 4

The interwell tracer tests results on Polymer Injector XX37 and surrounding producers

| Date | Tracer type | Injected Mass, kg | Injected V, m ³ | Prod-ed M, kg | Prod/Inj M, % | A tracer reached well number | Tracer max velocity, m/d | Tracer min velocity, m/d | Tracer average velocity, m/d |
|-----------|----------------------|-------------------|----------------------------|---------------|---------------|------------------------------|--------------------------|--------------------------|------------------------------|
| Nov. 2017 | Urea | 5000 | 18 | 147.8 | 2.96 | 25 | 1808 | 188 | 638 |
| Nov. 2019 | Fluorescein (Uranin) | 60 | 9 | 0.6172 | 1.03 | 1 (XX87) | 2781 | 2781 | 2781 |
| Nov. 2020 | Rhodamine C | 60 | 18 | 0.1 | 0.11 | 6 | 1162 | 62 | 210 |

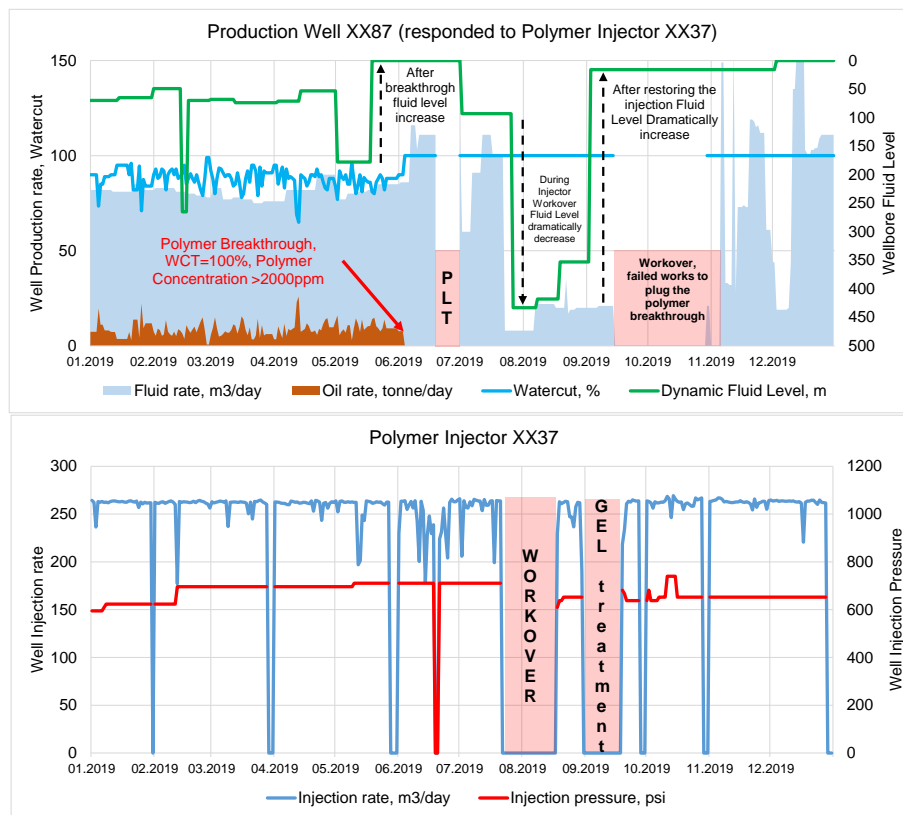


Figure 5. Well XX87 production and Well XX37 injection history, where polymer breakthrough was observed

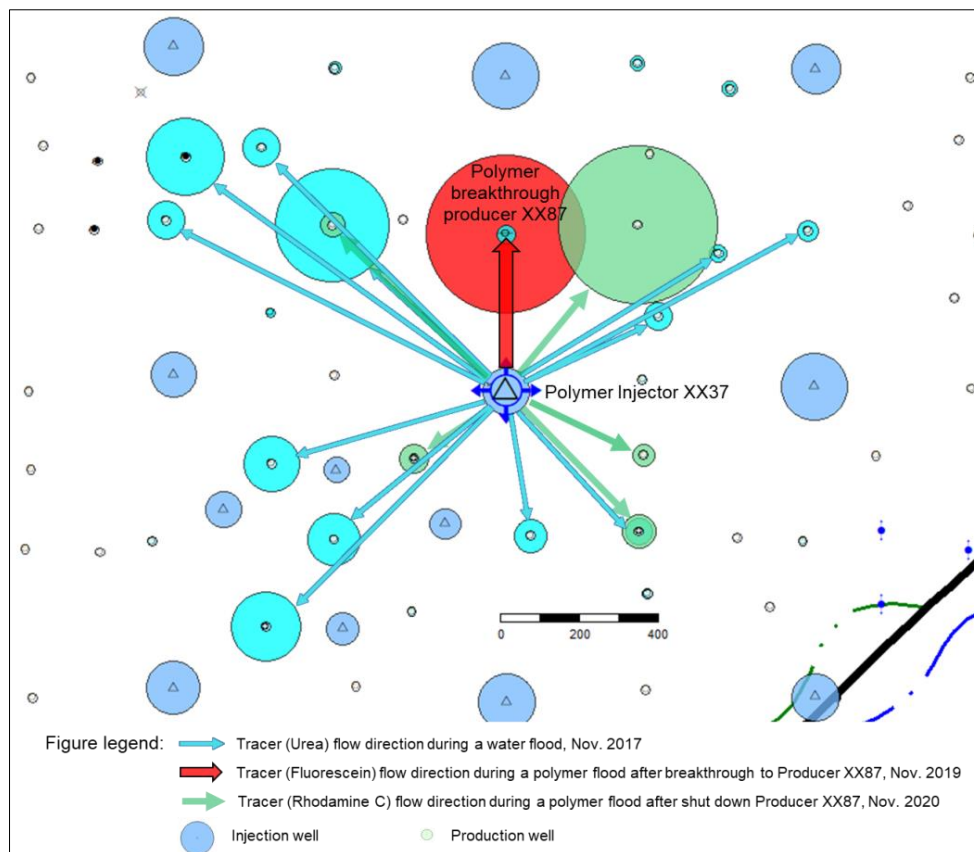


Figure 6. The interwell tracer tests results on Injection well XX37 and surrounding producers

A special scheme (Fig. 7) and procedure were developed to collect produced polymer solution samples from Producer XX87 and assess in situ polymer stability. The production well was equipped with a production line valve, check valve, annulus valve, wing valve, pressure gauge, sampler, and X-mas tree. The well downhole was equipped with tubing and a rod pump. The top of the perforation interval was at 806 m MD (measured depth), and the tubing end was at 590 m MD. A dedicated high-pressure hose was installed to connect the sampler to the pressurized cylinder to collect polymer solution samples at the wellhead. The special procedure was as follows as applied in Well XX87:

- Stop polymer solution injection unit (including Injector XX37) for planned repair work for >6 hours.
- Install pressure gauge flow meter, and connect the pressurized cylinder to collect samples before putting on production well XX87.
- Open wing and production line valve to put the well on the production and start to collect samples.
- Open the sampler valve and flush several-cylinder volumes with the produced polymer solution to prevent air from entering the sample.
- Collect six samples (total) at different cumulative production volumes with the same procedure described above and measure dissolved oxygen level.
- Collect injecting polymer solution at Well XX37 (source of the polymer breakthrough) and measure dissolved oxygen level.
- After collecting all samples, immediately transport pressurized cylinders to the field lab to measure viscosity.
- Viscosity measurements proceed as described above in the subsection “A field sampling of polymer solutions” and determine the rheological power-law index [21].

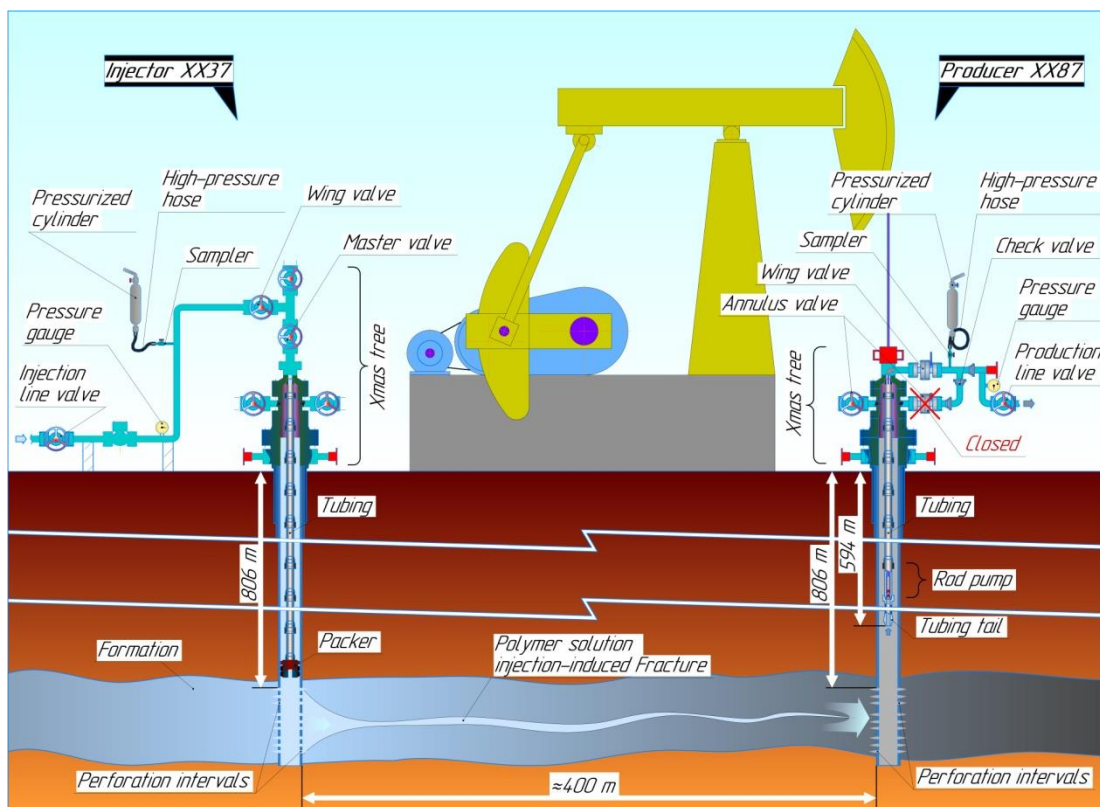


Figure 7. Scheme to collect polymer solutions from Producer XX87

Results and Discussion

Effect of Dissolved Oxygen

As shown in Table 2, process water has high dissolved iron content. Therefore, if dissolved oxygen is introduced to the polymer injection system, it will cause chemical degradation. The PSU is designed to keep dissolved oxygen low, and the eductor-type unit has no action to treat the oxygen or iron. Further, the effects of dissolved oxygen and Fe^{2+} on polymer viscosity for three polymer units are demonstrated in Table 5. Examination of this table first reveals that the PSU for both projects (West and East) has a good performance due to chemical stability. Chemical stability provided by nitrogen blanketing system and its efficiency is consistent with [6] work. The field viscosity of the PSU mother solution did not reach the lab viscosity. However, after subsequent dissolution processes (Fig. 1), the solution reached the required polymer viscosity and dissolving quality at the wellhead. Finally, viscosity losses were zero at the injector wellhead for the West and East PSUs, demonstrating high technical efficiency.

For the East eductor, both mother and polymer solutions showed a high level of viscosity losses. The viscosity loss for the mother solution and the injector wellhead were 36 and 45 %, respectively. These losses are unrelated to dissolving quality but are due to oxidative (chemical) degradation caused by dissolved oxygen and divalent iron reactions. As shown in Fig. 2, the dissolved oxygen was introduced by air injection associated with the polymer powder supply. At the first mixing step, the mother solution had 2–3 ppm dissolved oxygen. Due to the absence of oxygen in the process water and the polymer dilution process, the oxygen level at the wellhead decreased to 1.5 ppm (Table 1). This oxygen content was higher than the acceptable range — by roughly ten times. The final viscosity loss was about 45 % or equivalent to a 25 % loss of polymer concentration. The primary oxidative degradation location in the system is the dispersion tank. Subsequently, during transit from the injection unit to the wellhead, it loses about 10 % more viscosity. We assume this process continues in the tubing before entering the formation. As will be shown later, after the polymer solution enters the formation, all oxygen will be consumed by the surrounding rock quickly and provide subsequent chemical stability. Even so, severe degradation at the surface affects project economics and feasibility.

Table 5

The viscosity measurement results at different injection units

| Polymer injection unit | Lab viscosity, cp | | Field viscosity, cp | | Viscosity loss, % | | Polymer concentration loss, % |
|------------------------|-------------------|-------------------|---------------------|-------------------|-------------------|-------------------|-------------------------------|
| | Mother solution | Injector wellhead | Mother solution | Injector wellhead | Mother solution | Injector wellhead | |
| West PSU | 680 | 20 | 652 | 20 | 4 | 0 | 0 |
| East PSU | 1 980 | 23 | 1 850 | 23 | 14 | 0 | 0 |
| East educator | 240 | 38 | 154 | 21 | 36 | 45 | 25 % |

Note: The viscosity of the polymer solution measured at 7.34 s⁻¹, T = 25 °C.

The polymer rheology and concentration loss

Figure 8 shows polymer concentration and viscosity relationship for two types of used polymers in the field. In our case, polymer viscosity roughly depended on the square of its concentration. This figure analysis reveals that 45 % viscosity loss for the East educator polymer injection unit corresponds to 25 % equivalent polymer concentration loss.

Several views exist on how to solve this problem. They include: (1) chemical/mechanical treatment of the process water to remove all iron from the solution [27], (2) chemical additives such as free-radical scavengers or pH adjustment [28, 29], (3) keeping dissolved oxygen at an undetectable or acceptable level (close to zero) [5], and (4) no action [25] as in our example of the East educator unit.

The viscosity measurement results at different injection units (Table 5) reveal that removing all oxygen from the system is the feasible and effective way to provide the chemical stability of the solution. Thus, we suggest modifying the East educator injection unit to ensure an undetectable or acceptable oxygen level that will save 25 % cost of chemicals.

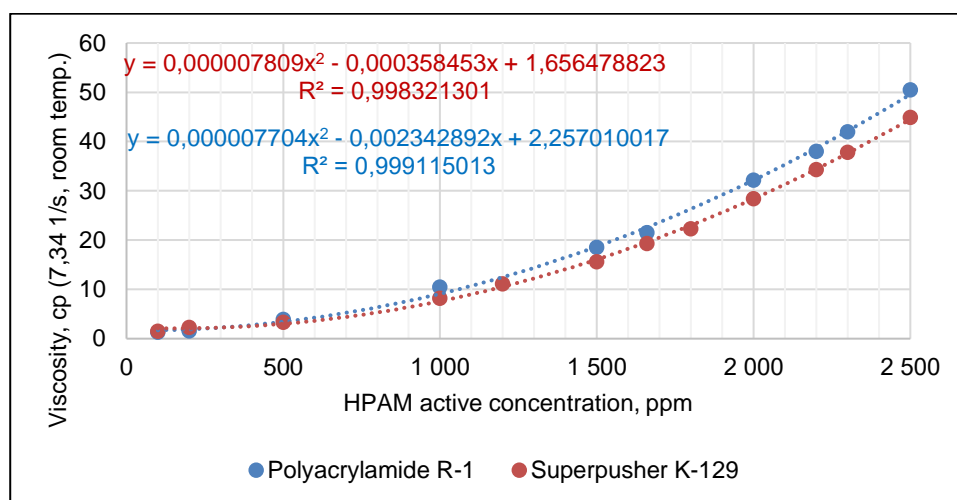


Figure 8. Polymer solution viscosities at different concentrations

Effect of the formation on the polymer stability

Fluid sampling for Producer XX87 and injection of polymer solution at the wellhead of Well XX37 occurred on 30th April 2021, as described above in the section “A sampling of producer fluid”. The typical surface temperature was +20 °C during the test. As shown in Fig. 7, samples from Producer XX87 were collected after polymer breakthrough and that polymer solution propagated over 400 m through the reservoir from Injector XX37. Additionally, the dissolved oxygen level was measured at the wellhead of Polymer Injection Well XX37 and the last four produced samples (# 3, 4, 5, 6) using CHEMets® colorimetric tests. The viscosity and oxygen measurement results are shown in Figure 9 and Table 6. Note in Table 6 that after the first listing (the original sample that was injected), the samples are listed in reverse chronological order of collection — i.e., Sample 6 was collected last from the formation, and Sample 1 was collected first in the tubing). Test results show that injected solution from Well XX37 had roughly 1.5 ppm (i.e., between 1 and 2 ppm) dissolved oxygen content and viscosity of 21.4 cp with a power-law index of 0.763. The first three produced samples (originating closest to the surface) contained 0.2 ppm dissolved oxygen and different degrees of vis-

cosity loss relative to the injected (25-50 %). The last three samples show undetectable dissolved oxygen levels (less than 0.025 ppm or 25 ppb) and minor viscosity loss, with a power-law index close to the injected solution. We presume that significant degradation was seen for the first collected samples because oxygen (air) was introduced into the production well during the well repair work. The gradual decrease in the level of degradation (i.e., increase in viscosity) with time reflected flushing this oxygen out of the system. These findings indicate that injected oxygen in the polymer solution (that transported 400 m through the Kalamkas reservoir) was consumed by the surrounding reservoir rock provided chemical (oxidative) stability of the solution (due to iron-containing minerals up to 2–4 %) [5].

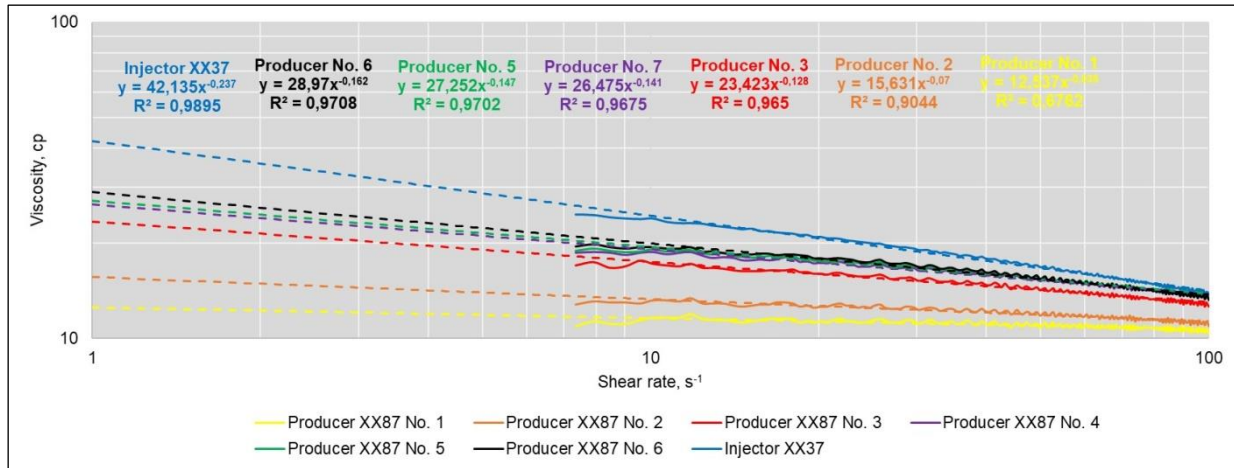


Figure 9. Rheological curve analysis of injected (Well XX37) and produced (Well XX87) polymer solutions

Table 6

Rheology measurements of the injected and produced polymer solution from Injector XX37 and Producer XX87

| Well | Produced Volume, m³ | Dissolved O ₂ concentration, ppm | The location of the collected sample | Viscosity at 7.34 s ⁻¹ , cp | The power law index (n), dimensionless* |
|---------------------|---------------------|---|--------------------------------------|--|---|
| Injector XX37 | | 1.5 | Injected | 25.1 | 1-0.237 = 0.763 |
| Producer XX87 No. 6 | 6.5 | 0 | Formation | 21.0 | 1-0.162 = 0.838 |
| Producer XX87 No. 5 | 4.4 | 0 | between tubing and perforation | 21.3 | 1-0.147 = 0.853 |
| Producer XX87 No. 4 | 3.6 | 0 | between tubing and perforation | 21.3 | 1-0.141 = 0.859 |
| Producer XX87 No. 3 | 3.3 | 0.2 | between tubing and perforation | 19.2 | 1-0.128 = 0.872 |
| Producer XX87 No. 2 | 2.9 | N/A | between tubing and perforation | 14.9 | 1-0.070 = 0.930 |
| Producer XX87 No. 1 | 2.0 | N/A | downhole tubing | 13.1 | 1-0.035 = 0.965 |

Note: *API RP 63 1990.

Pressure fall-off test

We ran pressure fall-off tests in injection wells to obtain valuable well test data. The Well XX37 pressure fall-off test analysis during polymer flood is presented in Fig. 10 and Table 7. The transient pressure analysis plots pressure versus time and the Bourdet derivative on a log-log scale [30]. Comparing and analyzing two pressure curves (original and derivative) for each flood can display the signature of numerous well, reservoir, and boundary behaviors. In our case, the analyses of pressure fall-off tests showed that during polymer flood injection occurs over formation parting pressure. The absence of fractures during water-flood showed in other wells similar to Well XX37. The fracture half-length for Well XX37 where severe channeling and polymer breakthrough was observed, fracture half-length is close to the well spacing. We can

see that polymer injection leads to natural well stimulation. Consequently, the polymer solution flows through the perforations and near wellbore zone with an area high enough to ensure mechanical stability of the solution. If Well XX37 were not fractured, injection of viscous polymer solution would necessarily decrease injectivity, roughly in proportion to the polymer solution viscosity [4; 7]. In our case, the expected injectivity without open fractures would be 20 times lower than that for water. Our injectivity was enhanced by a factor of 1.6.

The presence of fractures during the polymer flood is consistent with most of the worldwide polymer flood projects injections in vertical wells occur above the formation parting pressure [4; 19; 31–32], where linear flow is expected. In contrast, if fractures or fracture-like features are not present during polymer injection, achieving a favorable economical injection rate and acceptable voidage replacement ratio (e.g., the same as during a waterflood) is impossible. Additionally, according to the analytical calculations of [19] and the work of [33], fractures do not seriously affect a sweeping efficiency if the fracture half-length is less than 1/3 of the well spacing. These findings reveal that the advantages of fracture features during polymer flood (i.e., little or no injectivity loss, the mechanical stability of the polymer solution) outweigh its disadvantages (e.g., possible severe channeling, jeopardized sweep efficiency).

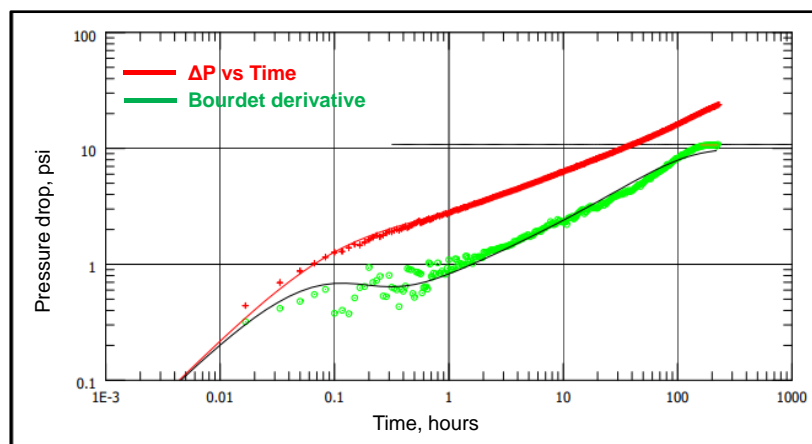


Figure 10. Analysis of pressure fall-off test during polymer injection into Well XX37 (2020)

Table 7

Analysis of pressure fall-off test during polymer injection into Well XX37

| No. | Parameters | Value | | | |
|-----|--|--|--|---------------------------|-----|
| | | During polymer flood (2021) | During polymer flood (2020) | During water flood (2018) | |
| 1 | Perforation interval, Top-Bottom | 806–810, 812.5–820.5 m | 806–810, 812.5–820.5 m | 806–810, 812.5–820.5 m | |
| 2 | Test duration, hours | 162.7 | 233.6 | N/A | |
| 3 | Wellbore storage (WBS) model | Changing WBS | Changing WBS | | |
| 4 | Well model | Vertical fractured finite conductivity | Vertical fractured finite conductivity | | |
| 5 | Reservoir model | Homogenous | Homogenous | | |
| 6 | Boundary model | Infinite | Infinite | | |
| 7 | Reservoir pressure, bar | 87.42 | 86.3 | | |
| 8 | Conductivity, mD·m | 5670 | 5 630 | | |
| 9 | Average permeability, mD | 506.5 | 503.1 | | |
| 10 | Total skin | –7.5 | –7.13 | | |
| 11 | Geometrical skin | 0 | 0.1 | | |
| 12 | Fracture half length, m | 396 | 308 | | |
| 13 | Fracture conductivity, mD·m | 6.13E+6 | 0.384E+6 | | |
| 14 | Fracture permeability, mD | 7 740 | 623 | | |
| 15 | Injectivity index, m ³ /(day·bar) | 6.7 | 5.7 | | 4.3 |

Conclusions

The large investment associated with the polymer bank during a polymer flood necessitates a determination that the polymer is not substantially degraded during the process of preparation and injection. This paper provides a methodology for assessing chemical degradation in the field, and the methodology is demonstrated for an important field of application in Kazakhstan. This study indicates the possibility of optimizing operational expenditure and increasing the economic efficiency of the polymer flood project operated by the eductor-type unit. Modifying the East eductor injection unit, which ensures the acceptable oxygen level, will save 25 % cost of chemicals. Consistent with [6], 300–400 ppb oxygen in polymer preparation and injection process does not degrade polymer viscosity. Furthermore, polymer solutions that propagated over 400 m through a fracture from the injector to the producer were depleted of dissolved oxygen from 1.5 to 0 ppm, thereby providing field-based support that the Kalamkas formation provides further chemical stability. The injector pressure fall-off test indicated that fracture is open during polymer flood. In addition, field studies reveal that the advantages of fracture features during polymer flood are no injectivity loss and stability of the polymer solution.

Acknowledgments

The authors express their gratitude to JSC “Mangistaumunaigas” and LLP “KMG Engineering” for providing the opportunity to publish the results of this field study.

References

- 1 Lake, L.W. (1989). *Enhanced Oil Recovery*. Englewood Cliffs, New Jersey, USA: Prentice Hall.
- 2 Maerker, J.M. (1975). Shear Degradation of Partially Hydrolyzed Polyacrylamide Solutions. *SPE J.*, 15(4), 311–322. SPE-5101-PA. <https://doi.org/10.2118/5101>.
- 3 Seright, R.S. (1983). The Effects of Mechanical Degradation and Viscoelastic Behavior on Injectivity of Polyacrylamide Solutions. *SPE J.* 23(3), 475–485. SPE-9297-PA. <https://doi.org/10.2118/9297-PA>.
- 4 Seright, R.S., Seheult, J.M., & Talashek, T.A. (2009). Injectivity Characteristics of EOR Polymers. *SPE Res Eval & Eng*, 12(5), 783–792. SPE-115142-PA. <https://doi.org/10.2118/115142-PA>.
- 5 Seright, R.S., Campbell, A.R., Mozley, P.S., & Han, P. (2010). Stability of Partially Hydrolyzed Polyacrylamides at Elevated Temperatures in the Absence of Divalent Cations. *SPE J.*, 15(2), 341–348. SPE-121460-PA. <https://doi.org/10.2118/121460-PA>.
- 6 Seright, R.S., & Skjevraak, I. (2015). Effect of Dissolved Iron and Oxygen on Stability of HPAM Polymers. *SPE J.*, 20(3), 433–441. SPE-169030-PA. <https://doi.org/10.2118/169030-PA>.
- 7 Manichand, R.N., Moe Soe Let, K.P., Gil, L., Quillien, B., & Seright, R.S. (2013). Effective Propagation of HPAM Solutions through the Tambaredjo Reservoir during a Polymer Flood. *SPE Prod & Oper*, 28(4), 358–368. SPE-164121-PA. <https://doi.org/10.2118/164121-PA>.
- 8 Vitor, H.S. Ferreira, & Rosangela, B. Moreno, Z.L. (2017). Polyacrylamide Mechanical Degradation and Stability in the Presence of Iron. *Offshore Technology Conference*, Rio de Janeiro, Brazil. OTC-27953-MS. <https://doi.org/10.4043/27953-MS>.
- 9 Jouenne, S., Klimenko, A., & Levitt, D. (2016). Polymer Flooding: Establishing Specifications for Dissolved Oxygen and Iron in Injection Water. *SPE J.*, 22(2), 438–446. SPE-179614-PA. <https://doi.org/10.2118/179614-PA>.
- 10 Jouenne, S., Chakibi, H., & Levitt, D. (2017). Polymer Stability After Successive Mechanical-Degradation Events. *SPE J.*, 23(1), 18–33. SPE-186103-PA. <https://doi.org/10.2118/186103-PA>.
- 11 Xu, T., White, S.P., Pruess, K., & Brimhall, G. (2000). Modeling Pyrite Oxidation in Saturated and Unsaturated Subsurface Flow Systems. *Transport in Porous Media*, 39, 25–56.
- 12 Wang, Z.W., Zhang, J.C., & Jiang, Y.L. (1988). Evaluation of Polymer Flooding in Daqing Oil Field and Analysis of Its Favorable Conditions. *SPE International Meeting on Petroleum Engineering*, Tianjin, China. SPE-17848-MS. <https://doi.org/10.2118/17848-MS>.
- 13 Zhao, Y., Yin, S.Z., Seright, R.S., Ning, S., Zhang, Y., & Bai, B.J. (2020). Enhancing Heavy-Oil-Recovery Efficiency by Combining Low-Salinity-Water and Polymer Flooding. *SPE J.*, 26(3), 1535–1551. SPE-204220-PA. <https://doi.org/10.2118/204220-PA>.
- 14 Leibin, E.L., & Ogay E.K. (1979). Technological scheme of the Kalamkas field development. *KazNIPIneft report*, Shevchenko [in Russian].
- 15 Sagyndikov, M., Mukhambetov, B., Orynbasar, Y., Nurbulatov, A., & Aidarbayev, S. (2018). Evaluation of Polymer Flooding Efficiency at brownfield development stage of giant Kalamkas oilfield, Western Kazakhstan. *SPE Annual Caspian Technical Conference and Exhibition*, Astana, Kazakhstan. SPE-192555-MS. <https://doi.org/10.2118/192555-MS>.
- 16 Wilson, A. (2017). Challenges During Surface-Facility-Project Implementation for a Full-Field Polymer Flood. *J Pet Technol*, 69(6), 81–28. SPE-0617-0081-JPT. <https://doi.org/10.2118/0617-0081-JPT>.

- 17 Sheng, J. (2011). *Modern Chemical Enhanced Oil Recovery: Theory and Practice, Chapter 5 — Polymer flooding*. Amsterdam: Elsevier.
- 18 Seright, R.S., Fan, T., Wavrik, K., & Balaban, R.C. (2011). New Insights into Polymer Rheology in Porous Media. *SPE J.*, 16(1), 35–42. SPE-129200-PA. <https://doi.org/10.2118/129200-PA>.
- 19 Seright, R.S. (2017). How Much Polymer Should Be Injected During a Polymer Flood? Previous and Current Practices. *SPE J.*, 22(1), 1–18. SPE-179543-PA. <https://doi.org/10.2118/179543-PA>.
- 20 Horne, R.A., & Johnson, D.S. (1966). The Viscosity of Water Under Pressure. *J. Phys. Chem.*, 70(7), 2182–2190. <https://doi.org/10.1021/j100879a018>.
- 21 American Petroleum Institute (1990). *Recommended Practices for Evaluation of Polymers Used in Enhanced Oil Recovery Operations*. API RP 63.
- 22 Sulin, V.A. (1946). *Waters of Petroleum Formations in the System of Nature Waters*. Moscow: Gostoptekhizdat [in Russian].
- 23 Zhang, J. (1995). *The EOR Technology*. Beijing: Petroleum Industry Publishing Company of China.
- 24 You, Q., F.L., Wang, Y.F., & Mu, L.N. (2007). Comparison of the Properties of Injected and Released Polyacrylamide in Polymer Flooding. *Journal of Beijing University of Chemical Technology*, 34(4), 414–417.
- 25 Wang, D., Seright, R., Shao, Z., & Wang, J. (2008). Key Aspects of Project Design for Polymer Flooding at the Daqing Oil Field. *SPE Res Eval & Eng*, 11(6), 1117–1124. Paper SPE 109682. <http://dx.doi.org/10.2118/109682-PA>.
- 26 Moe Soe Let, K.P., Manichand, R.N., & Seright R.S. (2012). Polymer flooding a ~500-cp Oil. *18th SPE Improved Oil Recovery Symposium*, Tulsa, Oklahoma, USA. SPE-154567-MS.
- 27 Levitt, D.B., Slaughter, W., Pope, G.A. et al. (2011). The Effect of Redox Potential and Metal Solubility on Oxidative Polymer Degradation. *SPE Res Eval & Eng*, 14(3), 287–298. SPE-129890-PA. <http://dx.doi.org/10.2118/129890-PA>.
- 28 Gaillard, N., Giovannetti, B., & Favero, C. (2010). Improved Oil Recovery Using Thermally and Chemically Protected Compositions Based on Co- and Terpolymers Containing Acrylamide. *SPE Improved Oil Recovery Symposium*, Tulsa, Oklahoma. SPE-129756-MS. <http://dx.doi.org/10.2118/129756-MS>.
- 29 Wellington, S.L. (1983). Biopolymer Solution Viscosity Stabilization — Polymer Degradation and Antioxidant Use. *SPE J.*, 23(6), 901–912. SPE-9296-PA. <http://dx.doi.org/10.2118/9296-PA>.
- 30 Houze, O., Viturat, D., Fjaere, O.S. et al. (2020). *Dynamic Data Analysis*. KAPPA. v5.30.01.
- 31 Van den Hoek, P.J., Al-Masfry, R.A., Zwartz, D. et al. (2009). Optimizing Recovery for Waterflooding under Dynamic Induced Fracturing Conditions. *SPE Res Eval & Eng*, 12(5), 671–682. SPE-110379-PA. <http://dx.doi.org/10.2118/110379-PA>.
- 32 Van den Hoek, P.J., Mahani, H., Sorop, T.G., Brooks, A.D., Sen, S., Shuaili K., & Saadi, F. (2012). Application of Injection Fall-Off Analysis in Polymer flooding. *74th EAGE Conference & Exhibition incorporating SPE EUROPEC 2012*, Copenhagen, Denmark. SPE-154376-MS. <https://doi.org/10.2118/154376-MS>.
- 33 Dyes, A.B., Kemp, C.E., & Caudle, B.H. (1958). Effect of Fractures on Sweep-Out Pattern. *Petroleum Transactions*, AIME, Vol. 213, 245–249, SPE-1071-G. Richardson, Texas: SPE.

М.С. Сагындиқов, И.И. Салимғараев, Е.К. Огай, Р.С. Серайт, С.Е. Кудайбергенов

Батыс Қазақстандағы Қаламқас кен орнында полимерлік суландыру кезінде полиакриламид ерітіндісінің химиялық тұрақтылығын бағалау

Полимерлі суландыру кезінде кен орнының операторы полимерді айдаудың алғашқы кезеңдерінде химияға айтарлықтай салынған қаражаттың бос кетпеуіне сенімді болуы қажет. Сонымен қатар, тұтқыр полимер ерітіндісіндегі ерітілген оттегінің деңгейі қауіпсіз деңгейде бақылануы керек, бұл жағдайда тұтқырлықтың жоғалуы айтарлықтай болмайды. Гидролизденген полиакриламидтің (ГПАА) ерітіндісі анаэробты жағдайда, тіпті технологиялық суда темір иондары болған жағдайда да өте тұрақты болатыны белгілі. Осылайша, кен орнында енгізілген оттегі мен суда бар темір иондары тұтқырлықтың төмендеуіне әкеледі. Геохимиялық есептеу Қаламқас кен орнының қабатына енгеннен кейін еріген оттегі тез сіңірілетінін көрсетеді. Осы мақалада зертханалық зерттеулер мен далалық бақылаулардың көмегімен бұл болжамдар расталған. Жүргізілген зерттеулер Батыс Қазақстандағы Қаламқас мұнай кен орнымен байланысты полимер ерітінділері мен реактивті өндіруші ұңғымадан алынған сұйықтықтың реологиясын өлшеуге негізделген. Жан-жақты талдау PSU типті қондырғыда (polymer slicing unit) полимерді дайындау және айдау кезінде беткі жабдықта тұтқырлық жоғалмағанын және полимер ерітіндісін дайындау кезінде енгізілген оттегі туындаған Educator типті қондырғыда полимердің тұтқырлығының айтарлықтай жоғалуын растайды. Алайда, бетінде химиялық ыдырау туғызатын еріген оттегінің жоғары деңгейінің өзі тау жыныстарымен байланысу кезінде тез сінеді, осылайша қабаттағы химиялық тұрақтылықты қамтамасыз етеді.

Кілт сөздер: полиакриламид, полимер ерітіндісі, химиялық бұзу, полимерлі суландыру, темір, оттегі, тұтқырлық, айдау.

М.С. Сагындииков, И.И. Салимгараев, Е.К. Огай, Р.С. Серайт, С.Е. Кудайбергенов

Оценка химической стабильности раствора полиакриламида при полимерном заводнении на месторождении Каламкас (Западный Казахстан)

При полимерном заводнении оператор месторождения должен быть убежден, что значительные инвестиции в химию не теряются на ранней стадии закачки полимера. Кроме этого, уровень растворенного кислорода в вязком полимерном растворе должен контролироваться на безопасном уровне, при котором потеря вязкости будет незначительной. Известно, что раствор гидролизованного полиакриламида в анаэробных условиях очень стабилен, даже при присутствии ионов железа в технологической воде. Таким образом, в полевых условиях введенный кислород и существующие ионы железа приведут к колоссальным потерям вязкости. Геохимический расчет показывает, что растворенный кислород после проникновения в пласт месторождения Каламкас будет быстро поглощен. Настоящая статья подтверждает эти предположения с помощью комбинации лабораторных исследований и полевых наблюдений. Проведенные исследования основаны на измерениях реологии полимерных растворов и жидкости из реагирующей добывающей скважины, связанной с нефтяным месторождением Каламкас в Западном Казахстане. Всесторонний анализ подтверждает отсутствие потери вязкости на поверхностном оборудовании во время подготовки и закачки полимера в установке типа PSU (polymer slicing unit) и значительную потерю вязкости полимера в установке типа Eductor, который вызван введенным кислородом при приготовлении полимерного раствора. Однако даже введенный высокий уровень растворенного кислорода, вызывающий химическую деструкцию на поверхности, быстро поглощается при контакте с породой, тем самым обеспечивая химическую стабильность в пласте.

Ключевые слова: полиакриламид, полимерный раствор, химическая деструкция, полимерное заводнение, железо, кислород, вязкость, закачка.

Information about the authors

Sagyndikov, Marat Serikovich (*corresponding author*) — PhD student, Satbayev University, Almaty, Kazakhstan; 050013, Satpayev str., 22; KMG Engineering LLC; E-mail: sagyndikov_marat@mail.ru; <https://orcid.org/0000-0003-0086-723X>;

Salimgarayev, Ishat Iskandarovich — Lead Engineer at Enhanced Oil Recovery Service, LLP “KMG Engineering” “KazNIPImunaygas”, Aktau, Kazakhstan; 130000, 35 mcr., plot 6/1. E-mail: Salimgarayev_I@kaznipi.kz; <https://orcid.org/0000-0002-9352-6743>;

Ogay, Evgeni Kiponiyevich — Chief Technical Adviser of KMG Engineering LLP, Doctor of Technical Sciences, Associate Professor, Academician of the Russian Academy of Sciences, Laureate of the State Prize of the RoK, Nur-Sultan, Kazakhstan; 010010, Kunayev str., 8, block B. E-mail: Y.Ogay@niikmg.kz; <https://orcid.org/0000-0002-5109-5623>;

Seright, Randall Scott — Senior Engineer and Associate Director of the New Mexico Petroleum Recovery Research Center, New Mexico Institute of Mining and Technology, PhD degree in Chemical Engineering from the University of Wisconsin (Madison), Adjunct Professor at New Mexico Tech’s Petroleum Engineering Department, NM 87801, Socorro, USA; 801 Leroy Place. E-mail: randy.seright@nmt.edu; <https://orcid.org/0000-0003-1734-5155>;

Kudaibergenov, Sarkyt Elekenovich — Full Professor, Doctor of Chemical Sciences, Director of Institute of Polymer Materials and Technology, Almaty, Kazakhstan; 050019, Atyrau-1, 3/1. E-mail: skudai@mail.ru; <https://orcid.org/0000-0002-1166-7826>

A.A. Yuminova^{1*}, E.A. Giniyatullina¹, L.M. Karieva¹, L.G. Chekanova²

¹Perm State National Research University, Perm, Russia;

²Institute of Technical Chemistry of Ural Branch of the RAS, Perm, Russia

(*Corresponding author's email: aleks3004@list.ru)

Physical-chemical properties of FM-1 reagent as a potential collector for ion flotation of lanthanoids

The physical-chemical properties of the industrial reagent “FM-1” have been investigated. These properties are necessary for evaluating its use as a collector in the processes of concentration of rare earth metal ions by ion flotation. “FM-1”, which is based on sodium salts of aminomethylenephosphonic acids, is used as a flocculant for oil production and purification of process waters from suspended particles and petroleum products. Protolytic equilibria in aqueous solutions of the reagents were studied. The values of dissociation constants equaling $pK_{a1} = 2.31 \pm 0.26$ and $pK_{a2} = 8.82 \pm 0.34$ were determined spectrophotometrically. Surface tension of the reagent solutions at the solution-air interface was studied. The “FM-1” reagent was classified as a strong surface-active substance with the following parameters: Minimal surface tension $\sigma_{\min} = 29 \text{ mN}\cdot\text{m}^{-1}$, surface activity $G = 0.031 \text{ N}\cdot\text{m}^2\cdot\text{mol}^{-1}$, critical concentration of micelle formation $1 \cdot 10^{-3} \text{ mol}\cdot\text{L}^{-1}$. The regularities of the reagent's interaction with lanthanum (III) ions were studied. A high degree of lanthanum ions' precipitation (over 99.7 %) was observed over a rather wide interval of pH values (4.00–12.00); at this point, at $\text{pH} \geq 7.5$, lanthanum hydroxide can co-precipitate. The formation of compounds in a solution with molar ratios $[\text{La}]:[\text{FM-1}] = 1:1$ and $1:2$ was established by conductometric titration method. The findings of chemical analysis, FTIR spectroscopy and elemental analysis of the isolated precipitates suggested their structural formula. A possibility for the “FM-1” reagent to be used as a collector for the ion flotation of lanthanum (III) ions was shown.

Keywords: ion flotation, rare-earth elements, aminomethylenephosphonic acid salts, collector, physical-chemical properties, surface-active substance, lanthanum, FM-1.

Introduction

Ion flotation has been one of promising techniques for extracting small amounts of rare-earth elements, first of all for producing collective concentrates from technological solutions [1–4]. In interaction with metal ions, collectors form highly stable structures and are of the most current importance [5]. Reagents having in their compositions heteroatoms capable of forming complex compounds are of most interest [6]. Three-valence lanthanoids form many complexes with organic ligands, more often with oxygen- and/or nitrogen-containing ones [7–10]. A commercial reagent termed FM-1 containing aminomethylenephosphonic acid salts is known as a flocculant for collecting suspended particles and oil products in the oil industry and purification of waste/technological waters [11]. The functional group “FM-1” contains nitrogen and oxygen atoms capable of interacting with rare earth element ions and long alkyl radicals that give the compound surfactant properties. Therefore, this reagent can be considered a potential collector for ion flotation processes.

The purpose of the research is to study the physical-chemical properties of the reagent “FM-1” to establish the possibility of using it in the processes of lanthanoids (III).

Experimental

We used solutions of $\text{La}(\text{NO}_3)_3$ prepared by dissolving a weighed portion of La_2O_3 in 6 M HNO_3 followed by evaporation of excess acid and dilution with distilled water. The FM-1 reagent (H_2L) as a 30 % aqueous solution served as an object to be assayed (formula 1).



Herein, R is a normal (linear) hydrocarbon radical $\text{C}_{10}\text{-C}_{14}$ (Technical Conditions 2483-001-79102376-2005, Russia). The main substance's content was calculated in terms of phosphorus content determined by

atomic-emission spectroscopy with inductively coupled plasma model ICAP 6500 DUO (Thermo Fisher Scientific, USA).

Protolytic equilibriums in the reagent solutes were studied spectrophotometrically [12]. The values pK_{a1} and pK_{a2} were calculated using the formulas below:

$$pK_{a_1} = pH + \lg \frac{A_{HL^-} - A_i}{A_i - A_{H_2L}}; \quad pK_{a_2} = pH + \lg \frac{A_{L^{2-}} - A_i}{A_i - A_{HL^-}}, \quad (2)$$

Here, pK_{a1} and pK_{a2} are negative logarithms of acidic dissociation constants for neutral and ionized forms of the reagent, respectively; A_{H_2L} is optical density of solution containing neutral form of the reagent; A_{HL^-} is optical density of solution containing ionized form of the reagent; $A_{L^{2-}}$ is optical density of solution containing doubly ionized form of the reagent; A_i is optical density of solution at a certain pH value.

UV spectra were acquired on a SF-2000 spectrophotometer (OKB-Spectr, Russia), pH values were measured on a MultiTest IPL-01c ionometer with use of a combined electrode ESK-10603/7 (Russia).

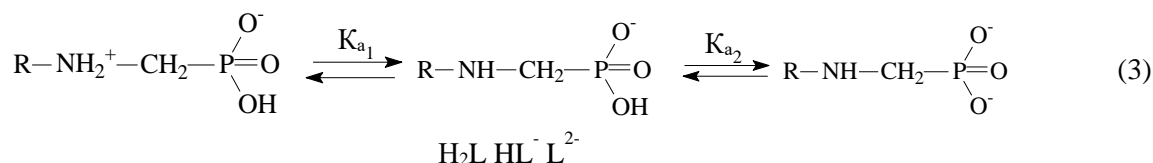
To determine adsorption of FM-1 on the water-air boundary interphase, the drop count method and a stalagmometer ST-1 (Russia) were employed [13, 14]. The first measurement was taken with a background solution (distilled water), all the successive ones — with the reagent solutes under study, at progressively increasing concentration.

The interaction processes between FM-1 and La (III) ions were explored by the precipitation technique [15]. HCl or NaOH solutions were used for creating necessary pH values of working solutions. The content of micro-amounts of La (III) in solution after precipitation was determined by atomic-emission spectroscopy (Thermo ICAP 6500 DUO, USA), that of macro-amounts of La (III) — by direct complexometric titration (Mettler Toledo T70, Switzerland) with xylenol orange [16]. The composition of La — FM-1 compounds being formed in solution was determined by the molar-ratio method [12]. The preparative isolation of precipitates and their analysis were performed in accord with a known method [15]. A Vario EL cube CHNS analyzer (Elementar, Germany) was used to determine the content of elements in precipitates; a Vertex 80V spectrometer (Bruker, Germany) was used to register the FTIR spectra of samples (a suspension in vaseline oil). Molar ratios [La]: [FM-1] in solutions were ascertained by conductometric titration with use of a SEVEN MULTI S70-K conductometer (Mettler Toledo, Switzerland). The experimental procedure used to study ion flotation, along with a laboratory flotation cell, is described in [17].

We used the following reagents: La_2O_3 (99,99 %, “TDM96”, Russia); HNO_3 (chemically pure, 65 %, “RM Engineering”, Russia); HCl (chemically pure, “Component-Reaktiv”, Russia); NaOH (chemically pure, “Vekton”, Russia).

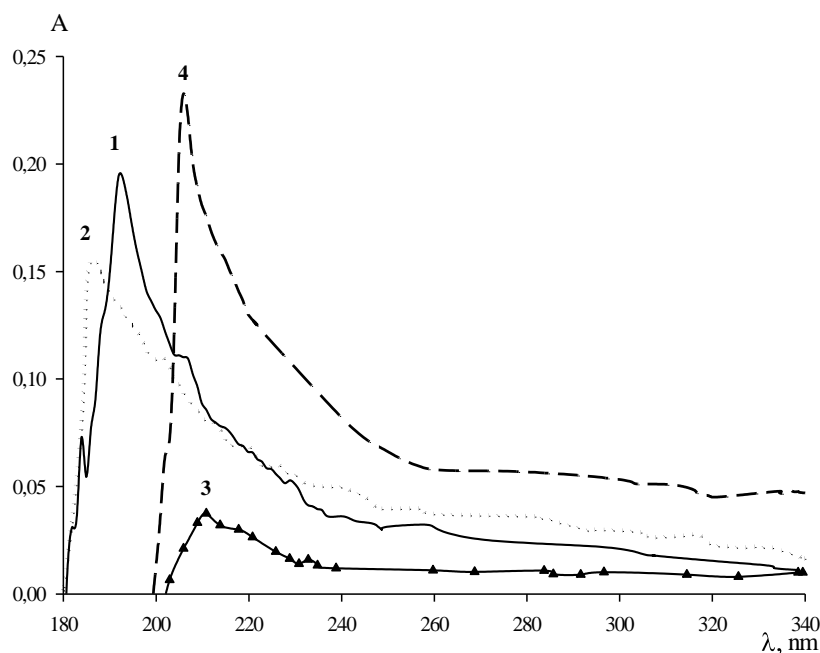
Results and Discussion

Based on the structure, it can be assumed that “FM-1” is an amphoteric compound. The protolytic equilibria can be represented by the following scheme:



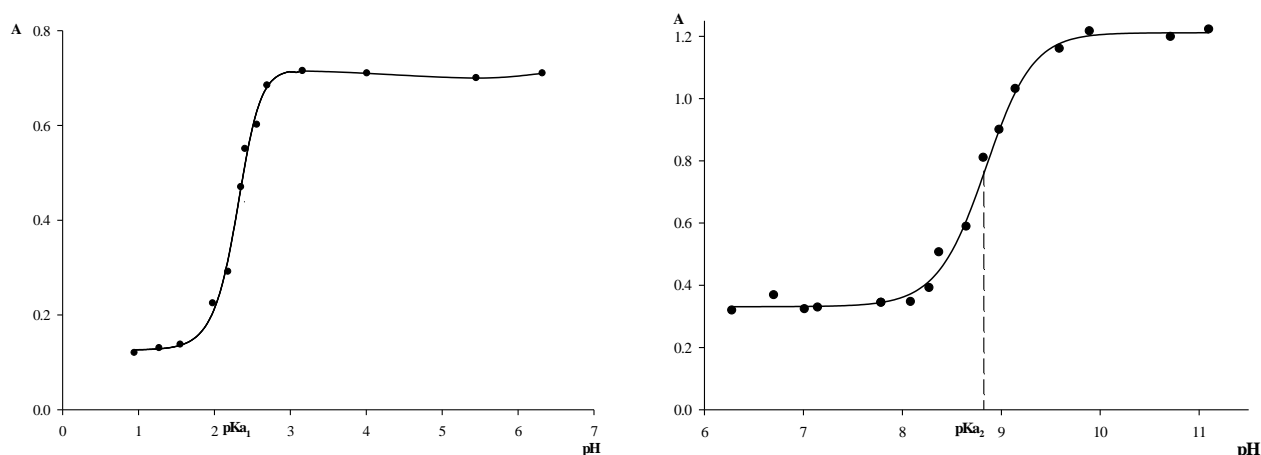
The electronic absorption spectra of solutions differ with varying pH values, thereby corroborating availability of different forms of the reagent (Figure 1).

The dependence of the optical density of FM-1 solutions on pH values was studied to calculate the values of ionization constants (Figure 2). The curves display two S-shaped inflections: the first one at pH 1.92-2.67, corresponding to dissociation of neutral form of FM-1 (H_2L) (Figure 2a), the second one — at pH 8.4-9.3, corresponding to dissociation of HL^- form (Figure 2b).



1 — pH 2.64; 2 — pH 6.06; 3 — pH 8.08; 4 — pH 10.81 (with KOH and HCl solutions used)

Figure 1. Absorption spectra of FM-1 reagent in water vs pH values. $C_{\text{FM-1}} = 1 \cdot 10^{-4} \text{ mol} \cdot \text{L}^{-1}$



$l = 1.0 \text{ cm}$; $\lambda, \text{ nm} = 184.9 \text{ (a) и } 196.9 \text{ (b)}$

Figure 2. Optical density (A) of FM-1 in aqueous solutions vs pH values. $C_{\text{FM-1}} = 1 \cdot 10^{-3} \text{ mol} \cdot \text{L}^{-1}$;

The ionization constants' values calculated as per formulas (2) equaled: $\text{pK}_{\text{a1}} = 2.31 \pm 0.26$ and $\text{pK}_{\text{a2}} = 8.82 \pm 0.34$.

One of characteristics enabling a possibility for a compound to be employed as a flotation reagent is its ability to lessen surface tension on a liquid-gas boundary [13]. Figure 3 presents the surface tension isotherm of FM-1 solutes. With the reagent at concentrations from $5.0 \cdot 10^{-5}$ to $1.0 \cdot 10^{-2}$ added, surface tension lessens by a factor of 2-2.5 as compared with the background solution (σ_{min} of FM-1 solutes equals $29 \text{ mN} \cdot \text{m}^{-1}$; $\sigma_{\text{H}_2\text{O}} = 72.75 \text{ mN} \cdot \text{m}^{-1}$ at 20°C). The results obtained enable the reagent to be classified as a strong surface-active substance.

The findings derived from Figure 3 gave rise to the following results: the surface activity (G) of the reagent calculated as the tangent value of the slope angle of the tangent line to the surface tension isotherm at $C \rightarrow 0$ [14] equaled $0.031 \text{ N} \cdot \text{m}^2 \cdot \text{mol}^{-1}$; the critical concentration of micelle formation equaled $1 \cdot 10^{-3} \text{ mol} \cdot \text{L}^{-1}$.

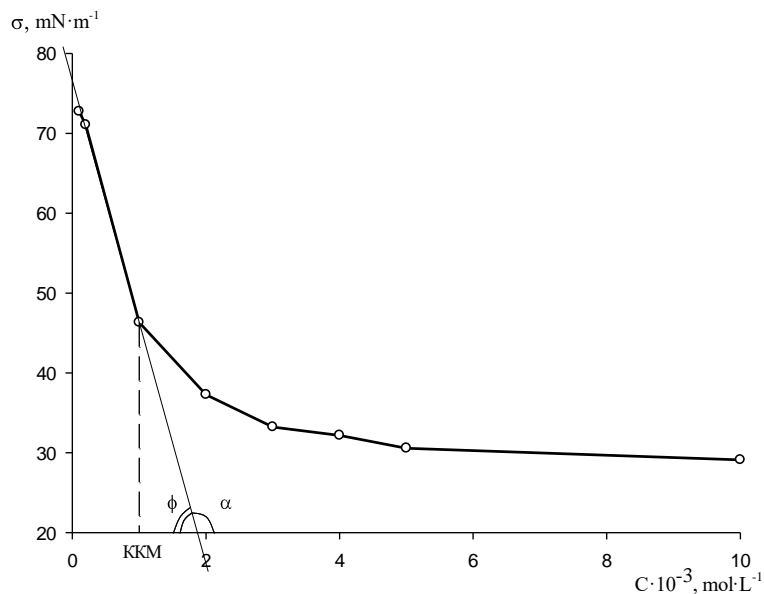


Figure 3. The surface tension isotherm of FM-1 solutions on liquid-gas boundary

Figure 4 shows the degree of precipitation (S , %) of La (III) ions with the reagent as dependent on the equilibrium pH value of solution.

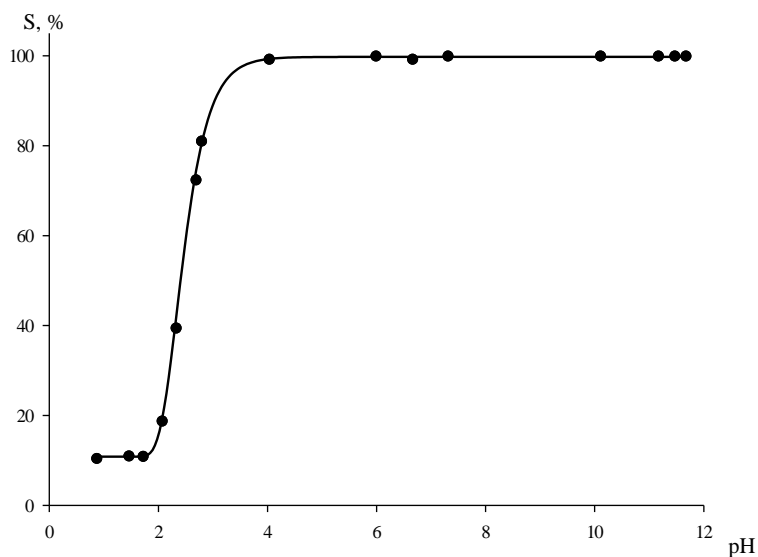
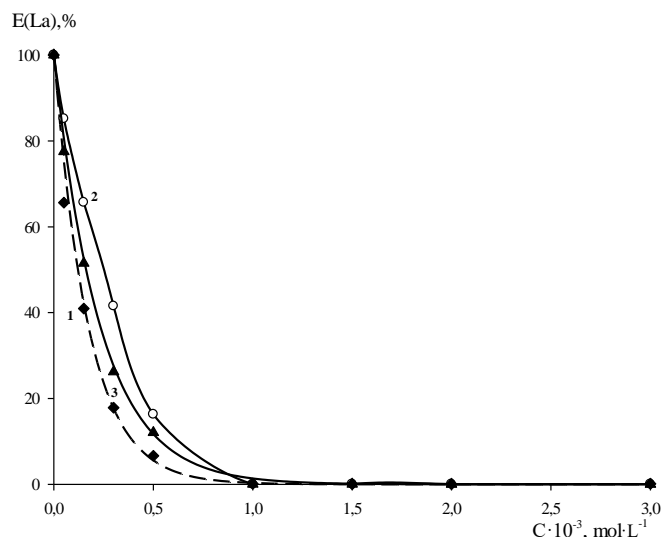


Figure 4. The degree of precipitation (S , %) of La (III) ions with FM-1 vs pH values of solution

A high degree of lanthanum ions' precipitation (over 99.7 %) was observed over a rather wide interval of pH values (4.00–12.00). It should be noted, however, that at $\text{pH} \geq 7.5$, lanthanum hydroxide can co-precipitate in solution [18]. Therefore, all the precipitation regularities were studied at $\text{pH} = 4.77; 5.70; 6.85$ (acetate-ammonium buffer solutions were used).

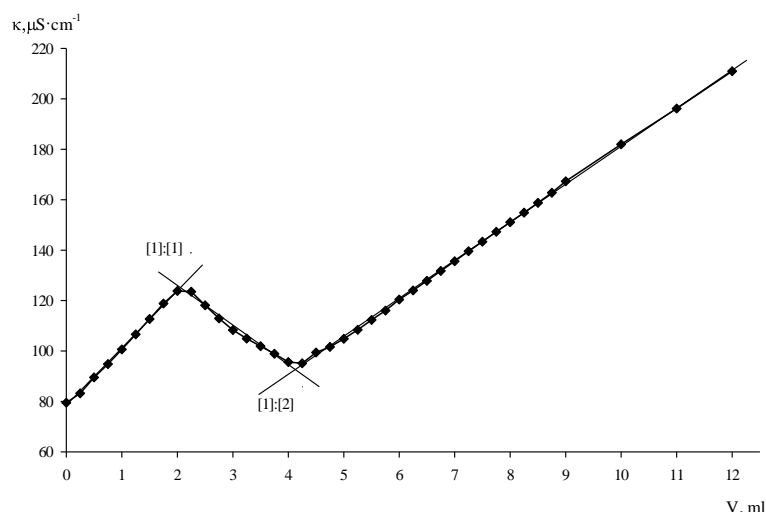
By using the saturation method (Figure 5), the qualitative binding of La^{3+} ions was ascertained to occur already at ratio $[\text{La}]:[\text{FM-1}] = 1:1$. Within the interval mentioned above, the pH values of the medium do not markedly affect the degree of precipitation.



$C_{\text{La(III)}} = 1 \cdot 10^{-3} \text{ mol} \cdot \text{L}^{-1}$; $V_{\text{(buffer)}} = 5.0 \text{ ml}$; $V_{\text{total}} = 25 \text{ ml}$; 1 — pH 4.77; 2 — pH 5.70; 3 — pH 6.85

Figure 5. The degree of extraction of La (III) ions vs concentration of FM-1

The conductometric titration method enabled the formation of compounds in solutions with molar ratios [La]:[FM-1] = 1:1 and 1:2 to be established (Figure 6).



$C_{\text{starting}}(\text{FM-1}) = C_{\text{starting}}(\text{La(III)}) = 1 \cdot 10^{-2} \text{ mol} \cdot \text{L}^{-1}$; $V_{\text{La(III)}} = 2.5 \text{ ml}$; $V_{\text{total}} = 60 \text{ ml}$; $[\text{EtOH}]:[\text{H}_2\text{O}] = 1:1$

Figure 6. Electrical conductivity of $\text{La}(\text{NO}_3)_3$ solution vs portions of the reagent added

The compounds with the ratios found were preparedly isolated. Elemental analysis of the compounds isolated at pH 5 is presented in Table 1. No sodium ions were detected in the samples after decomposition. The results of the analysis corroborated the ratio [metal]:[reagent] as equaling 1:1 for both compounds and were well in line with theoretical calculations.

Table 1

Chemical analysis of the compounds isolated

| Compounds | Molecular mass | Found, % | | | Calculated*, % | | |
|-------------------|----------------|----------|------|-------|----------------|------|-------|
| | | N | P | La | N | P | La |
| [La]:[FM-1] = 1:1 | 416 | 3.30 | 8.51 | 35.47 | 3.38 | 7.45 | 33.41 |
| [La]:[FM-1] = 1:2 | 693 | 3.36 | 8.34 | 36.41 | 4.04 | 8.95 | 20.06 |

Note: *In terms of average molecular mass ($R = \text{C}_{12}\text{H}_{25}^-$).

The analyzed FTIR spectra of the compounds isolated also corroborated them as being identical. In the FTIR spectra of La – FM-1 compounds, P–OH absorption bands typical of the reagent in the range 2700–2550 cm^{-1} are absent. The wide band appears in the La – FM-1 compounds in the region of 3500–3300 cm^{-1} . It can be considered as a result of the superposition of bands of N–H valence vibrations and the formed new O–H bond (Figure 7) [19].

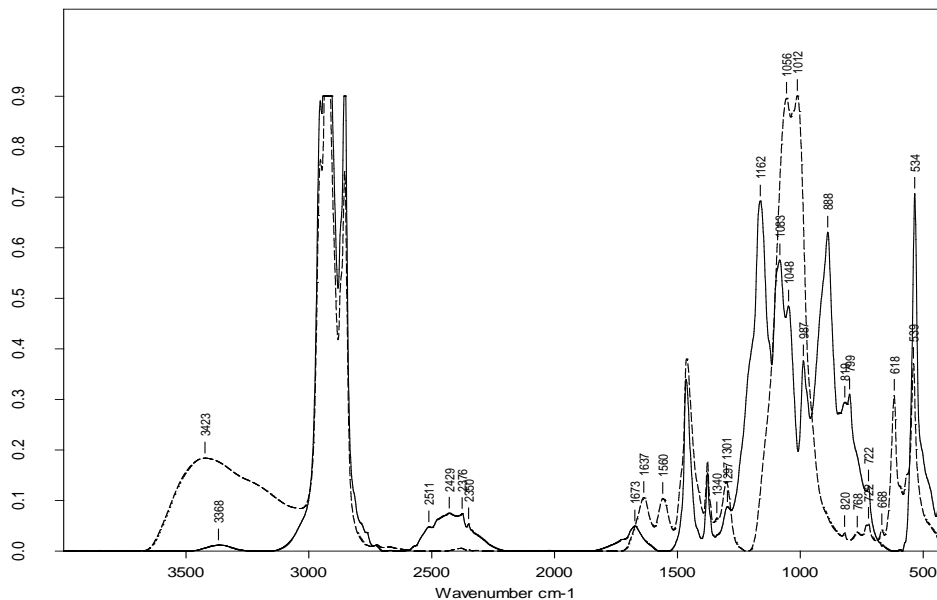


Figure 7. FTIR spectra of the reagent (firm line) and of its compound with lanthanum (III) at ratio 1:1 (dotted line)

With the findings of elemental analysis and FTIR spectroscopy as an underlying basis, the following structural formula of the reagent can presumably be presented:



Table 2 lists the findings of FM-1 investigated as a collector for the ion extraction of lanthanum.

Table 2

Ion flotation of La (III) with FM-1 reagent;
 $C_{\text{La(III)}} = 1 \cdot 10^{-3} \text{ mol} \cdot \text{L}^{-1}$; $C_{\text{R}} = 1 \cdot 10^{-3} \text{ mol} \cdot \text{L}^{-1}$; flotation duration 5 minutes

| № | pH | $C_{\text{remaining La}} \text{ mg} \cdot \text{L}^{-1}$ | E, % |
|---|------|--|------|
| 1 | 3.25 | 97.02 | 30.2 |
| 2 | 5.61 | 15.29 | 89.1 |
| 3 | 8.78 | 16.26 | 88.3 |

Conclusions

Based on the research results of the reagent “FM-1” properties, it can be recommended as a collector in the processes of rare earth elements ion flotation. The FM-1 reagent was evinced to be an amphoteric compound ($\text{pK}_{\text{a}1} = 2,31 \pm 0,26$; $\text{pK}_{\text{a}2} = 8,82 \pm 0,34$) and was classified as a strong surface-active substance (with the reagent at concentrations from $5.0 \cdot 10^{-5}$ to $1.0 \cdot 10^{-2}$ added, surface tension lessens by a factor of 2–2.5 as compared with the background solution). Strong surface-active properties enable the “FM-1” compound to be employed in ion flotation procedures with no additional foaming agents added. In conjoint presence with lanthanum (III) ions in a solution, the reagent forms hardly-soluble compounds over a rather wide interval of pH values (4.00–12.00). The formation of compounds with molar ratios $[\text{La}]:[\text{FM-1}] = 1:1$ and $1:2$ was established in a solution (pH 4,8–6,8). The findings of chemical analysis, FTIR spectroscopy and elemental analysis of the isolated precipitates suggested their structure. A possibility for the “FM-1” reagent to be used

as a collector for the ion flotation of lanthanum (III) ions was shown, with a maximal degree of extraction equaling 89.1 % ($C_{\text{remaining}} = 15.29 \text{ mg/l}$ at pH 5.61, $[\text{La}]:[\text{R}] = 1:1$).

Acknowledgments

This work was partially financed under the State Contract Order No. AAAA-A18-118032790022-7. The authors acknowledge Chemical company “Technology – Ural” for specimens of “FM-1”.

References

- 1 Чиркст Д.Э. Ионная флотация редкоземельных металлов с додецилсульфатом натрия / Д.Э. Чиркст, О.Л. Лобачева, Н.В. Джевага // Журн. прикл. хим. — 2011. — Т. 84, № 9. — С. 1424–1430.
- 2 Lobacheva, O.L., Dzhevaga, N.V., & Danilov A.S. (2016). The method of removal yttrium (III) and ytterbium (III) from dilute aqueous solutions. *Journal of Ecological Engineering*, 17(2), 38-42.
- 3 Shetty, S., Ponnurangam, S., & Chernyshova I.V. (2020). Foam flotation of rare earth elements by conventional and green surfactants. *Minerals Engineering*, 158, 106585.
- 4 Abaka-Wood, G.B., Zanin, M., Addai-Mensah, J., & Skinner, W. (2019). Recovery of rare earth elements minerals from iron oxide–silicate rich tailings — Part 2: Froth flotation separation. *Minerals Engineering*, 142, 105888.
- 5 Радусhev А.В. Реагенты для ионной флотации цветных металлов / А.В. Радусhev, Л.Г. Чеканова, Г.В. Чернова // Цветные металлы. — 2005. — № 7. — С. 34–39.
- 6 Marion, C., Li, R.H., & Waters K.E. (2020). A review of reagents applied to rare-earth mineral flotation. *Advances in Colloid and Interface Science*, 279, 102142.
- 7 Мартыненко Л.И. Особенности комплексообразования редкоземельных элементов (III) / Л.И. Мартыненко // Успехи химии. — 1991. — Т. 60, № 9. — С. 1969–1998.
- 8 Belova, V.V., Tsareva, Y.V., Zakhodyaeva, Y.A., Ivanov, V.K., & Voshkin A.A. (2021). Solvent extraction of lanthanides (III) in the presence of the acetate ion acting as a complexing agent using mixtures of cyanex 272 and caprylic acid in hexane. *Processes*, 9(12), 2222.
- 9 Radushev A. V. α -Branched tertiary carboxylic acid hydrazides as extractants of rare-earth metal ions from sulfate media / A.V. Radushev, V.A. Nikitina, T.D. Batueva // *Russian Journal of Applied Chemistry*, 2021. — Vol. 94, No. 5. — P. 595–600.
- 10 Healy, M.R., Ivanov, A.S., Karslyan, Y., Bryantsev, V.S., Moyer, B.A., & Jansone-Popova S. (2019). Efficient separation of light lanthanides(III) by using bis-lactam phenanthroline ligands. *Chemistry A European Journal*, 25(25), 6326-6331.
- 11 Евразийский патент № 014001. Способ воздействия на нефтяной пласт / А.Г. Тэслер, С.Н. Кайдалов, И.А. Перминов, И.В. Бармин, С.Е. Ильясов, Л.В. Закшевская и др. // Оpubл. 2010.
- 12 Бернштейн И.Я. Спектрофотометрический анализ в органической химии / И.Я. Бернштейн, Ю.Л. Каминский. — Л.: Химия, 1975. — 232 с.
- 13 Фролов В.И. Методы определения поверхностного натяжения / В.И. Фролов, Д.Ю. Митюк, Р.Е. Твердый. — М.: РГУ нефти и газа им. И.М. Губкина, 2013. — 48 с.
- 14 Ланге К.Р. Поверхностно-активные вещества: синтез, свойства, анализ, применение; пер. с англ. / К.Р. Ланге. — СПб.: Профессия, 2004. — 240 с.
- 15 Chekanova, L.G., Manylova, K.O., Pavlov, P.T., Baigacheva, E.V. & Tiunova T.G. (2015). Complexation of ethyl 2-aryl(alkyl)sulfonylamino-4,5,6,7-tetrahydrobenzo[b]thiophene-3-carboxylates with nonferrous metal ions. *Russian Journal of Inorganic Chemistry*, 60(4), 531–535.
- 16 Шварценбах Г. Комплексонометрическое титрование / Г. Шварценбах, Г. Флашка. — М.: Химия, 1970. — 360 с.
- 17 Чеканова Л.Г. N', N'-Диалкилгидразиды как потенциальные реагенты для ионной флотации меди (II) / Л.Г. Чеканова, Е.В. Байгачева, А.В. Радусhev, Т.Д. Батуева // *Химическая технология*. — 2008. — Т. 9, № 9. — С. 476–480.
- 18 Химия и технология редких и рассеянных элементов. Ч. 2 / под ред. К.А. Большакова. — М.: Высш. шк., 1976. — 360 с.
- 19 Тарасевич Б.Н. ИК спектры основных классов органических соединений / Б.Н. Тарасевич. — М.: МГУ, 2012. — 55 с.

А.А. Юминова, Е.А. Гиниятуллина, Л.М. Кариева, Л.Г. Чеканова

Лантаноидтардың иондық флотациясы үшін потенциалды жинақтаушы – «ФМ-1» реагентінің физика-химиялық қасиеттері

«ФМ-1» өнеркәсіптік реагентінің иондық флотация әдісімен сирекжер металл иондарын концентрлеу процестерінде жинақтаушы ретінде пайдалануды бағалау үшін қажетті физика-химиялық қасиеттері зерттелді. Негізгі аминдіметилфосфон қышқылдарының натрий тұздары болатын «ФМ-1» мұнай

өндіру және технологиялық суларды қалқыма бөлшектер мен мұнай өнімдерінен тазарту үшін флокулянт ретінде қолданылады. Реагенттің сулы ерітінділеріндегі протолиттік тепе-теңдігі зерттелді. Диссоциация тұрақтыларының мәндері спектрофотометриялық әдіспен анықталды: $pK_{a1} = 2,31 \pm 0,26$ және $pK_{a2} = 8,82 \pm 0,34$. Ерітінді-ауа шекарасындағы реагент ерітінділерінің беттік керілуі анықталған. «ФМ-1» күшті беттік белсенді заттар класына жататыны дәлелденген. Ерітінділердің беттік керілуінің минималды мәні ($\sigma_{\text{мин}}$) 29,0 мН/м құрады; беттік белсенділігі (G) — $0,031 \text{ Н} \cdot \text{м}^2/\text{моль}$, мицеллалардың шекті концентрациясы (МШК) — $1 \cdot 10^{-3}$ моль/л шамасына тең болды. «ФМ-1» реагентінің лантан (III) иондарымен әрекеттесу заңдылықтары зерттелді. «ФМ-1» лантан (III) иондарымен өзара әрекеттесу заңдылықтары зерттелді. La (III) иондарының реагентпен тұндырылуының жоғары деңгейі (99,7 % — дан астам) рН мәндерінің жеткілікті кең диапазонында байқалады (4,0-ден 12,0-ге дейін ($\text{pH} \geq 7,5$ кезінде лантан гидроксидінің тұндырылуы мүмкін). Кондуктометриялық титрлеу ($\text{pH} 4,8\text{--}6,8$) әдісі молярлық қатынасы бар ерітіндіде қосылыстардың түзілуін анықтады $[\text{La(III)}]:[\text{R}] = 1:1$ және $1:2$. Химиялық талдау, ИК-спектроскопия және бөлінген шөгінділерді элементтік талдау деректері негізінде олардың құрылымдық формуласы ұсынылды. «ФМ-1» реагентін лантанның (III) иондық флотациясы үшін жинақтаушы ретінде пайдалану мүмкіндігі көрсетілген.

Клт сөздер: иондық флотация, сирекжер элементтері, аминдиметиленфосфон қышқылдары, жинақтаушы, физико-химиялық қасиеттері, беттік белсенді заттар, лантан, ФМ-1.

А.А. Юминова, Е.А. Гиниятуллина, Л.М. Кариева, Л.Г. Чеканова

Физико-химические свойства реагента «ФМ-1» — потенциального собирателя для ионной флотации лантаноидов

Исследованы физико-химические свойства промышленного реагента «ФМ-1», необходимые для оценки его применения в качестве собирателя в процессах концентрирования ионов редкоземельных металлов методом ионной флотации. «ФМ-1», основу которого составляют натриевые соли аминометиленфосфоновых кислот, применяется в качестве флокулянта для нефтедобычи и очистки технологических вод от взвешенных частиц и нефтепродуктов. Изучены протолитические равновесия в водных растворах реагента. Спектрофотометрическим методом определены значения констант диссоциации: $pK_{a1} = 2,31 \pm 0,26$ и $pK_{a2} = 8,82 \pm 0,34$. Изучено поверхностное натяжение растворов реагента на границе раствор-воздух. Установлено, что «ФМ-1» относится к классу сильных ПАВ. Минимальное значение поверхностного натяжения ($\sigma_{\text{мин}}$) растворов составило 29,0 мН/м; поверхностная активность (G) — $0,031 \text{ Н} \cdot \text{м}^2/\text{моль}$, критическая концентрация мицеллообразования (ККМ) — $1 \cdot 10^{-3}$ моль/л. Исследованы закономерности взаимодействия «ФМ-1» с ионами лантана (III). Найдено, что высокая степень осаждения ионов La (III) реагентом (более 99,7 %) наблюдается в достаточно широком диапазоне значений рН — от 4,0 до 12,0 (при $\text{pH} \geq 7,5$ возможно соосаждение гидроксида лантана). Методом кондуктометрического титрования ($\text{pH} 4,8\text{--}6,8$) установлено образование соединений в растворе с молярными соотношениями $[\text{La(III)}]:[\text{R}] = 1:1$ и $1:2$. На основании данных химического анализа, ИК-спектроскопии и элементного анализа выделенных осадков, предложена их структурная формула. Показана возможность применения реагента «ФМ-1» в качестве собирателя для ионной флотации лантана (III).

Ключевые слова: ионная флотация, редкоземельные элементы, аминометиленфосфоновые кислоты, собиратель, физико-химические свойства, поверхностно-активное вещество, лантан, ФМ-1.

References

- 1 Chirkst, D.E., Lobacheva, O.L., & Dzhevaga, N.V. (2011). Ionnaia flotatsiia redkozemelnykh metallov s dodetsilsulfatom natriia [Ion flotation of rare-earth metals with sodium dodecyl sulfate]. *Zhurnal prikladnoi khimii — Russian Journal of Applied Chemistry*, 84, 9, 1424–1430 [in Russian].
- 2 Lobacheva, O.L., Dzhevaga, N.V., & Danilov, A.S. (2016). The method of removal yttrium (III) and ytterbium (III) from dilute aqueous solutions. *Russian Journal of Ecological Engineering*, 17(2), 38–42.
- 3 Shetty, S., Ponnurangam, S., & Chernyshova I.V. (2020). Foam flotation of rare earth elements by conventional and green surfactants. *Minerals Engineering*, 158, 106585.
- 4 Abaka-Wood, G.B., Zanin, M., Addai-Mensah, J., & Skinner, W. (2019). Recovery of rare earth elements minerals from iron oxide-silicate rich tailings — Part 2: Froth flotation separation. *Minerals Engineering*, 142, 105888.
- 5 Radushev, A.V., Chekanova, L.G., & Chernova, G.V. (2005). Reagenty dlia ionnoi flotatsii tsvetnykh metallov [Reagents for ion flotation of non-ferrous metals]. *Tsvetnye metally — Russian Journal "Non-Ferrous Metals"*, 7, 34–39 [in Russian].
- 6 Marion, C., Li, R.H., & Waters K.E. (2020). A review of reagents applied to rare-earth mineral flotation. *Advances in Colloid and Interface Science*, 279, 102142.

- 7 Martynenko, L.I. (1991). Osobennosti kompleksobrazovaniia redkozemelnykh elementov (III) [Peculiarities of rare-earth metals (III) complexation]. *Uspekhi khimii — Russian Chemical Reviews*, 60(9), 1969–1998 [in Russian].
- 8 Belova, V.V., Tsareva, Y.V., Zakhodyaeva, Y.A., Ivanov, V.K., & Voshkin A.A. (2021). Solvent extraction of lanthanides (III) in the presence of the acetate ion acting as a complexing agent using mixtures of cyanex 272 and caprylic acid in hexane. *Processes*, 9(12), 2222.
- 9 Radushev, A.V. (2021) α -Branched tertiary carboxylic acid hydrazides as extractants of rare-earth metal ions from sulfate media. *Russian Journal of Applied Chemistry*, 94(5), 595–600.
- 10 Healy, M.R., Ivanov, A.S., Karslyan, Y., Bryantsev, V.S., Moyer, B.A., & Jansone-Popova, S. (2019). Efficient separation of light lanthanides(III) by using bis-lactam phenanthroline ligands. *Chemistry A European Journal*, 25(25), 6326–6331.
- 11 Tesler, A.G., Kajdalov, S.N., Perminov, I.A., Barmin, I.V., Ilyasov, S.E., Zakshevskaya, L.V. et al. (2010). Sposob vozdeistviia na nefianoi plast [A method of acting on an oil reservoir]. *Yevraziiskii patent – Eurasian patent No. 014001* [in Russian].
- 12 Bernstein, I.Ya., & Kaminsky, Yu.L. (1986). *Spektrofotometricheskii analiz v organicheskoi khimii [Spectrophotometric analysis in organic chemistry]*. Leningrad: Khimiia [in Russian].
- 13 Frolov, V.I., Mityuk, D.Yu., & Tverdyi, R.E. (2013). *Metody opredeleniia poverkhnostnogo natiazheniia [Methods for determining surface tension]*. Moscow: RGU nefi i gaza imeni I.M. Gubkina [in Russian].
- 14 Lange, K.R. (2004). *Poverkhnostno-aktivnye veshchestva: sintez, svoistva, analiz, primeneniie [Surface-active substances: synthesis, properties, analysis, application]*. Saint Petersburg: Professiiia [in Russian].
- 15 Chekanova, L.G., Manylova, K.O., Pavlov, P.T., Baigacheva, E.V., & Tiunova T.G. (2015). Complexation of ethyl 2-aryl(alkyl)sulfonylamino-4,5,6,7-tetrahydrobenzo[b]thiophene-3-carboxylates with nonferrous metal ions. *Russian Journal of Inorganic Chemistry*, 60(4), 531–535.
- 16 Shvarcenbah, G., & Flashka, G. (1970). *Kompleksonometricheskoe titrovaniie [Complexometric titration]*. Moscow: Khimiia [in Russian].
- 17 Chekanova, L.G., Bajgacheva, E.V., Radushev, A.V., & Batueva, T.D. (2008). N',N'-Dialkilgidrazidy kak potentsialnye reagenty dlia ionnoi flotatsii medi (II) [N',N'-Dialkylhydrazides as potential reagents for ionic flotation of copper (II)]. *Khimicheskaiia tekhnologiia — Russian Journal of Chemical Technology*, 9, 9, 476–480 [in Russian].
- 18 Bolshakov, K.A. (1976). *Khimiia i tekhnologiia redkikh i rasseiannykh elementov [Chemistry and technology of rare and dispersed elements]*. Moscow: Vysshiaia shkola [in Russian].
- 19 Tarasevich, B.N. (2012). *IK spektry osnovnykh klassov organicheskikh soedinenii [IR-spectra of basic classes of organic compounds]*. Moscow: MGU [in Russian].

Information on the authors

Yuminova, Aleksandra Aleksandrovna (*corresponding author*) — PhD in Chemistry, Associate Professor, Department of Analytical Chemistry and Expertise, Perm State National Research University; Bukirev St. 15, 614097, Perm, Russia, e-mail: aleks3004@list.ru; <https://orcid.org/0000-0003-0168-9885>;

Giniyatullina, Elizaveta Albertovna — Student, Department of Analytical Chemistry and Expertise at Perm State National Research University; Bukirev St. 15, 614097, Perm, Russia, e-mail: 1.7582@yandex.ru; <https://orcid.org/0000-0002-6442-0501>;

Karieva, Leysan Midkhatovna — Student, Department of Analytical Chemistry and Expertise, Perm State National Research University; Bukirev St. 15, 614097, Perm, Russia, e-mail: 1.karieva@yandex.ru; <https://orcid.org/0000-0001-9959-3464>;

Chekanova, Larisa Gennad'evna — PhD in Chemistry, Associate Professor, Head of Laboratory of organic complexing reagents, Institute of Technical Chemistry of the Ural Branch of RAS; Korolev St. 3, 614013, Perm, Russia, e-mail: larchek.07@mail.ru; <https://orcid.org/0000-0003-1792-6945>.

R.M. Shlyapov¹, Sh.K. Amerkhanova¹, A.S. Uali¹, T.B. Omarbekov², D.S. Belgibayeva¹

¹*L.N. Gumilyov Eurasian National University, Nur-Sultan, Kazakhstan;*

²*Autonomous Cluster Fund “Park of Innovative Technologies”, Almaty, Kazakhstan*

(*Corresponding author's e-mail: rustamshlyapow@gmail.com)

Thermodynamics of chalcocite dissolving in solutions of flotation reagents

This work describes the formation of the ionic composition of the sorption layer during the concentration of copper-lead and pyrite-copper-zinc ore. The thermodynamics of the sorption layer of a sulfhydryl collector (sodium diisobutyl thiophosphate and potassium butyl xanthate) on the surface of chalcocite under various conditions of its oxidation has been studied using pH- and redoxometry. The nature of the change in the chalcocite electrode potential depending on the type of modifier and storage device, as well as on pH, has been experimentally clarified. The differences in the collective action of a one-component accumulator and a mixture of flotation reagents were revealed based on the thermodynamics analysis of the flotation process reactions. In addition, the optimal conditions for the flotation were determined. It was found that the quality of the concentrate is mainly influenced by two factors, such as the pulp redox potential and the pH of the medium. Mathematical equations of the optimal reagent and hydrodynamic enrichment regimes with the maximum dissolution of ore minerals in solutions of flotation reagents were modeled.

Keywords: flotation, hydrophobicity, sorption layer of collector, the ionic composition of the pulp in a liquid phase, flotation reagents, sulfide minerals.

Introduction

Modernized technologies of the enrichment of ores from new deposits should ensure the production of high-quality products from raw materials of medium and low quality [1–3]. However, most of the resources of ore raw materials in the Republic of Kazakhstan (pyrite-copper-zinc, copper, copper-lead, iron-manganese) are at a great depth and scattered over a large area. In this regard, the intensification of enrichment processes based on an integrated approach, which uses various enrichment methods in one technological scheme and reagent compositions selective for a specific mineral, takes on high relevance [4–6].

Improving polymetallic ores in production is predicated on examining economically profitable and environmentally friendly flotation reagents from a scientific research perspective, providing the necessary enrichment indicators [7–10].

The selection of flotation reagents for ore beneficiation is acquired from the ability of adsorption complexes on the surfaces of minerals. The sorption capacity is determined by the strength of the complex, poorly soluble compounds of metal ions that make up the crystal lattices. In this regard, the literature analysis of sorption processes on the surface of ore minerals is currently considered relevant and forward-looking to select cost-effective storage devices [11–16].

Along with the above, general criteria of selection of collector compositions capable of directional action on the surface of ore material are the quantitative indices of absolute stiffness and electronegativity, according to the theory of HSAB and Pearson principle, the affinity of individual collectors or their mixtures for cations of heavy metals in solution, based on the recovery of valuable components in concentrate [17].

The evaluation sources of physicochemical characteristics of dissolution of sulfide ores and minerals included in their composition have also been analyzed. It was shown that the processes of dissolution of sulfide minerals (CuFeS₂) are significantly intensified in the presence of catalysts (Ag). The dissolution mechanism is entirely determined by the semiconductor properties of chalcopyrite, namely, the electronic conductivity [18]. The solubility of minerals increases in the presence of potent oxidizing agents in an acidic medium. In particular, the dissolving ability of an electrolyte containing H₂SO₄ and Fe³⁺ has been studied. Moreover, the presence of Fe³⁺ ions plays a key role.

On the other hand, the possibility of dissolution of copper sulfides in solutions of complexing agents is traced [19]. At the same time, the results of elemental and phase analyses of leaching products were used to establish the dissolution mechanism. The complete theoretical description of the mineral dissolution process

is given in [20]. In the example of a waste rock mineral (serpentine), using the DLFO theory, a relationship was established between the intensive dissolution of serpentine and a decrease in brucite extraction. However, more attention is paid to the practical side of the issue. The relationship of the physicochemical characteristics of minerals in the dissolution process with the extraction efficiency of valuable components is poorly expressed.

Experimental

Flotation experiments were carried out on an FML-1 laboratory flotation machine with a chamber volume of 0.5 l according to the following procedure: a sample of ore (size 0.074 mm, weight 10 g) is loaded into the flotation cell and mixed with water.

Potentiometric measurements were performed using an ion-selective chalcogenide (Cu_2S) electrode based on the pH meter-ionomer (I-500). A chlorinated ESL-1M electrode was used as an electrode for comparison. The solutions were stirred using a magnetic stirrer.

During the experiment, tannin solutions with a concentration of 10^{-4} mol/l, potassium bichromate ($\text{K}_2\text{Cr}_2\text{O}_7$) 10^{-2} mol/l, hydrogen peroxide (H_2O_2) 10^{-2} mol/l were used. To maintain the required pH level, solutions of sodium hydroxide (NaOH) and sulfuric acid (H_2SO_4) were used in the concentration range from 10^{-2} – 10^{-6} mol/l. A mixture of $(\text{C}_4\text{H}_9\text{O})_2\text{PSSNa}$ (main substance is sodium diisobutyl dithiophosphate ($w((i\text{-C}_4\text{H}_9\text{O})_2\text{PS}_2\text{Na})=65\%$)) with butyl, potassium xanthogenate was used as a floater agent. All measurements were made in the temperature range 298–318 K. The electrode stationary potential was fixed within 30 minutes.

The values of activation energy, activation enthalpy, and activation entropy of chalcocite dissolution were calculated using the Arrhenius equation and the transition state equation [21]:

$$\lg W = \lg A - \frac{E_a}{2.303RT} \quad (1)$$

$$\Delta S^\# = R \ln A - \ln \frac{k}{Th} - 1 \quad (2)$$

$$\Delta H^\# = E_a - 2RT \quad (3)$$

The method of the full factorial experiment was chosen for optimal control. This method involves the use of 4 factors 3 level matrices and allows obtaining generalized regression equations that consider the influence of all factors [22]. The calculation and evaluation of the results of flotation studies were carried out by the statistical options of the Excel application.

X-ray phase analysis of ore samples was carried out on an X-ray diffractometer (XRD-7000 Shimadzu, Shimadzu, Japan). The valuable part of copper-lead ore is represented mainly by chalcocite, pyrite, galena, and cuprite. Gangue is silica, aluminosilicates, calcium carbonates. Elemental analysis of the initial ores was carried out on the ore grade instrument (Spektrolab, SPECTRO Analytical Instruments GmbH, Germany). The study of the results showed that sulfide ore > copper-zinc ore > oxide ore > tailings (primary enrichment) are the richest in the content of Cu, Pb, Zn industrial elements.

Results and Discussion

In this work, the process of collective absorption of minerals on the surface of a chalcocite electrode was studied using a mixture of potassium butyl xanthogenate and sodium diisobutyl dithiophosphate as flotation reagents, as well as potassium dichromate as an activator and sodium hydroxide as a depressor.

Considering the experimental data on the potential of a multi-component system, the values of the activation energy, entropy and enthalpy of the process were calculated using the Excel application (Table 1).

Under the data of [15], interpreting the achieved values of the activation energy specified in Table 1 indicates that the electrode potential ($E\{\text{mV}\}$) in the diffusion mode occurs on the surface of the mineral. Activation energy is diffused during the limitation period.

The negative value of the enthalpy of activation in a weakly alkaline medium has a combined structure, which leads to a decrease in the number of “active” particles. On the contrary, a change to positive values of the enthalpy of activation indicates an increase in the number of “active” particles. By the obtained values of the activation entropy, it can be assumed that compounds of variable composition in the anionic form are formed on the surface of the mineral.

Thermodynamic parameters of the theory of absolute speeds in the system NaOH – K₂Cr₂O₇ – (i-C₄H₉O)₂PS₂Na

| T {K} | 298 | 303 | 308 | 313 | 318 |
|-------------------------|-------------|-------------|--------------|--------------|--------------|
| pH=8 | | | | | |
| E _a {kJ/mol} | 43.93±0.01 | | | | |
| ΔS# {J/mol K} | -41.59±0.01 | -41.61±0.01 | -41.627±0.01 | -41.643±0.01 | -41.659±0.01 |
| ΔH# {kJ/mol} | -4.95±0.01 | -5.038±0.01 | -5.121±0.01 | -5.205±0.01 | -5.288±0.01 |
| pH=10 | | | | | |
| E _a {kJ/mol} | 45.81±0.02 | | | | |
| ΔS# {J/mol K} | 102.9±0.01 | 102.89±0.01 | 102.87±0.01 | 102.86±0.01 | 102.84±0.01 |
| ΔH# {kJ/mol} | 40.85±0.01 | 40.77±0.01 | 40.68±0.03 | 40.60±0.01 | 40.52±0.01 |
| pH=12 | | | | | |
| E _a {kJ/mol} | 49.00±0.01 | | | | |
| ΔS# {J/mol K} | 122.80±0.01 | 122.78±0.01 | 122.76±0.01 | 122.75±0.01 | 122.73±0.01 |
| ΔH# {kJ/mol} | 44.05±0.01 | 43.96±0.01 | 43.88±0.01 | 43.80±0.01 | 43.71±0.01 |

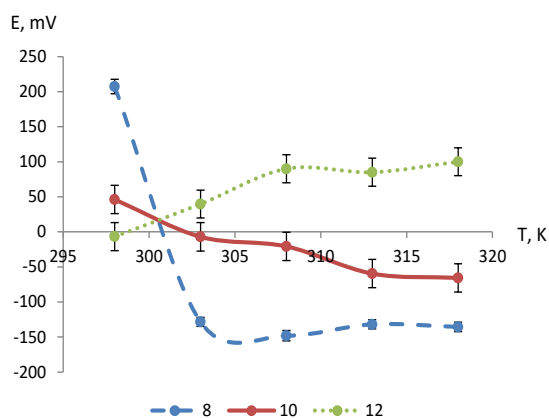


Figure 1. The investigation of the behaviour of the surface potential of the working electrode in solutions (K₂Cr₂O₇ – NaOH) with increasing temperature and pH

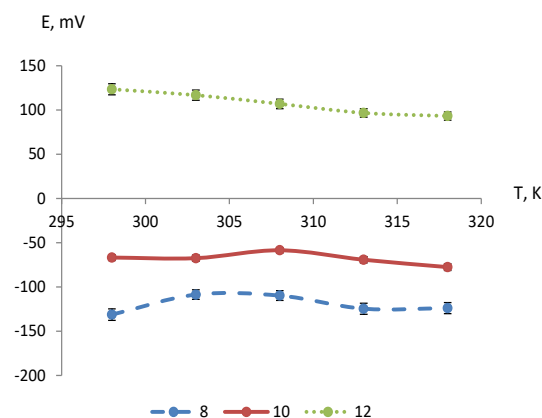
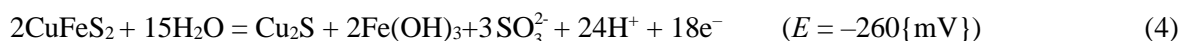


Figure 2. The behaviour of the electrode potential in the K₂Cr₂O₇ – NaOH – (i-C₄H₉O)₂PS₂Na system in the range of temperature 298–318 K and pH 8–12

Figure 1 demonstrates that the working area of the stationary potential of the chalcosine electrode in potassium dichromate solutions (pH = 8±0.3) is abruptly shifted to the electronegative region with increasing temperature. Cuprite (Cu₂O) formation occurs on the Cu₂S surface in these solutions. The following fact is confirmed by the results of the phase diagram in [23], where the analysis of CuFeS₂ oxidation is described in three stages:



The E{mV} curve in the K₂Cr₂O₇ – NaOH subsystem at pH = (10±0.3) is expressed by the ambiguous destabilization of the electrode potential of the chalcocite dissolution process in potassium dichromate solutions. With a stepwise increase in hydrogen concentration (pH = 12±0.3), the dependence of the electrode potential is formed on an electropositive scale. This indicates the formation of copper chromate, according to reaction (7):



Analyzing the obtained low values of the electrochemical potential in the system K₂Cr₂O₇ – NaOH – (i-C₄H₉O)₂PS₂Na (Figure 2), we suggest that copper and butyl xanthate interact at (pH = 8) with the formation of CuC₄H₉OPSS. In this experiment, the oxidation of chalcocite sulfide sulfur proceeds intensively

due to the influence of $\text{Cr}_2\text{O}_7^{2-}$ ions. The chalcocite electrode potential dependence in an alkaline solution of potassium dichromate in the presence of a mixture of a sulfhydryl collector at $\text{pH} = 12$ confirms the passage of ionic flotation due to the oxidation of sulfide sulfur and dissolution of copper ions. The thermodynamic characteristics, in particular, the activation energy and enthalpy values (Table 1), agree with the above reactions.

Despite specific achievements in expanding the list of effective reagents-fillers for flotation, the domestic industry is experiencing a shortage of its products. Based on the foregoing, in this work, a set of experimental studies has been carried out to develop the subsystems using tannin ($\text{C}_{76}\text{H}_{52}\text{O}_{46}$) as a complexing reagent-collector for refractory ores flotation concentration. The experimental results of the dependence of the Cu_2S potential in the H_2O_2 -tannin- H_2SO_4 system are shown in Figures 3-4.

A stable complex of tannin with copper ions is formed on the surface of the mineral at $\text{pH} = 4$. It was found that the oxidation of sulfide sulfur of chalcocite by dichromate ions promotes the binding of copper ions with tannin (Figure 4). An increase in the pH of solutions leads to a shift in the equilibrium of the reaction. It may be due to the hydrophilization of the chalcocite surface. The calculated values of the reaction thermodynamics in $\text{K}_2\text{Cr}_2\text{O}_7$ -Tannin- H_2SO_4 confirm the exothermicity of the process of Cu^{2+} binding with tannin at $\text{pH} = 4$ and $318\{\text{K}\}$ (Table 2).

Table 2

Thermodynamic factors of the system $\text{K}_2\text{Cr}_2\text{O}_7$ -Tannin- H_2SO_4

| T {K} | 298 | 303 | 308 | 313 | 318 |
|-------------------------|--------------|--------------|--------------|--------------|--------------|
| | pH=4 | | | | |
| E_a {kJ/mol} | 25.3±0.01 | | | | |
| $\Delta S^\#$ {J/mol K} | -391.82±0.01 | -391.94±0.01 | -391.98±0.01 | -391.97±0.01 | -391.99±0.01 |
| $\Delta H^\#$ {kJ/mol} | -49.55±0.01 | -50.38±0.01 | -51.21±0.01 | -52.04±0.01 | -52.87±0.01 |
| | pH=5 | | | | |
| E_a {kJ/mol} | 48.53±0.01 | | | | |
| $\Delta S^\#$ {J/mol K} | 109.05±0.01 | 109.03±0.01 | 109.01±0.01 | 109.01±0.01 | 108.95±0.01 |
| $\Delta H^\#$ {kJ/mol} | 43.63±0.01 | 43.55±0.01 | 43.46±0.01 | 43.38±0.01 | 43.36±0.01 |
| | pH=6 | | | | |
| E_a {kJ/mol} | 32.39±0.01 | | | | |
| $\Delta S^\#$ {J/mol K} | 58.47±0.01 | 58.46±0.01 | 58.44±0.01 | 58.43±0.01 | 58.41±0.01 |
| $\Delta H^\#$ {kJ/mol} | 27.45±0.01 | 27.35±0.01 | 27.27±0.01 | 27.18±0.01 | 27.14±0.01 |

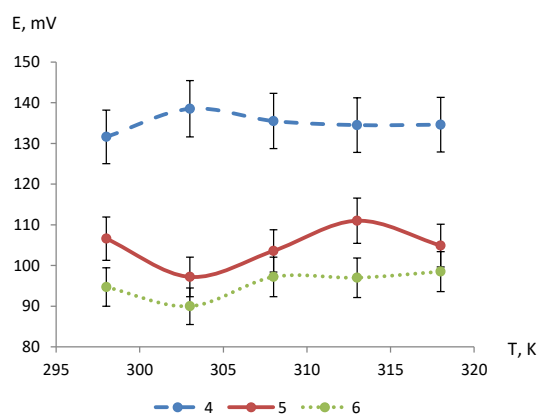


Figure 3. Characteristics of the electrode potential in the solutions (H_2O_2 – tannin – H_2SO_4) with increasing temperature and pH

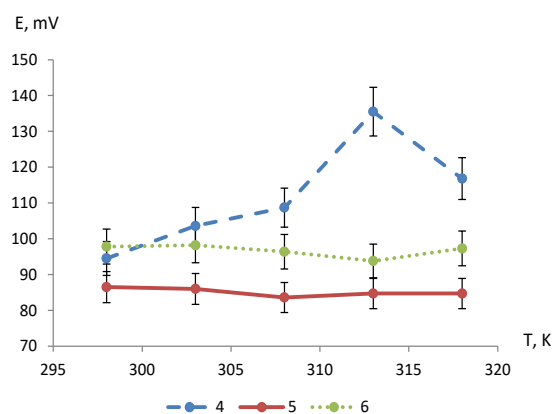


Figure 4. The behaviour of the electrode potential in the $\text{K}_2\text{Cr}_2\text{O}_7$ – tannin – H_2SO_4 system with a change in the pH range from 4 to 6

The thermodynamic characteristics of the copper-zinc ore beneficiation process were determined to test the optimal reagent modes of the modified polyfunctional collector (based on a mixture of potassium butyl xanthogenate-sodium diisobutyl dithiophosphate ($w((i\text{-C}_4\text{H}_9\text{O})_2\text{PS}_2\text{Na}))$) flotation reagents. The results are presented in Table 3.

Table 3

Thermodynamic values of the formation of a flotation complex of potassium butylxanthogenate – sodium diisobutyldithiophosphate on the surface of copper-lead ore

| T {K} | 298 | 303 | 308 | 313 | 318 |
|-------------------------|--------------|--------------|--------------|--------------|--------------|
| 1 | 2 | 3 | 4 | 5 | 6 |
| pH=8 | | | | | |
| E_a {kJ/mol} | 68.89±0.01 | | | | |
| lgA | 11.44 | | | | |
| $\Delta S^\#$ {J/mol K} | 187.93±0.01 | 187.92±0.01 | 187.94±0.01 | 187.87±0.01 | 187.87±0.01 |
| $\Delta H^\#$ {kJ/mol} | 63.94±0.01 | 63.86±0.01 | 63.77±0.01 | 63.69±0.01 | 63.61±0.01 |
| pH=10 | | | | | |
| $\Delta S^\#$ {J/mol K} | -31.28±0.01 | -31.31±0.01 | -31.37±0.01 | -31.33±0.01 | -31.34±0.01 |
| $\Delta H^\#$ {kJ/mol} | 156.02±0.01 | 155.94±0.01 | 155.85±0.01 | 155.77±0.01 | 155.69±0.01 |
| pH=12 | | | | | |
| E_a {kJ/mol} | 173.65±0.01 | | | | |
| lgA | -30.41 | | | | |
| $\Delta S^\#$ {J/mol K} | -613.7±0.01 | -613.72±0.01 | -613.73±0.01 | -613.75±0.01 | -613.77±0.01 |
| $\Delta H^\#$ {kJ/mol} | -178.68±0.01 | -178.62±0.01 | -178.75±0.01 | -178.85±0.01 | -178.94±0.01 |

The indicated activation entropy data suggest that the flotation reagent has an active effect on the interaction of copper with butyl xanthogenate with the formation of CuC_4H_9OCSS . Furthermore, the exothermicity of the process is confirmed by the maximum value of work and entropy, which indicates the direction. The potentiometric method results for determining the dependence of the electrode potential in an alkaline medium in the presence of a mixture of flotation reagents are shown in Figures 5-6.

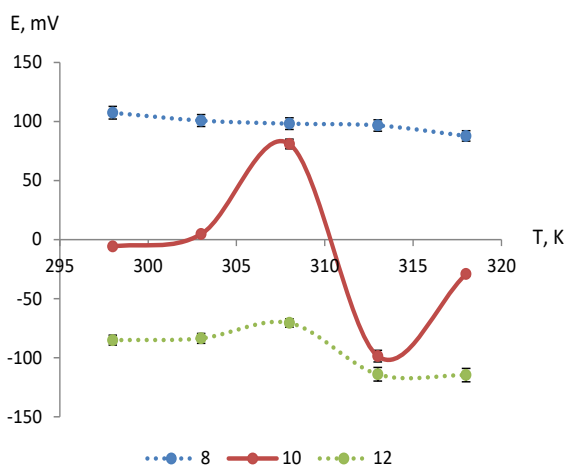


Figure 5. Dependence of the change in the potential of the working electrode in an alkaline medium with increasing temperature

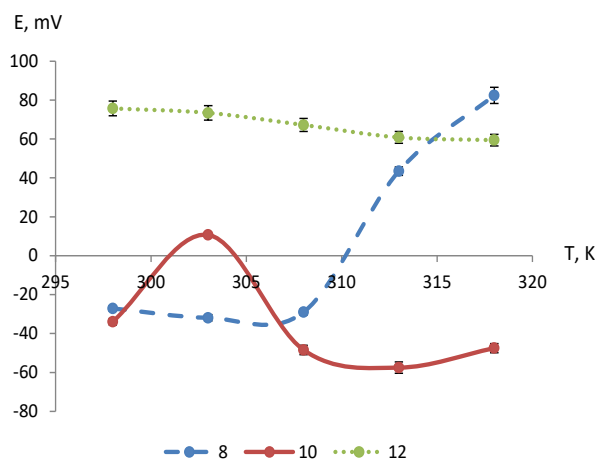


Figure 6. Changes in electrode potential in the system (NaOH – H₂O₂ – (i-C₄H₉O)₂PS₂Na) from temperature and pH

The potential shift to the electronegative region at pH = 10 is caused by the formation of poorly soluble copper hydroxides on the surface of the mineral. Sulfide sulfur oxidation to SO_3^{2-} and SO_4^{2-} is due to the adsorption of OH-radicals and atomic oxygen on the Cu_2S surface.

Taking into account all the revealed trends in the various-component systems of the model ore beneficiation process, the activation process of the “intermediate” copper complex occurs. In this study, using the Gauss method in the calculations, the equations of the electrode function are derived with temperature and pH change. The temperature dependence of the Cu_2S potential with a variable value of pH solutions is presented in Figure 7.

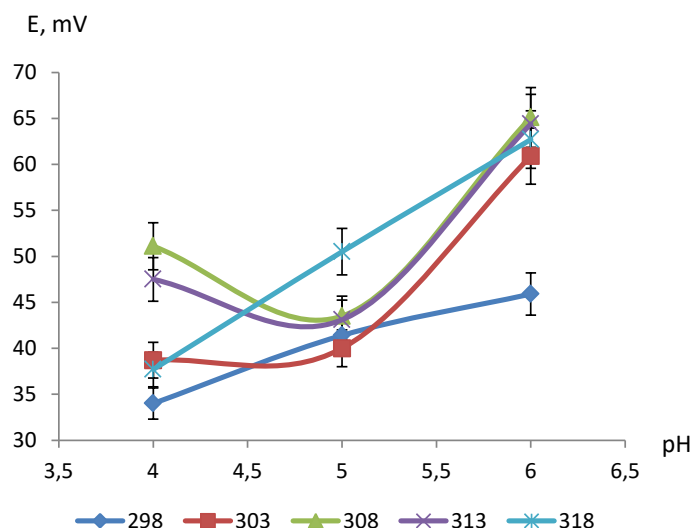


Figure 7. Effect of temperature and pH on the potential of the chalcocite electrode

The optimal mode for the maximum enrichment process of copper-lead and pyrite-copper-zinc ores was found using a mixture of flotation reagents according to the obtained obtained linear equations (8–10):

$$E = 1.9997t^2 - 153.77t + 2764.8 \quad (\text{pH}=8) \quad (8)$$

$$E = 471.34t^2 - 10562t + 87407 \quad (\text{pH}=10) \quad (9)$$

$$E = -0.8491t^2 + 61.04t - 1010.1 \quad (\text{pH}=12) \quad (10)$$

The method of mathematical planning was applied to establish the optimal reagent and hydrodynamic enrichment modes.

Table 4 represents the generalized equation of surface modelling changes in the dissolving mineral raw materials process based on the changed electrode potential in multicomponent flotation process systems.

Table 4

The generalized equation of surface modelling changes in the process of dissolving mineral raw materials

| Systems | Mathematical model | R |
|---|--|------|
| $\text{K}_2\text{Cr}_2\text{O}_7 - \text{NaOH}$ | $y = (20.475 + (-3.061) \cdot (\text{pH}) + 0.106 \cdot (\text{pH})^2) + ((-1.08) + 0.157 \cdot \text{pH} + (-0.005) \cdot (\text{pH})^2 \cdot t^\circ\text{C}) + (0.0124 + (-0.002) \cdot \text{pH} + 0.0001 \cdot (\text{pH})^2 \cdot (t^\circ\text{C})^2)$ | 0.99 |
| $\text{K}_2\text{Cr}_2\text{O}_7 - \text{H}_2\text{SO}_4 - \text{tannin}$ | $y = ((-107.79 + 73.019 \cdot \text{pH} + (-5.396) \cdot (\text{pH})^2) + ((419.280 + 88.824 \cdot \text{pH} + (-3.979) \cdot (\text{pH})^2 \cdot t^\circ\text{C}) + (16.48 + (-3.294) \cdot \text{pH} + 0.1597 \cdot (\text{pH})^2 \cdot (t^\circ\text{C})^2)$ | 0.98 |
| $\text{H}_2\text{O}_2 - \text{NaOH}$ | $y = ((-50.813) + 1.349 \cdot \text{pH} + (-8.7358) \cdot (\text{pH})^2) + (2.725 + 2.552 \cdot \text{pH} + (-7.563) \cdot (\text{pH})^2 \cdot t^\circ\text{C}) + (1.7329 + (-1.756) \cdot \text{pH} + (0.0283) \cdot (\text{pH})^2 \cdot (t^\circ\text{C})^2)$ | 0.99 |
| $\text{NaOH} - \text{H}_2\text{O}_2 - (\text{C}_4\text{H}_9\text{O})_2\text{PS}_2\text{Na}$ | $y = ((-388.08 + 94.877 \cdot \text{pH} + (-5.1541) \cdot (\text{pH})^2) + (341.397 + (-82.957) \cdot \text{pH} + 0.453 \cdot (\text{pH})^2 \cdot t^\circ\text{C}) + ((-1.355) + 0.286 \cdot \text{pH} + (-0.0137) \cdot (\text{pH})^2 \cdot (t^\circ\text{C})^2)$ | 0.99 |

It can be seen that the potential of the halcosin is shifted to the negative area with an increased temperature in a weakly alkaline medium (pH = 8) and to the positive zone in a more alkaline medium, which indicates an intensive occurrence of oxidative processes due to hydroxide and bichromate ions. This model is characterized by the interaction of the mineral in an alkaline oxidant solution; therefore, it may be tested to calculate the values of stationary potentials of copper sulfide (I) in the temperature range and the acidity of the medium.

It should be noted that the steady-state potential data (Figures 1–7) indicate that the sulfur oxidation reactions of copper and lead minerals to thiosulfate ions occur most fully in alkaline media. These ions are replaced by xanthogenate and dibutyldithiophosphate to form complex compounds. Moreover, sulfur oxidation products are thiosulfate and sulfate ions in the medium with high redox potential. These ions, which have a higher ability to hydrate, contribute to the formation of poorly soluble copper xanthates and copper diisobutyldithiophosphates in the volume of the solution, reducing the hydrophobicity of the surface, and consequently the quality of the concentrate [24].

In pursuance of the probabilistic-deterministic approach, the optimization of copper-lead ore concentration was carried out. Likewise, the partial dependences of chemical and technological parameters on variable factors of air supply rate, impeller speed, consumption of the $(C_4H_9O)_2PSSNa$ collector mixture and potassium butyl xanthogenate were obtained (Table 5).

Table 5

Dependence of the degree of copper extraction and the degree of ore reduction for the process of concentration of copper ore using a mixture of potassium butyl xanthogenate – sodium diisobutyl dithiophosphate

| Factors (x) | $\varepsilon_{Me}, \% (y)$ | R | K (y) | R |
|-------------------------|-------------------------------------|------|-------------------------------------|------|
| $v_{air} \{l/h\}$ | $y = -0.05x^2 + 4.4819x - 5.6996$ | 0.99 | $y = -0.0063x^2 + 0.3594x + 12.035$ | 0.99 |
| $v_{rot} \{Hz\}$ | $y = -0.0039x^2 + 0.2767x + 95.093$ | 0.99 | $y = -0.0146x^2 + 0.956x - 10.853$ | 0.99 |
| $C_{flotation} \{g/t\}$ | $y = -0.0246x^2 + 4.484x - 109.17$ | 0.99 | $y = 0.0042x + 4.1161$ | 0.99 |

For lead minerals, the high redox potential of the pulp initiates the reaction of the formation of poorly soluble lead sulfate at low pH and high pH of lead hydroxocarbonate. Therefore, hydrophobization in the presence of oxidized lead sulfide is difficult, which reduces the amount of metal extracted into the concentrate [25].

The large-scale laboratory studies have been carried out to recommend the use of a mixture of a flotation reagent (potassium butyl xanthogenate and sodium diisobutyl dithiophosphate ($w((i-C_4H_9O)_2PS_2Na)$) for flotation of copper ore from the Nurkazgan deposit.

Conclusions

The thermodynamic parameters characterizing the chalcocite dissolution process in copper minerals flotation solutions have been determined. The progress of the enrichment process is mainly determined not only by the change in the pulp potential's redox action, but also by the electrode potential of dissolution of chalcogenide minerals.

Due to this fact, it is possible to eliminate the formation of hydroxide compounds at the stage of selective flotation of copper concentrates in alkaline media due to the equalization of the chromate- and xanthogenate ions concentration in the liquid phase.

A qualitatively new approach to the prediction of the behavior of sulfide minerals is proposed. It consists in considering the relationship between the redox ability of minerals and the flotation characteristics of polymetallic ores and the hydrodynamic enrichment regime. It was shown that copper recovery degree into concentrate is closely related to air consumption and dispersion degree of bubbles for copper-lead ore samples. These factors directly affect the oxidation-reduction balance in the pulp. Namely, they increase the probability of the formation reactions of hydroxo complexes, thiosulfates, copper, lead sulfates on the surface of sulfide minerals.

A statistical model was proposed to calculate the value of the relative fractions of the surface sorption layer of the pulp during the flotation of copper ore from the "Nurkazgan" deposit.

This model takes into account the oxidation processes occurring in parallel on the surface of the mixed sorption layer of the collector of potassium butyl xanthogenate and sodium diisobutyl dithiophosphate ($w((i-C_4H_9O)_2PS_2Na)$).

References

- 1 Стрельцова А.А. Флотационные извлечения поверхностно-активных веществ различной природы из смешанных растворов, содержащих высокомолекулярный реагент / А.А. Стрельцова, А.А. Мазурик Е.А. Хромышева // Химическая безопасность. — 2018. — Т. 2, № 1. — С. 116–126. <http://chemsafety.ru/index.php/chemsafety/article/view/44>
- 2 Германов А.А. Новые технические средства автоматического контроля технологических параметров в обогащительном производстве / А.А. Германов, А.А. Трушин, Н.О. Тихонов, А.А. Трегубов // Горн. инф.-аналит. бюлл. (Науч.-тех. журн.). — 2019. — № 2. — С. 114–122. <https://giab-online.ru/catalog/12694>
- 3 Tinashe O. Nodoro. A Review of the Flotation of Copper Minerals / Tinashe O. Nodoro, Lordwell K. Witika // International Journal of Sciences: Basic and Applied Research (IJSBAR), 2017. — Vol. 34(2). — P. 145–165. <https://www.researchgate.net/publication/318284476>

- 4 Авагян А.В. Термодинамическое обоснование процесса сульфидирования окисленных медных минералов серой / А.В. Авагян // Вестн. Нац. политех. ун-та Армении. Metallurgy, материаловедение, недропользование. — 2018. — № 2. — С. 34–44. http://test.journals.sci.am/index.php/polytech_banber-metallurgia/issue/view/228
- 5 Горячев Б.Е. Термодинамика формирования сорбционного слоя тиольных собирателей на поверхности сфалерита при условии окисления сульфидной серы минерала до элементной [Электронный ресурс] / Б.Е. Горячев, А.А. Николаев, Зай Яа Чжо, А.А. Моргун // Цветные металлы. — 2018. — № 4. — С. 2–10. <http://www.rudmet.ru/journal/1715/article/29442/>
- 6 Александрова Т.Н. Метод типизации медно-цинковых руд сложного состава с применением нейросетевых моделей / Т.Н. Александрова, Е.К. Ушаков, А.В. Орлова // Горн. инф.-аналит. бюлл. (Науч.-тех. журн.). — 2020. — № 5. — С. 140–147. <https://cyberleninka.ru/article/n/metod-tipizatsii-medno-tsinkovyh-rud-slozhnogo-sostava-s-primeneniem-neyrosetevykh-modeley>
- 7 Заварухина Е.А. Влияние дополнительного собирателя на селективность флотационного разделения сульфидов меди и цинка / Е.А. Заварухина, Н.Н. Орехова // Гор. инф.-аналит. бюлл. (Науч.-тех. журн.). — 2017. — № 3. — С. 305–311. <https://cyberleninka.ru/article/n/vliyanie-dopolnitelnogo-sobiratelya-na-selektivnost-flotatsionnogo-razdeleniya-sulfidov-medi-i-tsinka>
- 8 Омарова Н.К. Флотация сульфидом медной руды с флотореагентом «PS» / Н.К. Омарова, Р.Т. Шерембаева // Обогащение руд. — 2015. — Т. 356, № 2. — С. 15–17. <http://dx.doi.org/10.17580/or.2015.02.03>
- 9 Кондратьев С.А. Оценка собирательной силы флотационного реагента / С.А. Кондратьев, В.И. Рябой // Физико-технические проблемы разработки полезных ископаемых. — 2015. — № 1. — С. 137–144. <http://www.rudmet.ru/journal/1428/article/24521/>
- 10 Рябой В.И. Собиратель для медно-мышьяковистых руд / В.И. Рябой, Е.Д. Шепета // Горные науки и технологии. — 2020. — Т. 5, № 4. — С. 297–306. <https://doi.org/10.17073/2500-0632-2020-4-297-306>
- 11 Игнаткина В.А. Экспериментальные исследования изменений контрастности флотационных свойств кальциевых минералов / В.А. Игнаткина // Физико-технические проблемы разработки полезных ископаемых. — 2017. — № 5. — С. 113–122. <https://elibrary.ru/item.asp?id=30488395>
- 12 Рамазанова В.Р. Перспективы использования нового реагента для флотации окисленных медных руд / В.Р. Рамазанова, А.С. Жилин / Актуальные проблемы развития технических наук: сб. ст. участн. XX Обл. конкурса науч.-исслед. работ «Научный олимп» по направлению «Технические науки». — М.: Эдитус, 2018. — С. 89–91. <https://elibrary.ru/item.asp?id=35049070>
- 13 Баласанян С.Ш. Компьютерная модель для стохастического управления технологическим процессом флотации руды с учетом надежности измельчительного оборудования / С.Ш. Баласанян, С.О. Симонян, Э.М. Геворгян // Изв. Том. политех. ун-та. — 2013. — Т. 323, № 5. — С. 50–57. <http://earchive.tpu.ru/handle/11683/5058>
- 14 Moses Nduna. A model for the zeta potential of copper sulphide/ Moses Nduna, Alison Emslie Lewis, Patrice Nortier // Colloids and Surfaces A: Physicochemical and Engineering Aspects, Elsevier, 2014. — Vol. 441. — P. 643–652. <https://www.sciencedirect.com/science/article/abs/pii/S0927775713007784>
- 15 Амерханова Ш.К. Кинетические особенности процесса сорбции серосодержащих собирателей на поверхности медной руды / Ш.К. Амерханова, Р.М. Шляпов, А.С. Уали // Вестн. Воронеж. гос. ун-та. Сер. Химия. Биология. Фармация. — 2017. — № 1. — С. 7–10. <https://elibrary.ru/item.asp?id=29025082>
- 16 Матвеева Т.Н. Новые флотационные реагенты для извлечения микро- и наночастиц благородных металлов из упорных руд / Т.Н. Матвеева, Т.А. Иванова, В.В. Гетман, Н.К. Громова // Горн. журн. — 2017. — № 11. — С. 89–93. — http://rudmet.net/media/articles/Article_MJ_11_17_pp.89-93_2.pdf
- 17 Kondratev, S.A., Bochkarev, I.G. Physically absorbable reagents-collectors in elementary flotation // J. Min. Sci, Elsevier, 2007. — Vol. 43. — P. 530–538. <https://doi.org/10.1007/s10913-007-0056-9>
- 18 Zand, L., Vakylabad, A.B. & Masoumi, M.E. Homogeneous Catalytic Dissolution of Recalcitrant Chalcocopyrite (CuFeS₂)// Top Catal, Elsevier, 2022. <https://doi.org/10.1007/s11244-022-01565-x>
- 19 Baba A.A., Balogun A.F., Olaoluwa D.T. Leaching kinetics of a Nigerian complex covellite ore by the ammonia-ammonium sulfate solution // Korean J. Chem. Eng., Elsevier, 2017. — Vol. 34. — P. 1133–1140. <https://doi.org/10.1007/s11814-017-0005-5>
- 20 Fu Yf., Yin Wz., Dong Xs. New insights into the flotation responses of brucite and serpentine for different conditioning times: Surface dissolution behavior // Int J Miner Metall Mater., Elsevier, 2021. — Vol. 28. — P. 1898–1907. <https://doi.org/10.1007/s12613-020-2158-1>
- 21 Al-Juaid S.S. Inhibition of carbon steel corrosion in hydrochloric acid solutions using polyoxyethylene sorbitan fatty acid esters (tween compounds). Chemistry and Technology of Fuels and Oils, Scopus, 2012. — Vol. 48. — P. 313–320. <https://doi.org/10.1007/s10553-012-0374-8>
- 22 Khovanskiy S., Pavlenko I., Pitel J., Mizakova J., Ochowiak M., Grechka I. Solving the coupled aerodynamic and thermal problem for modeling the air distribution devices with perforated plates // Energies, Elsevier, 2019. — Vol. 12. — P. 3488. <https://doi.org/10.3390/en12183488>
- 23 Николаев А.А. Термодинамика взаимодействия хромат-ионов с минеральным комплексом полиметаллических руд халькопирит / А.А. Николаев, Б.Е. Горячев // Изв. вузов. Цветная металлургия. — 2013. — № 5. — С. 3–9. <https://doi.org/10.17073/0021-3438-2013-5-3-9>
- 24 Vigdergauz V.E., Makarov D.V., Zorenko I.V. Effect exerted by structural features of copper-zinc ores on their oxidation and technological properties// J Min Sci., Elsevier, 2008. — Vol. 44. — P. 413–420. <https://doi.org/10.1007/s10913-008-0046-6>
- 25 Chander S. Oxidation/Reduction Effects in Depression of Sulfide Minerals — A Review // Mining, Metallurgy & Exploration, Scopus, 1985. — Vol. 2. — P. 26–35. <https://doi.org/10.1007/bf03402591>

Р.М. Шляпов, Ш.К. Амерханова, А.С. Уали, Т.Б. Омарбеков, Д.С. Бельгибаева

Флотациялық реагенттер қоспаларының ерітінділерінде халькозиннің еруінің термодинамикасы

Мыс-қорғасын және колчедан-мыс-мырыш кендерін байыту кезінде сорбциялық кабаттың иондық құрамын қалыптастыру процесі қарастырылды. рН метрия мен редоксометрияны қолдана отырып, халькозин бетінің әр түрлі тотығу жағдайларында сульфогидрил жинағышының сорбциялық қабатының (натрий динизобутилтиофосфаты және калий бутил ксантогенаты) термодинамикасы зерттелді. Халькозин электродының электрод потенциалының рН-ға байланысты модификатор мен жинақтау түріне өзгеру сипаты эксперименталды түрде түсіндірілді. Флотация процесінің реакцияларының термодинамикасын талдау негізінде бір компонентті жинақтау пен флотореагенттер қоспасының ұжымдық әсерінің айырмашылықтары анықталды. Флотация жүргізудің оңтайлы шарттары анықталды, қойыртпақ пен рН ортаның тотығу-тотықсыздану әлеуетінің екі факторының концентрат сапасына басым әсері дәлелденді. Флотациялық реагенттер ерітінділерінде кен минералдарын барынша ерітумен байытудың оңтайлы реагенттік және гидродинамикалық режимдерінің математикалық теңдеулері модельденді.

Кілт сөздер: флотация, гидрофобтылық, жинағыштың сорбциялық қабаты, қойыртпақтың сұйық фазасының иондық құрамы, флотациялық реагенттер, сульфидті минералдар.

Р.М. Шляпов, Ш.К. Амерханова, А.С. Уали, Т.Б. Омарбеков, Д.С. Бельгибаева

Термодинамика растворения халькозина в растворах флотационных реагентов

Рассмотрен процесс формирования ионного состава сорбционного слоя при обогащении медно-свинцовой и колчеданно-медно-цинковой руды. С применением рН и редоксометрии изучена термодинамика сорбционного слоя сульфогидрильного собирателя (динизобутилтиофосфата натрия и бутилового ксантогената калия) на поверхности халькозина в различных условиях его окисления. Экспериментально выяснен характер изменения электродного потенциала халькозинового электрода от типа модификатора и накопителя в зависимости от рН. На основании анализа термодинамики реакций процесса флотации выявлены различия собирательного действия однокомпонентного накопителя и смеси флотореагентов. Определены оптимальные условия проведения флотации, установлено преобладающее влияние двух факторов окислительно-восстановительного потенциала пульпы и рН среды на качество концентрата. Смоделированы математические уравнения оптимальных реагентных и гидродинамических режимов обогащения с максимальным растворением рудных минералов в растворах флотационных реагентов.

Ключевые слова: флотация, гидрофобность, сорбционный слой собирателя, ионный состав жидкой фазы пульпы, флотационные реагенты, сульфидные минералы.

References

- 1 Strelzova, A.A., Mazuric, A.A., & Hromysheva, E.A. (2018). Flotazionnye izvlecheniia poverkhnostno-aktivnykh veshchestv razlichnoi prirody iz smeshannykh rastvorov, sodержashchikh vysokomolekuliarnyi reagent [Flotation extraction of surfactants of various nature from mixed solutions containing high-molecular reagents]. *Khimicheskaja bezopasnost — Russian Journal of Chemical safety*, 2, 1, 116–126. <http://chemsafety.ru/index.php/chemsafety/article/view/44> [in Russian].
- 2 Germanov, A.A., Trushin, A.A., Tikhonov, N.O., & Tregubov, A.A. (2019). Noveye tekhnicheskie sredstva avtomaticheskogo kontrolya tekhnologicheskikh parametrov [New technical means of automatic control of technological parameters in concentration production]. *Gornyi informatsionno-analiticheskiiulleten (Nauchno-tekhnicheskii zhurnal) — Mining informational and analytical bulletin (scientific and technical journal)*, 2, 114–122. <https://giab-online.ru/catalog/12694> [in Russian].
- 3 Tinashe, O. Nodoro, & Lordwell, K. Witika. (2017). A Review of the Flotation of Copper Minerals. *International Journal of Sciences: Basic and Applied Research (IJSBAR)*, 34(2), 145–165. <https://www.researchgate.net/publication/318284476>
- 4 Avagyan, A.V. (2018). Termodinamicheskoe obosnovanie protsessa sulfidirovaniia okislennykh mednykh mineralov seroi [Thermodynamic justification for the sulphide process of oxidized copper minerals with sulfur], *Vestnik Natsionalnogo politekhnicheskogo universiteta Armenii. Metallurgiya, materialovedenie, nedropolzovanie. Herald of the National Polytechnic University of Armenia. Metallurgy, materials science, Subsoil use*, 2, 34–44. http://test.journals.sci.am/index.php/polytech_banber-metalurgia/issue/view/228 [in Russian].
- 5 Goriachev, B.E., Nikolaev, A.A., Zai Ya, Chzho, & Morgun, A.A. (2018). Termodinamika formirovaniia sorbtionnogo sloia tiolnykh sobiratelei na poverkhnosti sfalerita pri uslovii okisleniia sulfidnoi sery minerala do elementnoi [Thermodynamics of the

formation of a sorption layer of thiol collectors on the surface of sphalerite under the condition of oxidation of sulfide sulfur of the mineral to elemental] *Tsvetnye metally — Non-ferrous metals*, 4, 2–10. <http://www.rudmet.ru/journal/1715/article/29442/> [in Russian].

6 Alexandrova, T.N., Ushakov, E.K., & Orlova, A.V. (2020). Metod tipizatsii medno-tsinkovykh rud slozhnogo sostava s primeneniem neirossetevykh modelei [Method of complex copper–zinc ore typification using neural network models]. *Gornyi informatsionno-analiticheskii bulletin (Nauchno-tehnicheskii zhurnal) — Mining informational and analytical bulletin (scientific and technical journal)*, 5, 140–147. <https://cyberleninka.ru/article/n/metod-tipizatsii-medno-tsinkovykh-rud-slozhnogo-sostava-s-primeneniem-neirossetevykh-modeley> [in Russian].

7 Zavarukhina, E.A., & Orekhova, N.N. (2017). Vliyanie dopolnitelnogo sobiratelya na selektivnost flotatsionnogo razdeleniya sulfidov medi i tsinka [Effect of additional collector on the selectivity of the flotation separation of copper and zinc sulphides]. *Gornyi informatsionno-analiticheskii bulletin (nauchno-tehnicheskii zhurnal) — Mining informational and analytical bulletin (scientific and technical journal)*, 3, 305–311. <https://cyberleninka.ru/article/n/vliyanie-dopolnitelnogo-sobiratelya-na-selektivnost-flotatsionnogo-razdeleniya-sulfidov-medi-i-tsinka> [in Russian].

8 Omarova, N.K. & Sherembayeva, R.T. (2015). Flotatsiia sulfidom mednoi rudy s flotoreagentom «PS» [Sulfide copper ore flotation with “PS” reagent], *Zhurnal «Obogashchenie rud» — Journal of Russia “Obogashchenie Rud”*, 356, 2, 15–17. <http://dx.doi.org/10.17580/or.2015.02.03> [in Russian].

9 Kondratiev, S.A., & Ryaboi, V.I. (2015). Otsenka sobiratelnoi sily ditiofosfatov i ee svyaz s selektivnostiu izvlecheniya poleznogo komponenta [Dithiophosphates collecting ability estimation and its relationship to selectivity of valuable component recovery] *Zhurnal «Obogashchenie rud» — Journal of Russia Obogashchenie Rud*, 1, 137–144. <http://www.rudmet.ru/journal/1428/article/24521/> [in Russian].

10 Ryaboy, V.I., & Shepeta, E.D. (2020). Sobiratel dlia medno-myshiakovykh rud [Collector for copper-arsenic ore flotation]. *Gornyi informatsionno-analiticheskii bulletin (Nauchno-tehnicheskii zhurnal) — Mining informational and analytical bulletin (scientific and technical journal)*, 5(4), 297–306. <https://doi.org/10.17073/2500-0632-2020-4-297-306> [in Russian].

11 Ignatkina, V.A. (2017). Eksperimentalnye issledovaniia izmeneniia kontrasnosti flotatsionnykh svoystv kaltsevykh mineralov [Experimental investigation of change in the contrast between flotation properties of calcic minerals]. *Fiziko-tehnicheskie problemy razrabotki poleznykh iskopaemykh*, 5, 113–122. <https://elibrary.ru/item.asp?id=30488395> [in Russian].

12 Ramazanova, V.R., & Zhilin, A.S. (2018). Perspektivy ispolzovaniia novogo reagenta dlia flotatsii okislennykh mednykh rud [Prospects for using a new reagent for the flotation of oxidized copper ores]. *Zhurnal «Aktualnye problemy razvitiia tehnikeskikh nauk» — Journal of Russia “Aktualnye problemy razvitiia tehnikeskikh nauk”*, 2, 89–95. <https://elibrary.ru/item.asp?id=35049070> [in Russian].

13 Balasanyan, S.S., Simonyan, S.O., & Gevorgyan, E.M. (2013). Kompiuternaia model dlia stokhasticheskogo upravleniia tekhnologicheskim protsessom flotatsii rudy s uchetom nadezhnosti izmelchitel'nogo oborudovaniia [Computer model for stochastic control of the ore flotation process considering grinding equipment reliability]. *Izvestiia Tomskogo politekhnicheskogo universiteta — Bulletin of the Tomsk Polytechnic University. Geo Assets Engineering*, 323(5), 50–57. <http://earchive.tpu.ru/handle/11683/5058> [in Russian].

14 Moses, N., Alison Emslie Lewis, & Patrice Nortier (2014). A model for the zeta potential of copper sulphide. *Colloids and Surfaces A: Physicochemical and Engineering Aspects, Elsevier*, 441, 643–652. <https://www.sciencedirect.com/science/article/abs/pii/S0927775713007784>

15 Amerkhanova, Sh.K., Shliapov, R.M. & Uali, A.S. (2017). Kiniticheskie osobennosti protsesa sorbtzii serosoderzhashchikh sobiratelya na poverkhnosti mednoi rudy [Kinetic features of sorption process of sulfur collectors on the surface of copper ore] *Vestnik Voronezhskogo gosudarstvennogo universiteta. Seriya Khimiia. Biologiia. Farmatsiia — Proceedings of Voronezh State University. Series Chemistry. Biology. Pharmacy*, 1, 7–10. <https://elibrary.ru/item.asp?id=29025082> [in Russian].

16 Matveeva, T.N., Ivanova, T.A., Getman, V.V. & Gromova, N.K. (2017). Novye flotatsionnye reagenty dlia izvlecheniya mikro- i nanochastits blagorodnykh metallov iz upornykh rud [New flotation agents for recovery of micro- and nanoparticles of precious metals from rebellious ore]. *Gornyi zhurnal — Journal of Russia “Gornyi Zhurnal”*, 1, 89–93. http://rudmet.net/media/articles/Article_MJ_11_17_pp.89-93_2.pdf [in Russian].

17 Kondratev, S.A., & Bochkarev, I.G. (2007). Physically absorbable reagents-collectors in elementary flotation. *J. Min. Sci, Elsevier*, 43, 530–538. <https://doi.org/10.1007/s10913-007-0056-9>

18 Zand, L., Vakylabad, A.B., & Masoumi, M.E. (2022). Homogeneous Catalytic Dissolution of Recalcitrant Chalcopyrite (CuFeS₂). *Top Catal, Elsevier*. <https://doi.org/10.1007/s11244-022-01565-x>

19 Baba, A.A., Balogun, A.F., & Olaoluwa, D.T. (2017). Leaching kinetics of a Nigerian complex covellite ore by the ammonia-ammonium sulfate solution. *Korean J. Chem. Eng., Elsevier*, 34, 1133–1140. <https://doi.org/10.1007/s11814-017-0005-5>

20 Fu, Yf., Yin, Wz., & Dong, Xs. (2021). New insights into the flotation responses of brucite and serpentine for different conditioning times: Surface dissolution behavior. *Int J Miner Metall Mater.*, 28, 1898–1907. <https://doi.org/10.1007/s12613-020-2158-1>

21 Al-Juaid, S.S. (2012). Inhibition of carbon steel corrosion in hydrochloric acid solutions using polyoxyethylene sorbitan fatty acid esters (tween compounds). *Chemistry and Technology of Fuels and Oils, Scopus.*, 48, 313–320. <https://doi.org/10.1007/s10553-012-0374-8>

22 Khovanskyi, S., Pavlenko, I., Pitel, J., Mizakova, J., Ochowiak, M., & Grechka, I. (2019). Solving the coupled aerodynamic and thermal problem for modeling the air distribution devices with perforated plates. *Energies*, 12, 3488. <https://doi.org/10.3390/en12183488>

23 Nikolaev, A.A. & Goryachev, B.E. (2013). Termodinamika vzaimodeistviia khromat-ionov s mineralnym kompleksom polimetallicheskikh rud khalkopirit [Thermodynamics of interchange of chromate ions with mineral complex of polymetal ores. Chalcopirit].

copyrite]. *Izvestiia vuzov. Tsvetnaia metallurgiiia — Izvestiya. Non-Ferrous Metallurgy*, 5, 3–9. <https://doi.org/10.17073/0021-3438-2013-5-3-9> [in Russian].

24 Vigdergauz, V.E., Makarov, D.V., & Zorenko, I.V. (2008). Effect exerted by structural features of copper-zinc ores on their oxidation and technological properties. *J. Min. Sci.*, 44, 413–420. <https://doi.org/10.1007/s10913-008-0046-6>

25 Chander, S. (1985). Oxidation/Reduction Effects in Depression of Sulfide Minerals — A Review. *Mining, Metallurgy & Exploration*, 2, 26–35. <https://doi.org/10.1007/bf03402591>

Information about authors

Shlyapov, Rustam Maratovich (corresponding author) — Candidate of Chemical Sciences, Associate Professor, L.N. Gumilyov Eurasian National University, Kazhymukan street, 13, 010000, Nur-Sultan, Kazakhstan, e-mail: rustamshlyapow@gmail.com; <https://orcid.org/0000-0003-0696-214X>;

Amerkhanova, Shamshiya Kenzhegazinovna — Doctor of Chemical Sciences, Full Professor, L.N. Gumilyov Eurasian National University, Kazhymukan street, 13, 010000, Nur-Sultan, Kazakhstan, e-mail: amerkhanovashk@gmail.com; <https://orcid.org/0000-0002-2492-4203>;

Uali, Aitolkyn Sailaubekkyzy — Candidate of Chemical Sciences, Associate Professor, L.N. Gumilyov Eurasian National University, Kazhymukan street, 13, 010000, Nur-Sultan, Kazakhstan, e-mail: ualiaitolkyn@gmail.com; <https://orcid.org/0000-0002-5851-6566>;

Omarbekov, Tolegen Bazarovich — Candidate of Chemical Sciences, Autonomous Cluster Fund “Park of Innovative Technologies”, Zhibek-Zholy Ave, 135, 050000, Almaty, Kazakhstan, e-mail: omar_toke@mail.ru;

Belgibayeva, Dana Sapargaliyevna — Candidate of Chemical Sciences, L.N. Gumilyov Eurasian National University, Kazhymukan street, 13, 010000, Nur-Sultan, Kazakhstan, e-mail: dana0577.77@gmail.com; <https://orcid.org/0000-0002-4225-600X>